In-situ Interface Chemical Characterisation of a Boundary Lubricated Contact

by

Yugal Rai

Submitted in accordance with the requirements for the degree of
Doctor of Philosophy (PhD)

The University of Leeds
School of Mechanical Engineering

August, 2015

The candidate confirms that the work submitted is his/her own and that appropriate credit has been given where reference has been made to the work of others.

This copy has been supplied on the understanding that it is copyright material and that no quotation from the thesis may be published without proper acknowledgement.

The right of Yugal Rai to be identified as Author of this work has been asserted by him in accordance with the Copyright, Designs and Patents Act 1988.

Acknowledgements

First and foremost, I would like to express my deepest and sincere gratitude towards my supervisors, Professor Ardian Morina and Professor Anne Neville for their continued support, enthusiasm, encouragement and advice throughout my study period. I highly appreciate their patience, guidance and motivation during tough time in PhD pursuit. It has been a great pleasure working with their expertise in the field. Without their contribution of time and dedication, the study would not have been possible.

My sincere thanks to the technical staff at iFS for their help and advice in the lab on a daily basis, in particular to Mr. Graham Brown, Ron Cellier and Brian Leach who helped to build, develop and set up the new *in-situ* rig. Thanks greatly to Dr. Michael Ward at LEMAS for his help in setting up and preparing the TEM samples, and also to Dr. Adrian Eagles for his help and patience in explaining the surface measurement techniques. I would also like to thank EPSRC for providing me with the funding.

I would like to also thank the members of the iFS research group. With a wide and multi-disciplined range of people in the group, it has always been a learning process to educate myself. I would like to thank my colleagues Falko Sautermeister, Yong Hua, Rai Singh Notay, James Hesketh and David Slade in office 339a. Also, to Doris Khaemba and Liuquin Yang, for sharing the joy and pain, whilst working with the high speed pin on disc and Raman spectroscopy.

I would like to acknowledge and appreciate my parents for their unconditional love, blessings and moral support they have given me over the years. To my brother, Yugant for helping me cope with stress of writing up and for being a great companion. I would also like to express my gratitude to Prasansa for her support and encouragement, and helping me get through some agonizing period in the most positive way.

Finally, I would like to dedicate this thesis to my late Grandfathers J.R.Rai and Purna Bahadur Rai. Even though you are no longer with us, I know you would be proud.

Abstract

An increasing demand for improved fuel efficiency and more reliable automotive engines has seen a number of approaches made to further improve the tribological performance in automotive engine parts. Engine oil lubricants extend the life of the moving parts operating under different conditions and also preventing any damages to these parts. However, although its applications are beneficial towards the moving parts, the environmental implications of these lubricants are somewhat harmful, leading to stricter regulations against its emissions.

Strict emission requirements have led to a greater interest in understanding the tribological performance of these lubricant additives. Hence, in order to develop more environmentally friendly additives, it is necessary to understand the tribochemical mechanism that occur at the lubricated systems. However, to date despite considerable efforts, a model to predict friction coefficient is only limited to elastohydrodynamic and hydrodynamic lubrication systems. Under boundary and mixed lubrication conditions, the friction and wear behaviour of the tribological system are characterised by the surface asperities of real contact and with the formation of thin surface films. Thus, sophisticated and reliable experimental techniques are required to investigate and assess the tribological systems under this conditions.

In-situ approaches can greatly enhance our understanding on the progressive developments between the contacting interfaces, including the detailed chemical, structural and physical interactions governing friction and wear.

The research focuses on developing a methodology for *in situ* and real time boundary lubricated surface optical and chemical characterisation with the aid of Raman Spectroscopy.

The techniques are developed with the lubricant additive of Molybdenum Dialkyldithiocarbamate (MoDTC) and used to experimentally evaluate the interface phenomena occurring in a bench tribometer. MoDTC under defined tribological conditions forms MoS_2 tribofilms which reduces friction. Surface analytical methodology of *ex-situ* and *in-situ* analysis is applied for the

lubricant additive to understand the tribochemical process occurring at the tribological contacts.

Table of Contents

List of Tables

List of Figures

Nomenclature

(Alphabetical order)

	Terms	**Units**
a	semi-major axes of the contact ellipse	m
AES	Auger electron spectroscopy	
AFM	Atomic Force Microscopy	
AISI	American Iron and Steel Institute	
ATF	Automatic transmission fluids	
ATR/FT-IR	Attenuated total reflection/Fourier transform infrared spectroscopy	
AW	Antiwear	
BL	Boundary Lubrication	
c	Velocity of light	3×10^{10} cm/s
CAD	Computer-aided design	
CCD	Charged Coupled Device	
DAQ	data acquisition	
DC	Direct current	
DLC	Diamond like Carbon	
E	Young's modulus	GPa
E	reduced Young's modulus	Pa
EDS	Energy dispersive X-ray spectroscopy	
EDX	Energy dispersive X-ray	
EELS	electron energy loss spectroscopy	
EHL	Elastohydrodynamic Lubrication	
EM	Electromagnetic	
FIB	focused ion beam	

FM	Friction modifier	
FWHM	full width at half maximum	
HL	Hydrodynamic Lubrication	
HRC	Rockwell Hardness	
HSAB	hard and soft acid and base	
HSPOD	High speed pin on disc	
I	Intensity	W . steradian^{-1}
IR	Infra-red	
LWD	Long working distance	
MoDTC	Molybdenum dialkyldithiocarbamate	
MTM	Mini traction machine	
N.A	Numerical aperture	
NIR	near infrared	
PAO	Poly-alpha-olefin	
PMT	Photomultiplier Tubes	
R	Reduced radius of curvature	m
R_a	Surface roughness	μm
RHEED	reflection high-energy electron diffraction	
rpm	Revolutions per minute	
SEM	Scanning Electron Microscope	
SERS	surface enhanced Raman spectroscopy	
SFA	surface force apparatus	
SIMS	Secondary Ion Mass Spectrometry	
SNR	Signal to Noise ratio	
SPM	Scanning Probe Microscopy	
TEM	Transmission Electron Microscopy	
UHV	Ultra high vacuum	

UV	Ultraviolet	
Vis	Visible	
VSI	Vertical Scanning interferometry	
W	Load	N
XPS	X-ray Photoelectron Spectroscopy	
ZDDP	Zinc dialkyldithiophosphate	
T_a	amplitude correlation time	
T_c	coherence lifetime	
v	Frequency	Hz
μ	Friction coefficient	
λ	Lambda ratio	
m	Mass	kg
h_{min}	Minimum film thickness	
h	Planck's constatnt	6.62×10^{-27} erg s
ϑ	Poisson's ratio	
Ω	Solid angle	
η	Viscosity	

.

Chapter 1
Introduction

1.1 Tribology

Tribology is formally defined as the science and technology concerned with 'interacting surfaces in relative motion' focusing on fundamental investigations of friction, wear and lubrication. The term 'tribology' is derived from the Greek word 'tribos' which relates to rubbing or sliding and was first coined in 1966 by a UK government committee.

However, the existence of tribology as a traditional form of science has been recognized before the initiation of any historical records. Ignition of fire by the Palaeolithic people, development of the wheel and use of lubricants to move heavy masses for the construction of pyramids in Egypt displays early practical applications of tribology [3]. Tribology exists in many mechanical systems but also in nature which affects our lives to a much greater degree than it is commonly realized. For example, the human body associates with interacting surfaces on a daily bases from human joints to the external surface interaction with the human skin.

Friction is defined as the resisting force between the surfaces in contact. Relative motion between the contacting surfaces, generally involves a progressive loss of material, inducing damage to the surface. This phenomenon is termed as wear and is a major cause of material depletion and loss of mechanical performance. Wear mechanisms are however defined by considering complex changes of energy dissipation that takes place during friction. Therefore, it has been recognised that friction and wear in major components has been the cause of much energy loss, and further understanding of these mechanism can result in considerable savings and economic efficiency [4]. One of the solutions for the reduction of friction and wear has always been the use of lubrication between any two surfaces in contact. Lubricants applied to rubbing surfaces are used to reduce friction and wear and provide smooth running and satisfactory life of tribological components.

However, minimization of friction and wear is not always the case for the application of tribology. Certain cases such as the application of brakes and lubricated clutch require high friction, whereas reduction of friction but not wear is desired in pencils.

The field of Tribology can be further subdivided into two main branches, namely *tribotechnology* and *triboscience*. *Tribotechnology* is the aspect of tribology that involves the technical considerations for tribological application, whereas *triboscience* devotes to the systematic study of interacting surfaces in relative motion. *Triboscience* includes the scientific aspects of tribochemistry, tribophysics, contact mechanics and materials and surface sciences as related to tribology [5].

Tribochemistry is the science concerned with all chemical reactions in mineral and synthetic formulation affecting the tribofilm formation on metal surfaces. It deals with the relations between tribosystem and chemical changes of the surface layer [6]. "*Tribochemistry*" is defined as the lubrication conditions which is a compromise between numerous limitations forced by the nature of the physical and chemical properties of the lubricant, the material surfaces, the oil formulation, and the life required.
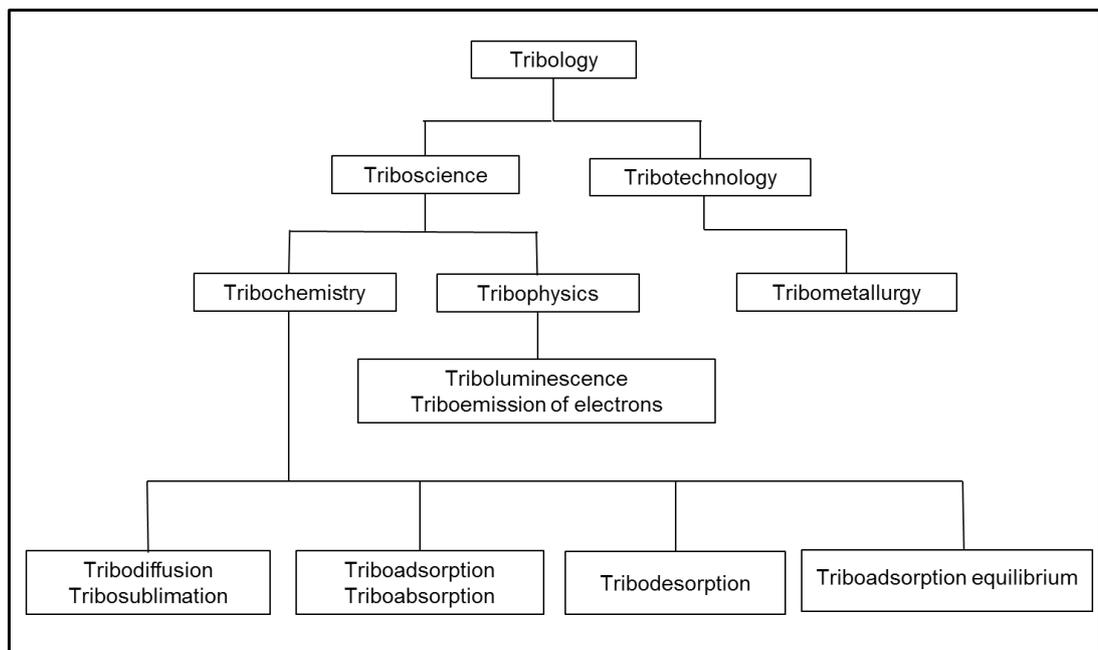
Figure 1.1 Branches of tribology [5].

1.1.1 Friction

Friction is described as the resistance to motion encountered when one body moves tangentially over another. It is commonly divided into *dry friction* and *viscous friction*. It may be *static* with the solid bodies having no relative motion or *dynamic*, when the solid bodies are moving relative to each other. Dry friction occurs between two solid bodies without any lubrication on the interface, whereas viscous friction occurs when two solid bodies are more or less separated by a fluid [7].

Hence, accordingly there are three laws of dry friction provided, where the friction force (*F*) is directly proportional to the applied load (*W*) and independent of apparent area of contact (*A*) and the sliding velocity (*V*) [8]. The first law gives rise to the definition of the coefficient of friction (*μ*), which is the ratio of the friction force *F* and the normal force between the bodies.

The normal force always acts perpendicular to the contact area, and under sliding, the friction force is the force required to maintain the sliding and always acts tangentially to the contact area. Therefore the coefficient of friction is obtained with the following well known equation.

$$\mu = \frac{F}{W} \tag{1-1}$$

In tribological experiments, the coefficient of friction is obtained from known or measured forces. Both F and W can be measured with the use of, for example, a load cell and may thus be logged as a function of time.
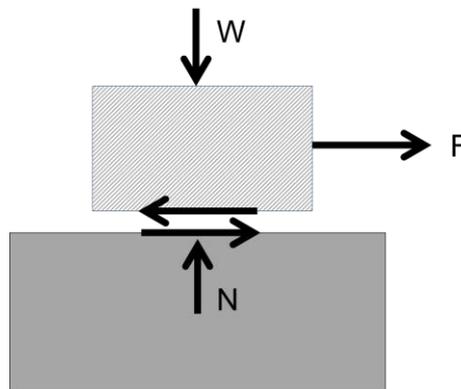
Figure 1.2 Visualization of friction under sliding motion, where various forces (F, (Friction force), W (Load) and N (Normal force)) acting on the contact is produced.

1.1.2 Wear

Wear occurs when a relative motion is established between the contacting surfaces and generally involves a progressive loss of material, inducing damage to the surface. Wear profile between the asperities of the two surfaces can be described by the Archard wear equation [9, 10]

$$V = kWx \qquad \text{(1-2)}$$

Where V is the worn volume, k is the dimensional wear factor, W is the load and x is the sliding distance. The wear factor, k, is a function of the interacting materials, their surface topography, the lubricant and the operating conditions.

1.1.3 Lubrication: Lubricants and lubricant additives

Lubrication is defined as an effective interposition of a solid, liquid or gas between two bodies to reduce friction and/or wear as one move over the other [7]. In a tribological interface, the form of lubrication is classified by their lubrication regimes, which allows us to consider the overall performance of a tribological interface in terms of basic parameters such as friction and wear. There are four lubrication regimes and can be distinguished accordingly [4, 11, 12]:

i. Hydrodynamic Lubrication – The interacting surfaces in a hydrodynamic lubrication are separated by a fluid lubricant film (1-100 μm) that is sufficiently thick to prevent them coming into contact. The behaviour of the contact is governed by the bulk physical properties of the lubricant, mainly viscosity and by the velocity of the relative motion.

ii. Boundary Lubrication – In boundary lubrication, the fluid lubricant (1-100 nm) does not separate the surfaces and contact takes place over an area comparable to that which develops in dry contact. The wear and friction are determined by the properties of the surface materials and the lubricant films at their common interfaces.

The physical and chemical properties of the thin lubricant films/boundary lubricants of molecular proportions govern the contact characteristics, which reduces friction and wear principally by minimising adhesion and abrasion. The boundary lubricant modifies the solid-solid interactions, due to various solid-lubricant reactions (physisorption, chemisorption, tribochemical reactions), which depend strongly on the environmental conditions and on the lubricant composition.

iii. Mixed Lubrication – Mixed Lubrication is a form of lubrication where the two extremes of hydrodynamic and boundary lubrication are encountered. Therefore there are regions in the interface separated by a fluid lubricant film and areas with contact between asperity peaks. Hence, the physical properties of the bulk lubricant governing the characteristics of the hydrodynamic lubrications and the chemical properties of the boundary lubricant determine the interface contact characteristics of the mixed lubrication regime.

iv. Elastrohydrodynamic Lubrication - Elastrohydrodynamic Lubrication occurs in low conformity, highly loaded tribological interfaces where effective hydrodynamic films often persist well into the regions where boundary lubrication would be expected. The high contact pressures generated due to low conformity, highly loaded interfaces results in a local elastic deformation of the surfaces with substantial viscosity increase.
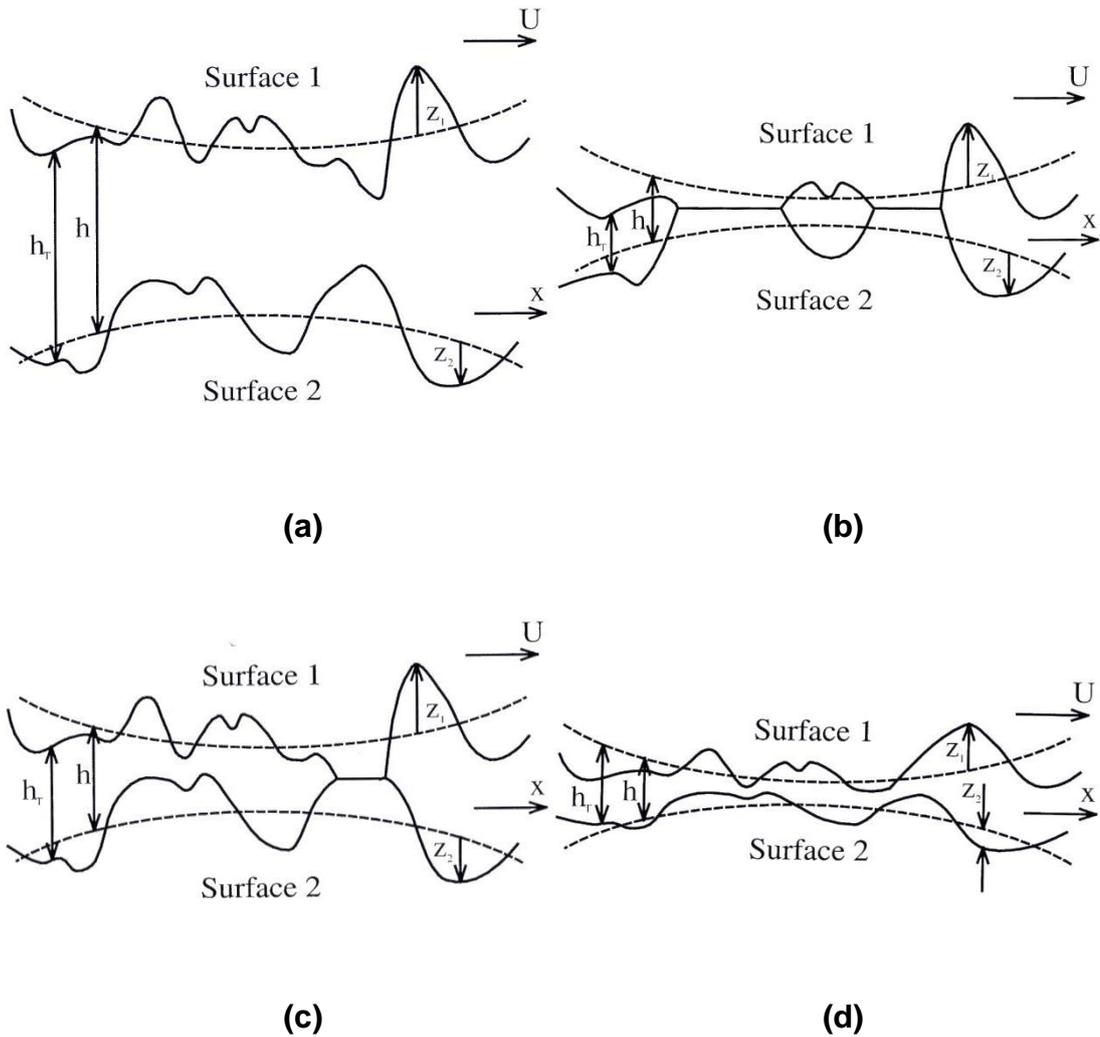
Figure 1.3 Lubrication regimes of (a) Hydrodynamic Lubrication (b) Boundary Lubrication (c) Mixed Lubrication and (d) Elastrohydrodynamic Lubrication between two interacting rough surfaces, where the dashed lines are the centre lines of the two surface profiles and (x), horizontal coordinate, (z_1), vertical displacement of surface 1 from the centre line at any x,(z_2), vertical displacement of surface 2 from the centre line at any x,(h), vertical separation of the centre line of surface 1 and 2 at any x, (h_T), vertical separation of surface 1 and 2 at any x, (U), relative sliding velocity between surface 1 and surface 2 [11].

Stribeck curve expresses the relationship between the friction coefficients, viscosity of the lubricating oil, load and velocity and expertly captures the characteristics of various lubrication regimes. The modified Stribeck diagram below (Figure 1.4) expresses the coefficient of friction against the Stribeck number which summarises the frictional behaviour of a tribological interface as it passes through the four lubrication regimes.
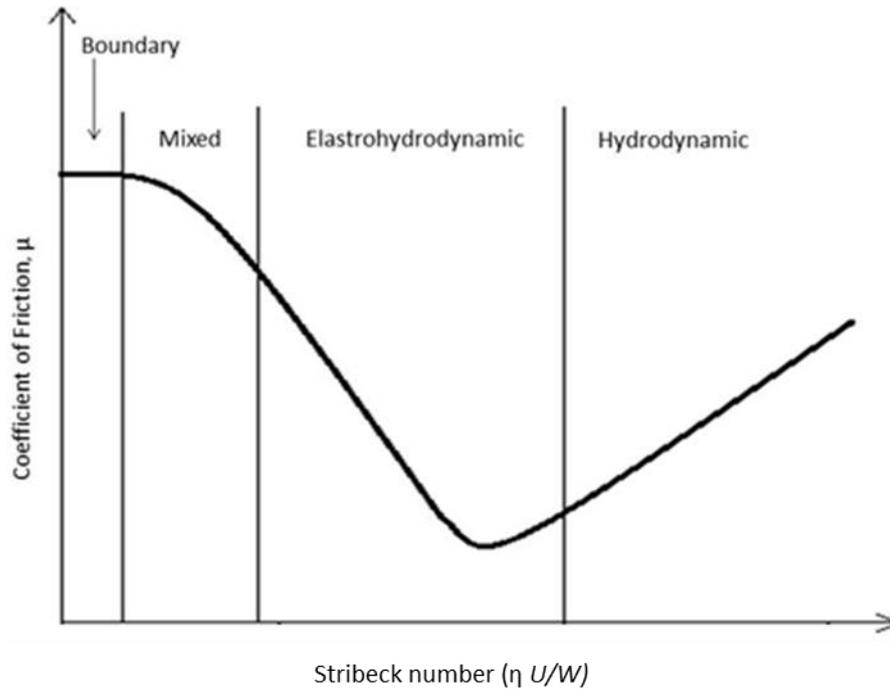
Figure 1.4 The Stribeck curve representing the general characteristic of lubricated moving surfaces as a function of Stribeck number where η, U and W are lubricant viscosity, the relative velocity and the normal force respectively. [13]

The relationship between the coefficient of friction against specific film thickness can also be displayed with the Stribeck curve. It is therefore convenient to discuss the transition from one lubrication regime to another in terms of a dimensionless film thickness ratio λ which is defined as

$$\lambda = \frac{minimum\ lubricant\ film\ thickness}{sum\ of\ the\ surface\ roughnesses} = \frac{h_{min}}{\sqrt{R_{q1}{}^2 + R_{q2}{}^2}} \qquad (1\text{-}3)$$

The minimum film thickness parameter h_{min} is subsequently used to calculate the lambda ratio, where the dimensionless minimum film thickness for a point contact is obtained using the Dowson and Hamrock equation [14]

$$h_{min} = 3.63 \times R \times G^{0.49} \times U^{0.68} \times W^{-0.073}(1 - e^{-0.68k_e}) \quad (1\text{-}4)$$

Where G is the dimensionless material parameter, U the dimensionless speed parameter, W is the dimensionless load parameter; R is the effective radius of the contact and k_e is the elliptical parameter. The surface films of the boundary lubrication vary in thickness from 0.005 µm to 0.01 µm and the specific film thickness of less than 1. The coefficient of friction experienced by the interfaces is also at its maximum, also with large applied load resulting in high friction force.

Figure 1.5 shows the wear rate in various lubrication regimes as determined with the Stribeck curve in Figure 1.4 [15]. Since there is no asperity contact, hydrodynamic and elastohydrodynamic regimes show little or no wear. Under boundary lubrication regime the degree of asperity interaction and the wear rate is high due to the increase in load. The coefficient of friction experienced by the interfaces is also at its maximum, also with large applied load resulting in high friction force.

Lubricants are used to reduce friction and wear between moving parts in most of the mechanical systems and a typical modern automotive engine lubricant consists of mineral or synthetic oils as the base oil and viscosity improver (72 – 96%) with an additive package comprising of 4-28% of the total engine oil [6]. Table 1.1 provides a typical concentration range of the main additives used in the formulation of engine oils.

Additives are chemicals added to the lubricant to perform specific function or achieve levels of performance not possible with the basic mineral oil alone. Modern engine lubricant additives, depending on the application, include a wider range of additive types, where some of the important ones are the antiwear additives, antioxidants, friction modifiers, detergents and dispersants.
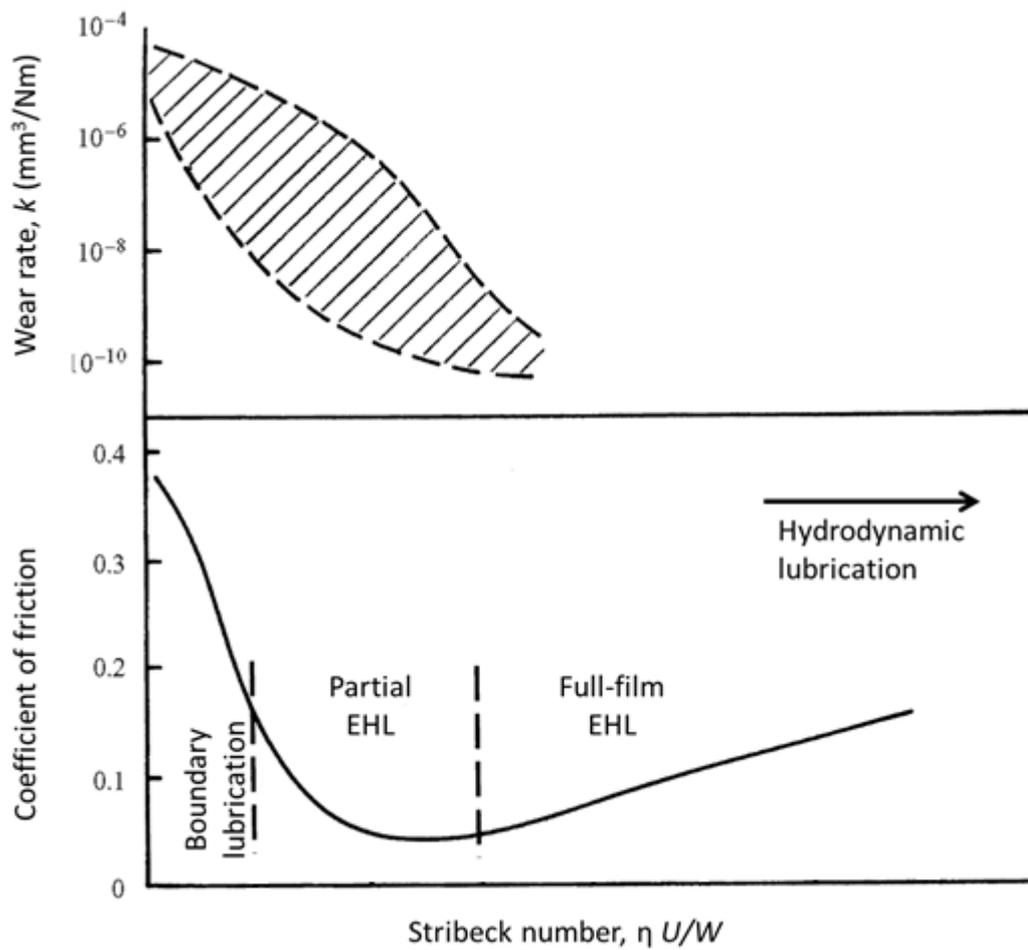
Figure 1.5 Regimes of lubrication and wear in the lubricated sliding of metal, as a function of Stribeck number. It also illustrates the variation of coefficient of friction, which follows the Stribeck curve familiar from Fig 1.4. [16]

Table 1.1 Concentration range of main additives used in the formulation of engine oils [6].

Material	Weight (%)	Material	Weight (%)
SAE 30 or 40 base oil	71.5 to 96.2	Antioxidant/Wear	0.1 to 2.0
Metallic detergent	2 to 10	Friction modifier	0.1 to 3.0
Ashless dispersant	1 to 9	Anti-foam agent	2 to 15 ppm
Zinc dithiophosphate	0.5 to 3.0	Pour point depressant	0.1 to 1.5

1.2 Tribology and tribochemistry modelling environment

Recent legislation demands the development of environmentally-friendly lubricant additives in order to meet the very strict emission requirements. Regulations governing environmentally friendly lubricating oils generally require that they be metal-free, readily biodegradable, display low ecotoxicity in water and soil, and exhibit a low tendency for bioaccumulation [17]. Zinc, phosphorus and sulphur containing additives are therefore proposed to be replaced by other ecologically compatible additives to facilitate even greater fuel efficiency and provide even longer catalyst life [18].

Strict emission requirements have led to a greater interest in further understanding the tribological performance of these additives in automotive engine parts with the development of environmentally-friendly lubricant additives [19]. Therefore, to develop a more environmentally friendly and ecologically compatible additives, it is necessary to understand the mechanisms of the tribochemical reaction that occur at the surfaces of the lubricated systems under tribological conditions.

However, tribology is a complex and multidisciplinary research field, with the influence of large number of factors affecting the tribological performance. Most tribological studies are based on experimental study of friction coefficient and wear rate, and are sensitive to running conditions such as load, speed, temperature and environment. To date ability to predict coefficient of friction is limited only to elastohydrodynamic lubrication (EHL) and hydrodynamic lubrication (HL) systems [20-24]. Boundary and mixed lubrication conditions are characterised with a direct contact between asperities of real areas of contact, which then repeat with lubrication additives to form surface films (tribofilms) that define friction and wear process. Due to such difficult tribological circumstances, modelling the tribology of boundary lubrication systems capable to predict friction and wear performance provides a challenge and a need to understand the tribochemistry processes in detail.

Our current understanding of tribology, especially tribochemistry are however, monitored and reported with experimental studies for friction coefficients and wear rates at steady-state conditions. The initial transient processes during the approach to steady state conditions are usually monitored but not modelled. Therefore, it is important that experimental studies are done with techniques that represent sophisticated and reliable approach towards investigating tribological interfaces. Hence, development of *in-situ* approaches and techniques can greatly enhance our tribological understanding, with further simulations of friction and wear processes to develop the kinetics of tribochemistry processes.

1.3 Objectives of the thesis

The current work aims to develop an *in-situ* experimental method to characterise boundary lubricated conditions, which will help to understand the tribochemical process occurring in a boundary lubricated interface. The main objectives of this thesis are as follows:

- To review literature on the application of *in-situ* experimental methods towards the understanding of boundary lubricated contacts.

- To determine the application of Raman spectroscopy towards the understanding of the tribofilms formed onto the surface with the validation of Raman operating parameters and its influence towards the characteristics response of the tribofilms in the Raman spectroscopy.

- To develop a suitable *in-situ* rig capable of utilising the surface analysis techniques of Raman spectroscopy, to conduct standard friction and wear tests along with the detection and chemical characterisation of various boundary lubricated films *in-situ*.

- To validate the performance of the new *in-situ* tribometer in accordance with the traditional High Speed Pin on Disc (HSPOD) tribometer to ensure the formation of the lubricant additives tribofilm.

- To study the performance of MoDTC lubricant additive with varying parameters and conditions along with its interaction with Zinc-dialkyldithiophosphate (ZDDP) lubricant additive

- To understand and characterise the time-transient tribochemical development of the MoDTC tribofilm under *ex-situ* and *in-situ* conditions without cleaning the sample.

- To develop a model of the tribochemical processes for the MoDTC lubricant additive compared with the tribo-nature of the film formed that can be adapted towards the understanding of the kinetics of the tribochemistry processes.

1.4 Structure of the thesis

Chapter 2 includes a literature review of boundary lubrication conditions and its current understanding in the field of tribochemistry of the MoDTC lubricant additives. In this chapter current experimental methodologies and techniques adapted towards the understanding of lubricant additives and its tribological phenomenon are reported. This chapter further reviews and highlights the importance of *in-situ* approaches towards the understanding of the tribochemical properties of the contacting surface.

Chapter 3 provides the relevant theories of Raman spectroscopy as a surface analytical technique, and its relevance as an *in-situ* approach towards understanding the tribochemical features of the contacting surface.

Chapter 4 describes the experimental methods, parameters, material used and its properties, and experimental procedures. Surface techniques of Raman spectroscopy, optical microscopy, Transmission electron microscope (TEM), Energy-dispersive X-ray spectroscopy (EDX) and optical profilometry used in this work has been described here. The development of *in-situ* tribometer has been described in the chapter along with its set-up of *in-situ* Raman analysis.

Chapter 5 presents an initial study conducted towards the application of Raman spectroscopy for understanding the characteristics nature of tribological samples. The chapter focusses on the optimisation of Raman spectroscopy and its parameters towards the influence of tribofilms formed onto the surface.

Chapter 6 presents the results of the tribological performance of MoDTC lubricant additive under boundary lubrication conditions. The effect of load,

speed and temperature are covered and discussed for both the HSPOD and *in-situ* rig. The effect of temperature was duly noted towards the formation of MoDTC tribofilms and further effect of temperature on the tribofilm formation is reported. MoDTC tribofilms were characterised with the surface analysis technique of Raman spectroscopy and wear data collected with the optical microscope and profilometry.

MoDTC tribofilm performance results are reported with longer duration test and under oil scarcity and the film characterise with Raman spectroscopy. Similarly the tribological performance results of MoDTC and its interaction with the ZDDP lubricant additive is presented. The characteristics of the tribofilms formed were identified with the use of Raman spectroscopy. The composition and the thickness of the tribofilm were identified by using a combination of TEM and EDX measurements.

Chapter 7 presents the results of time transient development of MoDTC lubricant additive under boundary lubrication conditions. The study presents the results of both *ex-situ* and *in-situ* analysis with Raman analysis and its influence on the time derived tribochemical formation. Combinatorial surface analysis technique of TEM, EDX and surface profilometry are used to further identify the nature of tribofilm formed onto the surface.

Chapter 8 discusses the main findings of the experiments, along with a comparison of experimental studies in literature.

Chapter 9 includes the conclusions and future work suggestions based on the current experimental data.

Chapter 2
Boundary Lubrication and Experimental Methodologies for Tribochemistry Studies: Literature review

Friction, wear and lubrication are prominent phenomena occurring within a tribological contact. Hence formulation and systematic testing of concepts and theories relating to friction, wear and lubrication are needed to obtain with designing and executing critical experiments and observations. A common approach to overcome the lack of theoretical understanding is to conduct experiments under controlled laboratory conditions.

This chapter is divided into three main parts, a review of boundary lubrication is presented firstly. A brief review of various friction modifiers additives which operates under these boundary conditions are presented, along with a detailed review of Molybdenum dialkyldithiocarbamate (MoDTC) as a friction modifier, which has been used extensively in this study.

Secondly various experimental methodologies in tribology are briefly described. The third part covers surface analysis methodology along with a review of various surface analytical techniques utilised for lubricant studies in tribology. Application of various surface analytical techniques and its importance towards the understanding of the interfacial properties of the contacting surface, particularly under boundary lubrication is highlighted.

2.1 Boundary Lubrication

Boundary lubrication is the lubrication regime where a fluid lubricant does not separate the surfaces and contact takes place over an area comparable to that which develops in dry contact. In a boundary lubrication the friction and wear characteristics are determined by the properties of the surface materials and the lubricant films at their common interfaces (Figure 2.1). The contact characteristics are governed by the physical and chemical properties of thin surface films of molecular proportions called boundary lubricants, which reduce friction and wear principally by minimising adhesion and abrasion [25].

High Loads/Low Speed force surfaces together

Lubricant film

Under boundary conditions, lubricant film is too thin to separate the contacting surface. Contact between surface asperities occurs, and the friction and wear protection is provided by lubricant additive.
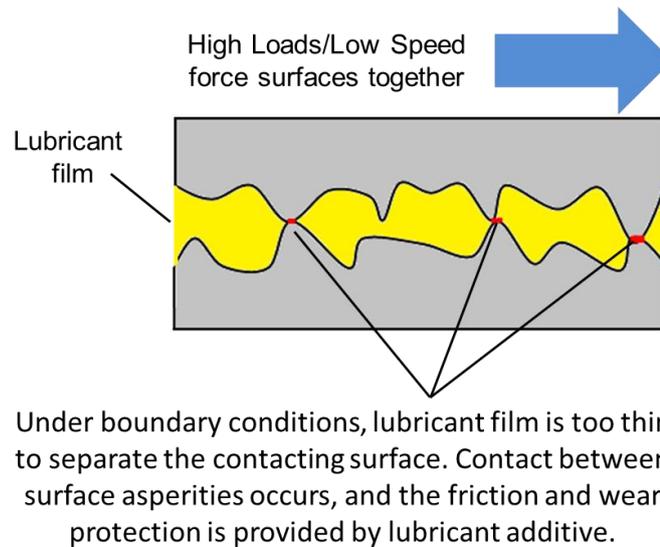
Figure 2.1 Contact between surfaces under boundary lubrication conditions.

Film strength is defined as the resistance of the boundary lubricant to wear and thereby being displaced from the surface, and therefore used to analyse boundary lubrication. Similarly, boundary lubricants can be classified according to the surface action that attaches them to the surface or led to their formation. There are three main types of surface action and listed according to their increasing order of film strength [12, 26] :

- *Physically adsorbed layers* of gaseous, liquid or solid lubricants are formed by short-range inter-molecular forces, such as van der Waal's forces, and the process is reversible. A layer of lubricant one or more molecules thick becomes attached to the surfaces of the solids which provide modest protection against wear. At higher transition temperature, usually close to the melting point of the lubricant, these layers loses their resistance to wear and are displaced from the surface.

- *Chemically adsorbed layers* involves a degree of chemical reaction, referred as chemisorption. Animal and vegetables fats and oils are added to the lubricant, and hence the additives contains long chain fatty acid molecules, which exhibit great chemical affinity for metals at their active ends. These polar molecules exhibit a usual representation like that of a carpet pile, and form metal soaps which are low shear strength materials. They provide satisfactory boundary lubrication at moderate loads, temperatures and speeds and are often successful in situations showing evidence of mild surface distress.

- *Films formed by chemical reaction* are components of the lubricant or lubricant additives which react with the surface to produce surface films of very different composition and physical properties to the original surface. High contact temperatures develop, due to frictional heating, when loads and sliding speeds are large and which is the most important condition to the success of boundary lubricants formed by chemical reaction. These films provide the greatest film strength and are used in the most severe operating conditions.

In the presence of anti-wear and friction-modifying additives, boundary lubrication is mainly governed by the formation of tribochemical films [27]. These films formed under the Hertzian contact are usually very thin <1 μm and confined by the bounding metal or ceramic surfaces in contact [28]. Therefore complementary information on the local chemical composition, rheology or molecular conformation has proved more difficult to obtain.

One of the solution to examine the behaviour in and around the contact region is the use of molecular vibrational spectroscopy, either infra-red (IR) or Raman [29]. And although IR techniques have been successfully applied to various different lubricant systems [30-33], a number of challenges still remain, where detection of boundary film formation with the use of IR techniques is a major challenge.

2.1.1 Friction modifiers

Friction modifiers (FMs) as the name suggests are additives which reduces friction when surfaces come into contact by the formation of surface films. At increased loads and low viscosities at higher temperatures the liquid lubrication can easily proceed to mixed and boundary friction conditions.

Friction modifiers are added to the lubricant to modify the friction in this lubrication regime of the tribological contact. They are added, for example, to engine oils and gear oils to reduce friction and to automatic transmission fluids (ATFs) to control friction [1, 34]

Friction modifiers adsorb by physisorption, even though chemisorption occurs. They adsorb in monolayers or multilayers. The FM molecules adsorb more strongly to the surface than to neighbouring FM molecules (Figure 2.2). The layers promote the separation of the surfaces by steric hindering, exhibiting strong anticompressive behaviour of the layers. On the other hand, the FM layers are easily sheared and thereby reduce friction. This combination of strong anticompressive properties and low resistance to shear gives FMs their superior properties [7].

Friction modifiers a classified into different groups regarding their function: mechanically working FMs, adsorption layers forming FMs, tribochemical reaction layers forming FMs, friction polymer-forming FMs and organometallic compounds [35]. However there are two types of friction modifiers: organic friction modifiers (carbon, hydrogen and oxygen only) and metal-containing friction modifiers (MFMs) such as molybdenum dithiocarbamate (MoDTC) [36].
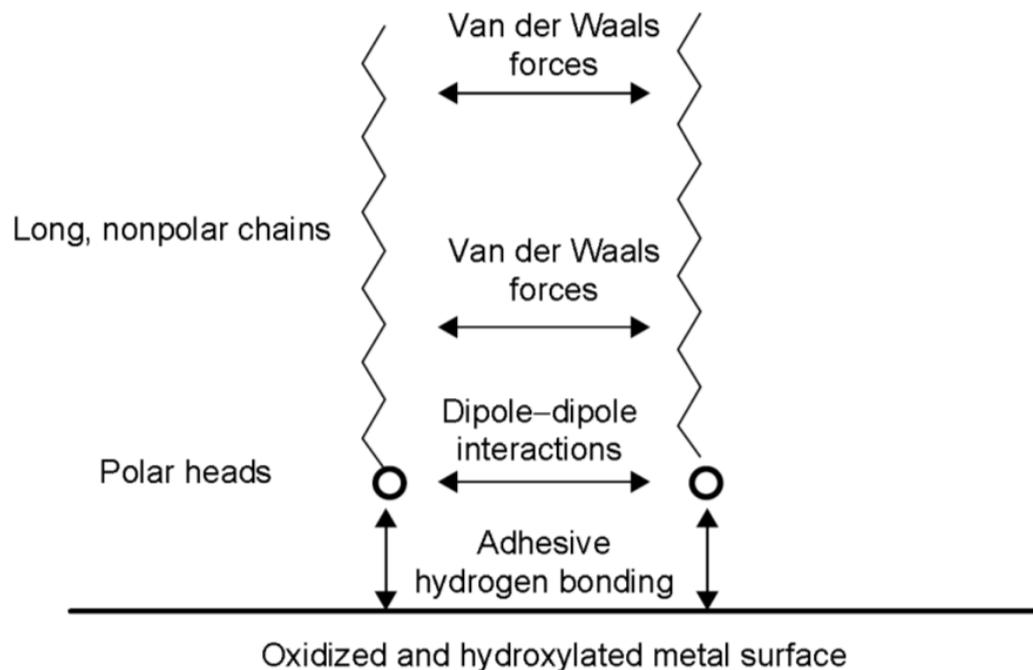
Figure 2.2 Formation of adsorbed layers of organic friction modifiers [1].

Organic friction modifiers chemistry comprises, for example, fatty alcohols, esters, fatty acids and fatty amides. These chemistries are all surface active, having a polar part of oxygen or nitrogen and a hydrophobic part. Long and linear chain materials reduce friction more effectively than short and branched chain FMs. Fatty acids reduce friction more effectively than both fatty amides and fatty alcohols. The preferred fatty acid FM is saturated and has 13 to 18 carbons. Shorter chained fatty acids may entail corrosion problems [1].

Organic FM (friction modifier) has been classified as a greener candidate to reduce the environmental damage caused by heavy elements present in the lubricant additives. A substantial amount of work [1, 37, 38] has been carried out with this type of friction modifiers at the moment. However, further understanding of the mechanisms of these friction modifiers are needed in relation to tribological parameters of friction, wear and surface interaction.

2.1.1.1 Molybdenum Dialkyldithiocarbamate (MoDTC)

Oil soluble organo-molybdenum compounds such as molybdenum dithiocarbamates (MoDTC) and molybdenum dithiophosphates (MoDTP) are well-known friction modifier additives. Since the late 1970s, considerable research has been undertaken to investigate the mechanisms of these additives [39]. Various molybdenum additives have been studied and analyzed for their friction reducing capabilities [40]. In particular, molybdenum dialkyl-dithiocarbamate (MoDTC) compounds containing both molybdenum and sulphur which are soluble in oil due to their hydrocarbon chain compounds are of interest [41, 42].
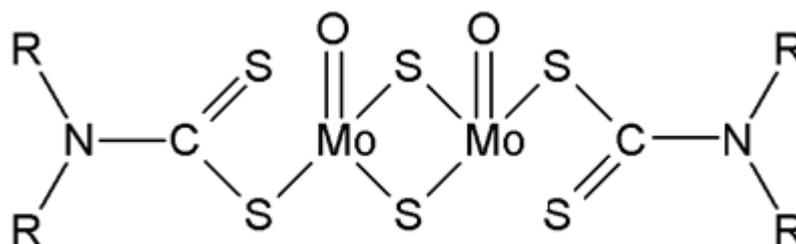
Figure 2.3 Molybdenum Dithiocarbamate structural drawing.

It is well documented under boundary lubrication conditions that this type of additive has been able to reduce friction to very low friction coefficient values of 0.04 to 0.075 [43, 44]. The tribological properties of this friction modifier have been attributed to the formation of the MoS_2 tribofilm. Various analytical techniques such as electron diffraction [45], X-ray methods [41, 46] and Raman spectroscopy [43, 44] detected the presence of the MoS_2 tribofilm on the rubbing surfaces. The MoS_2 tribofilm has a lattice-layered structure with low shear strength which makes it possible for low friction between the tribology components [42, 47-50]. These tribofilms were reported to form on the rubbing surfaces in the presence of air and oxygen [42].

Graham *et al*. [43] concluded that the friction reducing capability of the MoDTC tribofilm is highly dependent upon the temperature and MoDTC concentration. They confirmed the formation of the MoS_2 tribofilm on the wear scar with the use of Raman spectroscopy, and further concluded that friction is reduced when MoS_2 forms and occurs only under true boundary lubrication conditions [51]. MoDTC was able to reduce friction effectively in the absence of other additives, but the range of conditions strongly depending on temperature and additive concentration. Friction coefficient values were produced in the range of 0.04 and 0.075, and lowest friction produced at high temperature and high additive concentrations.

Yamamoto and Gondo [50] also showed with a constant temperature of 120⁰C, with increasing concentration the final coefficient of friction was decreased to a low value of about 0.05 independent of the concentration of MoDTC. Induction time necessary for the coefficient of friction to decrease was short with higher concentration and smaller the amount of wear. MoS_2 was detected at a shorter time period for high concentration of MoDTC, where friction coefficient was decreased more quickly due to the rapid formation of MoS_2 on the surface. However, at concentration ranging above 500 ppm improvement by the addition of MoDTC seems to be saturated and reduction of friction and wear was not expected.

Similarly, Kasrai *et al* [46] related the friction reduction to the formation of a ''pure '' MoS_2-like film with MoDTC. The tribofilms generated from MoDTC indicates that the film is composed of an MoS_2 like film and a sulphate. The sulphate was present mostly on the surface. The proportion of sulphate was reduced when the concentration was increased. However, a small amount of sulphate can apparently affect the friction reducing properties of the film and suggested that the presence of sulphate is the cause of the increase in friction. However, the mechanism of how this tribofilm are formed onto the surface is subjected to end of test analysis and transient process that leads to the development of these tribofilms needed further understanding, prior to its formation.

Grossiord *et al*. [47], explains the tribofilm formation of MoS_2 with a two-step tribochemical reaction of MoDTC (Figure 2.4). Ultrahigh vacuum friction tests were conducted on MoDTC tribofilms, and analyzed utilizing various surface techniques. Formation of the MoS_2 was proposed to be initiated by the degradation of the MoDTC molecule through electron transfer mechanism activated by the friction process.

The initial step of MoS_2 formation was suggested via electron transfer at the Mo-S bond in MoDTC which led to the formation of three free radicals. One of them corresponded to the core of the MoDTC and the other two to the chain end. The decomposition of the MoDTC core radical followed and MoS_2 and MoO_2 were formed, which could further oxidise in the presence of O_2, and the chain end radical recombined to form thiuram disulphides [47].

It has also been stated that sulphur-containing additives such as zinc dialkyldithiophosphates (ZDDP) are needed to promote MoS_2 formation [30, 52-56] . Ligand exchange between the dialkyldithiocarbamate moiety and the dialkylthiophosphate in ZDDP influences the friction modifying reaction of MoDTC. The antioxidants were required to prevent molybdenum additives from behaving as peroxide-decomposers and thereby being consumed and the antiwear additives promoting the formation of MoS_2 films by reducing the rate of their removal by wear [51].
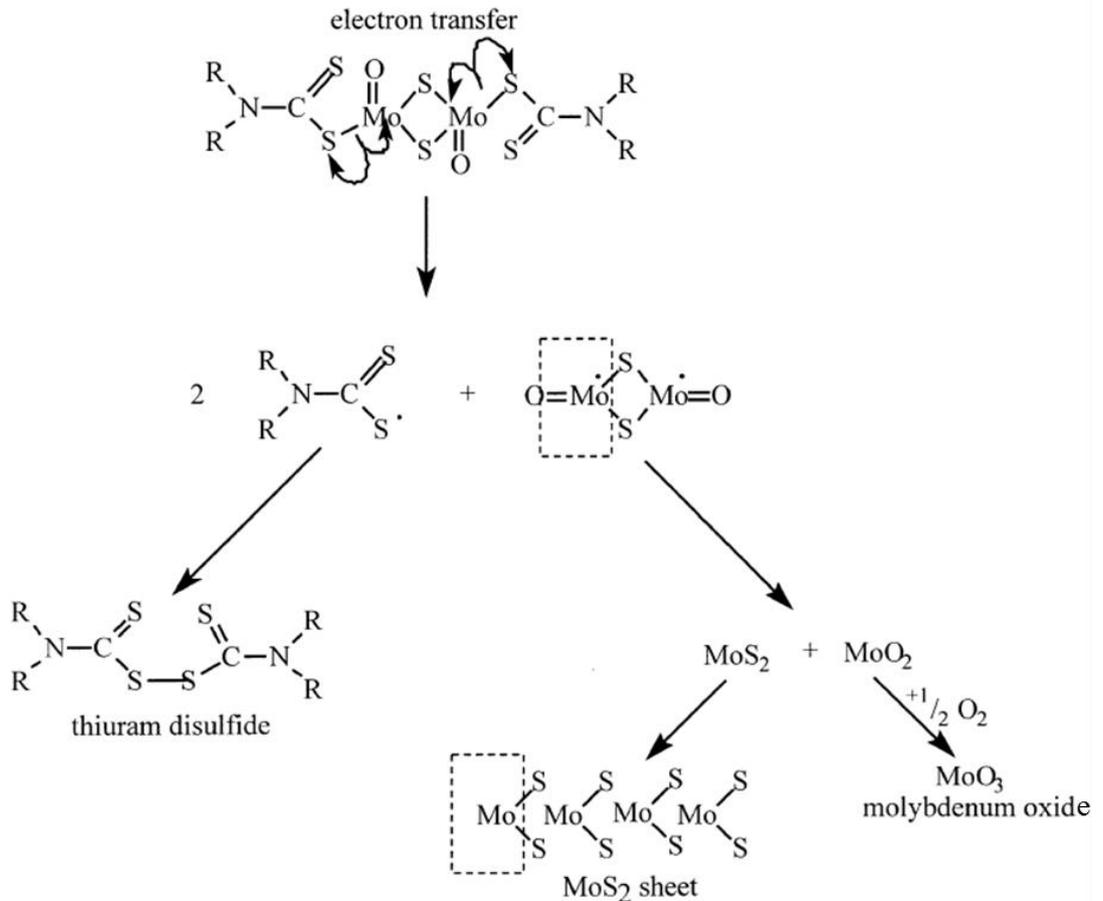
Figure 2.4 Chemical decomposition model of Molybdenum Dithiocarbamate (MoDTC) to form MoS_2 as proposed by Grossoird et al [47].

Similarly, Graham and Spikes [51] suggested that in optimal conditions MoDTC additives produced very low friction coefficients in the range of 0.06 to 0.075 in boundary lubrication conditions. Further suggestion also stated that (i) sulphur-containing additives are needed to promote MoS_2 formation (ii) antioxidants were required to prevent molybdenum additives from behaving as peroxide-decomposers and thereby being consumed, (iii) ligand exchange between the dialkyldithiocarbamate moiety and the dialkylthiophosphate in ZDDP was an important stage in the friction modifying reaction of MoDTC (iv) antiwear additives promote the formation of MoS_2 films by reducing the rate of their removal by wear.

Korcek, Jensen and Johnson [52] likewise, studied the interactions leading to formation of low friction films in systems containing MoDTC and ZDDP additives. The friction reducing ability of these oil additives were known to gradually diminish with mileage accumulation due to oil oxidation. Under

ligand exchange reactions, MoDTC and ZDDP produce products which are known to be antioxidant, which interacts with peroxy radicals and hydroperoxides under oxidant to produce secondary antioxidants under a series of oxidative conversions. Zn containing products were obviously recorded to be stronger antioxidants than the corresponding Mo compounds. The occurrence of friction reducing efficiency in the system was presented because the polar base oil oxidation products and polar base oil components interfere with friction reducing process involving MoDTC and its ligand exchange products.

Martin *et al* [57] studied the effect of oxidative degeneration on the mechanism of friction reduction by MoDTC and showed significant decrease of friction reduction ability when about 80% of the additive content had been consumed by oxidation. It was suggested that the formation of MoS_2 sheets was delayed and/or inhibited due to the concentration of MoDTC being too low.

Morina et al [53] studied the effect of MoDTC and ZDDP tribofilm characteristics and its evolution on tribological performance. Using surface analysis techniques, a link between the theory of MoDTC additive chemical decomposition model and formed MoDTC tribofilm chemical characteristics were obtained. Low friction obtained was confirmed with the detection of MoS_2 in tribofilm formed from MoDTC alone and in a blend with ZDDP. Prior to the formation of MoS_2, FeS_2 was formed which served as a protective layer for retaining MoS_2. When ZDDP was used with MoDTC, phosphate layer was found to be formed beside FeS_2 and deposition of N organic layer. Similarly, the wear in ZDDP/MoDTC lubricant was higher than with ZDDP alone and etching showed that ZDDP/MoDTC lubricants formed phosphate film with higher chain length then the ZDDP one.

Equally, in another journal, Morina et al [54] studied the effect of temperature and ZDDP/MoDTC ratio in boundary lubrication. An increase of MoDTC concentration in the ZDDP containing lubricant caused an increase in MoS_2 formation which resulted in further reduction of friction and similarly, the presence of MoDTC in the ZDDP containing lubricant caused a marginal increase of wear when compared to the ZDDP alone.

Although there exists a wide range of experimental studies conducted on the MoDTC lubricant additive, the tribochemical mechanism that leads to the formation of MoS_2 films is not fully understood. In the presence of ZDDP and MoDTC additive, tribofilms formed onto the surface shows a characteristic properties of friction reduction and anti-wear. Most of the tribochemistry understanding of MoDTC is based on the end of test tribofilm composition and therefore transient tribochemical processes that leads to the formation of these tribofilm is essential to understand the kinetics of the tribofilm formation.

2.2 Experimental methods in Tribology

In order to overcome the lack of understanding friction and wear, it is a common approach to measure them in a laboratory experiment. It can always be argued that friction and wear measurements should be undertaken on the actual component or system in service. However, due to the various difficulties and complexities associated with the real life system or components, it is generally not viable along with the high cost and their lack of availability. On the other hand, laboratory friction and wear experiments provide that control and ease of instrumentation as well as that of the environment whilst conducting experiment, at a relatively low cost [58].

2.2.1 Laboratory tribology tests

Laboratory friction and wear experiments can conveniently be categorised under two headings

- *Standard Tribology* tests using specimens with simple controllable geometries. Friction and wear testing machines often referred to as tribometers or tribotesters are used to measure basic friction and wear. These tribometers are classified according to their relationship between sliding surfaces, being symmetrical or asymmetrical (Figure 2.5). These standard tribology tests using tribometers are more popular with tribologist for measuring friction and wear and hence accordingly a large number of national and international standards have been developed to rationalise friction and wear testing with tribometers.

- *Service Simulation* of the real component and system. High repeatability of friction and wear results provided by the standard tribology test can always be questioned regarding its applicability to the results of a real component or system. Similarly, friction and wear measurement on a real life component or system is not viable. Therefore service simulation involves the design and manufacture of a specialist test apparatus, which on a graduated scale are laboratory simulations of service conditions between the simple tribometers and the real system.
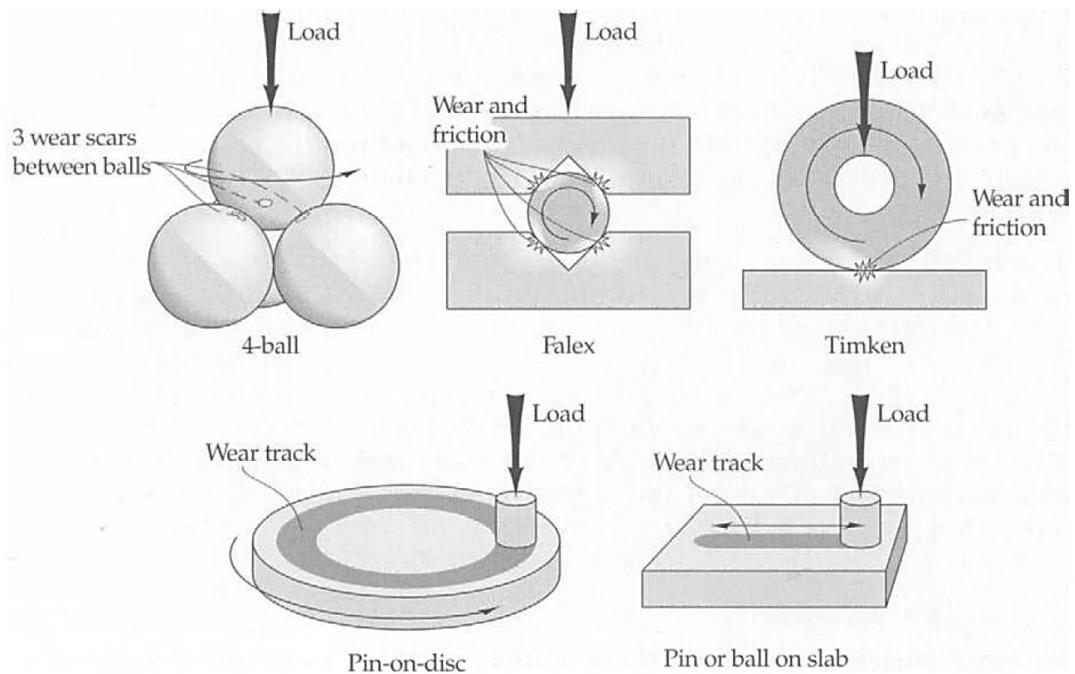
Figure 2.5 Schematic illustration of the basic sample configuration used in dry or partially lubricated sliding contacts of a tribometer [58].

2.2.2 Surface analysis

Hence, when two materials are loaded together, the surface of the material is the interface between the bulk and the external phase in direct contact with the material. Surface roughness is the most important aspect of the surface texture, as it is an important factor in predicting the overall performance or likely the life history of the contact. A wide variety of methods exist to investigate the texture of the surfaces and producing qualitative or quantitative information on the nature of the surface topography [59].

In fundamental terms, the outermost layer of atoms of the material composes the surface. The physical and chemical behaviour of these atoms is strongly influenced by the atomic layers in the vicinity, to a depth of the order of several nanometres into the bulk. Physical characteristics involves the recognition of surface structure, morphology, topography, mechanical properties and stress. Equally, the chemical characteristics involves its elemental, chemical and molecular composition.

Therefore, controlling and characterizing the behaviour of the surfaces is central to physical and chemical tribology and necessarily involves the determination of the chemical, electronic, and structural characteristics of the surface and wear debris [60]. A wide variety of analytical techniques and methodologies are available to supply the necessary information required and hence the selection of the appropriate analytical methods have been done suitably.

Gellman and Spencer [61] reviewed the areas in which surface chemistry has played an important role in enhancing tribological understanding. One of these areas includes the vital importance of boundary lubrication, and the challenges associated with it, along with the impact of surface science. They summarises the development of the understanding of boundary layers through the historical mechanism and techniques applied by researchers to understand this phenomenon.

With the evolution of technologies, the tribological understanding has been pushed to new frontiers and similarly demand solutions to tribology problems in new environments. It is understood that the types of chemistry that are implicated in tribological phenomena are broad and varied, and hence demands a challenge of extensive understanding of the chemical and mechanical aspects of tribology.

Further investigations and the development of the boundary lubrication theory should apparently be directed at developing more efficient techniques (Figure 2.6). Studies for adsorption and chemically modified boundary layers, kinetics of the physico-chemical processes, the structure, composition and mechanical behaviour of these layers under various loading, temperature and

environmental effects using sophisticated equipment to perform spectral analysis, electromagnetic resonance, electron microscopy at the level of atomic interactions between boundary layers and the solid body surface under the effect of surface forces are required [27].
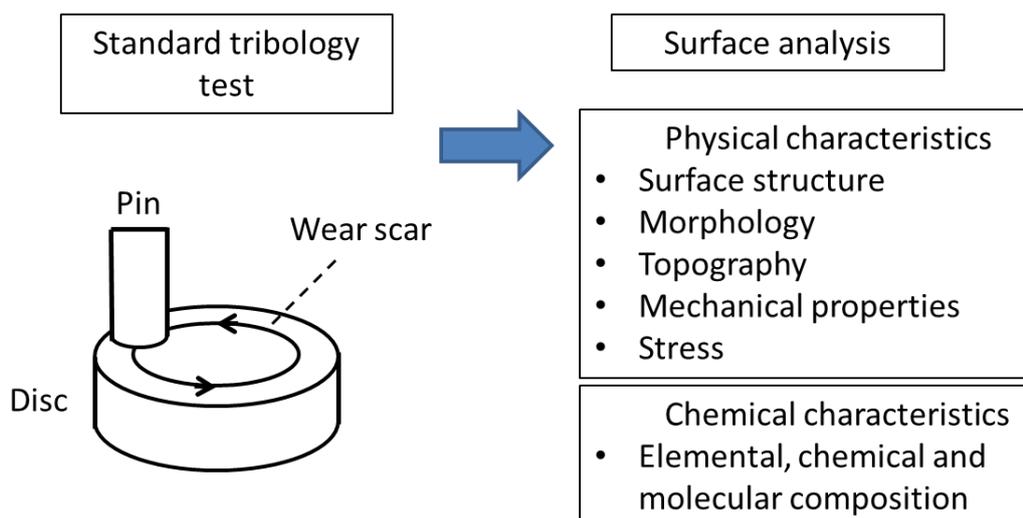
Figure 2.6 Standard experimental procedure of tribology test, along with the combination of appropriate surface analysis technique to characterise the surface.

2.3 Surface analysis methodologies

Three modes of surface and interface analysis methodology are possible for the investigation of a tribological contact, within which the friction experiment and the surface analysis of the contacting surfaces can be arranged [62]. The three modes of *ex-situ*, *in-situ* and *in-vivo* (Figure 2.7) analysis allow the identification of friction-induced surface modifications, such as the development of transfer films, tribochemical phase formation, or the removal of material and lubricant films by wear. Hence, correlations may be revealed that might help to elucidate the friction and wear mechanisms.

Historically tribology experiments have been conducted *ex-situ*, with the combination of utilising laboratory friction and wear experiments and following it up with the surface analysis of the materials in contact. *Ex-situ* analysis provides the possibility of using the great potential of various complementary modern surface analysis techniques, providing sensitive measurements from

ever more restricted areas. However, regarding *ex-situ* approach, important information of the tribological processes or performance can be lost, as properties of the surface and the tribofilms analysed after the experiments may not be similar to that when they are in their active states [8]. Similarly, the properties of the surfaces and the tribofilms formed may change after the removal of rubbing contacts from the tribometer [9]. Although this method can produce useful information, identifying the development of any interaction processes during the experiment is difficult.

In situ analysis involves surface analysis performed inside the tribometer, inside the wear scars but outside the contact. This mode allows exploration of friction and adhesion of clean solid surfaces, the effect of adsorbed species, or the nature of the lubricant phase, in order to illuminate the tribo-induced surface modifications in as direct a manner as possible. This mode can be performed in either of the two configurations of *post mortem* and *pre mortem* analysis (Figure 2.7). The configuration of pre mortem obviously comes with difficulties as the analysed area changes continuously, with a period related to the rotation speed, and most of the analytical techniques require acquisition times longer than the normal rotation periods.

Lastly *In vivo* mode performs surface analysis inside the tribometer, inside the wear scars, and inside the contact. They consist of performing spatially resolved surface analysis directly inside the contact. This mode imposes drastic conditions on both the tribometer configuration and the performance of the analytical technique. Therefore the use of electron or x-ray transparent materials is necessary in order that the probe may reach the interface with only minimal interaction with the bulk contacting bodies and a dedicated tribometer must be compatible with the analytical configuration.

As similar to the *in-situ* analysis, two time-scale criterion of *post mortem* and *pre mortem* are possible (Figure 2.7). *In vivo post mortem analysis* performed after the friction stage provides analytical data relating to the contact with minimal perturbation. *In vivo pre mortem analysis* can be performed during the friction stage. The analysis corresponds to the ultimate goal in recording real-time and spatially resolved information from the friction interface, which can then be correlated with simultaneous friction forces, surface forces, or

wear rate measurement. However a balance has to be struck between the dynamic of the friction movement on the one hand, and the spatial resolution/acquisition time of the analysis on the other.

Ex situ Outside the tribometer	Post mortem After friction	
In situ Inside the tribometer Outside the contact	Pre mortem During friction	
	Post mortem After friction	
In vivo Inside the tribometer Inside the contact	Pre mortem During friction	
	Post mortem After friction	
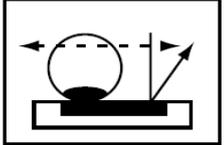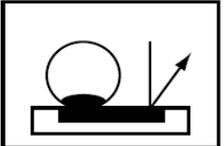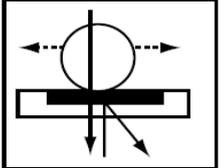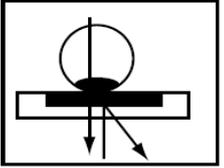
Figure 2.7 Time scale criteria combining friction experiments and surface analysis in different modes [62].

2.3.1 Commonly used surface techniques to study lubricated surfaces

Tribological contact results in microstructural changes of the surfaces, and the performance of lubricated contacts depends on the formation of lubricant films on the contact. Commonly used methods are therefore categorised according to the scale of information required. Figure 2.8 shows the various aspects of surface characterization for tribological surfaces and in order to characterize friction, wear and lubricant mechanisms, a combination of different methods are usually required.
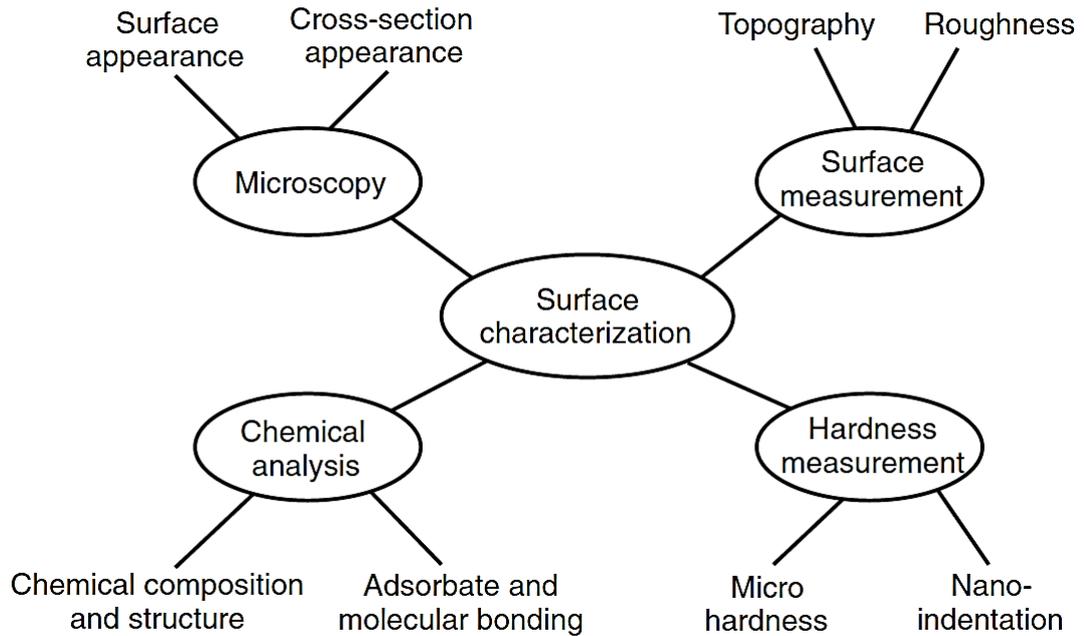
Figure 2.8 Various surface characterization of tribological surfaces [62].

2.3.1.1 Surface and hardness measurement

The surface topography can be divided into form, waviness and roughness. Surface roughness affects the lubricant film parameter directly but also the friction and wear of the lubricated contact. The surface measurement data that quantitatively describe a surface can be expressed by different statistical parameters. Statistical parameters are defined using surface measurement data, such as the R_a (average roughness) and R_q (root mean square roughness) parameters. It is an important parameter directly affecting the tribological contact and can be utilized to describe used and fresh samples [63].

However, R_a and R_q parameters can prove too general to describe a roughness profile with different measurement techniques, as commonly measured roughness parameters depend strongly on the resolution of the measuring instrument and are not unique for a surface [63]. Therefore, one should be careful when using these parameters and when comparing surfaces on the basis of parameter values.

Most surfaces, including contaminated surfaces, can be measured with a contacting stylus profiler. The surface profile is measured by moving a diamond stylus or a glass sphere along the surface. Since the stylus is

touching the surface there may be a risk of deforming the surface. Microscopy techniques such as optical interference microscopes and AFM microscopy techniques also provide surface measurement data, and can provide both contact and non-contact analysis of surface roughness.

Hardness of the component describes the material's resistance to plastic deformation and affects the lubrication conditions in a tribological contact. The hardness of the surfaces and possible tribofilms are often different from those of the bulk material and are therefore of great importance for understanding the tribological contact.

In order to get the hardness value of a bulk material a macro hardness test is used, for example the Rockwell or Brinell tests. Similarly to get information from the surface region rather than from the bulk material, micro hardness techniques such as Vickers test are applied. Nanoindentation is a method which uses very small loads and indentation tips. The indentation load is recorded against the indentation depth during loading and unloading and gives information about hardness, but also about the elastic modulus of the surface [64].

2.3.1.2 Optical and microscopy techniques

Microscopy techniques are usually utilised to reveal surface and cross-section appearances of the sample. Surface appearance can indicate the occurrence of oxides, tribofilms, deformation or wear on the sample. Similarly, cross section of the surfaces can reveal information on thickness and structure of tribofilms, coatings or deformed surface layers and bulk materials.

Popular techniques such as optical light microscope, optical interference microscopy are usually utilised to obtain surface information at higher resolution. Similarly, techniques such as scanning electron microscopy (SEM), Atomic force microscopy (AFM), focused ion beam (FIB) and transmission electron microscopy (TEM) provides very detailed information from small surface areas.

Optical light microscope is the most common microscopy technique because of its ease of use. They can be used in room atmosphere and images all

surfaces that reflect light. Conventional optical microscopes have a short depth of field and all parts of an uneven or rough surface will not be in focus, but new techniques for optical 3D (three-dimensional) measurement and microscopy are evolving [65].

Optical interference microscopes combines optical microscope with an interferometer into one instrument that produces 3D images and measurements of the surface. An interferometer is an optical device that splits a beam of light into two separate beams and then combines them. One beam is reflected from the sample surface and the other beam is reflected from a reference mirror. When the beams are recombined they create an interferogram that reflects their difference in travel length, that is the height of the surface (Figure 2.9).

However, there are some requirements on the surface. The surface must reflect light, because the beam reflected by the sample surface must be reflected back through the objective lens. Therefore, the surface cannot be completely black. It can also be difficult to measure very rough or porous surfaces, since tilted surfaces will reflect the light away from the lens [66].
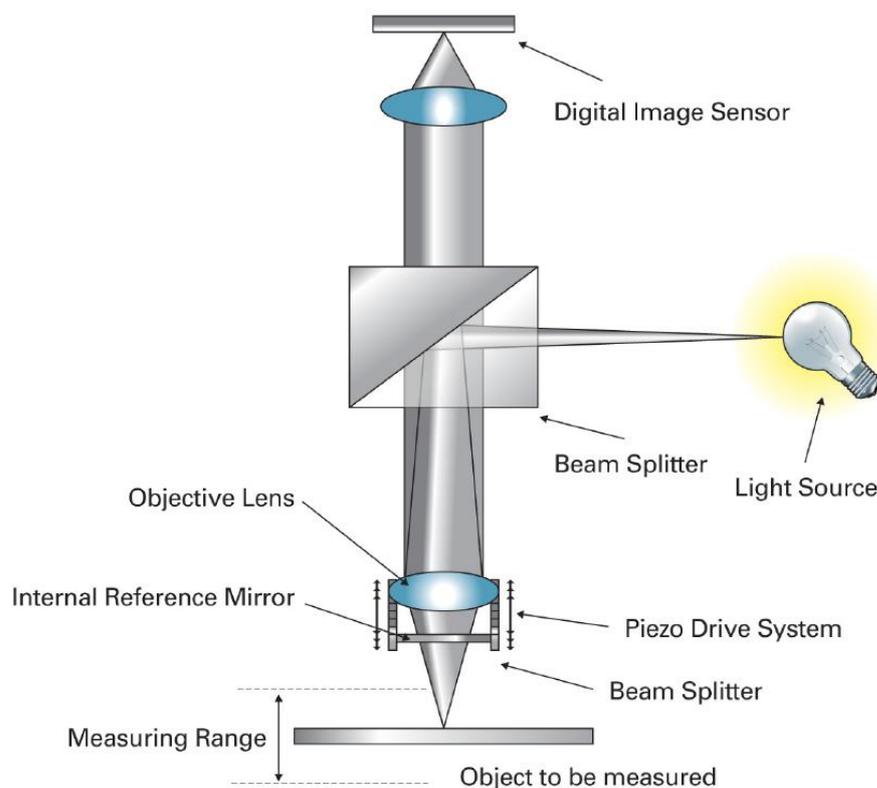
Figure 2.9 A typical optical interference microscope design [67].

Atomic Force Microscopy (AFM) belongs to a family of Scanning Probe Microscopy (SPM) techniques and commonly used to study friction and wear in a small area. SPM techniques are based on scanning a small tip over the surface, monitoring some kind of interaction between the tip and the surface [68]. With AFM the surface is imaged and the topography is measured with very high resolution. The surface is mechanically examined using a very sensitive tip mounted on the end of a flexible cantilever. This tip is scanned across the surface while recording very small attractive or repulsive force between the outmost atoms of the tip and the surface atoms. The force magnitude depends on the tip–sample distance. A piezoelectric scanner provides the scanning motion. A laser beam monitors the movement of the cantilever caused by the tip–sample interaction (Figure 2.10).

Along with images of surface topography, AFM can also provide information on film thickness, frictional properties and elastic compliances of thin films. Scanning probe technique capability of extremely high resolution imaging (atomic level in certain favourable cases) without sample treatment of coating, can be run under vacuum, air or liquid environment, with possibility of quantitative measurements of sample form, distribution, roughness over a large range of magnifications, friction, adhesion, wear etc [69].
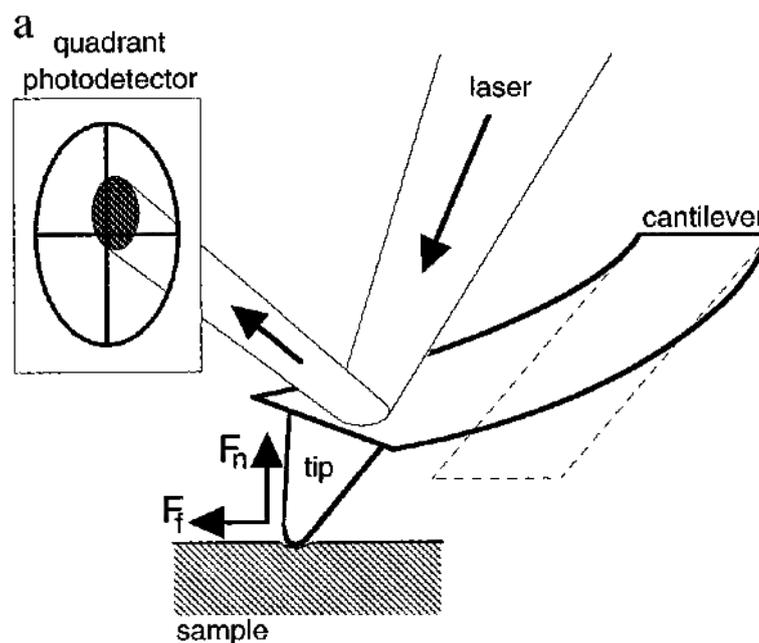
Figure 2.10 Working principle of AFM (Atomic Force Microscopy) [69].

However, compared to the single scan image size and the slow scan time of AFM, electron microscope such as SEM provide high spatial resolution and large depth of field at a relatively high speed. It is the prime technique for imaging and examining wear and damage mechanisms along with the study of contaminations and tribofilm formation. A finely focused electron beam is scanned over the surface to be imaged and the incident electrons interact with the sample atoms within a few microns of the surface. This interaction generates various signals emitting from the surface, for example electrons and X-ray photons (Figure 2.11) [70].

The SEM image is formed from the intensity of electron emissions from the surface. Another advantage of this technique is the possibility to combine imaging with elemental analysis using EDS (Energy dispersive X-ray spectroscopy). By combining the SEM with EDS elemental information can also be obtained. SEM for tribology studies is diverse and very effective for examining wear and damage mechanisms. However, SEM analysis are made in vacuum environment and requires dry surfaces; thus the surfaces must be clean from, for example, lubricants.
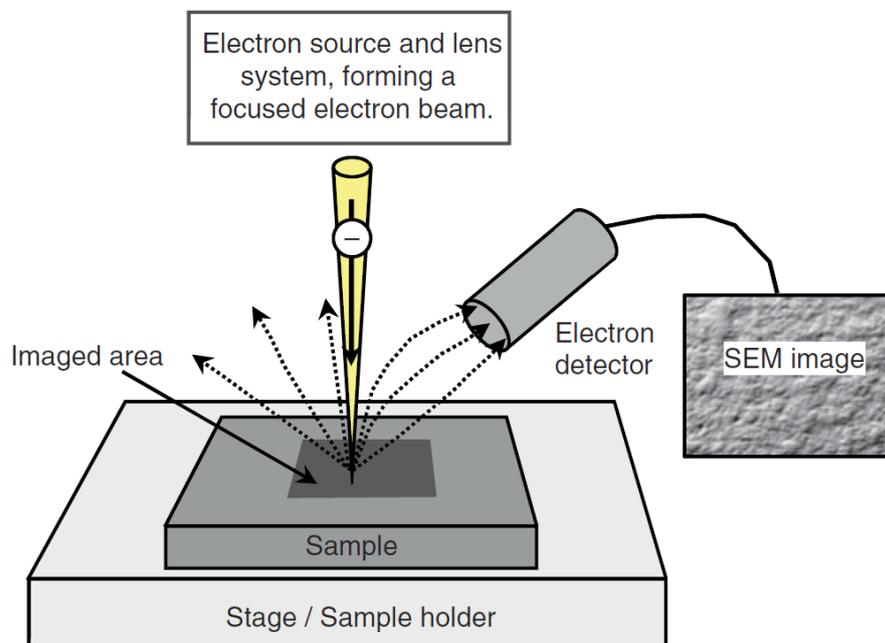
Figure 2.11 Principle of SEM. The focused electron beam is scanned over the surface (scanned area = imaged area). The electron detector counts the emitted electrons. The intensity of emitted electrons sets the contrast of the SEM image [71].

Focused ion beam (FIB) is another technique used to analyse and manipulate small surface area using a well-controlled beam of Gallium (Ga) ions. It is usually integrated with SEM, making it possible to select a surface area of interest and to position the ion beam more accurately. It is usually used for preparing cross-section surfaces for further SEM studies and for preparing cross-section samples for TEM.

A thin coating of platinum is deposited on the surface in order to protect the interest surface area from the ion bombardment during etching. The focused ion beam is then used for etching a crater into the surface. For TEM analysis a sample is cut as a thin slice of the surface (Figure 2.12).

Transmission Electron Microscopy (TEM) provides high-resolution imaging and analysis. Both imaging at atomic resolution and chemical analysis of a very small sample volume are possible. In a conventional TEM a thin specimen (<100 nm in thickness) is irradiated with an electron beam. The electrons interact with the specimen when passing through the sample. When the electrons exit the specimen, they may be unaffected, they may have lost some energy or they may have altered direction.

The TEM image contrast is caused by variations in absorption and diffraction of electrons, for example due to differences in thickness, composition and crystal orientation. A lens system provides the formation of an image of the specimen captured on a screen. The TEM instrument is also often equipped with an EDS detector for elemental analysis. TEM provides detailed information about, for example, crystal structure, grain size and elemental composition, which may be crucial for the fundamental understanding of, for example, lubricant film formation and friction mechanisms [72].
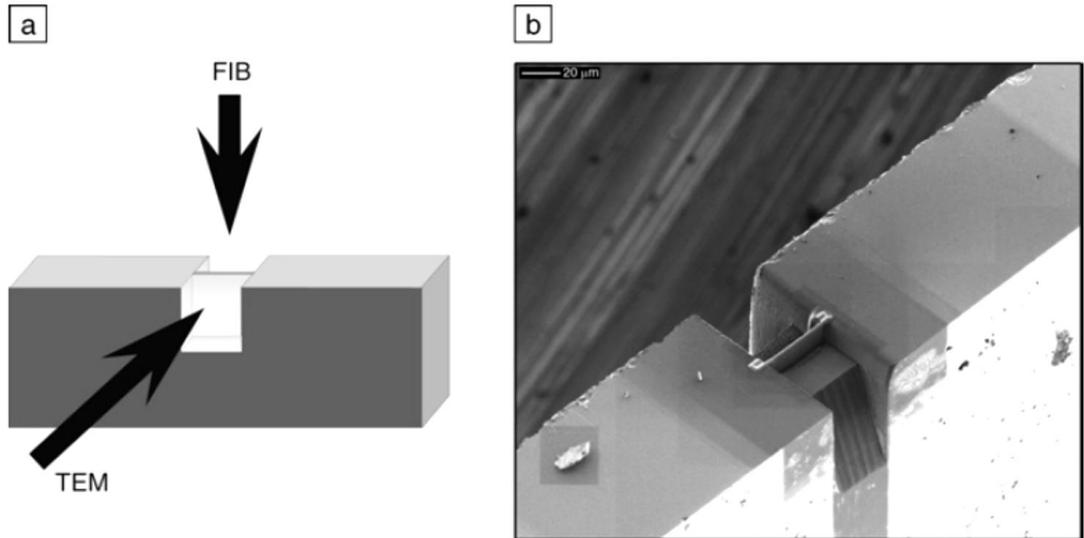
Figure 2.12 (a) Schematic illustration of focused ion beam (FIB) technique. (b) Scanning electron microscopy (SEM) image showing the FIB specimen in progress [72].
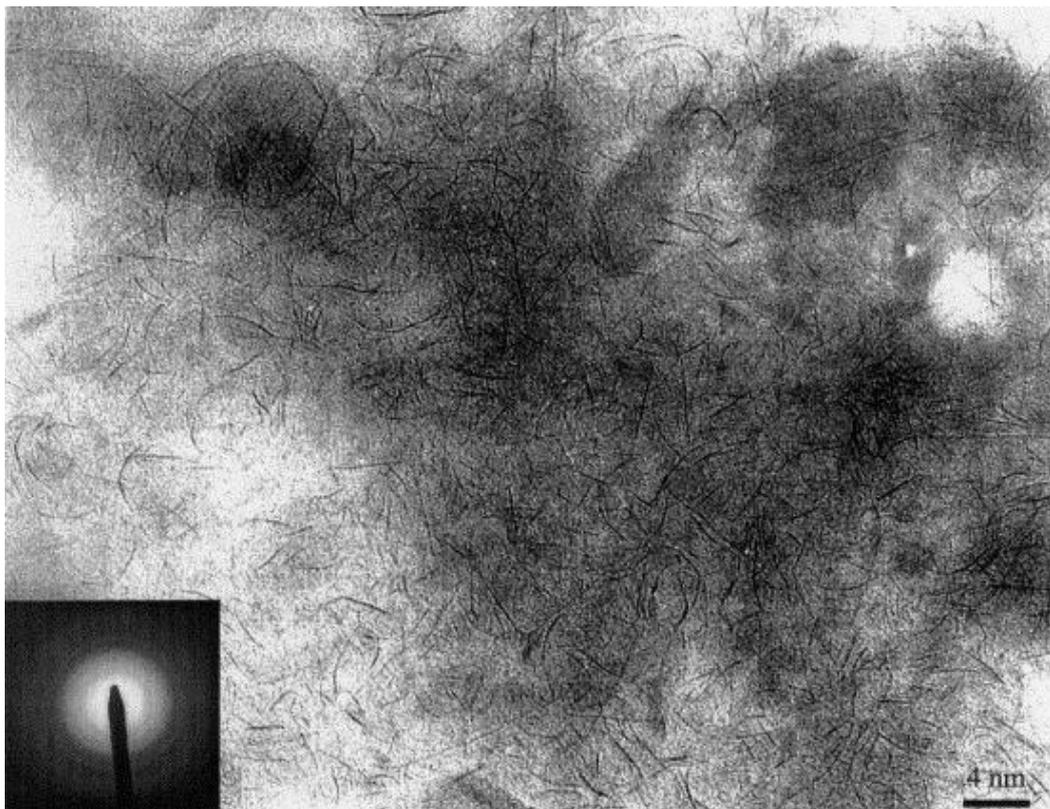
Figure 2.13 TEM images of wear debris showing the presence of MoS_2 'eyelashes' tribofilm [47].

2.3.1.3 Spectroscopy techniques

Spectroscopy is a technique that uses the interaction of energy with a sample to perform an analysis on the composition and chemistry of the surface material. Depending on what information is required an appropriate method is selected. All spectroscopic methods usually stimulates the surface by some form of irradiation. The interaction processes with the surface material result in a response from the surface and a spectrum is created from the detected signal.

Every surface analysis method has its benefits and limitations. The method to use for a specific analysis problem depends on one or more performance parameters. Different spectroscopy methods provide different levels of information. Some methods give only elemental information, that is information of what kind of atoms or elements are present. Other methods also give chemical information, that is information about how the atoms are bonded to each other. Some methods give molecular information, for example on how specific molecules are adsorbed to a surface.

In X-ray spectroscopy characteristic X-rays are used to identify the elements of a sample. In combination with SEM and TEM, EDS technique is used to detect X-ray photons. EDS provides elemental information, where characteristic X-rays are generated from the interaction process between the electron beam and the sample atoms. The sample is irradiated with electrons with energy high enough to ionize the atom. The interaction process includes an electron from the beam, which knocks out an inner shell electron and creates an inner shell vacancy. An electron from a higher shell fills the vacancy and an X-ray photon is emitted (Figure 2.14). The energies of the emitted X-ray photons are characteristic since the electron binding energies of different elements are characteristic. Hence, chemical elements of the sample is identified from the energy of the emitted characteristic X-rays.

Combination of EDS with SEM gives the possibility to combine good imaging with elemental analysis. Similarly, EDS analysis in TEM the analysis volume can be kept very small since the TEM sample is very thin. Therefore, the lateral resolution is better for EDS in TEM compared to SEM [71].
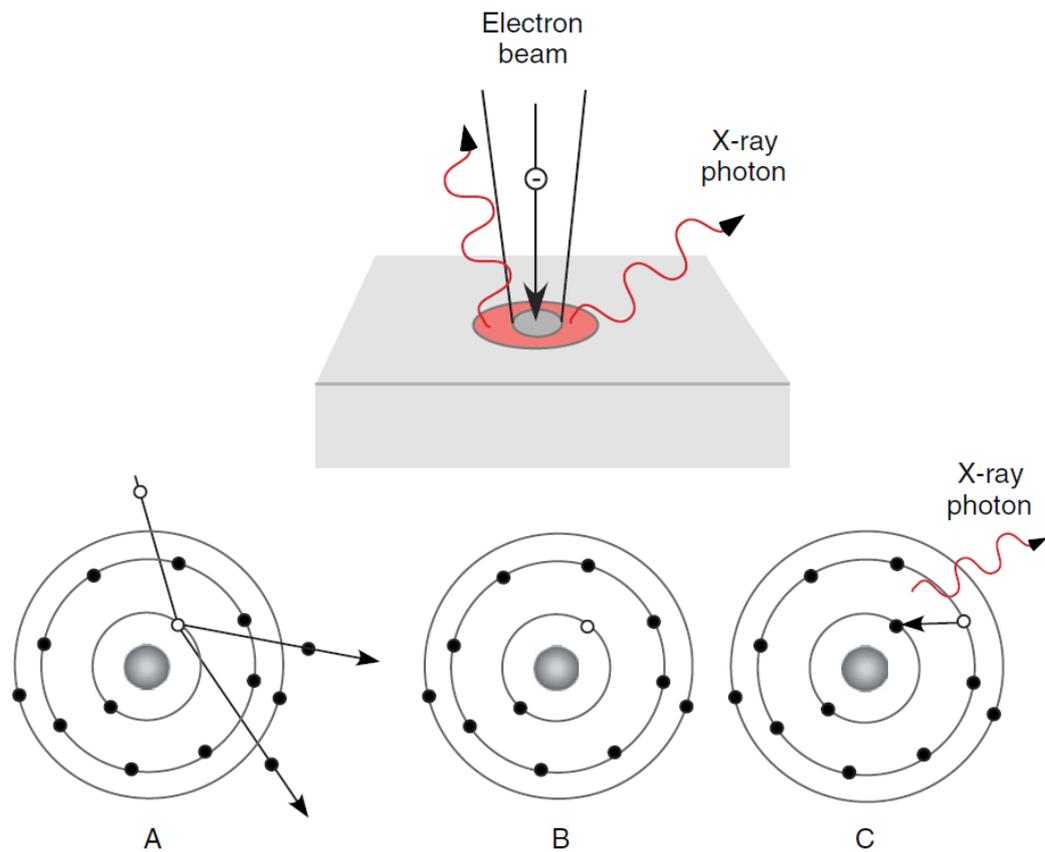
Figure 2.14 Principle of EDS technique. The surface is irradiated with an electron beam. Interaction process includes an electron from the beam which knocks out an inner shell electron (A), an inner shell vacancy is created (B), an electron from a higher shell is filling the vacancy and an X-ray photon is emitted (C) [71]

Similarly, Auger electron spectroscopy (AES) generates Auger electrons from the interaction process between the electron beam and the sample atoms. It is a useful method for analysis of very small surface features for high resolution elemental mapping and for depth profiling using ion sputtering. The surface is irradiated with a focused electron beam (as in EDS in SEM). Auger electrons are emitted from the surface when the incoming electrons interact with the sample atoms. An incoming electron knocks out an inner shell electron, thus creating an inner shell vacancy. The following relaxation of the atom includes the process where an electron from an outer shell moves to the inner shell vacancy. The excess energy is released as an Auger electron (or as an X-ray photon, as detected in EDS) (Figure 2.15). The emitted Auger electrons are detected and their energies are measured. The energy of the

Auger electron depends on the binding energies of the electrons involved in the Auger process [71].

Most AES instruments are equipped with an electron detector for SEM imaging. Thus, the surfaces can be imaged using the SEM function and the electron beam can be positioned very precisely for the AES analysis. However, samples must be electrically conductive to be analysed since the electron beam will cause an electric charge-up of electrically insulating surfaces. The samples must also be clean and dry since the analysis is performed in ultra-high vacuum (UHV). All elements, except for hydrogen (H) and helium (He) can be detected [73].
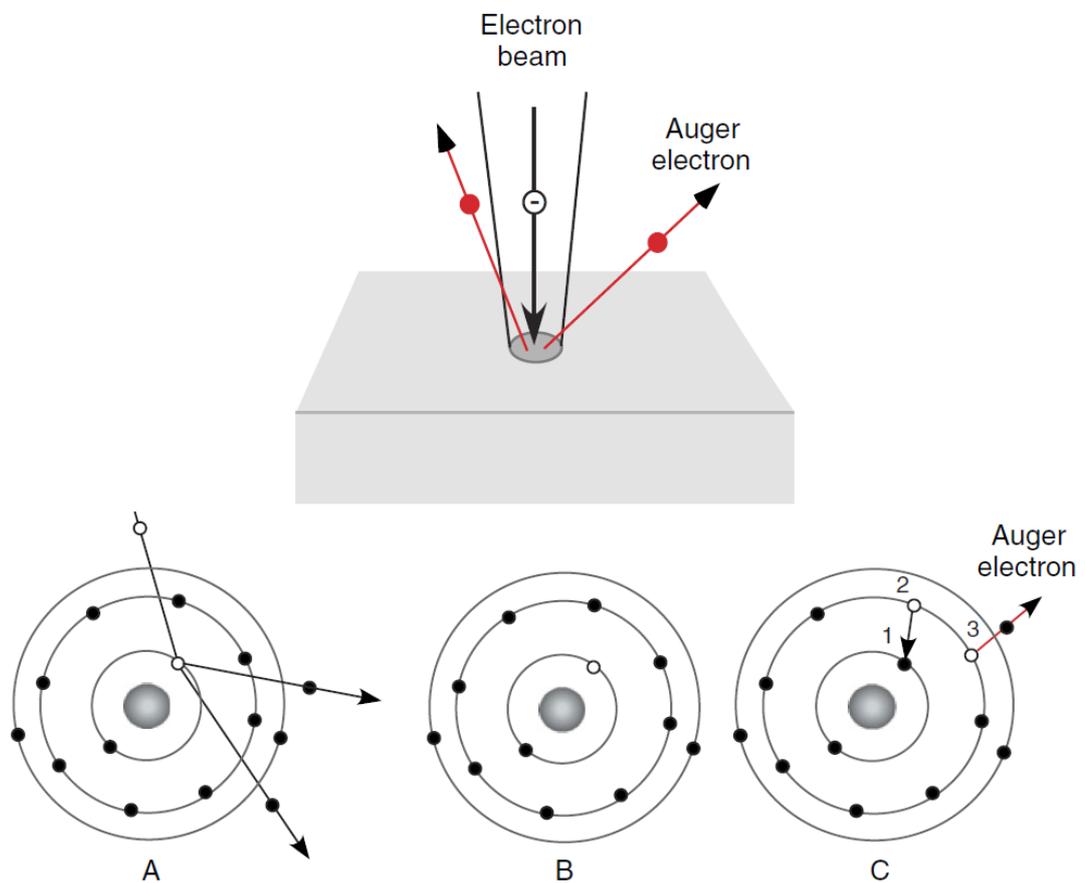
Figure 2.15 Principle of AES technique. The surface is irradiated with an electron beam. The Auger process includes an electron from the beam which knocks out an inner shell electron (A), an inner shell vacancy is created (B), an electron from a higher shell is filling the vacancy and an Auger electron is emitted (C) [71].

X-ray Photoelectron Spectroscopy (XPS) is one of the most widely used surface analysis methods. It is used for analysis of thin surface layers, giving information about both elements and chemical bonding. In XPS the surface is irradiated with X-ray photons which interacts with an atom and an inner shell electron (by the photoelectric effect). This means that an electron, referred to as the photoelectron, is emitted from the atom. The X-ray photon energy is well defined. Thus, the kinetic energy of the photoelectron gives a direct measurement of its original binding energy to the atom. An important benefit of XPS is the small information depth. The X-ray photons penetrate deep into the sample surface. However, only photoelectrons generated from near the surface can travel to the surface and escape from it without losing any energy (Figure 2.16). For tribology studies XPS is very useful for identifying the chemical composition and structure of thin surface films, for example thin tribofilms, lubricant films or other reaction layers. However, samples must be clean and dry since the analysis is performed in ultra-high vacuum (UHV) environment. All types of materials that can withstand the UHV can be analysed [74].
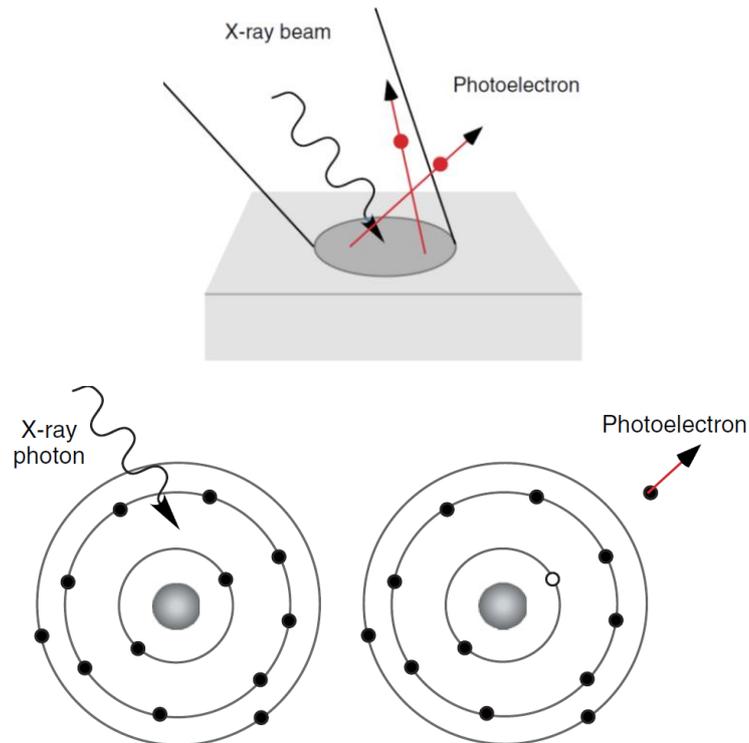
Figure 2.16 In XPS the surface is irradiated with X-ray photons. The interaction process includes absorption of the X-ray photon and emission of a photoelectron [71].

Secondary ion mass spectroscopy (SIMS) provides a very detailed chemical analysis of the surface. It is possible to detect low concentrations of all elements including hydrogen. It is very surface-sensitive, allowing for detection of the top one or two atomic layers. A relatively narrow spot can be used, allowing for analysis and chemical mapping of small surface features. The analysis is performed in UHV. Therefore, it is important to handle the surfaces carefully prior to analysis since the top layers are investigated. All types of materials that can withstand the UHV can be analysed [75].

The surface is bombarded with a beam of ions (i.e. primary ions). The energy is transferred to the atoms of the sample surface. This results in sputtering of atoms, atom clusters, molecules or molecular fragments. Some of the sputtered particles are ionized, that is negatively or positively charged (Figure 2.17). These are the secondary ions, which are separated and analysed by a mass spectrometer. Thus, in SIMS the masses of the secondary ions are examined. There are different modes and types of SIMS operation and mass detection systems.
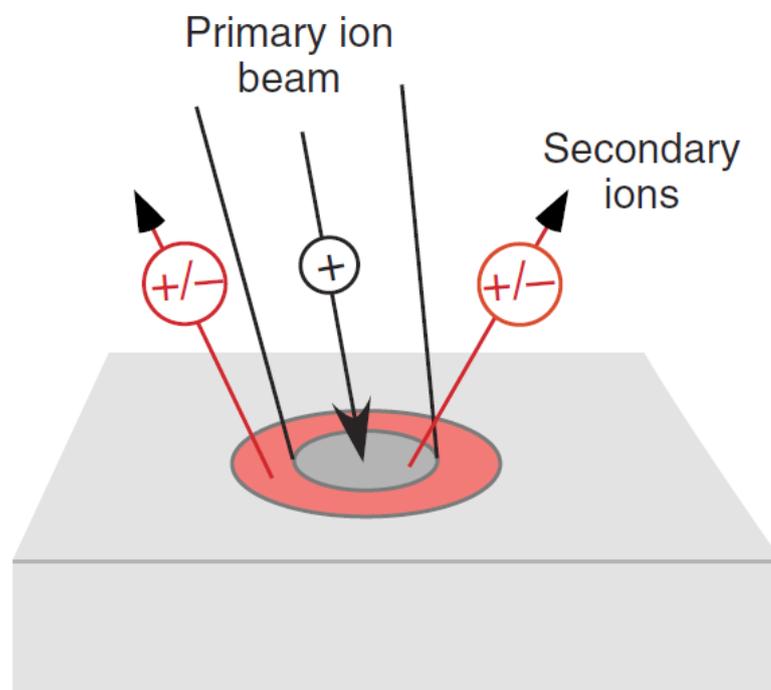
Figure 2.17 In SIMS the surface is irradiated with an ion beam (primary ions), for example gallium ions (Ga). As a result secondary ions (ionized atoms or fragments) are emitted from the surface [71].

Spectroscopy analysis usually requires some form of cleaning and conduction of analysis under high vacuum conditions. However vibrational spectroscopy such as Fourier transform infrared spectroscopy (FTIR) and Raman does not require any form of cleaning and analysis to be conducted under ambient conditions.

Vibrational spectroscopy is particularly useful in detecting lubricant films on surfaces. It can provide binding and chemical information for adsorbed large molecules. The specimen is illuminated with infrared light or laser wavelength of well-defined energy. Depending on the structure of a molecule, it will vibrate at different frequencies. If the energy of the incident light corresponds to a transition between vibrational energy levels in the specimen, the light can be absorbed or scattered. Hence, characteristic response of the molecule bonds are measured and information regarding the sample characteristics are obtained [76].

Hence, usability of the various surface analysis techniques depends on what type of information is required. For example, SIMS and XPS are good choices to reveal the chemical composition of tribofilms combined with depth profiling. However AES may be a good choice if the films have varying thickness and/or are unevenly distributed over the surface. Therefore, with AES a depth profile over a small surface area can be obtained, but the chemical information will not be as detailed as with XPS or SIMS.

Similarly, samples which are affected with sample cleaning process and affected with vacuum conditions, vibrational spectroscopy is a choice to negate this effects.

2.3.2 *In-situ* analytical techniques

With the need to study the kinetics of tribofilm formation and the way in which they are influenced by different parameters, development of several *in-situ* technologies have been encouraged. Various *in-situ* approaches including contact resistance, conductance, thermoelectric, interferometric, thermal measurement and a number of analytical techniques have been employed in tribological studies. A number of these analytical techniques have been listed out in Table 2.1, with examples of the measurement application, resolution and limitations.

The importance and methods of the *in-situ* approaches, underlining *in situ* approaches as applied to the study the interaction between surfaces during contact and sliding have been highlighted by a number of researchers and has been a focus of special issues [77-79]. The common goal for *in-situ* approaches is the fundamental measurement of the real area of contact, the interfacial film or tribofilm chemistry and the wear track morphology and wear rates where microscope objectives illustrate pathways for *in-situ* studies.

Wahl and Sawyer [80] reviewed various approaches for real time experimental methods of the tribological contacts and highlights an understanding of issues such as: What causes friction instabilities? How do chemistry and mechanics combine to provide low friction? How does varying the ambient environment change the interfacial film morphology and rheology? How do crystal structure and size influence lubricant performance?

The most common *in-situ* approach however, has been to perform detailed measurement on the surface of the sample within the environment but outside the contact (*post mortem analysis*). A more complex approach can be employed to perform the measurements within the contact; however some compromise of the sliding contact is typically required to achieve an *in-situ* measurement of this type [77].

Table 2.1: *In situ* approaches used for tribological interface studies [77].

Technique	Measurement	Spatial Resolution	Limitations	Ref.
Optical Microscopy	Tribofilm formation and motion, contact size	~ 1 µm	One counterface must be optically transparent	[81]
Interferometry (contact)	Contact separation	~ 1 µm	One counterface must be optically transparent	[28]
Interferometry (wear track)	Wear	~ 1 µm	Index of refraction or reflectivity changes can distort results	[82]
Raman microscopy	Composition/chemistry, film thickness	~ 1 µm	One counterface must be optically transparent	[83-85]
ATR-FTIR spectroscopy	Chemical bonding	mm to cm (width of crystal)	One counterface must be IR-transparent	[31, 86]
TEM + EELS + AFM / nanoindentation	Microstructural transformation, interfacial film formation composition, chemistry	0.1 nm	Interface region must be electron-transparent;vacuum environment	[87]
SEM/EDX	Surface morphology, composition	10 nm	Contact charging, contamination in low vacuum environments	[88, 89]
SEM + FIB	Cross section of sliding surface w/o separation	0.1 nm	Potential beam damage from FIB sectioning	[90]
SFA + x-ray diffraction or neutron relativity	Structure	µm's	Requires synchrotron access	[91-93]
AFM	Friction, surface topography, contact stiffness, wear	~ 1 µm	Difficult to ascertain contact size, chemistry	[94, 95]
AES	Composition	10 nm	Cannot probe inside contact zone	[96, 97]
XPS	Composition, chemical state	10s of µm	Cannot probe inside contact zone	[96]
Contact resistance	Coating thickness, damage, interfacial film formation			[98, 99]

Note: ATR-FTIR, attenuated total reflection Fourier transform infrared spectroscopy; TEM, transmission electron microscopy; AFM, atomic force microscopy; EELS, electron energy loss spectroscopy; SEM, scanning electron microscopy; EDX, energy dispersive x-ray spectroscopy; FIB, focused ion beam; SFA, surface force apparatus; AES, Auger electron spectroscopy; XPS, x-ray photoelectron spectroscopy.

However, *in-situ* approaches in the test environment provide an improvement along with several benefits. Firstly, the correlation between friction data and interface events are simplified. Secondly, the need for the sample to be removed from the test environment is eliminated, thus reducing the risk of surface contamination. Most importantly from direct observation of contact events in real time, much of the highly speculative nature of deriving explanations for friction changes can be eliminated [80].

Cann and Spikes [100] classifies *in-situ* methods into two categories, surface microtransducer methods and techniques based upon electromagnetic radiation. Microtransducer methods uses miniaturized signal-conversion devices deposited to measure pressure, surface temperature and local film thickness. The latter approach however, is subjected to limitations and that one of the two rubbing surfaces must be made of a material transparent in the frequency range of radiation. Other *in-situ* approach employed a range of techniques such as scanning electron microscopy (SEM)/ transmission electron microscopy, reflection high-energy electron diffraction (RHEED), x-ray reflectivity, attenuated total reflection Fourier transform infrared, visual imaging, spacer layer imaging method (SLIM) and ellipsometry.

Similarly Rossi and group [31, 86, 101-103], executed a series of *in situ* analysis of the lubricant – substrate interface under tribological conditions. Quantitative tribological measurements were conducted by combining an attenuated total reflection Fourier-transform infrared (ATR/FT-IR) spectrometer with a reciprocating tribometer (Figure 2.18). ATR spectra were obtained from metal-coated monocrystalline Germanium ATR crystal and therefore the metal/lubricant interface was analysed as a function of time under both purely thermal and tribological conditions. However, the metal coating on the ATR crystal is very thin in terms of nanometres; hence under the applied load during rubbing, the coating is prone to be removed very easily during the course of experiment.

Further on, Rossi and her group [102] combined this approach of *in-situ* study along with other *ex-situ* characterization utilising specially X-ray photoelectron spectroscopy (XPS), in order to compare the correlation between the XPS spectra results with that of *in-situ* ATR FT-IR spectra. Recently, Rossi et al

[103] developed the new version of the *In situ* ATR/FT-IR tribometer which comprises a testing block and a control block, with the incorporation of a force-measuring system which allowed the measurement of the friction force during tribological experiments and its correlation with infrared spectroscopic results that provided insights into the chemical reactions taking place at the metal/oil interface.
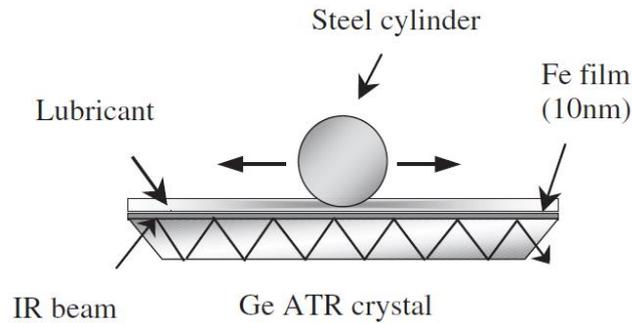
Figure 2.18 Diagram of the in situ ATR tribometer as executed by Rossi and group [31, 86, 101-103]

Spikes and group [28, 104-107] utilised the optically-based technique of ultra-thin film interferometry to study the film-forming properties of lubricant films (Figure 2.19). The ultra-thin film interferometry is able to measure nanometre-thickness lubricant films in very high pressure and shear rate conditions, very similar to those found in machine component contacts. Spikes and group were successful in utilising the ultra-thin interferometry in studying and testing the applicability of the Elastrohydrodynamic (EHL) theory down to very thin films.

Application of this very thin film EHL measurement allowed the exploration of possible changes in the rheology of lubricant layers next to solid surfaces and also confirmation of possible film formations. Lubricant film up to nanometre thickness was possible to be measured in very high pressure and shear rate conditions, very similar to those found in real machine component contacts.

However, although the method of ultra-thin film interferometry measures the film thickness of the lubricant and its possible changes in the surface rheology, the interferometry methods lacks in providing the chemical characterisation of the possible chemical changes of the lubricant. Similarly, Spikes and group, whilst utilising the ultra-thin film interferometry, needed one of the contacting

surfaces to be transparent in order to enable the optical interference to be observed. Therefore considering real life situation on a metal on metal contact, the influence of the third body particles on the thickness of the lubricant as well as on its influence on the surface rheology has been neglected.
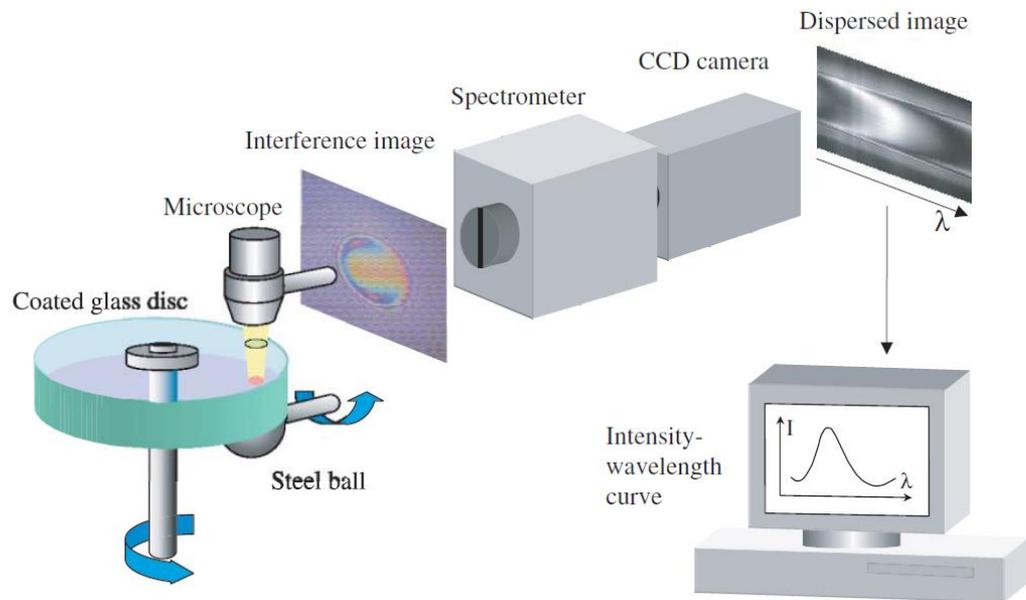
Figure 2.19 Schematic diagram of the ultra-thin interferometry as utilised by R.P.Glovnea et al [105] to measure the sub-nanometer lubricant films.

Fujita and Spikes [108] utilised an *in-situ* spacer layer interferometry to monitor and compare the formation of both tribo- and thermal zinc dialkyldithiophosphate (ZDDP) films on steel surfaces. They applied spacer layer interferometry to study ZDDP films '*in situ*', i.e. on the rubbing tracks formed within a tribometer but not within the rubbing contact itself and a schematic diagram of their test set-up can be observed in Figure 2.20.

A sliding-rolling contact was generated between the steel ball and the steel disc with the use of mini traction machine (MTM) and a specially built optical attachment was developed as shown in Figure 2.20, which consisted of a spacer layer-coated glass window which can be loaded against the wear track on the steel ball. The optical interference image was captured from the loaded glass window/steel ball contact with the use of a microscope, colour video camera and microcomputer and hence, analysed to determine the thickness of separating film within this contact. However, one limitation of this technique is that it required the knowledge of the refractive index of the film being

measured in order to convert the measured optical thickness to the true film thickness.

This technique utilised by Fujita and Spikes also relied in the assumption that when loaded against the antiwear film-coated steel ball, the glass surface wholly elastically conforms to it. Therefore they believed that the non-conformity of the steel ball did not affect the measurements of tribofilm thickness. However, they established that the rate of ZDDP tribofilm formation is proportional to the product of sliding distance and rubbing time and it does not occur if the elastohydrodynamic film thickness is significantly greater than the surface roughness.
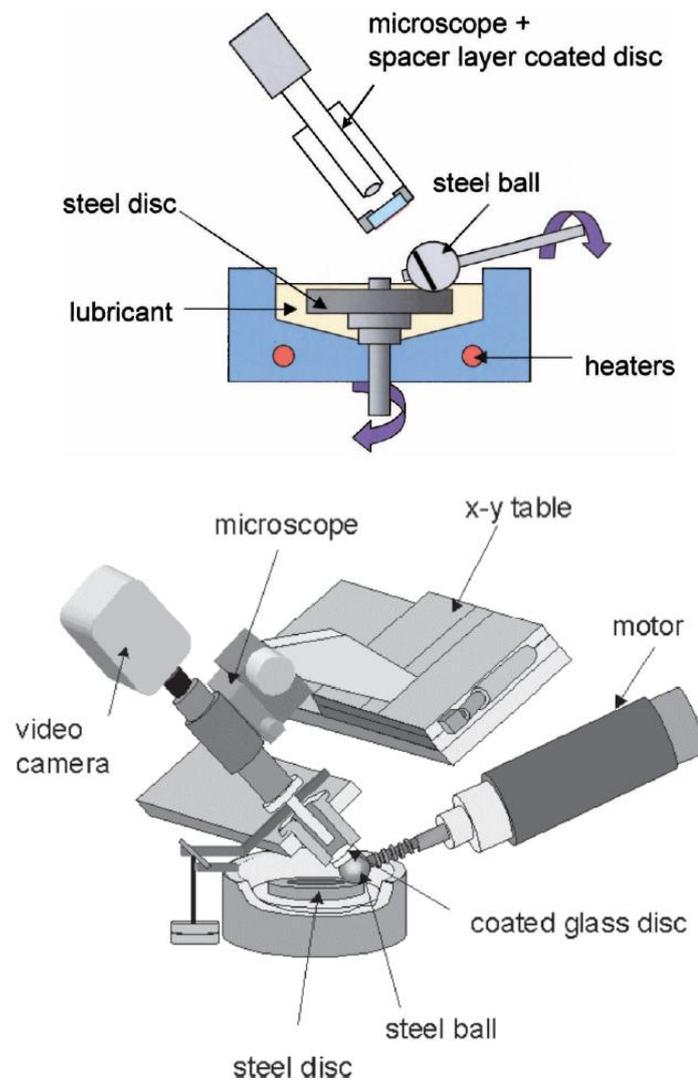
Figure 2.20 Schematic diagram of the in situ spacer layer interferometry set-up on the MTM, along with the coated glass window loaded on a stationary steel ball wear track [108].

Martin et al [30, 109, 110] has extensively utilised the ultrahigh vacuum techniques (UHV) for the characterization of the surfaces with the help of X-ray photoelectron spectroscopy (XPS). Since boundary lubrication is mainly governed by the formation of tribofilms in the presence of antiwear and friction modifying additives, they have tried to relate friction coefficient values to surface chemistry and transfer film formation.

A pin on flat friction tribometer machine with a very well controlled environment (Figure 2.21) had been developed and assumed that a steady-state lubricated test in the presence of additives can be experimentally modelled by a short friction test on the tribofilm which is actually formed, but in ultrahigh vacuum conditions.

Surface investigations performed *ex-situ,* requires the necessity of separating the two bodies in contact, and being exposed to environment where various reaction of the tribofilm might occur. Similarly the surface chemistry might also be modified after a typical cleaning procedure by organic solvents before the AES/XPS analysis, which is necessary to eliminate the contamination (carbon-rich layer) which generally strongly offsets the XPS photopeaks of interest.

Therefore Martin *et al* developed an alternative to *in-situ* analysis of the tribo-chemistry of the two counter faces with limited tribological perturbations, where friction experiments in ultrahigh vacuum on a tribofilm simulated a snapshot of the boundary lubricated contact, but isolated from its surrounding environment. However, the analysis provided an advantage of conducting experiments without the effect of contaminants which are always present in the lubricated test, while it provided a disadvantage of the quick wear of the tribofilm in vacuum conditions compared with the lubricated test.
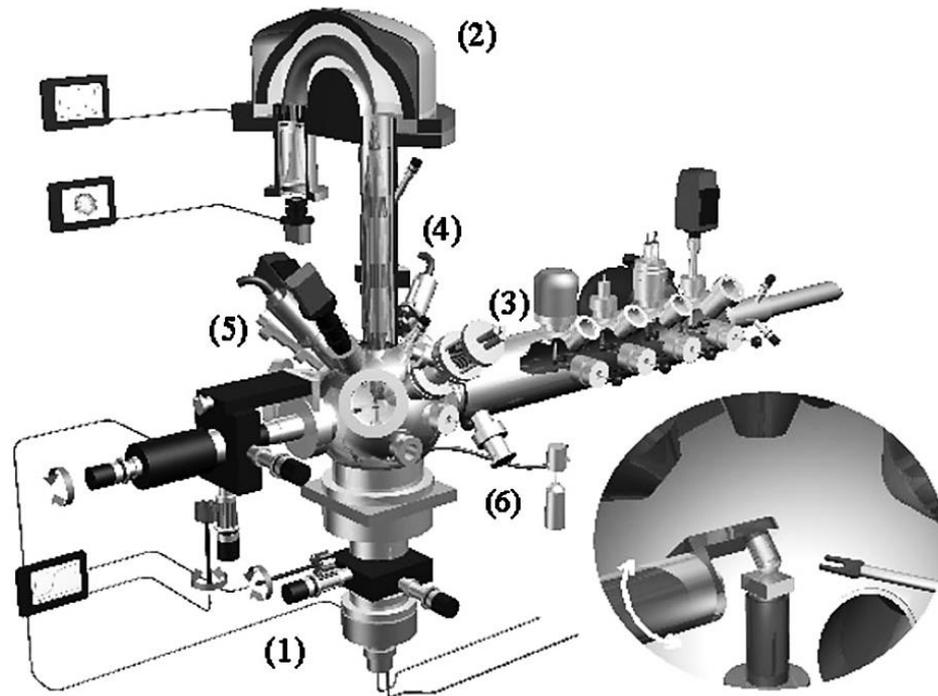
Figure 2.21 Schematic representation of the ultrahigh vacuum analytical tribometer. (1) pin-on-flat computer-controlled tribometer; (2) electron spectrometer; (3) electron gun for AES and SEM; (4) X-ray source for XPS; (5) ion gun for etching; (6) gas partial pressure inlet. In insert, the pin is clamped in the rubbing position. After the friction test the pin is turned up towards the analytical tools so that the scars could be observed [30].

Spikes [107] reviewed the various experimental techniques that have contributed towards the understanding of the EHD lubrication, therefore highlighting the contribution of *in situ* techniques for studying the behaviour of the lubricant films. Spikes definitely highlights the importance of the application of infrared and Raman spectroscopy, in order to yield information on film composition and molecular alignment and to even enable a study of lubricant degradation processes caused by the severe temperature and stress conditions present in thin-film contacts.

Lauer and Peterkin [111, 112], first applied IR spectroscopy to the study of lubricants in order to study base stock and additive response in sliding contacts and provided evidence of molecular alignment, glass transition, temperature gradients and additive shear effects. However the technique applied, posed many experimental problems and the resulting spectra are

often poor in quality and hence difficult to interpret the results. Since then IR-contact techniques has been successfully applied to several different lubricant system and further in contact methods have been reported.

Lubricant films in high pressure inlet region are subjected to severe mechanical and thermal stresses, where the film in this region is usually very thin < 1 µm and confined by the bounding metal or ceramic surfaces in contact. Under these severe conditions molecular rupture can occur resulting in chemical degradation and the formation of new chemical species. However, these severe conditions experienced by the lubricant as it passes through the contact are difficult to reproduce in a bulk reactor. But as explained by Cann and Spikes [29], an alternative approach is to use the Elastrohydrodynamic (EHL) contact as the experimental chamber and develop analytical techniques capable of examining lubricant properties from within the Hertzian zone.

However, complementary information on the local chemical composition, rheology or molecular conformation has proved more difficult to obtain. Therefore one of the solutions has been the persistent use of molecular vibrational, either IR or Raman techniques used in conventional analysis to provide information on the chemical composition of bulk organic materials [29]. Recent issue of the *MRS bulletin* [77], focuses on the development of experimental approaches allowing direct probing of materials mechanics and chemistry active in sliding contacts.

Cann [113] reviews the application of infrared and Raman microscopy to liquid-lubricated contacts, showing how the relationship between molecular conformation, pressure, additives and lubricant degradation can be correlated to friction performance. Thus, also stating the experimental challenges regarding the application of the method such as detecting very thin films and also obtaining depth profile information.

Similarly, Wahl and Sawyer [80] reviews optical microscopy and spectroscopy approaches to understand the solid lubrication phenomena. Examples of optical and interference microscopy, Raman microscopy and electron microscopy are provided to display the importance of *in-situ* applications to

link real-time changes in interfacial film chemistry, morphology, and rheology to friction and wear events.

However, considering the examination of the contact with the molecular spectroscopy, a number of technical constraints and challenges still exist. Firstly, spectroscopic techniques sensitive enough to detect lubricant films down to few angstroms are required to study the boundary regime. Secondly, the application of these developed techniques to obtain good quality noise free spectra, in order to obtain the information on the molecular response of the fluid within the contact zone, with clear detailed interpretation of band shape changes and peak shifts.

One of the practical problems associated with the application of Raman and IR spectroscopy to perform *in-situ* studies is the necessity to replace one of the contacting surfaces with a transparent window. Therefore the choice of window comes as a compromise between the requirements of an acceptable wavelength range, strength and refractive index. Use of a transparent window is obviously not a real life ideal simulation, as it replaces one of the surfaces but, it has little impact for studies of fluid film behaviour and more important implications for the study of chemically reacted or adsorbed films [29].

2.4 Summary of Surface Analytical Approach Towards Understanding Boundary Lubricated Conditions.

The friction and wear characteristics of boundary lubrication in the presence of lubricant additives is mainly governed with the formation of tribochemical film on the surface. These tribofilms are usually very thin and the approach of understanding the chemical information on the surface has been difficult to obtain. Surface analytical methods aids to enhance our understanding towards the characteristics of these tribofilm nature on the surface. However applications of various techniques has been limited towards the type of information that is desired.

To date, despite considerable efforts towards understanding the friction and wear nature of boundary lubricated contacts, a model capable of predicting friction coefficients and wear rate from first principles has not been established. Therefore, a requirement of developing sophisticated and reliable

experimental techniques for investigating and assessing tribological contact is highly needed. *In-situ* techniques shows a potential towards understanding the development of tribofilms between the contacts and link it with the friction and wear measurement under appropriate tribological system conditions. In the literature review presented in this section, many researchers have shown to apply *in-situ* techniques towards the investigation of tribofilm development under boundary conditions. However due to the limiting factors provided by the surface analytical method and the techniques applied, such approaches require a compromise of sample composition, geometry and the testing environment.

In this work, molybdenum dialkyldithiocarbamate (MoDTC) lubricant additive as a friction modifier has been used extensively in this study. Although substantial research have been conducted towards understanding the tribochemical phenomena of this additive, most of the work has been based on end of test analysis. The project in hand aims to develop an *in-situ* technique capable of investigating transient processes of these lubricant additives to fill in the knowledge gaps of the lubricant film formation.

Chapter 3
Application of Raman Spectroscopy for Tribochemistry Studies: Theory and Literature review

Practical applications of molecular vibrational of Infra-red or Raman spectroscopy as an *in-situ* analytical technique is strongly highlighted in Chapter 2. Advantage of molecular vibrational spectroscopy not requiring any sample preparation and analysis undertaken at ambient conditions, in comparison to conventional methods of X-Ray spectroscopy, electron microscopy etc. shows a great potential to analyse sample under real time conditions.

Raman spectroscopy is a surface analytical technique which is concerned with the phenomenon of a change of frequency when light is scattered by molecules. This change in frequency is relative to the primary light corresponding to the shift in the energy and provides information about vibrational, rotational and other low frequency transitions in molecules. This process is called the Raman effect and explained further in this chapter. Similarly compared to other Infrared Spectroscopy studies, Raman possesses several advantages in terms of gathering information. Raman spectroscopy has been extensively used in my research project and to understand the underlying theory behind the working of Raman spectroscopy, the study of the interactions of the conducting material or a dielectric substance with an external electric field is essential.

This chapter outlines the basic principles of light and matter, along with its effect on molecular vibration for the first part. Theory regarding Raman spectroscopy is highlighted in the second part of the chapter along with the significance of Raman spectrum and its instrumentation detailed. Lastly, a brief review of Raman spectroscopy as an *in-situ* approach has been reviewed.

3.1 Basic Theory

3.1.1 Interaction of light with matter

Interaction of light and molecules forms the basis of IR spectroscopy. When light interacts with matter, the photons which make up the light may be absorbed or scattered, or may not interact with the material and may pass straight through it. If the energy of an incident photon corresponds to the energy gap between the ground state of a molecule and an excited state, the photon may be absorbed and the molecule promoted to the higher energy excited state. It is this change which is measured in absorption spectroscopy by the detection of the loss of that energy of radiation from the light. However, it is also possible for the photon to interact with the molecule and scatter from it. In this case there is no need for the photon to have an energy which matches the difference between two energy levels of the molecule. The scattered photons can be observed by collecting light at an angle to the incident light beam, and provided there is no absorption from any electronic transitions which have similar energies to that of the incident light, the efficiency increases as the fourth power of the frequency of the incident light [114].

3.1.2 Electromagnetic radiation

All light (including infrared) is classified as electromagnetic radiation and consists of alternating electric and magnetic fields and is described classically by a continuous sinusoidal wave like motion of the electric and magnetic fields in Figure 3.1 [115]. A wave of polarized electromagnetic radiation traveling in the z-direction, consists of the electric component (x-direction) and magnetic component (y-direction), which are perpendicular to each other. The magnetic field component is neglected in this section and for a typical Raman spectroscopy, only the electric field is considered with the classical approach.
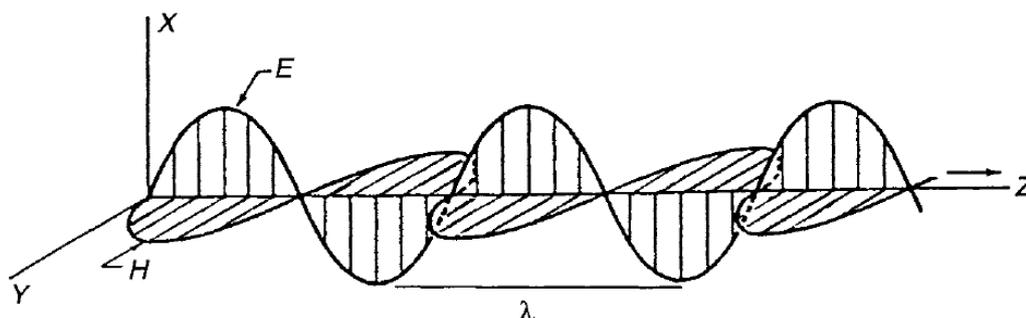
Figure 3.1 Plane-polarized electromagnetic radiation [116].

The electric field strength (E) at a given time (t) is expressed by

$$E = E_0 cos 2\pi v t \qquad (3\text{-}1)$$

where E_0 is the amplitude and v is the frequency of radiation (number of cycles per unit time)

The distance between two points of the same phase in successive waves is called the "wavelength," λ and related with the frequency by the following expression:

$$v = \frac{c}{\lambda} \qquad (3\text{-}2)$$

where c is the velocity of light (3 x 10^{10} cm/s). If λ is in the unit of centimetres, its dimension is (cm/s)/(cm) = 1/s. This "reciprocal second" unit is also called the "hertz" (Hz).

The third parameter, which is most common to vibrational spectroscopy, is the "wavenumber," $\tilde{v}$, defined by

$$\tilde{v} = \frac{v}{c} \qquad (3\text{-}3)$$

Hence combining equation (3-2) and (3-3)

$$\tilde{v} = \frac{v}{c} = \frac{1}{\lambda} \; (cm^{-1}) \qquad (3\text{-}4)$$

And similarly

$$v = \frac{c}{\lambda} = c\tilde{v} \qquad (3\text{-}5)$$

The difference between the frequency and wavenumber is apparent with equation (3-4), however this two terms are often used interchangeably as frequency shift and used conventionally in IR and Raman methods.

However, if a molecule interacts with an electromagnetic field, a transfer of energy from the field to the molecule can occur when Bohr's frequency condition is satisfied [116]. Hence,

$$\Delta E = h v = h\frac{c}{\lambda} = hc\tilde{v} \qquad (3\text{-}6)$$

Where ΔE is the difference in energy between two quantized states, h is Planck's constant (6.62 x 10^{-27} erg s) and c is the velocity of light. Thus, v is directly proportional to the energy of transition.

Therefore photons of specific energy may be absorbed or emitted by a molecule resulting in a transfer of energy, where the difference in energy ΔE can be categorised as

$$\Delta E = E_2 - E_1 \qquad (3\text{-}7)$$

Where E_2 and E_2 are energies of the excited and ground states, respectively. Hence, when the molecule is excited from E_1 to E_2 , the molecule absorbs ΔE and emits ΔE when it reverts from E_2 to E_1.
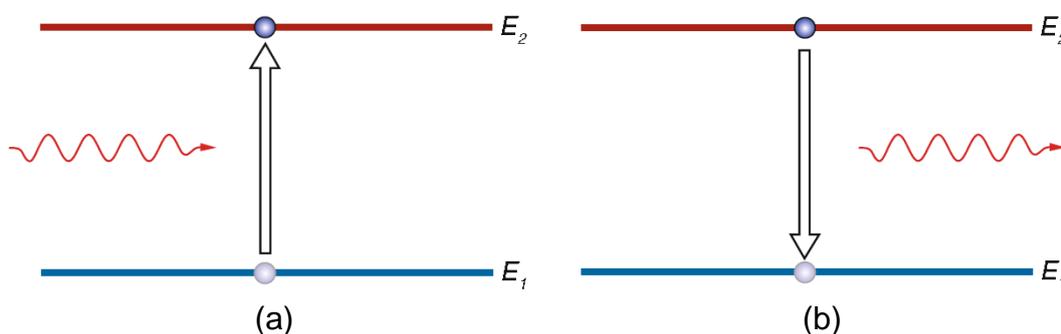
Figure 3.2 (a) Absorption of a photon. Its energy is transferred to the atom and raises its electron shell onto a higher energetic state. (b) Spontaneous emission of a photon by an excited atom or molecule. The energy difference between the two atomic states determines the frequency (and, thus, the wavelength) of the departing photon.

3.1.3 Molecular vibrations

To better understand the molecular vibrations responsible for the characteristic bands observed in Raman spectra, a simple model derived from classical mechanics is considered. A diatomic molecule with two masses m_1 and m_2 connected by a massless spring is depicted in Figure 3.3. In the classical treatment, the chemical bond is regarded as a spring that obeys Hooke's law [115]. The displacement of each mass from equilibrium along the spring axis is X_1 and X_2. The displacement of the two masses as a function of time for a harmonic oscillator varies periodically as a sine (or cosine) function.

In the given diatomic system, although each mass oscillates along the axis with different amplitudes, both atoms share the same frequency and both masses go through their equilibrium positions simultaneously. The observed amplitudes are therefore inversely proportional to the mass of the atoms which keeps the centre of mass stationary.

$$\frac{X_1}{X_2} = \frac{m_2}{m_1} \tag{3-8}$$
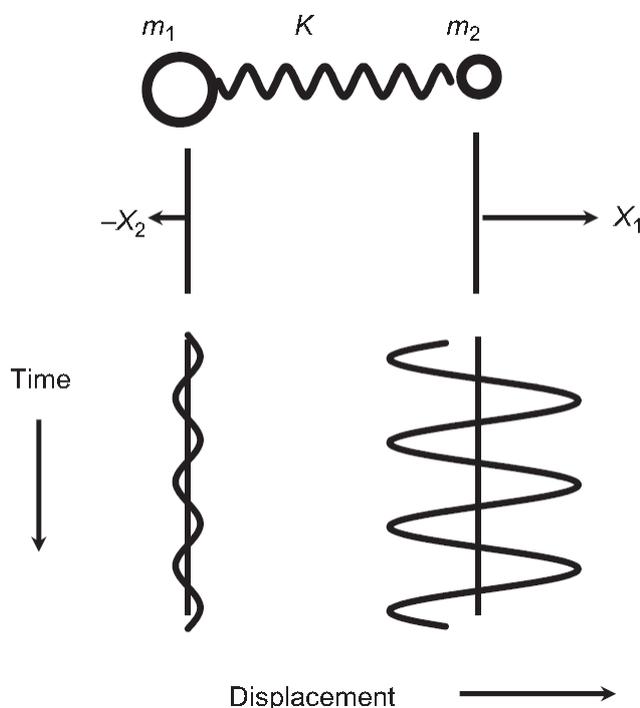
Figure 3.3 Motion of a simple diatomic molecule. The spring constant is K, the masses are m_1 and m_2, and X_1 and X_2 are the displacement vectors of each mass from equilibrium where the oscillator is assumed to be harmonic [115].

The classical vibrational frequency for a diatomic molecule is given by

$$v = \frac{1}{2\pi}\sqrt{K\left(\frac{1}{m_1}+\frac{1}{m_2}\right)} \tag{3-9}$$

where K is the force constant in dynes/cm and m_1 and m_2 are the masses in grams and v is in cycles per second. This expression is also encountered using the reduced mass where

$$\frac{1}{\mu} = \frac{1}{m_1}+\frac{1}{m_1} \quad \text{or} \quad \mu = \frac{m_1 m_2}{m_{1+m_2}} \tag{3-10}$$

In vibrational spectroscopy wavenumber units, $\tilde{v}$ (waves per unit length) are more typically used, and hence replacing (3-9) with (3-5)

$$\tilde{v} = \frac{1}{2\pi c}\sqrt{K\left(\frac{1}{m_1}+\frac{1}{m_2}\right)} \tag{3-11}$$

where v is in waves per centimetre and is sometimes called the frequency in cm^{-1} and c is the speed of light in cm/s.

Therefore this simple expression shows that the observed frequency of a diatomic oscillator is a function of the force constant K, which relates to the bond energy of a two atom bond and inversely proportional to the atomic masses of the two atoms involved in the vibration. Therefore with the knowledge of the masses and frequency, calculation of a diatomic force constant is possible [115]. In diatomic molecules, the vibration occurs only along the chemical bond connecting the nuclei. However in polyatomic molecules, the situation is complicated because all the nuclei perform their own harmonic oscillations [116]. However, these complicated vibrations of a molecule can be expressed as a superposition of a number of "normal vibrations" that are completely independent of each other [116].

Normal vibrations includes symmetric (in phase) stretching, antisymmetric (out of phase) stretching and bending vibration. Since each atom can move in three direction (x,y,z), an N-atom molecule has 3N degrees of motion, which includes six degrees of freedom originating from translational and rotational

motions of the whole molecule about the three principal axes of rotation. Thus the net vibrational degrees of freedom is 3N – 6, and 3N – 5 in case of linear molecules [116].

3.2 Raman spectroscopy

Raman spectroscopy is based on an inelastic scattering or Raman scattering of monochromatic light, usually from a laser source. The laser light interacts with molecular vibrations, photons or other excitations in the system, resulting in the Raman Effect where the energy of the laser photons is shifted up or down in comparison with original monochromatic frequency. This shift in the energy provides information about vibrational, rotational and other low frequency transitions in molecules.

3.2.1 Theoretical aspects

Light scattering phenomena may be classically described in terms of electromagnetic (EM) radiation produced by oscillating dipoles induced in the molecule by the EM fields of the incident radiation [117]. Raman scattering is the polarization induced in a molecule by the oscillating electric field of the incoming light, and the induced dipole then radiates the scattered light, with or without exchanging energy with vibrations in the molecule. The strength of the induced polarization, P, is given as

$$P \ = \ \alpha E \ (\alpha, \text{ polarizability and } E, \text{ incident electric field})$$ (3-12)

The incident Electric field E due to electromagnetic wave with the frequency of the laser light v_0 is given as

$$E \ = \ E_0 cos 2\pi v_0 t$$ (3-13)

The molecular vibrations are usually considered to be composed of normal modes, Q_j, of which there is 3N - 6 in a molecule or 3N - 5 for a linear molecule with N atoms.

$$Q_j = Q_j^0 cos 2\pi v_j t$$ (3-14)

Where v_j is the characteristic harmonic frequency of the *j*th normal mode and hence the polarizability *P* of electrons in the molecule will be modulated by the molecular vibration so that it develops in series of

$$\alpha = \alpha_o + \left(\frac{\delta\alpha}{\delta Q_j}\right) Q_j + higher\ order\ terms \qquad (3\text{-}15)$$

Therefore from (3-12), the polarization is the product of eq. (3-13) and (3-15), which yields noting cos a cos b = [cos (a+b) + cos (a-b)]/2 and ignoring higher order terms

$$P = \alpha_O E_O cos2\pi v_O t + E_O Q°_j \left(\frac{\delta\alpha}{\delta Q_j}\right) \frac{cos2\pi(v_O+v_j)t+cos2\pi(v_O-v_j)t}{2} \qquad (3.16)$$

Therefore, after assuming that the polarized electrons will radiate light at the frequency of their oscillations, (3-16) demonstrates that light will be scattered at three frequencies. The first term of $\alpha_O E_O cos2\pi v_O t$ is the Rayleigh scattering, which is at the same frequency as the laser and has a magnitude proportional to α~O~, the inherent polarizability of the molecule. The second term is anti-Stokes Raman scattering, which occurs at $v_O + v_j$ and the third term is Stokes Raman scattering at $v_O - v_j$. [118].

Therefore eq. (3.16) shows that polarization and scattering intensities are linear with the laser intensity, where nonlinear Raman scattering can occur at higher values of E_O and secondly only vibrations that change the polarizability yield Raman scattering. Thirdly, eq. (3-16) signifies that Raman shifts may be positive and negative. The $\frac{\delta\alpha}{\delta Q_j}$ may vary significantly for different molecules and for different modes in a given molecule, leading to wide variations in Raman scattering intensities. Lastly, although not apparent from eq. (3-16), $\frac{\delta\alpha}{\delta Q_j}$ is generally smaller than α~O~, and Raman scattering is much weaker than Rayleigh scattering [118].

inelastic impact	elastic impact	inelastic impact
$\Delta E_M > 0$	$\Delta E_M = 0$	$\Delta E_M < 0$
$v = v_0 - v_{vib} < v_0$	$v = v_0$	$v' = v_0 - v_{vib} > v_0$
Stokes	Rayleigh	Anti-Stokes

Figure 3.4 The elastic and inelastic scattering of the radiated light at different frequencies [119].

3.2.2 Raman spectrum

The position of a Raman band in the spectrum is determined by the energy difference between the ground state and the first vibrationally excited state (Figure 3.4). Equation 3-11 forms the basis of interpretation of the Raman spectra. From this equation, two factors determine the Raman band position: the force constant of the bond and the type of vibration (K) and the reduced mass (μ).

Once these two properties are known, the Raman band position can be calculated. Since K and μ are relatively stable for a specific type of bond or a particular functional group, for a series of functional groups so-called group frequencies can be determined. These characteristic wavenumbers give an indication about the region where a particular Raman band can be expected, but don't say whether this band is present or not, as this is dependent on the selection rules and the final appearance of the spectrum is strongly dependent on the symmetry of the molecule [117].

The idea of group frequencies is based on the simplification that vibrations in a specific functional group are independent of the other vibrations in the molecule. These group frequencies have mainly practical value for the interpretation of Raman spectra of organic molecules. Often Raman spectra of inorganic molecules are more influenced by the symmetry properties of the molecule. Moreover, strong band shifts occur frequently as well as possible overlap between functional groups [117].

The overall intensity of a Raman band is the result of a whole series of influences and basically divided into two groups [117]:

$$I = \alpha \cdot \beta \qquad (3.17)$$

where α refers to parameters related to the sample and β are parameters that are instrument-related. From a fundamental point of view, where the instrumental factor are not taken into account, Raman intensity of a scattered light equals the change in electromagnetic flux $d\phi$, considered over a specific solid angle Ω:

$$I = \frac{d\phi}{d\Omega} \qquad (3.18)$$

Intensity has a unit of W . steradian^{-1}. The solid angle describes a circle with area A, on a distance r of the source of the scattered radiation, resulting in:

$$dA = r^2 \cdot d\Omega \qquad (3.19)$$

For a specific considered area A (e.g. the size of the collection optics), the measured intensity is inversely proportional to the square of the distance to the source [117].

Further elaboration of the Intensity equation with the classic eqn of 3.16 shows that the intensity of a Raman band due to a molecular vibration depends on the quantity [117]. However scattering intensities depends upon various factors such as particular experimental methods, the state of the incident polarization, the size of the scattering volume etc.

Hence, for Raman fundamentals which arise from localized normal vibrations, some general principles can be applied to relative band intensities [120]. For example, a Raman band is more intense for a mode which involves primarily a bond stretching coordinate than for that which is predominantly an angular deformation. The intensity of a band due primarily to the stretching of a covalent bond increases with bond order and for a mode which is largely localized in a given bond, the intensity increases with the atomic numbers of the bonded atoms [120].

In consideration to the shape or profile of a Raman band, the relative intensity of a Raman band is correctly obtained by integration over the entire spectral profile and presented over as some form of 'spectral lines' (Figure 3.5). The resulting lines are the result of the slit images employed in the monochromator [117]. Therefore a bandshape of the Raman spectral profile is produced depending on the spectral resolution of the spectrometer.
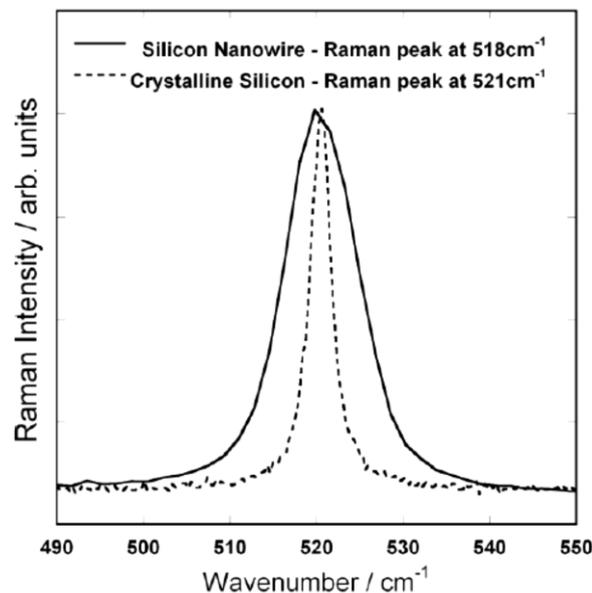
Figure 3.5 Raman spectrum of a Silicon at 532 nm laser excitation [121] .

The Raman bandwidth or the bandshapes is determined by a number of factors. However, for most materials, the local molecular neighbourhood is the most important source of band broadening. Therefore with eqn 3-11, the chemical environment does not influence the reduced mass but it does influence the force constant of the chemical bond. In the presence of different chemical environment the bonds present in the measured volume of the

sample, a range of slightly different force constant may cause band broadening. Hence amorphous materials have broader Raman bands compared to crystalline materials. Similarly, Raman band broadening is affected with various environment such as temperature and pressure and various instrumental parameters [117].

3.2.3 Raman instrumentation

Typically, a Raman spectrometer contains at least four major components: a monochromatic light source usually a laser, a sample area with collection optics, a light dispersing unit (Filter or Spectrophotometer) and a detector (Photodiode array, Charged Coupled Device CCD or Photomultiplier Tubes PMT).

A sample is normally illuminated with a laser beam in the ultraviolet (UV), visible (Vis) or near infrared (NIR) range. Scattered light is collected with a lens and is sent through interference filter or spectrophotometer to obtain Raman spectrum of a sample [122]. Therefore Raman spectroscopy is suitable to investigate the physical contact parameters as it measures the molecular vibrational levels, it is sensitive to tiny chemical changes and different physical conditions.

Modern Raman techniques utilises highly sophisticated methods to enhance the collection of Raman signals from specific molecules and aims to highlight very thin layer of the analyte on the substrate. Technique such as Resonance enhanced Raman spectroscopy, surface enhanced Raman spectroscopy (SERS) has been successfully adapted to study such samples.

A laser (light amplification through stimulated emission of radiation) produces an intense, monochromatic light beam and when they hit a material, they can interact in different ways. Various types of lasers are available on the market, and depending on their specific optical characteristics, the desired power and wavelength, one or other type is selected. The laser's performance is based on the amplification of the signal through stimulated emission. The result of the stimulated emission is that all atoms in the laser together emit

electromagnetic radiation whereby an intense, coherent laser beam is formed [122].

Taking into account the very weak Raman signals, it is necessary to utilise sensitive detectors. For Raman spectroscopy, different types of detectors are used. For dispersive instruments we distinguish single-channel detectors and multi-channel detectors, while for Fourier-transform instruments semiconductor detectors are used (mostly Si, InGaAs or Ge) [122].

Since the Raman effect is an intrinsically weak effect, it is important that the Rayleigh signal is suppressed. Various different filter such as natural density filters, long pass filters, low pass filters, band pass filters and band block filters or polarisation filters are considered according to its usage [122].

All spectrometers need to be able to disperse the light, in function of their wavelength. Light of different wavelengths can be separated either as function of space or in function of time. The most simple diffraction instrument is a prism, where diffraction is based on the wavelength-dependent (angle of) refraction of the light in the prism. However, in modern spectrometers, usually diffraction gratings are used as dispersion system [122].
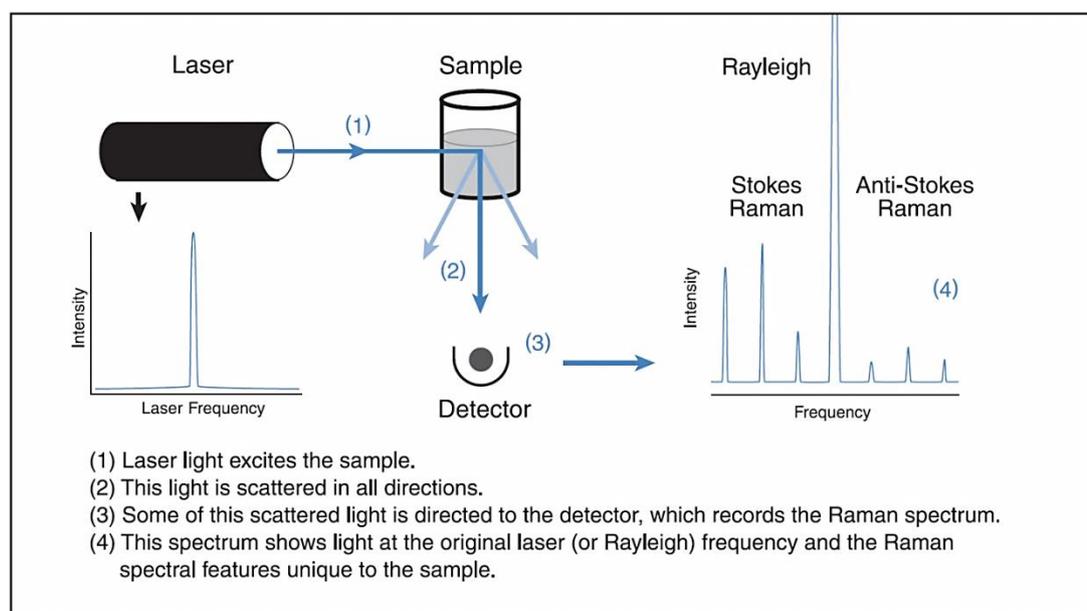
Figure 3.6 Illustration of the Raman theory from its source to its detection.

3.3 Application of Raman spectroscopy as an *in-situ* technique

Raman spectroscopy is a well-known useful technique for determining the molecular structures. It is the most primitive level of structure determination and its application depends heavily on the use of characteristic group frequencies [123]. Compared to other Infrared Spectroscopy studies, Raman possesses several advantages in terms of gathering information. Therefore, Raman spectra are more sensitive to the lengths, strengths, and arrangements of bonds in a material than to chemical composition.

Although various *in-situ* approaches has been applied for tribological interface studies, the severe conditions experienced by the lubricant as it passes through the contact are difficult to reproduce in a bulk reactor [29].

One solution, in order to achieve this complementary information is the use of molecular vibrational spectroscopy, either IR or Raman, to examine the lubricant behaviour in and around the contact region [29]. IR and Raman spectroscopies provide information on the chemical bonding in covalent molecules, which absorb energy at wavelengths characteristic of the various bond vibrations [113]. These techniques are usually used in conventional analysis to provide information on the chemical composition of the bulk organic materials. However, due to the constriction of the set-up, it has been recognised to replace one of the surfaces with a transparent window for the application of IR or Raman spectroscopy to in-contact studies [113].

Glass, quartz or sapphire are usually used as the transparent counter face in Raman spectroscopy, with further consideration of mechanical strength, sufficient transmission in a wavelength range of interest and acceptable cost [29]. Use of a transparent window is obviously not a real life ideal simulation, as it replaces one of the surfaces but, it has little impact for studies of fluid film behaviour and more important implications for the study of chemically reacted or adsorbed films [113]. Although IR and Raman spectroscopies suffer from limitations, it provides simpler methods for probing lubricated contacts but techniques sensitive enough to detect thin lubricant films from small sample area is a major goal and a requirement.

Singer *et al* [84, 85, 124-127] utilised a tribometer incorporating *in situ* optical microscopy and Raman spectroscopy to study the third body processes and friction during sliding. Hence, reciprocating sliding tests were performed with an *in situ* tribometer that allowed real-time visualization and Raman analysis of the sliding contact through a transparent hemisphere.

The friction behaviour therefore could be explained in terms of the relative motion between a transfer film on the hemisphere and the wear track. This approach therefore allowed Singer *et al* to identify the composition of third bodies at the sliding interface and correlate third bodies' processes with friction and wear behaviour for various coatings, also demonstrating that in situ optical and Raman tribometry can be joined to identify near surface chemistry.

Further on, similar approach has been utilised by others [128] to understand the friction and wear process of the third body particles with the use of protective solid coatings. However, most of this approach has been utilised with a transparent hemisphere pin to allow real time visualization and Raman analysis, which might not exactly simulate the real contact.
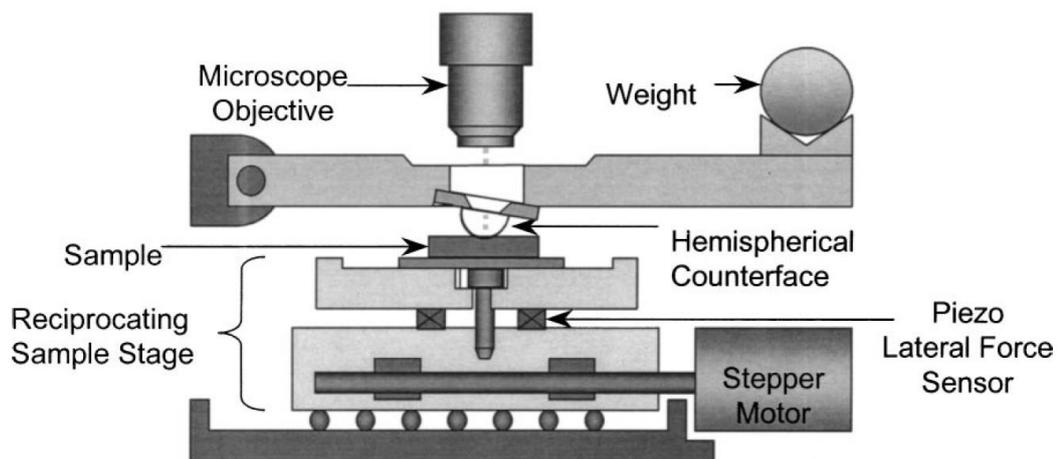
Figure 3.7 Schematic illustration of the *in situ* Raman tribometer utilised by Singer *et al* [84, 85, 124-127]. Micro-Raman spectroscopy and optical microscopy of the sliding contact can be performed through the objective positioned above the transparent hemisphere.

Muratore *et al* [33] employed Raman spectroscopy for real-time correlation of sliding contact surface chemistry to the measured friction coefficient of solid lubricant coatings during high temperature (300–700 ºC) wear testing. The system consisted of a ball on flat tribometer with a heated enclosure that allows heating of the film surface up to 700 ºC, with an optical assembly enclosed in a stainless steel tube probe inserted into the heated zone, focused on the wear track (Figure 3.8). They were successful in observing the mechanisms contributing towards the understanding of the various coating chemistry with the measured friction coefficient utilising the Raman spectroscopy. Similarly, Mcdevitt et al [129] also developed an *in-situ* tribotester (Pin on disc) in conjugation with a Raman spectrometer to obtain chemical information from the wear track of solid lubricants.

In-situ techniques with Raman spectroscopy has been mostly applied towards understanding the tribochemical process of solid lubricants. Graham et al [43], Miklozic et al [44] has characterise the lubricant tribofilms of MoS_2 with *ex-situ* analysis. However, compared to all of the *in-situ* techniques, Raman spectroscopy has yet to be utilised with the effect of lubricants on the analysis of the tribofilms, setting a challenge towards the understanding of the limits of the spectroscopy towards the research.
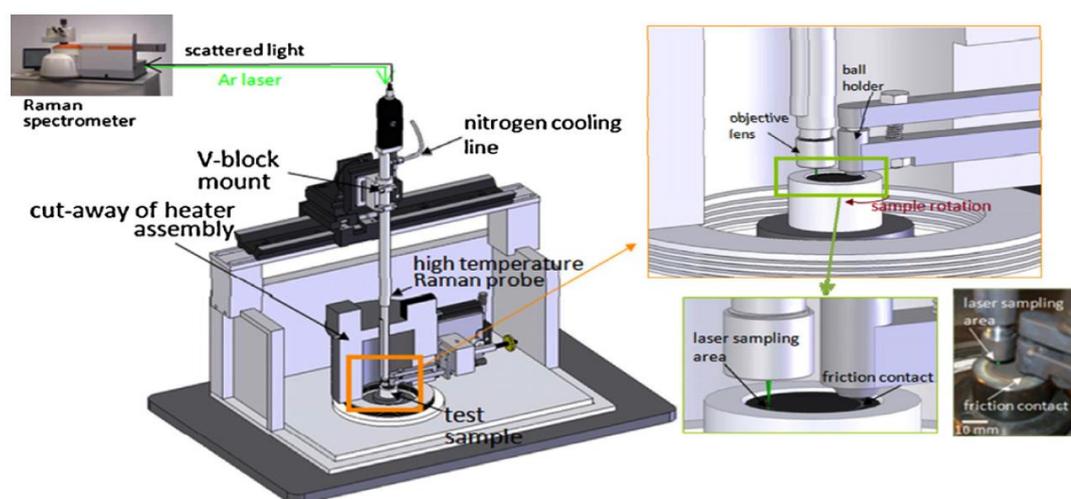
Figure 3.8 Schematics and photograph of the *in situ* Raman testing apparatus designed by Muratore *et al* [33]. The *in situ* set up consists of a tribometer with a heatable enclosure designed to accommodate a gas-cooled tube fitted with the optics necessary to guide the excitation laser to the sample and the resulting backscattered luminescence to the spectrometer.

3.4 Summary

This chapter describes the theory and principle of Raman spectroscopy as a surface analytical technique. The working principle and the information obtained to understand the tribochemical mechanism is presented.

Raman spectroscopy as an *in-situ* technique has seen its numerous application towards understanding the tribochemical processes of solid lubricants and coatings. However, such approaches have been utilised with a transparent window which does not necessarily replicate a real life ideal simulation. Similarly, an ideal compromise has also been made by various researchers where Raman analysis is conducted on the wear track without replacing any ideal samples. However, most of these *in-situ* technique have been utilised to understand the tribochemistry of solid lubricants, hence setting a challenge towards it application towards understanding tribofilms formed under lubricated conditions.

Chapter 4
Experimental Methods

Chapter 4 provides an insight into the various experimental methods and methodology adapted to conduct a series of experiments and analysis for this work. The first part presents the principle of the tribometers and surface analytical techniques are discussed in the second part of the chapter. All of the ex-situ experiments have been conducted in the traditional high speed pin on disc tribometer, followed with a surface analysis technique of Raman spectroscopy.

Complementary surface analytical techniques utilised with the analysis on the surface are also provided. In reference to Chapter 2, description of the principles of Transmission electron microscope (TEM), White Light interferometry, Profile projector and Optical Microscope, respectively are provided.

The development of the new *in-situ* tribometer and its principles is discussed in section 4.2, along with its validation for *in-situ* approaches for real time experimental conditions.

Section 4.3 presents the lubricant additive of Molybdenum dialkyldithiocarbamate (MoDTC) and Zinc dialkyldithiophosphate (ZDDP) investigated in this study, along with their physical and chemical properties listed.

4.1 Methods

Initial experiments were conducted with the high speed pin on disc (HSPOD) tribometer to produce the tribological phenomena occurring on the contact. Surface analytical technique of Raman spectroscopy is used to characterize the tribofilms formed on the contacting surface after the test.

Transmission electron microscope (TEM) is used as a complementary ex-situ technique to observe the tribofilm at a higher resolution and measure the thickness of the tribofilm. Similarly, tribofilm elements are characterized with the aid of Energy-dispersive X-ray spectroscopy (EDX), which is equipped within the TEM instrument.

Optical microscopes are utilised to obtain the surface information at a higher resolution. Wear scar profile on the disc are obtained with the white light interferometer and the wear scar diameter of the ball obtained with the profile projector.

In-situ tribometer is developed in this research with the capability of working in conjunction with the Raman spectroscopy to monitor the tribological phenomenon occurring within the boundary lubricated surface *in-situ*.

4.1.1 High Speed Pin on Disc (HSPOD) tribometer

The High Speed Pin on Disc tribometer, as the name suggests is a standard tribometer which produces comparable friction and wear data. It can reach speeds up to of 5000 rpm. The rig is powered by a D.C brush motor, placed below the set-up of the rig to rotate the sample disc at the required speed. The motor is placed with two switches, where one of it switches the motor box on and off, and the other powers the motor to produce the rotational effect needed on the disc itself. The motor box is provided with a rotor switch which helps to vary the speed of the shaft with a variable frequency inverter.
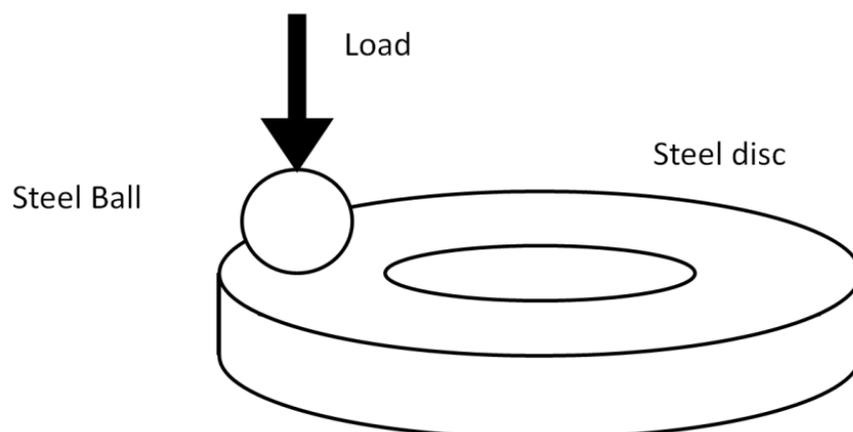
Figure 4.1 Representative illustration of the contact between the steel ball and disc sample in the High Speed Pin on Disc tribometer (HSPOD).

The tribometer consists of a fixed long arm perpendicular to the rotating disc with a load attachment on one end and also the pin holder on its arm length. The tribometer is equipped with its own calibration system and consists of a counter weight at the opposite end of the load attachment to balance the distributed weight. The tribometer was instrumented to measure friction force via a transducer rod on the load arm which provided the friction force on the load cell, and recorded through a Labview based data acquisition system.

The motor rotates the sample disc, which is screwed onto the sample tray at the desired speed and the friction produced against the ball bearing measured through the transducer rod (Figure 4.1). The friction coefficients of the rotating disc on the pin was therefore measured and calculated by the Labview based data acquisition system available on the attached PC. The data corresponded to given frequency measurement/data collection and plotted against time for friction analysis.

Experimental samples comprised of a steel disc and a ball bearing, clamped to a holder to be used instead of a pin. The steel disc was an AS Series Thrust Washers made of spring steel AISI 1050 and the ball bearing was AISI 52100 Chrome Steel Ball Bearings (60 - 67 HRC, 0.2 - 0.3 µm R_a) .The sample disk had the dimension of 25 mm inner diameter/42 mm outer diameter with a thickness of 1 mm and the ball bearing had a 6.35 mm diameter. The sample pin and disc was cleaned with acetone before each experiment to ensure that no other contaminants would affect the experiment being conducted.

Similarly an electrical heater was connected to the tribometer system which was used to heat the lubricant injected into the sample tray. To ensure the disc and the ball were always submerged in the lubricant, 35 - 40 ml of lubricant was injected into the sample tray. The tribometer also had a pipe in the sample tray, where once the sample tray was rotating with the lubricants, the flow mechanism produced in the tray would deliver the lubricant into the pipe and onto the surface of the rotating disc to always provide the presence of lubricant on it.

The experiments conducted on the High Speed Pin on Disc Tribometer, were operated at various temperature, speed and contact load, for the lubricants additives and for different time duration. All of the experiments are ensured to be conducted under boundary lubrication conditions and a detailed calculation regarding the contact pressure and lubrication regimes is included in Appendix 1.

Table 4.1 and 4.2 show a comparative tribological conditions and parameters applied for the tests conducted with various lubricant additives on the high sped pin on disc tribometer (HSPOD). These following tests were conducted to understand the friction and wear performance of the lubricants, at various stated parameters. The samples were further analysed with various surface analytical techniques discussed in the following section.

Table 4.1 Tribological experimental conditions for the lubricant additive of Molybdenum dialkyldithiocarbamate (MoDTC) at the stated parameters in the high speed pin on disc (HSPOD).

Sliding velocity	0.44 m/s			0.88 m/s			1.75 m/s		
Normal load	7 N	14 N	29 N	7 N	14 N	29 N	7 N	14 N	29 N
Apparent contact pressure	0.8 GPa	1.02 GPa	1.29 GPa	0.8 GPa	1.02 GPa	1.29 GPa	0.8 GPa	1.02 GPa	1.29 GPa
Lubricant	Poly-α-olefin 4 (PAO4) + Molybdenum dialkyldithiocarbamate (MoDTC)			Poly-α-olefin 4 (PAO4) + Molybdenum dialkyldithiocarbamate (MoDTC)			Poly-α-olefin 4 (PAO4) + Molybdenum dialkyldithiocarbamate (MoDTC)		
Tempera-ture	25ºC , 100ºC			25ºC , 100ºC			25ºC , 100ºC		

Table 4.2 Tribological experimental conditions conducted in the high speed pin on disc (HSPOD) for the lubricant additive of Molybdenum dialkyldithiocarbamate (MoDTC) at various temperature. Experiment conditions for lubricant of polyalphaolefin 4 (PAO4) and additives of Molybdenum dialkyldithiocarbamate (MoTDC) and Zinc dialkyldithiophosphate (ZDDP).

Sliding velocity	0.88 m/s	0.88 m/s
Normal load	14 N	14 N
Apparent contact pressure	1.02 GPa	1.02 GPa
Lubricant	Poly-α-olefin 4 (PAO4) + Molybdenum dialkyldithiocarbamate (MoDTC)	Poly-α-olefin 4 (PAO4)
		Poly-α-olefin 4 (PAO4) + Molybdenum dialkyldithiocarbamate (MoDTC) + Zinc dialkyldithiophosphate (ZDDP)
		Poly-α-olefin 4 (PAO4) + Zinc dialkyldithiophosphate (ZDDP)
Temperature	25ºC , 50ºC, 80ºC, 100ºC, 120ºC	25ºC , 100ºC

4.1.2 Raman Microscope

The Raman spectrometer used in this work is based on a commercial Raman microscope (inVia Raman microscope, Renishaw plc.)(Figure 4.2). A light source is directed onto the sample and the scattered light collected by a Leica microscope, equipped with a 5X, 20X, 50X and 50X LWD (Olympus) objective. A 488 nm wavelength (30 mW) Modu-laser Stellar REN Argon laser and 785 nm (300 mW) diode laser is provided as the exciting light source. In order to increase the effective field of view a 50X LWD, 0.55 N.A objective with a spot diameter size of 800 nm was used for various experiments conducted. The Raman spectrometer provided a maximum depth and lateral resolution of 2 μm.

The Raman signal was collected at 180° backscattering geometry and the scattered light passes through a notch filter that removes Rayleigh scattering

and then focused by a lens through a slit, and directed onto a diffraction grating. The Raman scattered light is split into component wavelengths or spectrum by the diffraction grating and detected on a CCD (charged-couple device) detector (Figure 4.3).

Figure 4.2 Renishaw inVia Raman microscope.
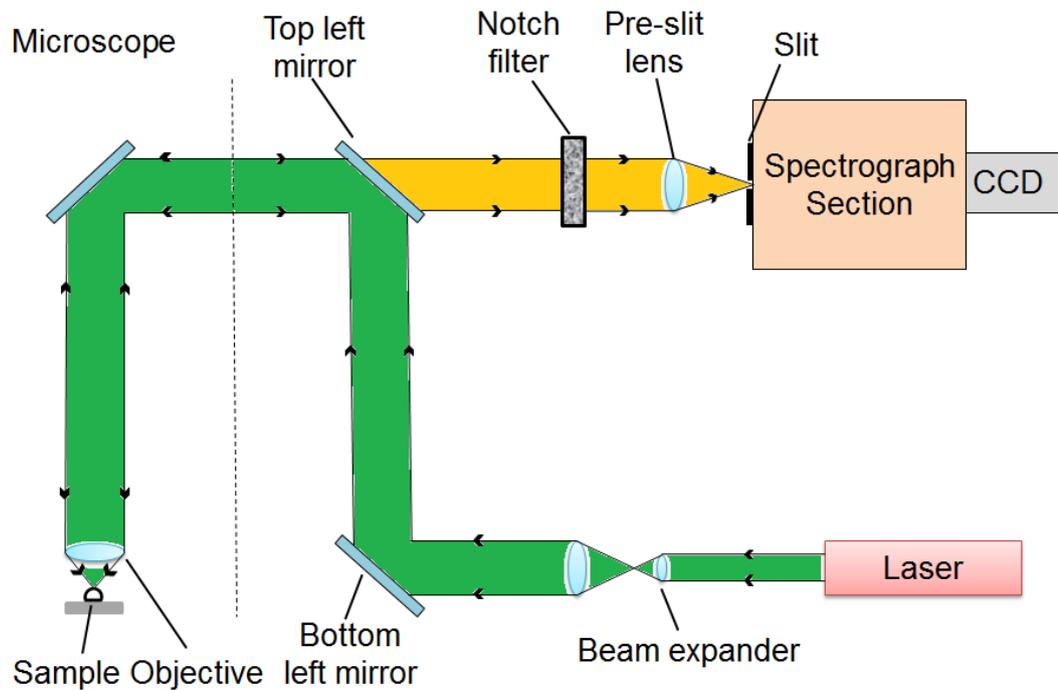
Figure 4.3 Instrument layout showing the laser beam pathway used as Raman excitation beam, excitation path, Raman scattering path, positions of objective lens, pin hole, grating, and CCD.

A software package provided by the Renishaw plc named WiRE 3.4 (Windows-based Raman Environment), is used to control the Raman system. It allowed system control and configuration as well as analysis and processing of the acquired data.

The WiRE 3.4 software permitted the adjustment of various parameters such as laser power, type of scans, exposure time etc. for the Raman system before the analysis could be undertaken. A procedure to optimize the laser power was therefore undertaken to obtain good quality signal with the various Raman parameters while ensuring no sample damage and discussed thoroughly in Chapter 5.

To calibrate the system an automatic silicon reference alignment procedure was conducted with a built in silicon band whenever the system was in use. This built-in calibration system consist of a silicon sample fitted inside the system where the lasers can be focused onto this sample. The corresponding Raman shift for the silicon of 520 cm^{-1} [130] is analysed with the lasers and any offset or change in the laser was calibrated accordingly. The calibrations for the lasers are performed every time the Raman system was in use and before any Raman analysis were undertaken.

Characteristics of the Raman spectra that have been investigated include shifts in Raman peak values and full width at half maximum (FWHM) Raman bands, and normalized intensity variations. A linear curve fit was provided for all spectra with a Gausian Lorentzian Product (Voight profile function) in the Originlab software to provide a satisfactory fit to the Raman data. For Raman map data, a Matlab program was utilised to provide a linear background subtraction to provide normalized intensity variations along the analyzed area.

4.1.3 Transmission Electron Microscopy (TEM)

Apart from Raman analysis, the surfaces of the samples were also analysed with the aid of Transmission Electron Microscopy (TEM) to characterise the tribofilm. Sample discs were collected after the tribometer test and observed in the TEM.

The sample preparation for the TEM analysis was conducted with the application of the focused ion beam (FIB), where sample around 15 X 2 µm is cut off the bulk of the wear scar. FEI Nova 200 NanoLab high resolution Field Emission Gun Scanning Electron Microscope (FEGSEM) with precise Focused Ion Beam (FIB) - etch and deposition capabilities were utilised to deposit platinum onto the surface, to protect the underlying surface. The chosen area was then treated with low-energy gallium ions for further thinning the sample area and to lift it out from the sample bulk and placed on a copper film suitable for high resolution TEM analysis [72, 131].

The TEM system utilised to analyse the sample wear scar surface was the FEI Tecnai TF20 and the Philips CM200. The sample is loaded onto the airlock entryway at the centre of the chamber of the TEM system. The pre pumping sequence takes place as soon as the sample is placed onto the chamber to create a vacuum, and the beam alignment is performed. After the pre setup and the parameters adjustment of the TEM system, the analysis was carried out on the sample.

The TEM system was also equipped with an Energy dispersive X-ray (EDX) analysis. X-rays are produced due to the ionisation of the specimen by the electron beam. These X-rays originated from atomic electrons dropping in energy to fill the holes created in the ionisation events. These X-rays have a characteristics energy, due to the unique electronic structure of each different element. This energy is used to identify the elements being analysed. A thorough principle of the X-ray technique is provided in Chapter 2 Section 2.3.1.3.

4.1.4 Optical Microscope

Optical Microscope was used to observe the tribological interface of the various experiments conducted. The microscope utilised in this work was the Leica DM6000 digital microscope. The microscope was provided with an objective lenses of 5X, 10X, 20X and 50X, which provided magnification of the sample according to purpose and its combination.

The Leica DM600 was provided with an automated stage with an external control panel, easing the convenient control of all functions including the focus wheel for fine and coarse adjustment and the x,y,z stage adjustment. Similarly, the microscope was provided with the Leica Application Suite (LAS) software, which provided a graphical user interface on the desktop for analysis purpose.

The microscope technique was used to reveal the surface information of wear scar and its appearances on the contacting sample. Images of the wear scar are obtained from the sample and the software could also be used to measure the 2D (two-dimensional) wear profile of the sample.

Figure 4.4 Leica DM6000 Optical digital microscope.

4.1.5 Wear measurement

The NPFLEX-LA Non-contact Optical Profiling system was used to obtain the measurement of the disc wear scar profiles. The system utilised a broadband light source which combined vertical scanning techniques with optical interferometry techniques to achieve a three-dimensional surface measurement. The samples were measured with the Vertical Scanning interferometry (VSI) mode which yields high resolution images of the surface up to a nanometer scale. Measurements were further interpreted utilizing the Vision64 software to obtain numerical data. Four different points on the wear scar of the disc was obtained from each sample, and the values averaged to obtain the wear volume (Figure 4.5).

Similarly, the wear scar diameter of the ball samples was obtained by using the Nikon profile projector. The wear scar was projected and magnified to measure the precise diameter across the x and y axis for each sample. An average of three readings was obtained across the wear scar and averaged to calculate the volume loss. The calculated volume loss was further divided by the sliding distance (m) multiplied by the unit of load (N) to produce the dimensional wear coefficient, which allows a comparison of the wear performance of the testing parameters.
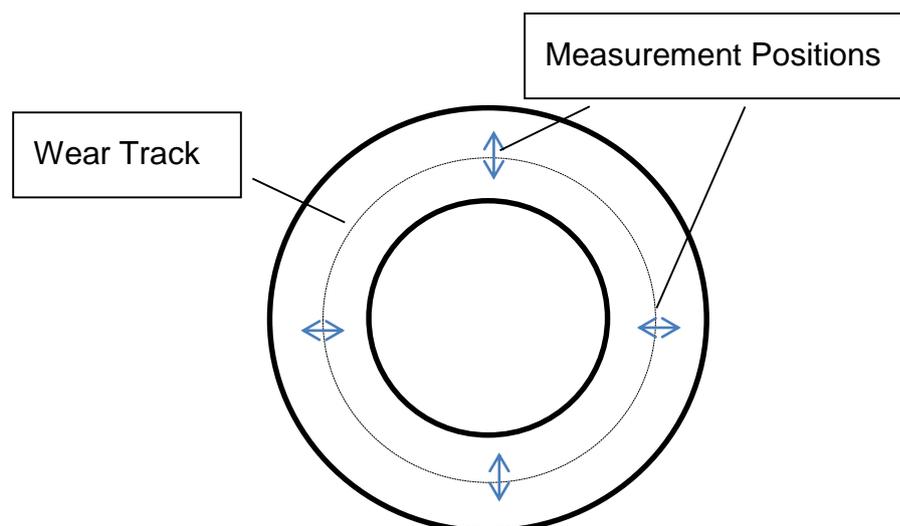
Figure 4.5 Measurement of disc samples wear scar highlighted with non – contact optical profilometer taken along 4 different positions of the samples. The analyses were carried out along the width of the wear scar.

4.2 Development of a new *in-situ* tribometer

In-situ Raman spectroscopy is a technique developed to understand the development of a tribochemical phenomenon occurring on a rubbing surface. The importance of *in-situ* approaches for tribological interface studies has been highlighted in Chapter 2. Therefore, a small scale, unidirectional tribometer capable of operating in conjunction with a Raman spectroscopy was designed and built in the university during the course of the PhD programme, in order to monitor the tribological phenomenon occurring within the boundary lubricated surface with *in-situ* capabilities.

The characteristics of the tribometer have been designed with parameters closely simulating a real tribological contact under boundary lubricated conditions. The tribometer was designed with a specific focus on the replication of surface interactions between an automotive engine's cam and followers system functioning under boundary conditions and with the purpose of viewing the wear scar *in-situ*.

4.2.1 *In-situ* tribometer set-up

The *in-situ* tribometer was designed with a set-up of a conventional pin on disc apparatus. Friction tests can be performed with the *in-situ* tribometer under dry and wet lubrication condition whilst varying the different operating parameters of temperature, load, and speed [Table 4-1]. The frictional force between the sample disc and bearing pin is measured by a compression load cell, which is integrated with a Labview based data acquisition system to store and collect the frictional force data.

Table 4.3 Parameter ranges of various operating conditions for the designed *in-situ* rig.

	Speed	Load/Contact pressure	Temperature
Max:	400 rpm	5 kg	100°C
Min:	10 rpm	0.2 kg	Ambient

The rotary motion of the tribometer consists of a sample disc sliding against the fixed ball bearing attached to a load arm. A unidirectional point contact is thus produced between the bearing ball and the flat disc. An electric spur gear motor (Anaheim Automation, BLWSG23 series) with a gear ratio of 7.5:1 is used to rotate the sample disc. The rotational speed is controlled with a dial and can be varied between the given speeds at Table 4-3.

The normal force acting on the contact is applied at the load arm with the application of different weights. The load arm consists of a clamp for the ball bearing which then applies the weight against the sample disc. The steel disc was an AS Series Thrust Washers made of spring steel AISI 1050, with a dimension of 85 mm inner diameter/110 mm outer diameter and a thickness of 1 mm. The ball bearing was AISI 52100 Chrome Steel Ball Bearings (60 - 67 HRC, 0.2 - 0.3 µm R_a) with a diameter of 5.5 mm. The samples utilised for the experiments of *in-situ* tribometer were replicated with similar sample materials of the high speed pin on disc (HSPOD).

In order to provide the system with adequate heating capabilities, four cartridge heaters (Acim Jouanin, France) are employed to provide uniform heat diffusion along the diameter of the disc. The heaters are placed beneath the sample disc and heatable up to 100°C, with the power provided by a temperature controller (IR32, Carel, Italy). The temperature was measured with a type K thermocouple.
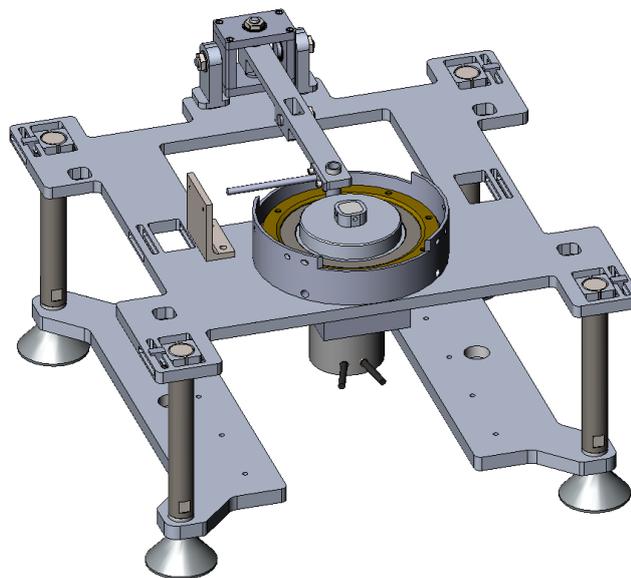
Figure 4.6 Computer-aided designed (CAD) model of the *in-situ* tribometer.

Lubricant was supplied to the system with the aid of a peristaltic pump (Watson Marlow 505S, UK) where the oil was drained from a container and poured onto the contact. The lubricant was run through a cyclic process where it drained from an outlet within the sample tray and poured back onto the container. Tribochemical reactions at elevated temperatures involved heating the lubricant by running the oil through an oil bath (Haake DC10-B3, Thermo-Scientific, U.S.A) at the desired temperature.
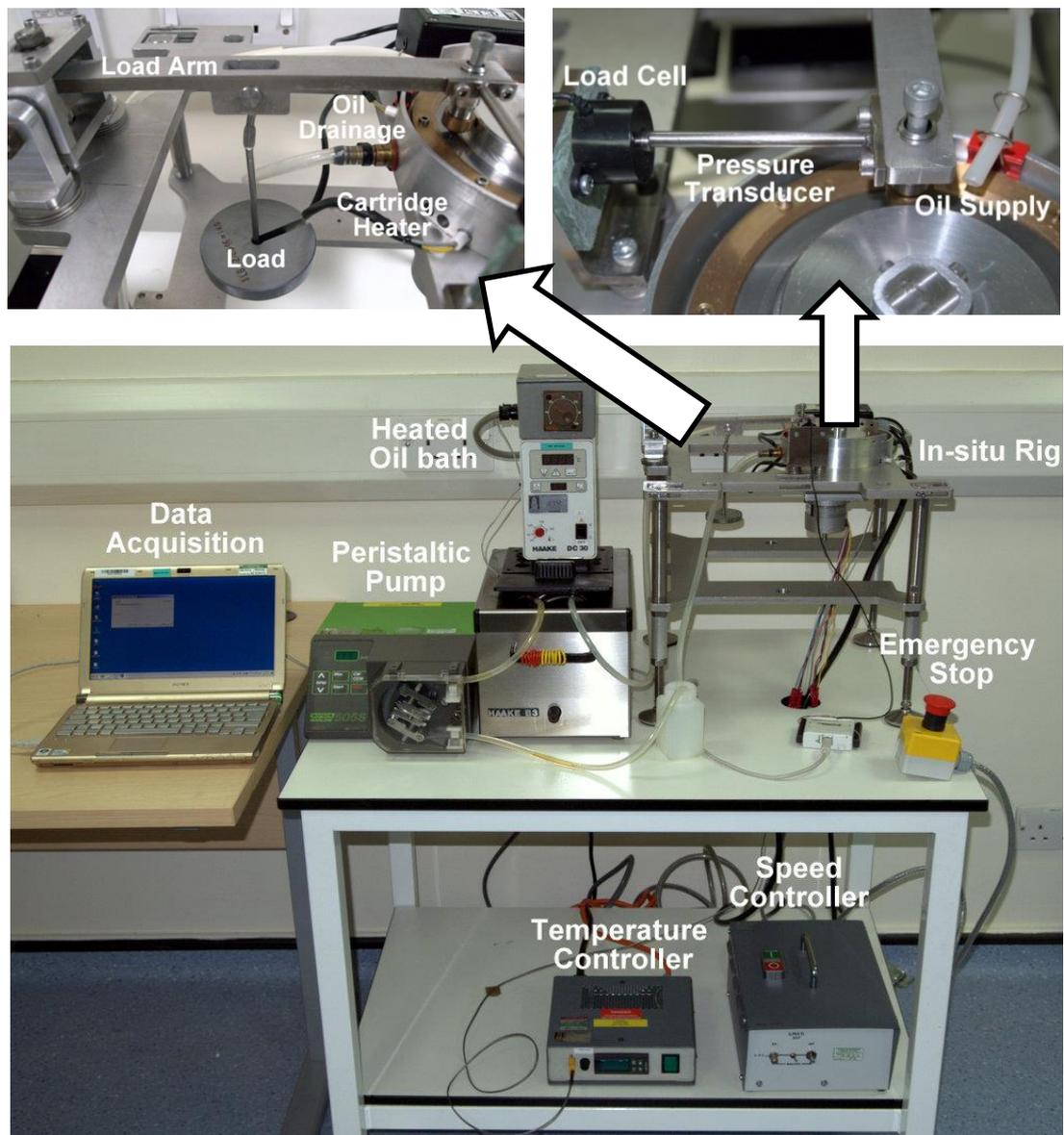
Figure 4.7 Experimental setup of the *in-situ* tribometer, with an enlarged view of the load arm assembly, along with the force between the ball and the disc generated with the pressure transducer and recorded with the load cell.

4.2.2 *In-situ* tribometer load cell voltage output readings and its calibration procedure

The frictional force generated between the sample disc and the bearing pin, is measured with the aid of a compression load cell (Phidgets FC Compression Load Cell, Calgary, Canada) (Measurement range 0 – 4.54 kg). A pressure transducer attached to the load arm (Figure 4.1) generates the pressure on the load cell and the voltage output is recorded.
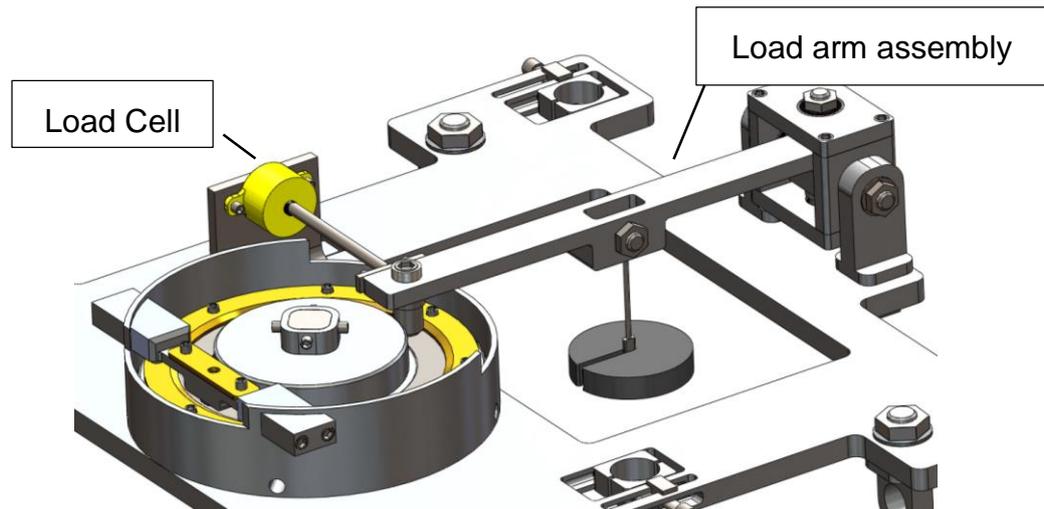
Figure 4.8 Illustration of pressure transducer attached with the load arm, generating the necessary force between the pin and disc and the output recorded with the load cell.

The load cell is connected with a bus-powered multifunction data acquisition (DAQ) USB device (NI USB-6008, National Instruments) which provides basic DAQ functionality for data logging and measurement applications. In accordance with the DAQ device, a Labview software program was developed to record data in the computer. The software sampled data at the rate of 1000 samples per 1000 milliseconds, and the averaged data recorded every single second.

To ensure reliable test results a calibration procedure of the load cell was also conducted before any tribometry test were conducted. The load cell is screwed onto the tribometer on a pressure transducer bracket and easily isolated from the system. The load cell was placed in a horizontal force test stand and compressive force applied on the load cell to record the voltage. The test stand was employed with a manual hand wheel to apply the force onto the load cell and the force displayed on a gauge.

The load cell is labelled to measure compressive forces of up to 10 pounds (~ 4.5 kg). The calibration procedure involved the application of forces up to 45 Newton, where voltage output data was measured at every 5 Newton force increase. To ensure repeatability, the load cell output readings were repeated with identical loadings under the procedure of loading and unloading the force values. The analytical response of the load cell output readings with the known quantity of the force was generated with a calibration curve graph. A linear response of the curve graph was produced with a 99% best fit and the slope calculated to interpret the voltage output readings.

4.2.3 Friction measurement with the *in-situ* tribometer

To ensure the formation of the lubricant additives tribofilms and to observe the friction coefficient values, experiments were conducted with the High Speed Pin on Disc (HSPOD) and *in-situ* tribometer with similar materials to observe the friction.

Table 4.4 provides a comparison of the tribological parameter utilised to conduct test between the HSPOD and the *in-situ* rig. Experiments were conducted with the lubricant of MoDTC at varying temperatures of room temperature and 100°C to observe the friction produced.

Figure 4.9 shows a comparative graph of the tests conducted for the lubricant of MoDTC at the stated parameters in the HSPOD and the *In-situ* rig. Test conducted at room temperature conditions showed the friction coefficient follows a similar trend in both tests conducted at both HSPOD and the *in-situ* rig. The significant drop of friction observed on the HSPOD test conducted at 100°C can be obtained with the *in-situ* tribometer too. HSPOD is an established tribometer, *in-situ* tribometer can obtain similar friction results when tested at same running conditions. A further discussion of the MoDTC tribofilm is provided in the following chapters, however similar observation of friction is observed with the *in-situ* rig and HSPOD which validates the *in-situ* tribometer.

Table 4.4 Parameters utilised in the tribological experiment of the HSPOD and *In-situ* rig to observe the friction produce with the load cell of the *in-situ* rig.

	HSPOD	***IN-SITU* RIG**
Samples	Steel Disc AISI 1050 (25 X 42 X 1mm)	Steel Disc AISI 1050 (85 X 110 X 1mm)
	Steel Ball Bearing AISI 52100 (6.45 mm Diameter)	Steel Ball Bearing AISI 52100 (5.5 mm Diameter)
Load	1.02 GPa	1.02 GPa
Speed	400 rpm	400 rpm
Sliding speed	0.7 m/s	2.04 m/s
Time	1 hour	1 hour
Temperature	Room Temperature (~25ºC) & 100°C	Room Temperature (25ºC) & 100°C
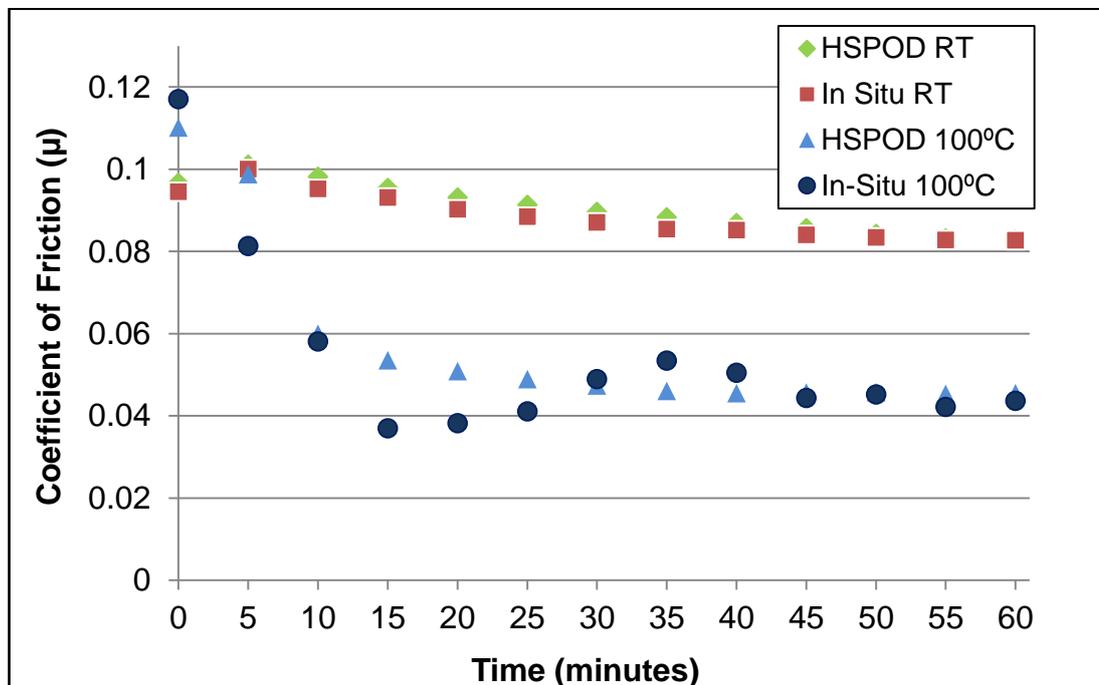
Figure 4.9 Friction coefficient graph of the test conducted at the HSPOD and the *in-situ* rig, with the lubricant of MoDTC under similar parameters of tribological conditions. An average friction value at every 5 minute has been highlighted at the graph.

4.2.4 *In-situ* Raman spectroscopy experimental set-up

In-situ tribometer is developed to produce the boundary lubricated tribological phenomenon occurring on the interface. Surface analysis on the sample are usually performed with the conventional methods of *ex-situ*, where the samples are taken out from the system. The designed *in-situ* tribometer utilises the flexible sampling arm provided with the Raman system, and analysis conducted without removing the samples from the system.

4.2.4.1 Flexible objective positioning (flexible sampling arm)

With the benefit of direct coupling with the Raman system, a flexible sampling arm is provided as an accessory from the Renishaw plc. to analyse samples out of the sampling stage. The sampling arm comprises of the arm itself and a support bracket. The arm comprises of an outer and inner tube with the outer tube cantilevered from a flexible mounting in a mounting block such that it can move simultaneously in both the vertical and horizontal planes, while the inner tube can slide in and out of the outer tube.

An objective lens screws into the end of the inner tube, alternatively, the 90° mirror is screwed in here and an objective lens is screwed to the other side of the mirror. The mounting block is intended to be supported from one of the positions in the turret of a microscope used with a Renishaw Raman system. It is attached by a detachable microscope adaptor.

The support bracket comprises a metal arm that is secured to the microscope stage. It has a spigot on the end which supports the end of the steerable arm and is adjustable for height. The steerable arm and support bracket are mounted on the microscope such that, as the microscope stage moves, the inner tube is pulled in and out and the outer tube support the rotation around its mounting as it is pulled by the spigot.
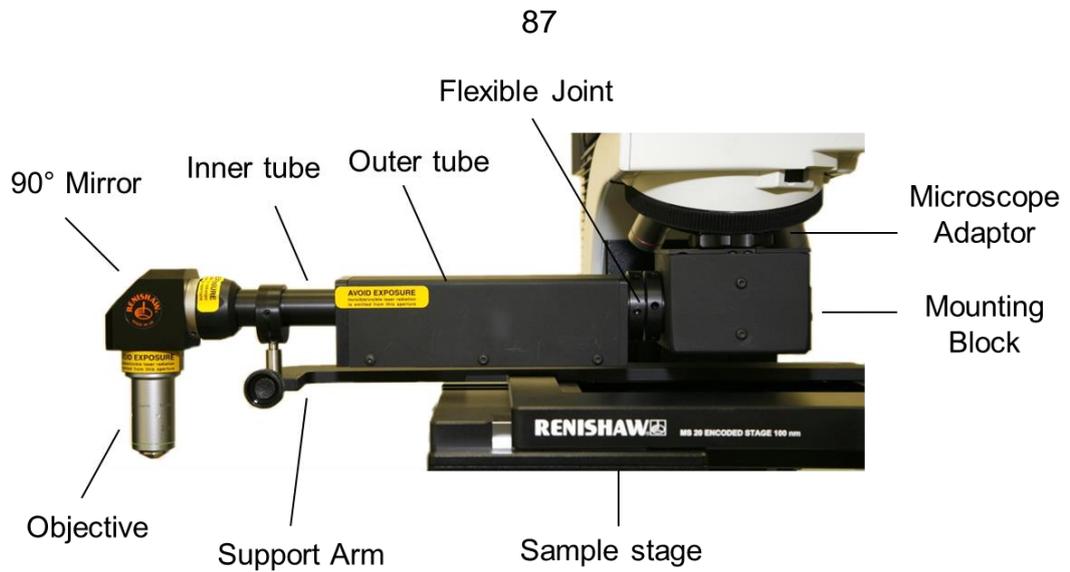
(a)
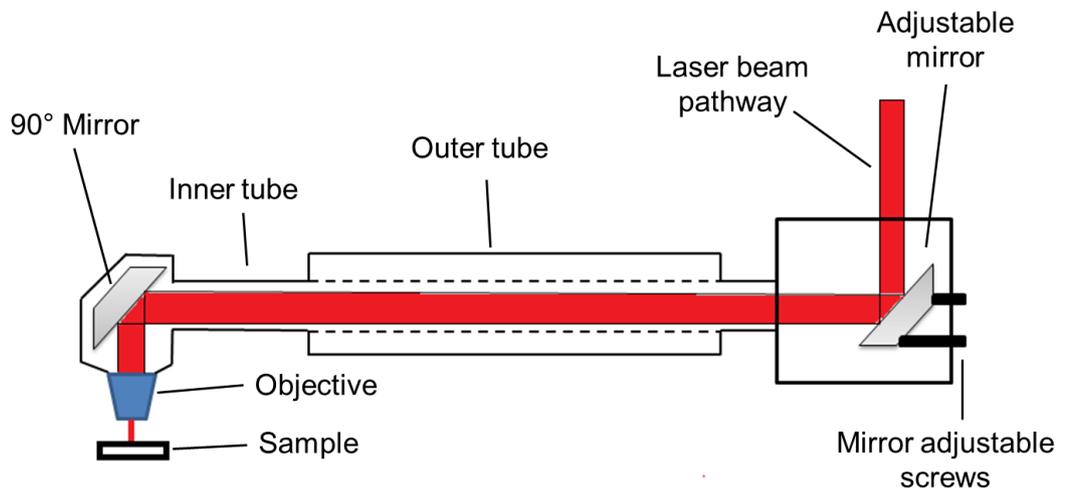
(b)

Figure 4.10 (a) Components of the steerable arm (flexible sampling arm) with the mirror installed onto the sampling stage of the Raman microscope. (b) Illustration of the laser beam pathway followed within the flexible sampling arm.

4.2.4.2 Flexible sampling arm calibration

The Raman system is provided with an automatic silicon reference and the laser is aligned with the calibration procedure. The calibration procedure is however limited to the enclosed chamber within the system. The sampling arm directs the laser from the enclosed chamber and onto the environment outside the chamber. To measure the laser position and the reliability of the data analysed, a method for determining Raman peak positions is needed. In order to calibrate the laser alignment of the flexible sampling arm, a Sapphire disc (Goodfellow, Al_2O_3, 99.9%) sample was used. Standard substances such as silicon, sapphire, diamond etc. have a strong and simple Raman spectrum making them very useful calibration reference in Raman. The Raman shift for these sub-standards are known and usually easy to detect due to its sharp peak. Raman spectra of a sapphire single crystal show visible peaks at 378, 418, 432, 451, 578, 645 and 751 cm^{-1} [132-134]. Figure 4.11 highlights the Raman response of the standard peak of sapphire conducted within the enclosed chamber and the flexible sampling arm. Before every experiment, Raman analysis was conducted on the sapphire for laser alignment within the enclosed chamber and followed with the flexible sampling arm.
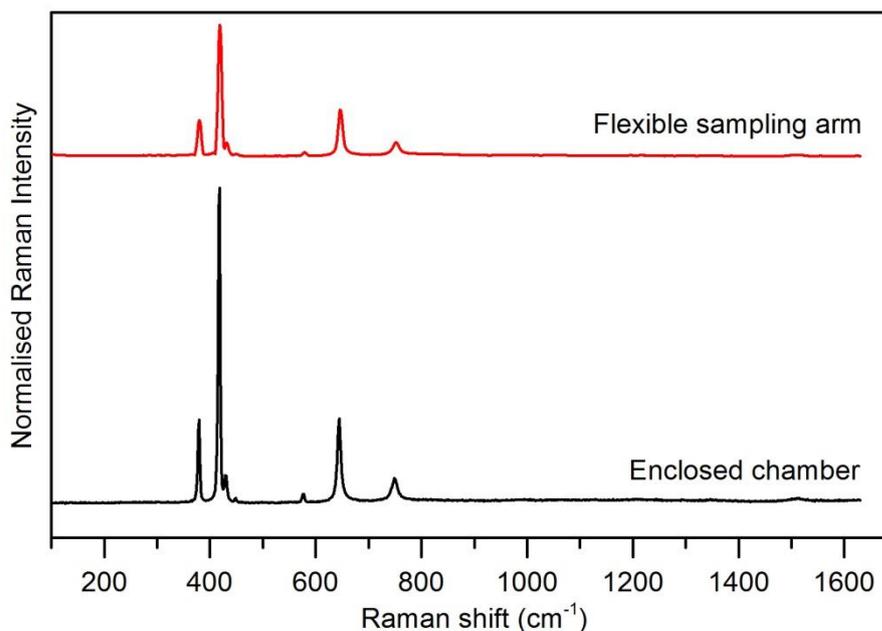
Figure 4.11 Raman spectrum (488 nm excitation) of the sapphire disc conducted within the enclosed chamber and with the flexible sampling arm under ambient conditions.

4.2.4.3 *In-situ* experimental set-up with the flexible sampling arm

Flexible sampling arm assists with *in-situ* microscopy access, as it directs the laser out of the enclosed chamber and exposes out on to the environment. Contact between the ball and the disc samples occurs on the rotating sample stage of the *in-situ* rig, and the flexible sampling arm is focused onto the opposite end of the contact (Figure 4.12). The base of the arm sits on the sample stage of the enclosed chamber and hence the focus can be adjusted with the aid of the sample stage adjuster. *In-situ* analysis was therefore performed with the aid of the flexible sampling arm.

To understand the development of lubricant additives tribofilm, experiments were conducted for a defined duration of time on the *in-situ* rig and the experiments were stopped at every defined time period. The supply of lubricant to the contact was paused and the contact between the ball and the disc was removed. The rotating disc was run for a period of 1 minute after the contact was removed to remove any excess oil from the surface of the sample. The sampling arm along with the objective was focused onto the wear scar of the disc and the Raman analysis undertaken. Raman spectra were undertaken with the laser of 488 nm at 100% with an exposure of 1 second and 30 accumulations. After the analysis was undertaken, the lubricant supply and the contact were restored and the experiment continued once again.
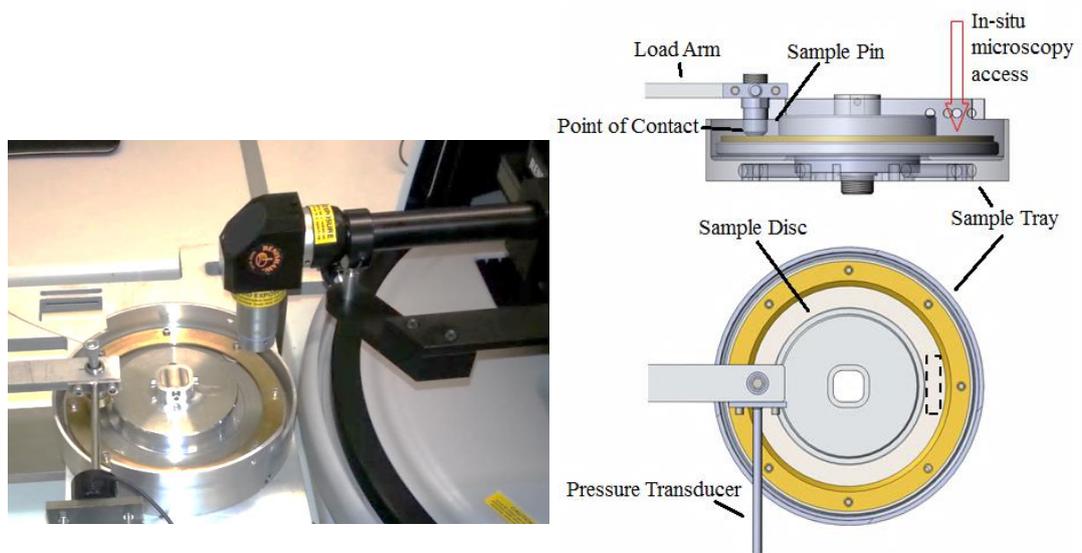
Figure 4.12 Experimental setup of the *in-situ* rig with the flexible sample arm to analyse the tribofilm development under real time conditions.

4.3 Materials

The chemical structures, chemical and physical properties of the specimens (lubricants and additives) investigated in this work are listed in the following paragraphs.

4.3.1 Poly-alpha-olefin Group IV base stock (PAO4).

Engine oil basestocks of poly-alpha-olefin Group IV, provided by Afton Chemical Ltd. is used as a base oil for all of the model oils. PAO4 is a synthetic high performance basestocks and used in many industrial and automotive lubricant applications. The primary function of the base fluid is to facilitate lubrication; that is, to provide a fluid layer between moving surfaces to minimize friction, hence heat and wear.

Polyalphaolefiin fluids, or PAOs, are synthetic, saturated hydrocarbons that are manufactured by a two-step process from linear alpha-olefins [135]. For the synthetic lubricant base fluids (PAOs 2-10 cSt), mainly 1-Decene is oligomerized. A molecular structure of a typical PAO components is shown in Figure 4.13 and typical properties of PAO4 provided in Table 4.5.
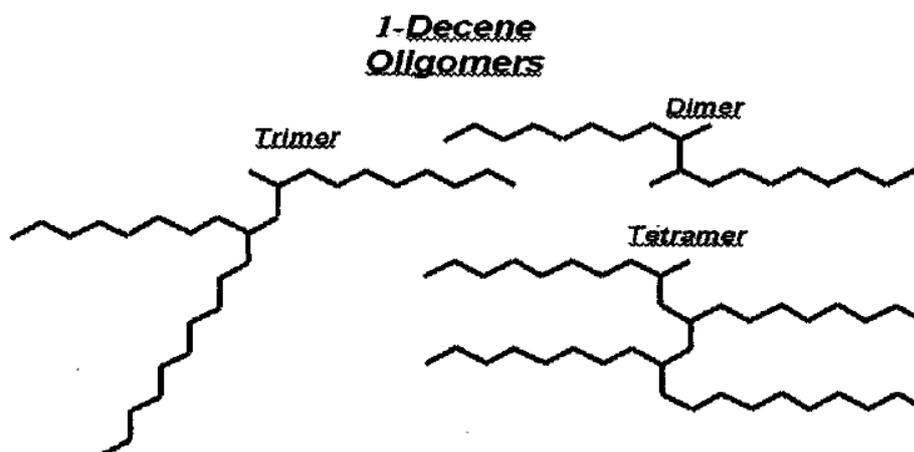
Figure 4.13 Typical molecular structures of a dimer, trimer and a tetramer of 1-decene. For PAO components, mainly 1-decene is usually oligomerized to manufacture the synthetic lubricant base fluids [135].

Table 4.5 Physical and chemical properties of PAO4

Form	Oily liquid
Appearance	Clear and bright
Pour point	-68ºC
Flash point	226ºC
Viscosity index	122
Viscosity at 40ºC	0.1267 Pa s
Viscosity at 100ºC	0.0026 Pa s

4.3.2 Lubricant additives

Model oils containing lubricant additives of Molybdenum dialkyldithiocarbamate (MoDTC), Zinc dialkyldithiophosphate (ZDDP) and the lubricant containing both the additives were blended and provided by Afton Chemical Ltd. All of the additives were blended with the base stock of PAO4 lubricant. Table 4.5 gives the physical properties of the model oils used.

Table 4.6 List of lubricant additives and their properties (Base oil of all the model oils are poly-alpha-olefin Group IV base stock PAO4)

	Molybdenum dialkyldihocarbam - ate (MoDTC)	Zinc dialkyldithiophosph - ate (ZDDP)	Molybdenum dialkyldithiocarbamate (MoDTC) + Zinc dialkyldithiophosphate (ZDDP)
Treat rate (%)	100 ppm Mo	0.08% P	100 ppm Mo, 0.08% P
Viscosity at 100ºC (Pa s)	0.0029	0.0032	0.0028

ZDDPs can be grouped in three sub-classes on the base of their chemical structure: primary, secondary and aryl ZDDP, where its chemical structure is dependent on the type of alcohols used for synthesis [136]. The anti-wear additive of ZDDP used in the research is that of the secondary type.
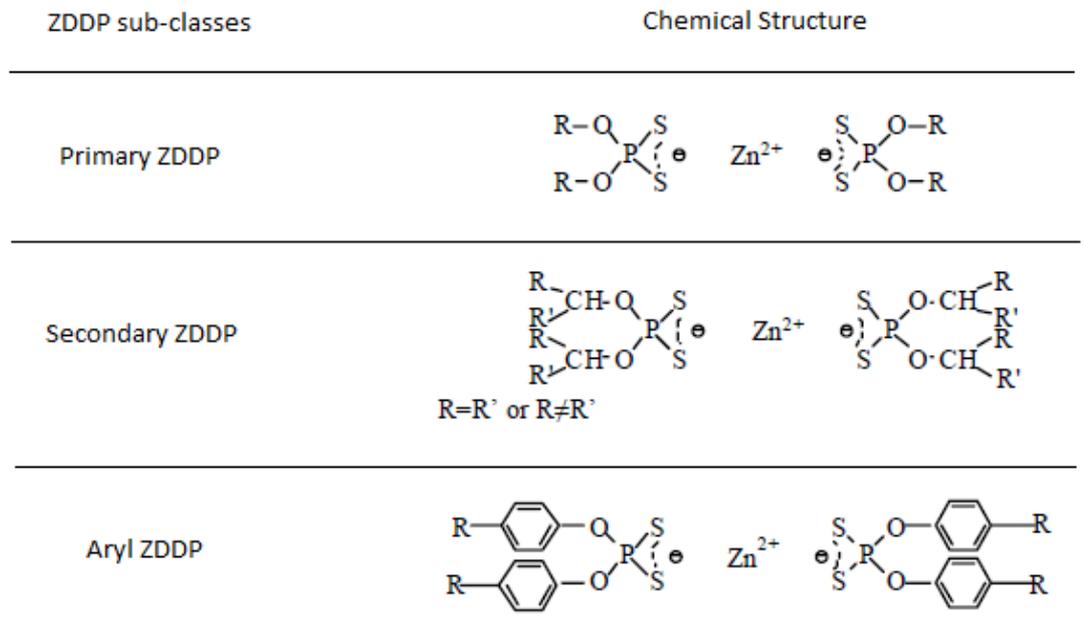
Figure 4.14 ZDDP sub-classes and their chemical structure [136].

4.4 Summary

This chapter describes the experimental techniques and methods of analysis which are used in the tribochemical study of lubricant additives of MoDTC and ZDDP. Methods of surface analysis used to conduct a comprehensive investigation on the tribofilms are presented. The development of the new *in-situ* rig has been presented along with its set-up with Raman for *in-situ* analysis. Figure 4.15 demonstrates the overall procedure of experimental work throughout the project.
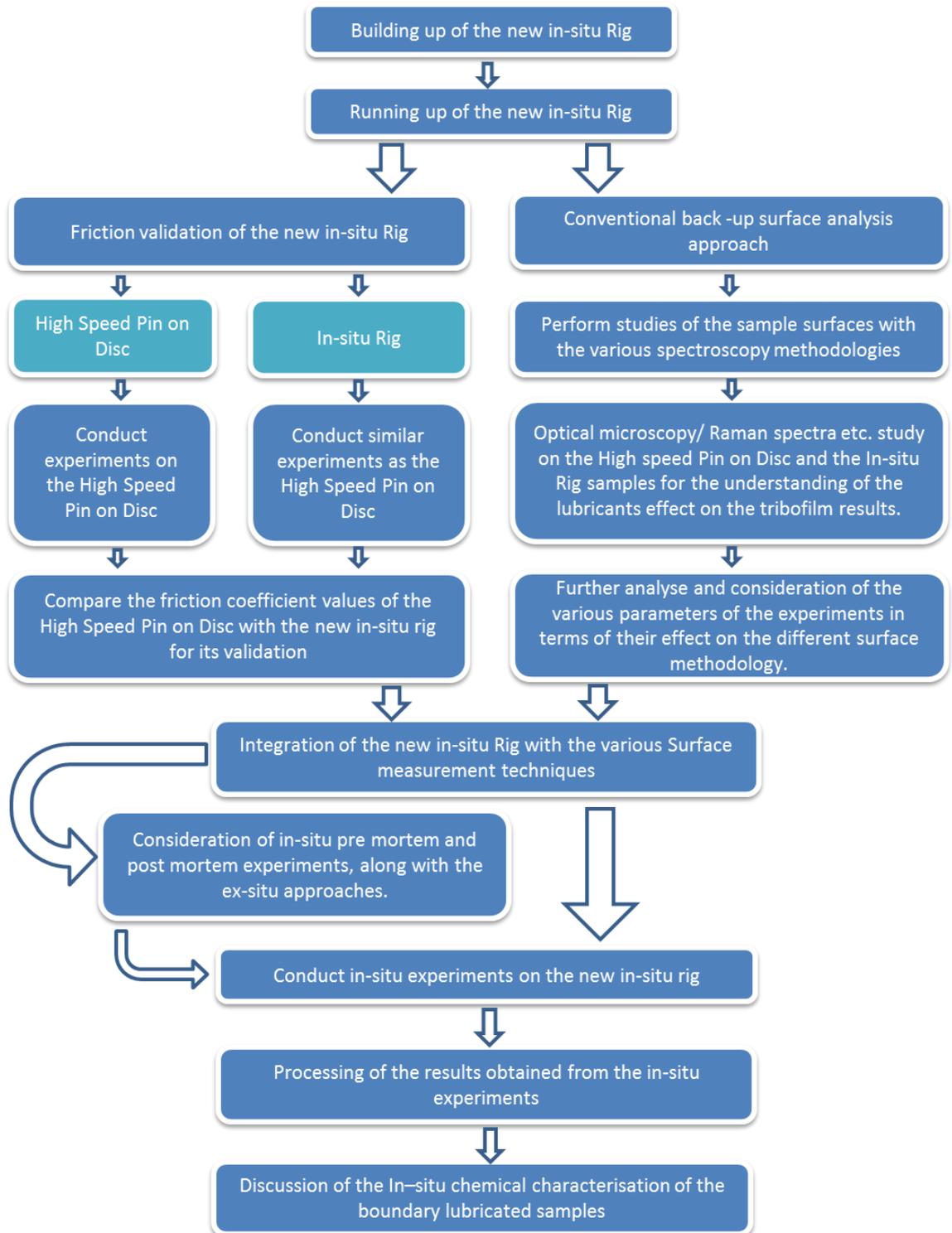
Figure 4.15 Procedures of experimental work outlined

Chapter 5
Influence of Raman Parameters and its Application Towards Understanding Tribological Processes

Raman spectroscopy is a well-known useful technique for determining molecular structure and possesses several advantages in terms of gathering information. Chapters 2 and 3 highlighted the application of Raman spectroscopy for various tribology studies and describes its potential towards the understanding of various tribological processses.

However Raman effect and its detection requires a sensitive and highly optimized instrumentation. Getting the signal optimised in Raman spectroscopy is challenging and there is also the potential for sample damage to occur due to excessive heating of the local area.

Phenomenon such as fluorescence are known to provide a major problem with respect to the collection of a Raman signal. Similarly various lasers are utilised as an ideal light source for the generation of Raman scattered photons. Optimisation is required since the higher power to obtain a better Raman signal leads to sample heating through intense laser radiation which can destroy the sample.

Therefore an initial study was conducted to understand the Raman effects and its influence on the characteristic nature of tribological samples. This chapter focusses on optimisation of Raman spectroscopy for the study of tribochemical surfaces.

5.1 Raman characteristics of MoS$_2$

MoS$_2$ is postulated to be an integral part of the tribofilms formed in this study. As such its molecular structure is vital towards understanding the performance of lubricants and tribocouples in boundary lubrication. Previous Raman spectroscopic studies of MoS$_2$ have specified the presence of four first-order Raman active modes that are present at 286 cm^{-1}, 383 cm^{-1}, 408 cm^{-1} and 32 cm^{-1} [2] (Figure 5.1).
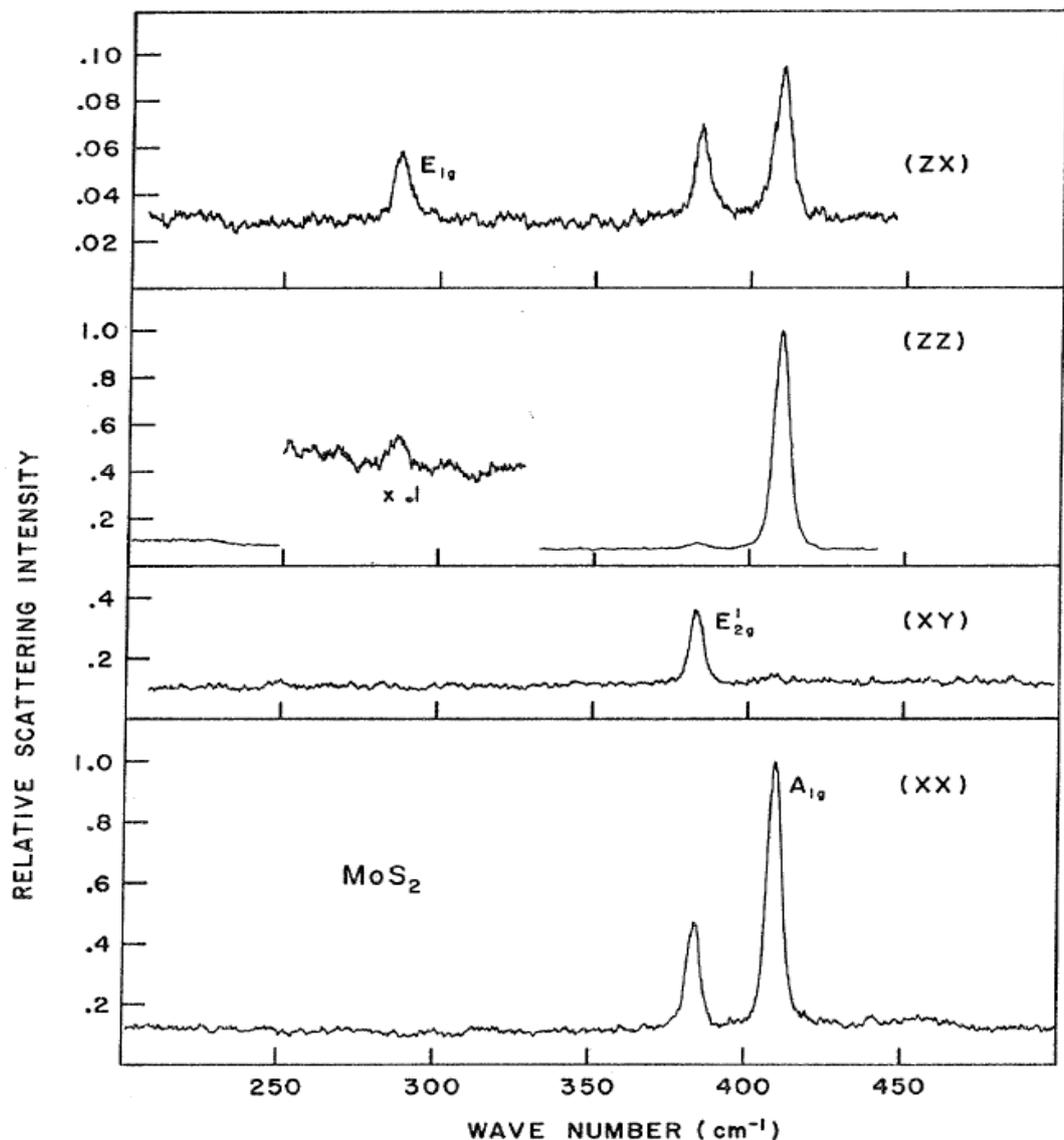
Figure 5.1 Raman spectrum of MoS$_2$(2H) at room temperature under different polarization [2].

The peaks at 286 cm^{-1}, 383 cm^{-1} and 408 cm^{-1} namely E_{1g}, E^1_{2g} and A_{1g} respectively, are the results of the vibrational mode within the sulphur-molybdenum-sulphur layer and the 32 cm^{-1} (E^2_{2g}) is due to the vibration of the adjoining rigid layers [2, 137]. Among the entire first order MoS$_2$ Raman active modes, two modes at 383 and 408 cm^{-1} show a well-defined peak for the structure of MoS$_2$.

The frequency mode of 383 cm^{-1} (in plane E^1_{2g} mode) has been assigned to the motion of the Mo+S atoms in the x-y layered plane of the unit cell, which results from the opposite vibration of two S atoms with respect to the Mo atom (Figure 5.2) [138]

The 408 cm^{-1} frequency (out of plane A_{1g} mode) is assigned to the motion of the S atoms along the z axis of the unit cell in opposite direction (Figure 5.2) [138]. Raman active modes for the MoS$_2$ therefore shows its characteristic peaks at 383 and 408 cm^{-1}.

Quantification of these Raman modes for the MoS$_2$ molecule are carried out by conducting a Raman analysis on a Molybdenum (IV) sulphide powder (Sigma-Aldrich, <2 micron. 99%) sample.

A_{1g} E^1_{2g} E^2_{2g} E_{1g}
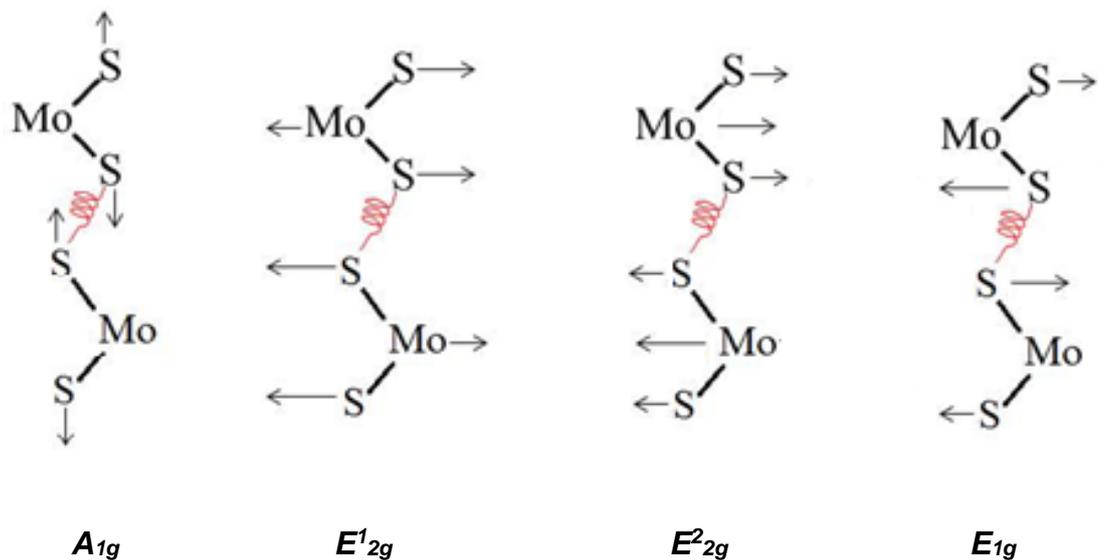
Figure 5.2 In plane phonon modes of E_{1g}, E^1_{2g} and E^2_{2g} and the out of plane phonon mode A_{1g} of the MoS$_2$ molecule [2].

5.1.1 Influence of Raman laser wavelength

Raman analysis of the Molybdenum (IV) sulphide powder sample was carried out with the laser wavelength of 488 nm and 785 nm at a laser power of 1% each. The 488 and 785 nm wavelength lasers operates at a maximum laser power of 10 and 220 mW at the source, respectively. The spectra for each laser wavelength is presented in Figure 5.3. MoS_2 powder sample was placed on a steel substrate and each scan was repeated over the same area to maintain the conformity of the analysis. Each scan was carried out with an exposure time of 1 second and an accumulation of 30 scans.
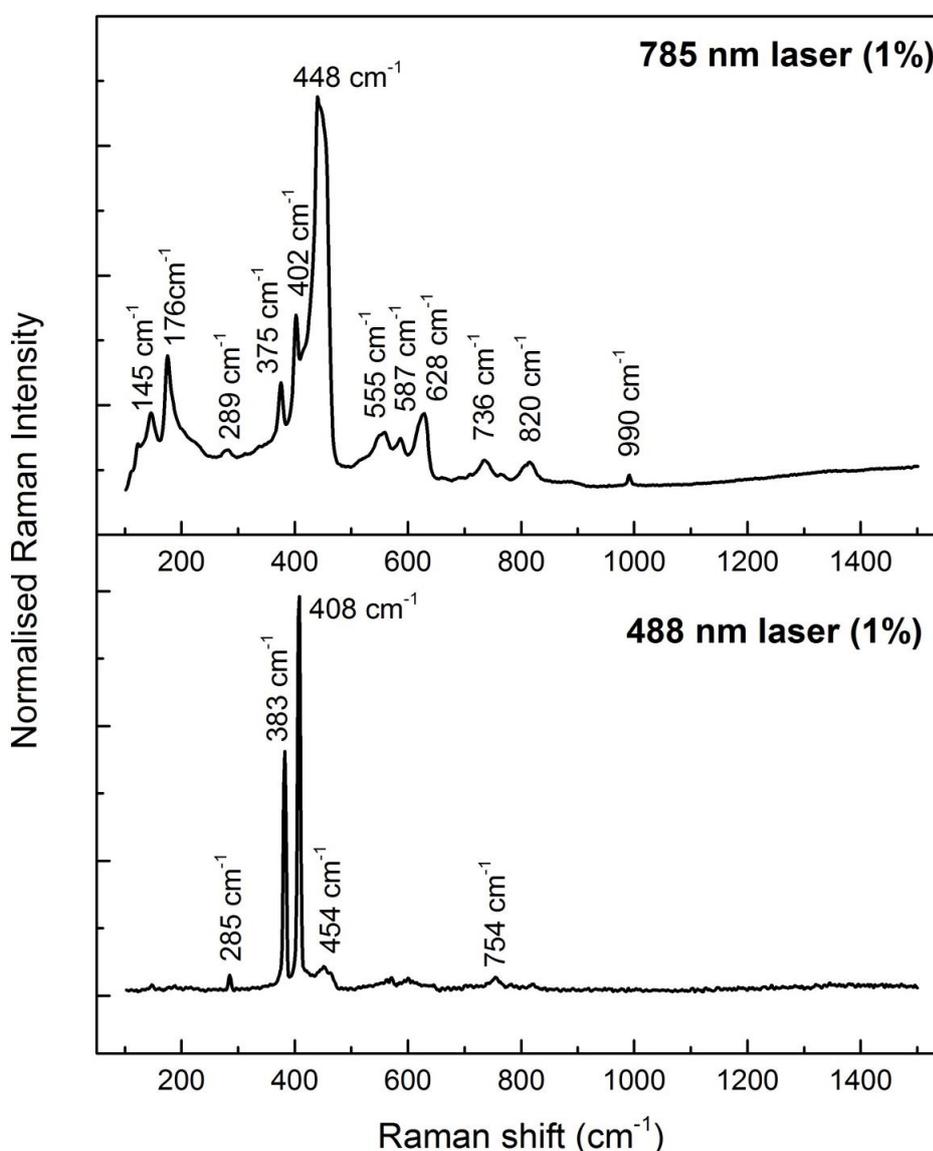
Figure 5.3 Raman analysis of the Molybdenum (IV) sulphide powder (Sigma-Aldrich, <2 micron. 99%) sample with 488 nm and 785 nm laser at 1 % power.

Use of 488 nm laser wavelength at 1% power shows the characteristic E_{1g}, E^1_{2g} and A_{1g} first order peaks at 285, 383 and 408 cm^{-1} for the MoS$_2$ powder sample. A broad band centred around 454 cm^{-1} is observed at the Raman spectra for the 488 nm laser. This band has been attributed to the 2LA(M) mode for the second order Raman bands of the MoS$_2$ molecule and a feature present typically because of a resonance effect [137, 139]. Similarly a peak at 754 cm^{-1} is also observed which is identified as $2E^1_{2g}$ which is produced due to the overtone process of E^1_{2g} modes itself [137, 139].

Windom *et al* [137] indicated that two wavelengths at 652.6 nm and 590.5 nm had strong absorption for MoS$_2$, similar to Stacy and Hodul [140]. The excitation laser photon energy corresponding with the absorption band causes strong coupling of energy into phonon modes. This energy therefore combines with the four first-order Raman frequencies creating additional energy states that can be excited, resulting in a variety of new second-order emission lines. They showed that the Raman spectra of MoS$_2$ are significantly different when an excitation source near the absorption band was used.

The use of 785 nm wavelength laser similarly shows the occurrence of various Raman peaks for the MoS$_2$ powder sample compared to that of the 488 nm laser wavelength (Figure 5.3). The first order peaks E^1_{2g} and A_{1g} at 383 and 408 cm^{-1} for the MoS$_2$ powder sample at 488 nm laser wavelength has been observed to be shifted towards 375 and 402 cm^{-1}. The band attributed to the 2LA(M) mode at 454 cm^{-1} has shifted to 448 cm^{-1} and a higher intensity is observed. Windom et al [137] explains the band around the 450 – 460 cm^{-1} may be a merger of the 2LA(M) mode with some additional mode that becomes more pronounced when resonance occurs, as photon energies near to that of the excitation energies. Raman peaks at 145 and 176 cm^{-1} could be probably because of resonance difference process, which creates a phonon and absorbs another [139]. Similarly, Raman peaks occurring at 555, 587, 628, 736 cm^{-1} are a combination of various resonance effects and optical mode peaks, giving rise to extensive second order peak of the MoS$_2$ powder sample [137].

However, a close observation on the MoS$_2$ powder sample following the analysis with the 785 nm laser wavelength even under a laser power of 1 %

showed the sample to be burned due to laser heating. Hence, the peak shift of E^1_{2g} and A_{1g} to lower cm^{-1} positions at 375 and 402 cm^{-1} was due to the heat induced phase transition [137].

Similarly, when the powder sample is irradiated with high laser power, the presence of the 820 and 994 cm^{-1} MoO_3 bands has also been reported for MoS_2 sample due to rapid oxidation [137]. Raman bands for the MoO_3 are exhibited at 998, 821, 668, 474, 381, 367, 341, 294, 286, 248, 220 and 200 cm^{-1} for different orders [141, 142]. The Raman band at 820 cm^{-1} is regarded as the symmetry related vibrational mode and is very sharp and the most intense Raman band in the spectrum. Similar Raman peaks at 820 and 990 cm^{-1} can be observed for the Raman spectrum of the 785 nm laser wavelength in Figure 5.3. These peaks corresponds to the oxidation of MoS_2 powder sample due to the local laser heating.

The Raman spectrum observed for the MoS_2 powder is therefore dependent on the laser wavelength. The Raman spectrum of MoS_2 powder is dominated by the two vibrational modes of E^1_{2g} and A_{1g} at 488 nm wavelength. However, more complex spectra are observed due to the resonant excitation of MoS_2 with the use of 785 nm wavelength laser.

Second-order Raman scattering processes, which are enhanced by the coupling of phonon modes to electronic states excited optically in the sample with the use of 785 nm wavelength laser, and are more effective than the modes related to the first-order Raman scattering. The use of 785 nm induced a rapid oxidation process even at a lower percentage due to its high rated power. The powder sample is easily subjected to local heating due to laser irradiation changing the phonon modes. Shift of the E^1_{2g} and A_{1g} to lower cm^{-1} positions, along with the origin of MoO_3 Raman band indicates the change in the structure of the MoS_2 powder sample due to the local laser heating.

5.1.2 Influence of Raman laser power

Laser power is the percentage of maximum laser power that is used for the acquisition of Raman spectrum. The influence of the laser power is a major concern due to induced damage in sample because of local heating. The 785 nm wavelength laser is rapid in inducing changes on the Raman spectrum of the MoS_2 powder due to its high rated power, and hence the 488 nm laser is subjected to increasing laser power to study the influence of local heating.

Figure 5.4 (a) shows the relative Raman spectra of the MoS_2 powder as a function of the various laser powers of the 488 nm laser. It can be observed that with the increase of power a better signal to noise ratio is achieved, with more defined peaks of MoS_2.

First order peaks of E_{1g}, E^1_{2g} and A_{1g} are observed along with the presence of 2LA(M) mode for the second order MoS_2 Raman bands. However, with higher laser power, oxidation peaks around 820 and 990 cm^{-1} become more defined and intense, indicating a transition of MoS_2 to MoO_3 with the increase in laser energy.

Figure 5.4 (b) shows the influence of 488 nm laser power on the characteristic vibrational modes of E^1_{2g} and A_{1g}. A closer observation shows the shift of the E^1_{2g} and A_{1g} peak to lower cm^{-1} with the increase in the laser power. The characteristic peaks of MoS_2 shift to 375 and 400 cm^{-1} at higher laser power, a peak value similar to those observed with the 785 nm laser.

The peaks identified in MoS_2 powder sample at higher laser power, shows the shift of E^1_{2g} and A_{1g} peak to lower cm^{-1} with the increase in laser power. This induced change is attributed to localized heating occurring from the laser interaction changing the phonon modes associated with the sample structure. The MoO_3 oxidation band around 820 cm^{-1} becomes more evident with increasing laser power which indicates a transition of MoS_2 to MoO_3 due to rapid oxidation.
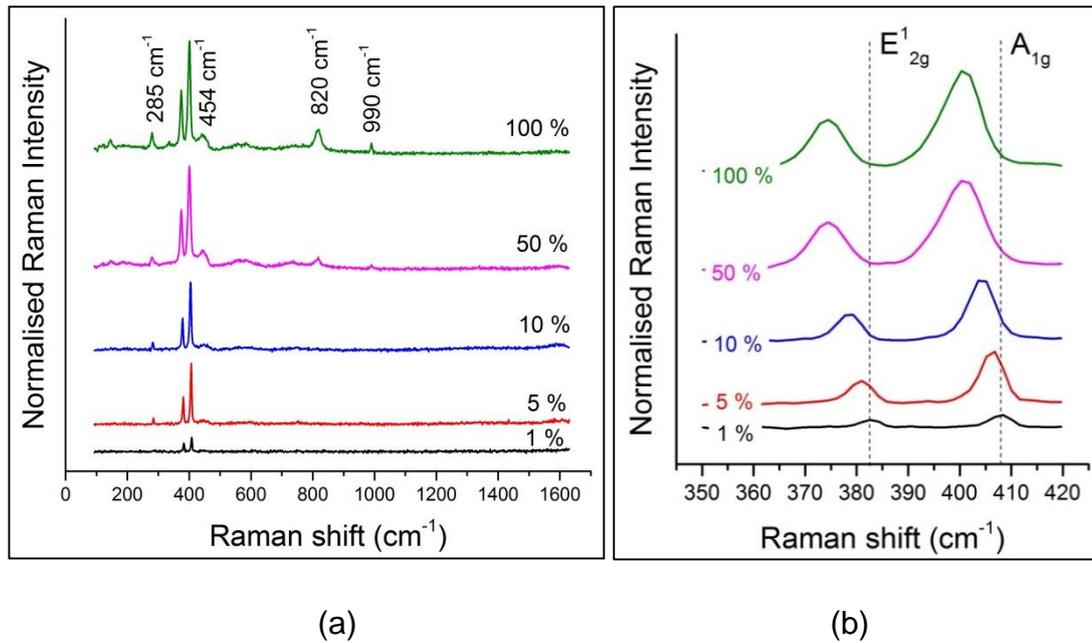
Figure 5.4 (a) Raman spectra (488 nm excitation) at room temperature of microcrystalline MoS_2 powder at various laser power values as indicated. (b) Raman spectra showing the shift of the E^1_{2g} and A_{1g} peaks of the microcrystalline MoS_2 powder at various laser power values as indicated.

5.1.3 Influence of oil on the Raman characteristic of MoS_2 powder

MoS_2 powder sample shows that the laser power causes localized heating which changes the phonon modes associated with the MoS_2 powder structure. The formation of a MoS_2 containing tribofilm from the MoDTC additive means that the MoS_2 is formed in a lubricated environment with the use of a certain base oil. Hence, the influence of the base oil on the Raman characteristic of MoS_2 is important to understand the characteristic of the MoS_2 tribofilms.

The synthetic poly (alpha-olefin) (PAO4) oil has been used as a base oil in all of the experiments. Polyalphaolefins (PAOs) are synthetic hydrocarbons and developed as a high performance base-stock for automotive and industrial applications [143]. Alpha-olefins are a class of olefins having a carbon–carbon double bond between the first and second carbon atoms of the hydrocarbon chain. PAOs are composed of hydrogenated olefin (alkene) oligomers having the general formula of C_nH_{2n}.

Figure 5.5 provides a Raman spectrum of the PAO4 base oil dispersed on a steel substrate with the 488 nm laser wavelength. Raman peaks at 1300 and 1447 cm^{-1} are CH deformation vibrations and are usually with a weak intensity. However, the Raman response of the PAO is usually characterised with various C-H stretching vibrations between 2800 – 3000 cm^{-1} [144].

To observe the Raman characteristics of the MoS$_2$ sample when covered with the base oil, MoS$_2$ powder was placed on a steel substrate and a drop of the base oil poured on to the powder. Similar procedures of Raman analysis conducted on the MoS$_2$ powder were followed (See section 5.1.2) with varying the laser power and an exposure time of 1 second and an accumulation of 30 scans.

Figure 5.6 shows a stronger signal to noise ratio is achieved on the sample when the laser power is increased. First order peaks of E_{1g}, E^1_{2g} and A_{1g} are observed along with the C-H stretching vibrations of the base oil PAO4. However, at a laser power of 100 %, a high background leading to signal saturation is observed for the sample analysed with the decrease in intensity for the E^1_{2g} and A_{1g} MoS$_2$ Raman peaks.

In particular, background includes luminescence of cell, sample, or optics (e.g., fluorescene, thermal emission), and stray laser light, including Rayleigh scattering, reflection from optics or dust [145]. Due to the high laser power of 100 %, some energy of the excitation photon can be absorbed by the molecule of the oil hence undergoing energy transmission. A phenomenon of fluorescence therefore occurs and provides a higher background, along with the decrease in intensity for the E^1_{2g} and A_{1g} MoS$_2$ Raman peaks.
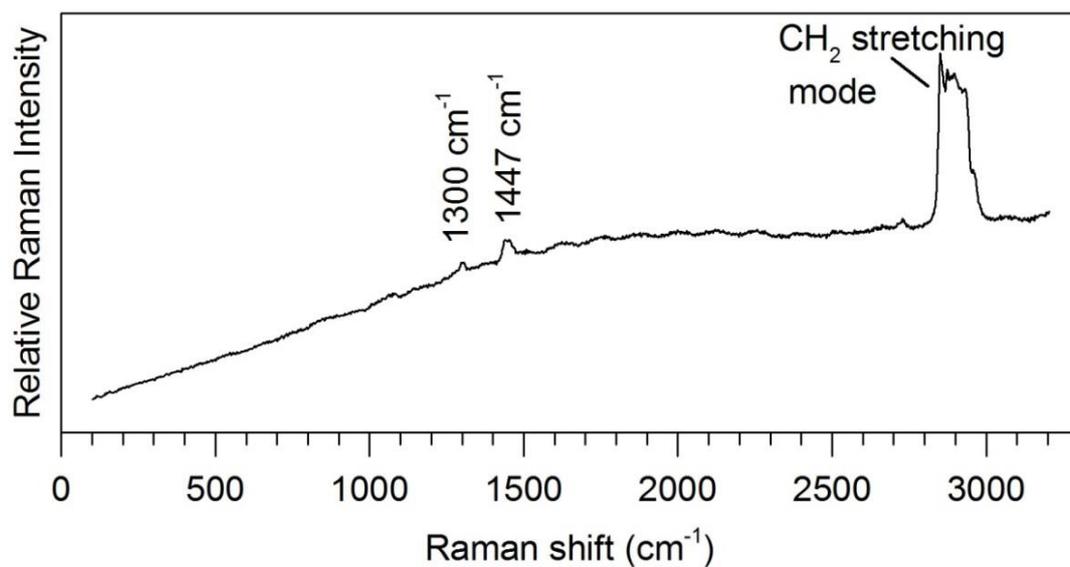
Figure 5.5 Raman spectrum (488 nm excitation at 100% laser power) of base oil polyalphaolefin (PAO4) layer dispersed on a steel sample.
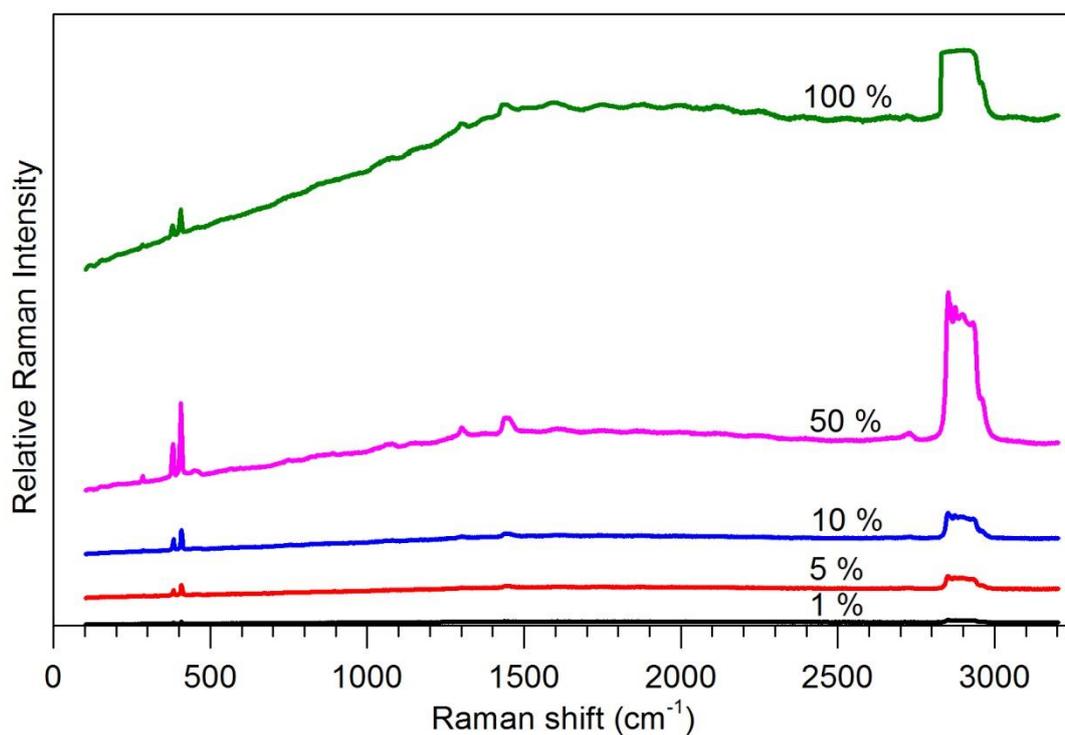
Figure 5.6 Raman spectra (488 nm excitation) of MoS_2 powder covered with base oil polyalphaolefin (PAO4).

Figure 5.7 gives a closer look on the E^1_{2g} and A_{1g} MoS$_2$ Raman peaks obtained in these conditions. With the increase of laser power, a minimal shift of the Raman peaks is observed. The reason for this shift could be explained when considering the results shown in Figure 5.4 (a). Any Raman response around the oxidation peak of 820 cm^{-1} is absent for the MoS$_2$ powder on oil, hence confirming that laser induced changes due to local heating has not occurred. The laser photon energy is therefore absorbed by the MoS$_2$ sample along with the oil and distributed to produce the Raman spectra. The influence of the base oil on the Raman spectra of the MoS$_2$ is observed to be minimal, however with higher laser energy the Raman spectra is bound to have a higher background due to the influence of fluorescence.
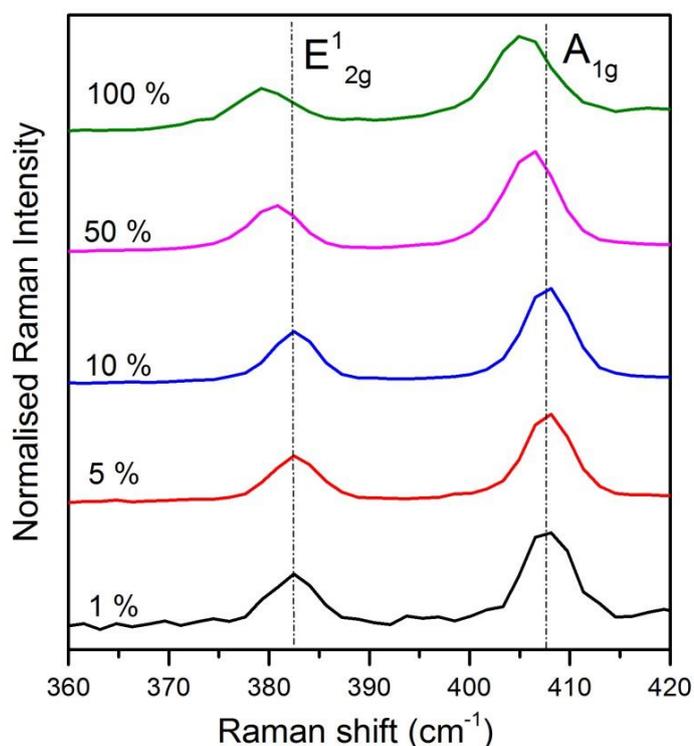
Figure 5.7 Raman spectra (488 nm excitation) of the E^1_{2g} and A_{1g} mode of the MoS$_2$ powder sample covered with the base oil polyalphaolefin (PAO4) at varying laser powers.

5.2 Raman characteristics of MoDTC tribofilm

Experiments were conducted using the High Speed Pin on Disc (HSPOD) tribometer to form MoS$_2$ tribofilms under boundary lubrication conditions. Operating parameters with a speed of 500 rpm, 1.02 GPa Hertzian pressure and a temperature of 100°C were chosen for the experiments. Test conditions were chosen to represent conditions where the friction reduction occurs due to the formation of a MoDTC tribofilm.

Figure 5.8 shows the friction coefficient of the MoDTC lubricant at a temperature of 100°C as a function of time. MoDTC lubricant, in the presence of high temperature reduces the friction coefficient dramatically within the first 10 to 20 minutes and reaches a constant value of around 0.04. The reduction of friction by the MoDTC additive has been attributed to the formation of a MoS$_2$-containing tribofilm on the tribological contact [41, 43, 44, 50, 146]. Raman analysis on the wear track was performed with the 488 nm laser, being guided by the analysis of MoS$_2$ powder as a function of various laser powers repeated in the previous section.
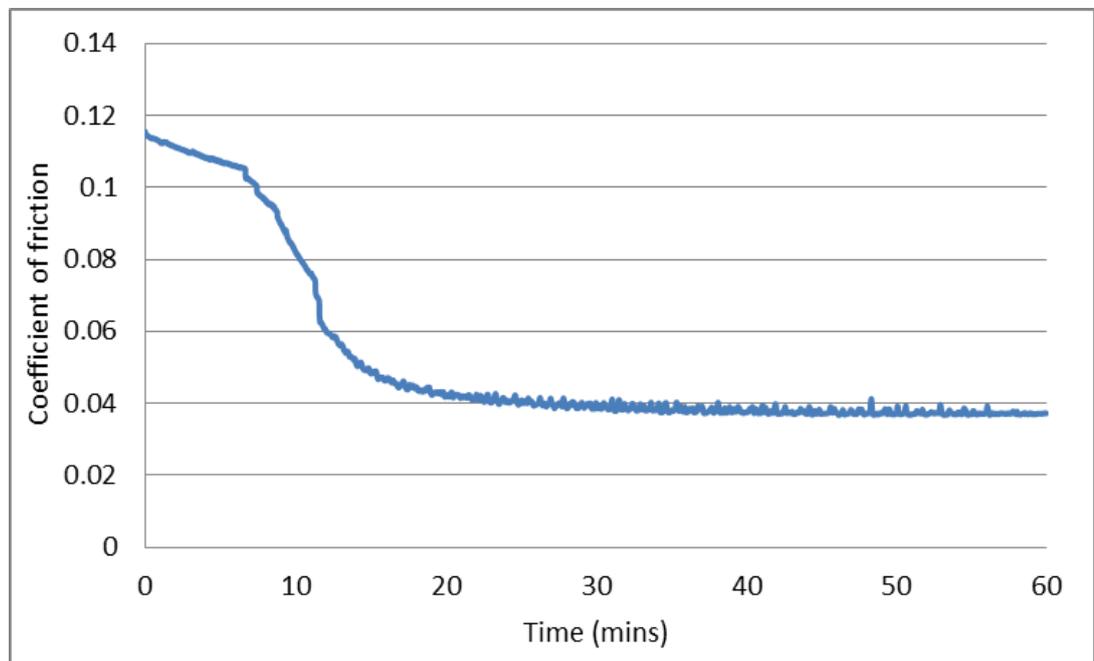
Figure 5.8 Friction values of the High Speed Pin on Disc experiment with the MoDTC lubricant at a temperature of 100°C under boundary lubricated conditions of 1.5 kg load and sliding speed of 500 rpm.

Figure 5.9 shows a Raman spectrum for the 1 hour time period 100°C HSPOD samples, which shows a typical characteristic of the MoS_2 tribofilm at 5% laser power. The two characteristic peaks have been defined at the peak position of 379 and 410 cm^{-1}, in agreement with what has has been observed and reported for the MoS_2 tribofilm in literature [43, 44].

In comparison to the Raman spectrum of the MoS_2 powder, the peaks of MoS_2 tribofilm have a shift of 2 -3 cm^{-1} in the peak values of E^1_{2g} and A_{1g} vibrational mode. The shift in the tribofilm could be a result of the induced pressure during the experiment which initiates vibrational changes in the multi-layered MoS_2 [147] due to stress-induced disorder. Kong et al [55] also showed that MoS_2 films with vertically aligned layers that expose edges of the layers to have exhibit high surface energy. The out-of plane Mo−S phonon mode (A_{1g}) was preferentially excited for edge-terminated film due to the polarization dependence, whereas the in-plane Mo−S phonon mode (E^1_{2g}) was preferentially excited for terrace-terminated film.

E^1_{2g} and A_{1g} Raman mode of MoS_2 tribofilm is also observed at a lower intensity in comparison to MoS_2 powder sample, along with a wider FWHM under similar Raman analysis parameter. The intensity of two characteristic Raman peaks significantly increases and the E^1_{2g} peak width narrows when the MoS_2 film is subjected to high crystalline [148]. Peak positions and FWHMs of the A_{1g} and E^1_{2g} peaks are also shown to be affected by temperature [149].

The Raman spectra of MoS_2 tribofilm also exhibited peaks at 660 and 923 cm^{-1} with higher laser powers, which corresponds to various Fe and Mo oxide [150, 151], along with the broad D and G graphitic carbon peaks arising from the steel substrate (Figure 5.10). Raman signal strength is directly proportional to the power of the Raman laser exciting the sample, hence with the increase in laser power, a higher response of Raman signal for the samples is achieved.

The spectrum from MoDTC tribofilm when analysed with the 788 nm laser wavelength did not show any significant peaks. A high background is observed in the region where MoS_2 first-order modes are expected to be observed.
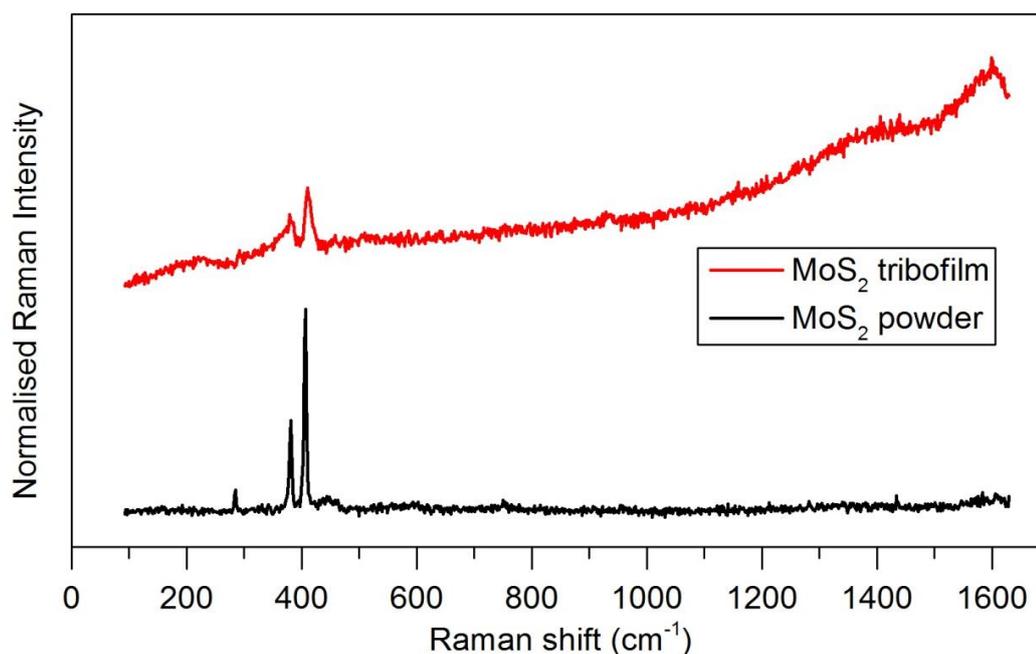
Figure 5.9 Raman spectrum (488 nm excitation) of the MoS_2 tribofilm, in comparison to the pure MoS_2 powder at a laser power of 5 %.

5.2.1 Influence of Raman laser power on MoS_2 tribofilm

In section 5.1 the Raman spectra of the MoS_2 powder sample are shown to be highly dependent of the laser power. High laser power can result in localized heating with rapid oxidation occurring from the laser interaction changing the phonon modes associated with the sample structure. Hence, similar laser excitation Raman study with various laser powers was conducted on the tribofilm of MoS_2.

Figure 5.10 presents the Raman spectra of the MoS_2 tribofilm conducted at various laser power intensity values. With the increase of laser power, a higher signal to noise ratio is achieved. The Raman peaks are more defined along with the observation of the D and G broad band occurring from the steel substrate and the hydrocarbon stretching bands from the oil. At a laser power of 1 % the Raman spectra was characterised with a lot of noise and no characteristic peaks were observed. The E^1_{2g} and A_{1g} vibrational mode of the MoS_2 tribofilm is defined at the peak position of 379 and 410 cm^{-1}. A closer observation of the E^1_{2g} and A_{1g} peak at Figure 5.11 shows that no shift occurs with the increase in laser power. Therefore, with the increase of laser power, the sample of MoS_2 tribofilm is not shown to experience any thermal or photolytic damage to the sample.
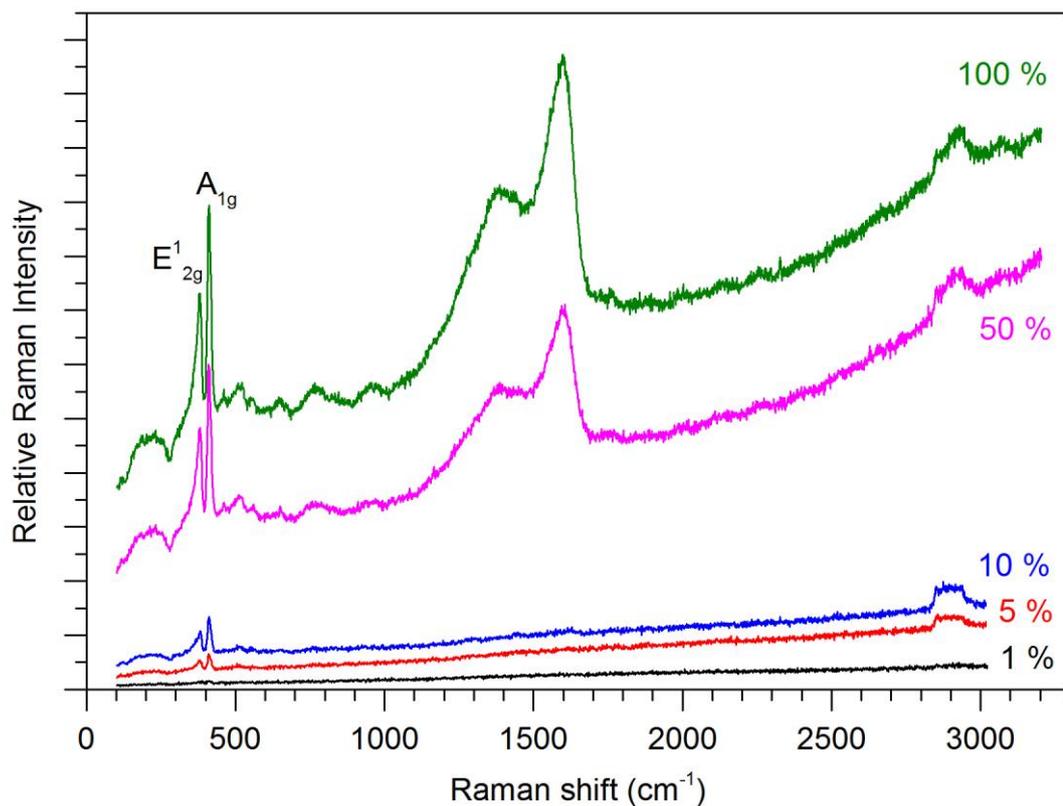
Figure 5.10 Raman spectra (488 nm excitation) of MoS$_2$ tribofilm conducted at ambient conditions with various laser power as indicated
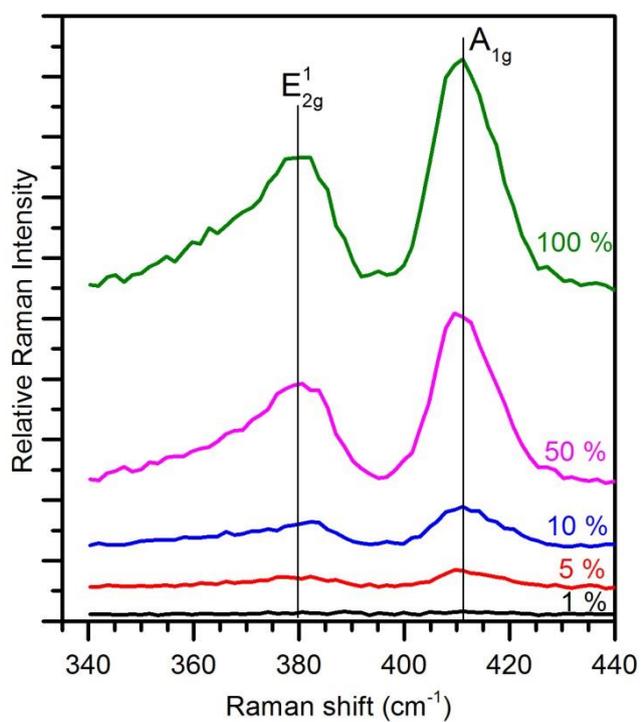
Figure 5.11 Raman spectra showing the shift of the E^1_{2g} and A_{1g} peaks of the MoS$_2$ tribofilm, at various laser power as indicated.

5.2.2 Influence of acquisition parameters on Raman results

For a given sample and laser power, increasing laser power will increase the signal and signal-to-noise ratio (SNR) and high laser power is desirable in this regard. Hence, the ability to extract analytical information from any spectroscopic technique is usually limited by the SNR for the conditions employed [145]. Exposure time and the number of accumulations enable the control of data acquisition and is usually related with the reduction of noise.

Figure 5.12 shows the Raman spectra of one accumulation for the MoS_2 tribofilm with various exposure times. Similarly, with an exposure time of 1 second, various accumulations of the MoS_2 tribofilm are obtained in Figure 5.13. The Raman spectra indicates with increase in the exposure time and accumulation, the spectra is enhanced with a high SNR. Any change in peak values for the MoS_2 tribofilm are not observed but weak scattered spectra can be enhanced with a reasonable combination of exposure time and accumulation. However with high exposure time, usually above 30 seconds the CCD detector of the Raman systems is saturated because of the high signal.

Hence, to obtain an optimal signal with a reasonable SNR, Raman spectrum was obtained with an exposure time of 1 second and an accumulation of 30 scans for the tribofilm of MoS_2 at 100 % laser power. High exposure time saturated the Raman signal and higher possibility of sample damage could occur due to extended period of laser exposure. Accumulation of 30 scans provided shorter time period to obtain the Raman spectrum, which provides a benefit towards analysing *in-situ* samples quicker to minimise the environmental effects on the sample.
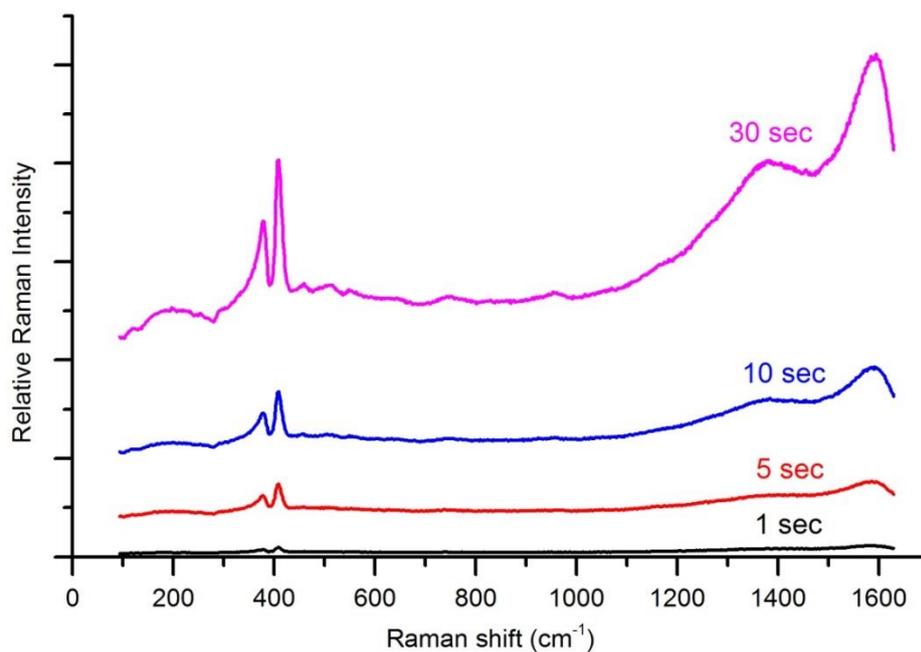
Figure 5.12 Raman spectra of MoS$_2$ tribofilm at 488 nm excitation (100 %) with 1 accumulation at various exposure time as indicated.
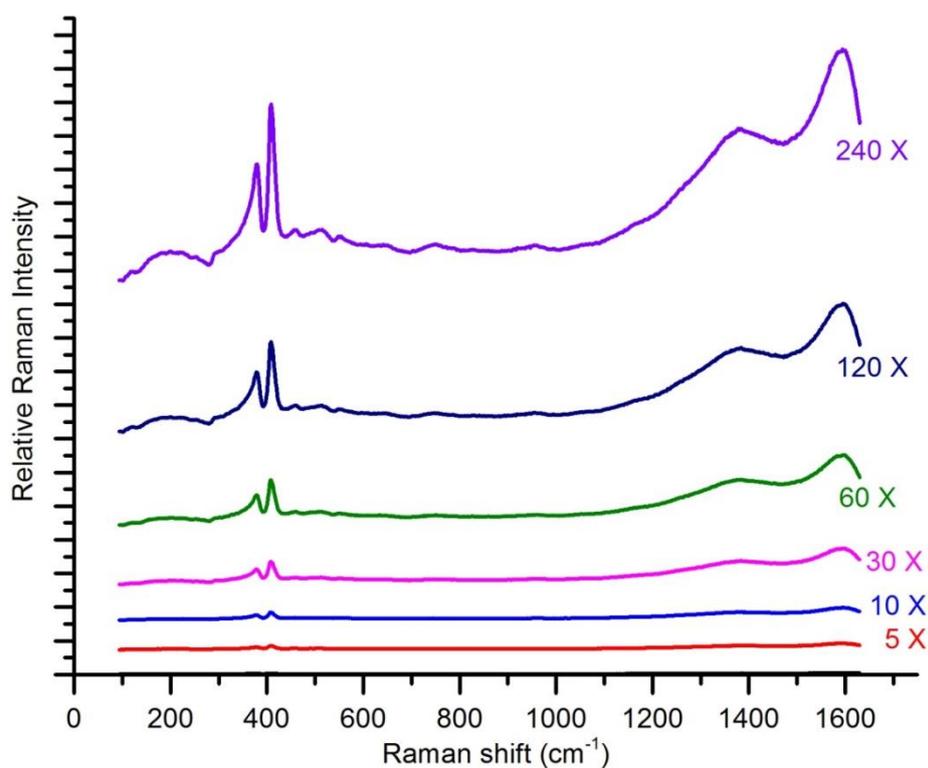
Figure 5.13 Raman spectra of MoS$_2$ tribofilm at 488 nm excitation (100 %) with 1 second exposure time at various accumulation as indicated.

5.2.3 Polarisation effect on Raman peaks obtained from MoS₂ tribofilm

Chen and Wang [139] showed that the first order Raman intensities of MoS_2 due to its crystal lattice layer structure differed due to the polarisation of laser light. The intensity of the A_{1g} mode was twice that of the E^1_{2g} mode using s-polarised laser, whereas the A_{1g} and E^1_{2g} mode have almost equal intensities in p-polarisation mode. Figure 5.14 shows the Raman spectra of the MoS_2 tribofilm obtained from the same spot within a wear scar. The spectra were obtained using three laser polarisations of circular, normal and orthogonal. In all the spectra, E^1_{2g} and A_{1g} peaks were observed at 380 cm^{-1} and 410 cm^{-1}, respectively. No significant differences in the peak intensities of the A_{1g} and E^1_{2g} mode were observed. The A_{1g}/E^1_{2g} ratio was 1.3, 1.25 and 1.27 for circular, normal (s-) and orthogonal (p-) polarisation, respectively. The Raman modes for the MoS_2 tribofilm were not altered with the change in laser polarisation and hence the analysis were conducted with normal (s-) polarisation mode.
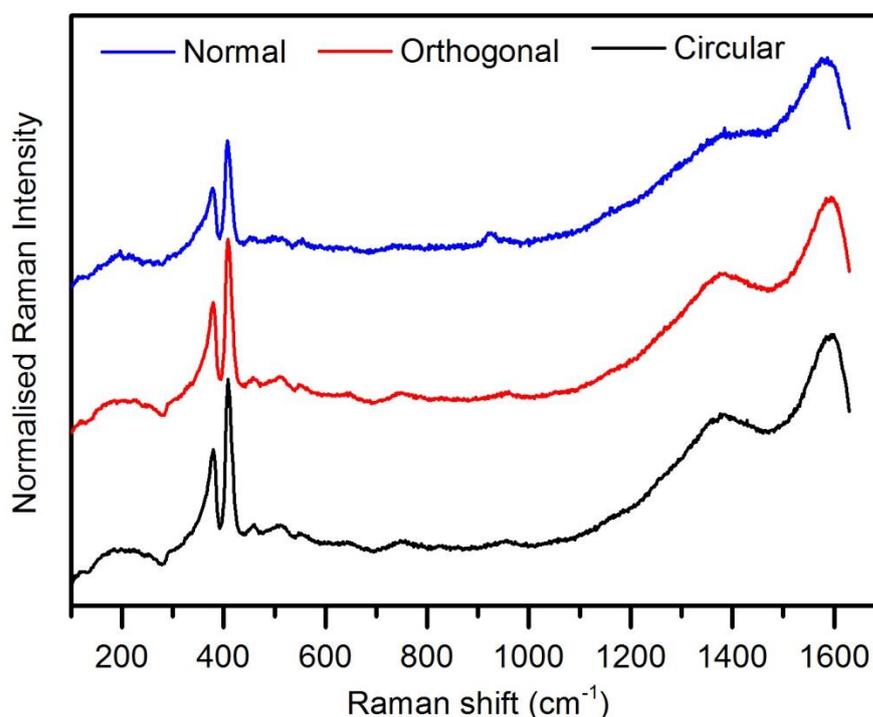
Figure 5.14 Raman spectra of the MoS_2 tribofilm at different laser polarisation. Raman analysis were conducted with the 488 nm laser power at 100%, with an exposure of 1 second and 30 accumulation.

5.2.4 Effect of sample cleaning on the MoS$_2$ tribofilm Raman results

Raman spectroscopy is a surface analysis technique which does not require any form of sample preparation and therefore can facilitate determination of sample surface chemistry without any form of cleaning. However, whilst analysing tribofilms and in the presence of any excess oil on the surface, there is a possibility to observe what is in the oil too. In contrast, vacuum based surface analysis techniques such as X-ray Photoelectron Spectroscopy (XPS), Scanning Electron Microscope (SEM), Secondary Ion Mass Spectrometry (SIMS) etc. require solvent-washed specimens. Therefore, in order to understand the effect of solvent washing on the characteristics of the tribofilm, a Raman analysis was undertaken on a rinsed and unrinsed sample.

The MoS$_2$ tribofilm formed at 100ºC for a time period of 1 hour was analysed with the 488 nm laser excitation at 100 % power with an exposure time of 1 second and 30 accumulations. The samples were analysed firstly without any form of cleaning and the sample was immersed in a chemical solution of pure heptane and rinsed ultrasonically in an ultrasonic bath for 1 minute. Raman analysis was conducted with the same parameters on the solvent cleaned samples.

Figure 5.14 shows comparative Raman spectra of the wear track before and after cleaning the sample. Raman spectra for the non-rinsed samples exhibit sharp and intense peaks for the A$_{1g}$ and E$^1_{2g}$ modes of the MoS$_2$ molecule. Broad and less intense peaks are also observed around the peak values of 454 cm^{-1}, 514 cm^{-1} and 555 cm^{-1} for the second order modes of the MoS$_2$ molecule [139]. A closer observation also shows a less intense and broad peak at 660 and 920 cm^{-1}, corresponding to various iron oxide and ferrous-molybdenum oxide peaks. The spectra of non rinsed samples are comprised with a hydrocarbon stretching bonds around 2800 – 3100 cm^{-1}, and usually supported with a higher spectrum background.

Rinsed samples do not contain the hydrocarbon stretching bonds but a less intensity and noisy spectrum is produced. Raman peaks for the A$_{1g}$ and E$^1_{2g}$ mode of the MoS$_2$ molecule is not affected and the peak values remain the

same. However weak bands around 660 cm^{-1} and 923 cm^{-1} corresponding to various oxides, are more prominent with the solvent rinsed samples.

The higher background produced due to the effect of the oil on the Raman spectrum, are subsided with rinsing the sample. Raman analysis of the samples are conducted on the samples without any rinsing to promote *in-lubro* analysis. Differences in the Raman spectrum for rinsed and non rinsed are not observed during the course of the study and hence provides a platform to examine the sample with *in-situ* analysis.
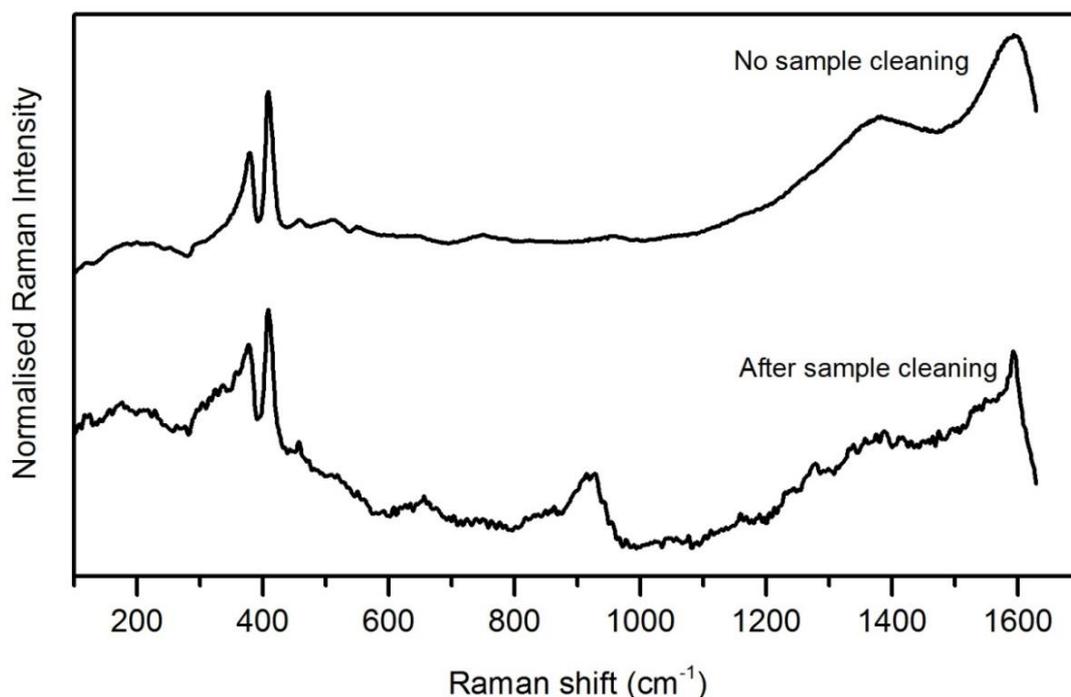
Figure 5.15 Raman spectrum (488 nm excitation) of the MoDTC tribofilm with samples rinsed and unrinsed with a solution of Heptane.

5.3 Summary

In this chapter, an optimisation of Raman spectroscopy parameters and its influence on the study of tribochemical surfaces was presented. Findings in this section can be summarised into the following:

- Raman spectrum of the MoS_2 powder sample was dependent on the laser wavelength. Visible laser wavelength of 488 nm gave a response of typical first order Raman scattering of MoS_2, whereas near infra-red lasers of 785 nm were complementary with first and second order Raman scattering.

- However, the Raman spectrum of the MoS_2 powder sample was more dependent on laser power. With higher laser power, Raman response showed a transition of MoS_2 powder to MoO_3 due to localized heating.

- With the presence of oil on the powder sample, some energy of the excitation photon can be absorbed by the molecule of the oil hence undergoing energy transmission and inhibiting localized heating changes in the MoS_2 powder sample.

- E^1_{2g} and A_{1g} Raman mode of MoS_2 tribofilm in comparison to the MoS_2 powder showed a shift in peak values, with less intensity and broader FWHM.

- The E^1_{2g} and A_{1g} Raman mode of MoS_2 tribofilm was independent of laser power. However when analysed with the 788 nm laser wavelength, Raman spectrum did not show any significant peaks for the MoS_2 tribofilm.

- A reasonable combination of exposure time and accumulation, enabled an optimum MoS_2 tribofilm signal.

- The Raman modes for the MoS_2 tribofilm were not altered with the change in laser polarisation.

- Rinsing the tribofilm, showed a major difference was not observed between rinsed and unrinsed sample. However a noisy spectrum with lower intensity is produced with higher response of weak Raman band in rinsed samples .

Chapter 6
Tribological Performance of Molybdenum Dialkyldithiocarbamate (MoDTC) Under Boundary Lubrication Conditions and its Interaction with Zinc Dialkyldithiophosphate (ZDDP)

Molybdenum Dialkyldithiocarbamate (MoDTC) is a widely known friction modifier additive and is generally accepted to reduce friction under boundary lubrication due to the formation of molybdenum disulphide (MoS_2) [41, 50]. The low friction boundary lubrication regime has been highly credited to the presence of the lattice layer structure of MoS_2 [40]. This level of friction reduction depends on MoDTC type and concentration, operational temperature and the characteristics of type of tribological system such as type of contact, load, surface roughness, type of base oil etc. [43]. However, although the presence of molybdenum disulphide is probable, the chemical pathway by which molybdenum additives react with rubbing surfaces is unclear.

In the first part of this chapter, tribological performance of the lubricant additive MoDTC under varying parameters of load, speed and temperature with the high speed pin on disc (HSPOD) and the new *in-situ* rig are presented. Tribological performance of the MoDTC lubricant additive are explained with reference to the formation of the MoS_2 tribofilm on the contacting surface. The effect of temperature on the rate of formation of MoS_2 is observed. Furthermore durability tests of the MoDTC tribofilm on the contacting surface is presented. The nature of the tribofilms of the MoDTC have been characterized by means of Raman spectroscopy.

The interaction of MoDTC with the ZDDP additive is observed in the second part of this chapter. Frictional results of the MoDTC/ZDDP additive are presented and the tribofilms characterized with Raman spectroscopy, TEM and EDX. Wear analysis for the end of test samples are compared for various lubricant additive systems.

6.1 Tribological performance of tests with MoDTC additive under boundary lubricated conditions

Initial tribological tests were conducted with the MoDTC additive under various operating parameters to understand the tribological performance of the MoDTC additive. Under boundary lubrication, thin surface films formed on the surface determine the nature of the tribological systems. Figure 6.1 shows comparative graphs of friction coefficient for the MoDTC lubricant additive under varying operating parameters of temperature, speed and load with the high speed pin on disc (HSPOD). Each test were conducted for a time period of 1 hour and each samples were analysed with Raman spectroscopy after the test. Among all of the experiments conducted, loads of 7 N and 14 N at the temperature of 100°C and sliding speed of 0.88 m/s, reduces friction instantly due to the formation of the MoS_2 tribofilm. This significant drop in friction is not observed with other experimental parameters for the MoDTC lubricant additive.

Figure 6.2 (a) and 6.3 (a) shows the friction coefficient values at the end of the 1 hour test for the lubricant additive of MoDTC at varying operating parameters of load and sliding speed at high temperature and low temperature respectively. An overall friction value is decreased with the increase of speed. However, with the load of 7 N and 14 N at high temperature of 100°C friction drops instantaneously with rubbing time, and an increase in friction is observed with 14 N load at low temperature.

At higher sliding speed of 1.75 m/s, friction values reaches minimum at the end of the 1 hour test when compared with the lower sliding speed of 0.44 m/s at every defined load. The change in sliding speed also changes the sliding distance over the time period and a detailed discussion is provided in Chapter 8 in relation to the friction and wear values.

Friction is observed to be lowest with the load of 14 N under all of the conditions except under room temperature with the load of 14 N and 0.88 m/s speed. Similarly an increase in friction value is observed with the increase in temperature, which could be due to the reduction in fluid viscosity with the increase in temperature. Friction values at speed of 0.88 m/s with 7 N and 14

N are reduced with high temperature in comparison to the values obtained at room temperature conditions.

At sliding speed of 0.88 m/s and temperature of 100°C, nominal conditions for MoS_2 tribofilm formation is achieved for the additive of MoDTC. Loads of 7 N and 14 N corresponds to 0.8 and 1.02 GPa respectively, and provide enough pressure to initiate the formation of MoS_2 tribofilm.

Raman spectroscopy confirmed the presence of MoS_2 tribofilm for the stated parameters. Raman peak values at 380 and 410 cm^{-1} were observed at the wear track which corresponded to the molecule of MoS_2 [43, 44, 152]. Under varying parameters of temperature and speed, the load of 14 N appears to have the lowest friction value for varying parameters, except for room temperature conditions at speeds of 0.88 m/s (Figure 6.2 (a) and 6.3 (a)).

Initial friction value usually decreases at time period of 1 hour for every varying conditions. Speeds of 1.75 m/s shows a steady friction reduction at varying conditions of load and temperature. However, presence of MoS_2 tribofilm is not detected with the analysis of Raman spectroscopy. High speed and contact pressure could promote non conformal lubricated contact at the surface hence affecting the fluid viscosity. Thin oil films supporting the load are produced and reducing the friction at 1.75 m/s. Low speeds of 0.44 m/s also does not show the presence of MoS_2 tribofilm on the surface. Low speed and the combining parameters of load and temperature does not promote MoS_2 tribofilm formation.

High friction values are witnessed with high temperatures however, speed of 0.88 m/s and contact loads of 7 N and 14 N promotes the formation of MoDTC tribofilm at high temperature which reduces friction. High temperature of 100°C displays an eminent effect towards the formation of MoS_2 tribofilm with the varying load and 0.88 m/s sliding speed.

Figure 6.2 (b) and 6.3 (b) shows the wear rate values of the ball sample of the HSPOD at the end of 1 hour test for the lubricant additive of MoDTC at low and high temperature respectively. Hence, wear rate value also follows a similar trend to friction values at different operating parameters. An overall

decrease in wear rate values is observed with increasing speed, except for conditions where friction was observed to be out of trend.

At slow speed of 0.44 m/s, a high wear rate and a lower wear rate is observed, usually in high speeds of 1.74 m/s. Wear rate for speed of 0.88 m/s usually lies in between the two low and high speed, however at contact load of 14 N, minimum wear is observed on the HSPOD pin. Avoidance of the excessive wear could be through a formation of a protective film under boundary lubricated contacts, hence providing a nominal conditions for the formation of MoDTC tribofilm.

Eqn 1-4 shows that the dimensional wear factor is indirectly proportional to the sliding distance. Therefore for a certain time criterion lower speed accounts to shorter sliding distance, and with increasing speed, longer sliding distance is achieved. With lower sliding speed therefore higher wear rate is generated, which decreases with an increase in speed. In relation to 0.44 m/s, the sliding distance for a one hour test only covers about one-fourth of the sliding distance for the speed of 1.75 m/s. Hence, in relation to sliding distance it can be stated wear factor is generated at a higher rate when the contact is initially produced.

However, with longer sliding distance wear induces non conformal lubricated contact at the surface and hence promoting mixed or elastohydrodynamic lubrication within the contact. Under this lubrication regime, a thicker entrained oil film is produced which leads to less solid contact and the wear rate is decreased along with the friction.

Certain conditions of operating parameter are needed to promote the formation of MoS_2 tribofilm. High temperature conditions of 100°C at speed of 0.88 m/s and contact load of 14 N are therefore chosen to reduce friction due to the formation of MoS_2 tribofilm at true boundary conditions.
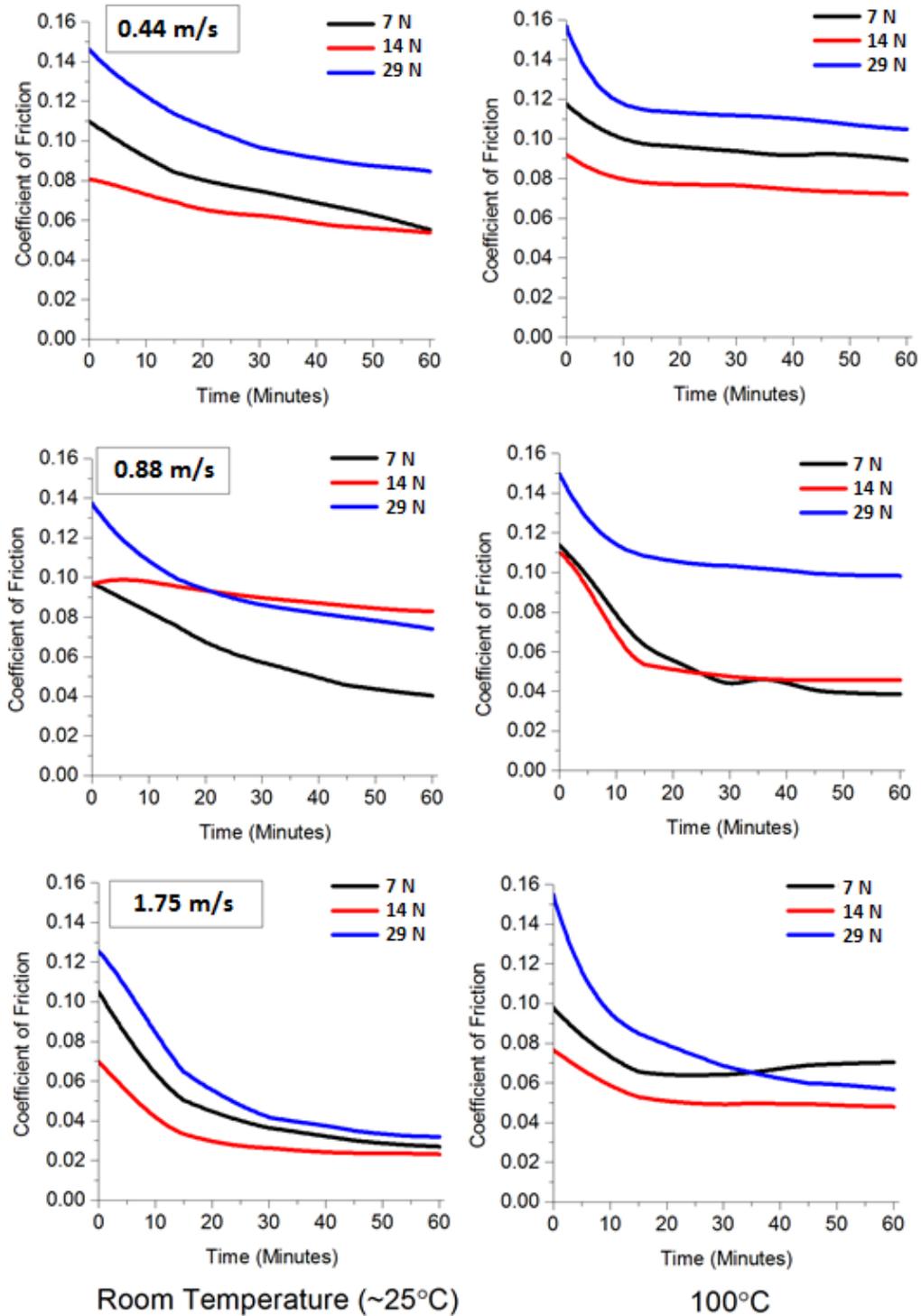
Figure 6.1 Friction coefficient graph at a time period of 1 hour for the additive of Molybdenum Dialkyldithiocarbamate (MoDTC) tested at the HSPOD with varying operating parameters of temperature (25⁰C and 100 °C), sliding speed (0.44, 0.88 and 1.75 m/s) and load (7 N, 14 N and 29 N).
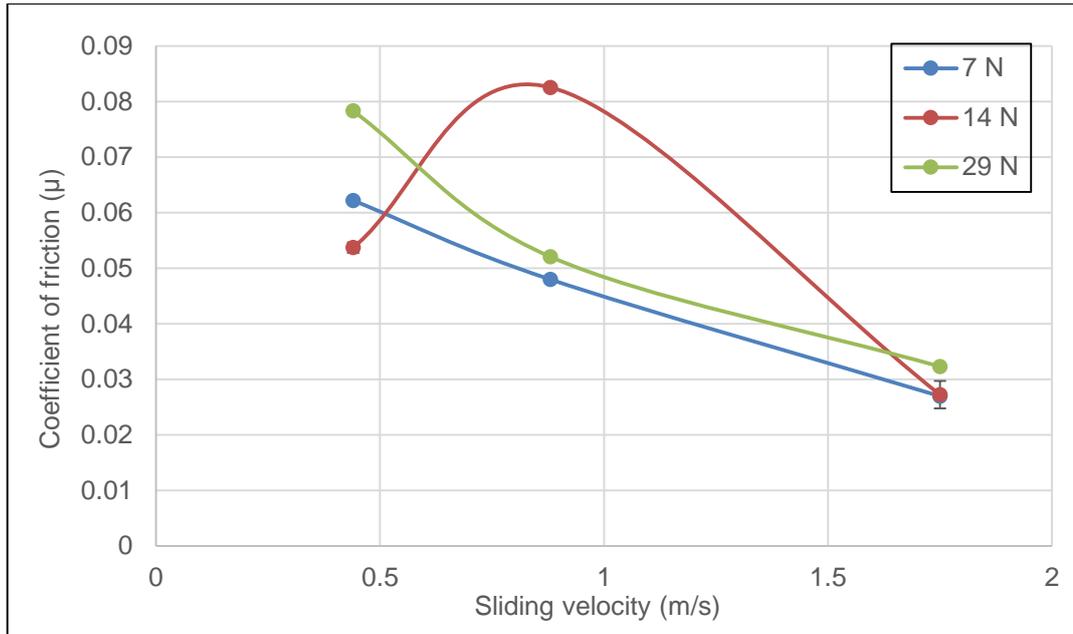
(a)
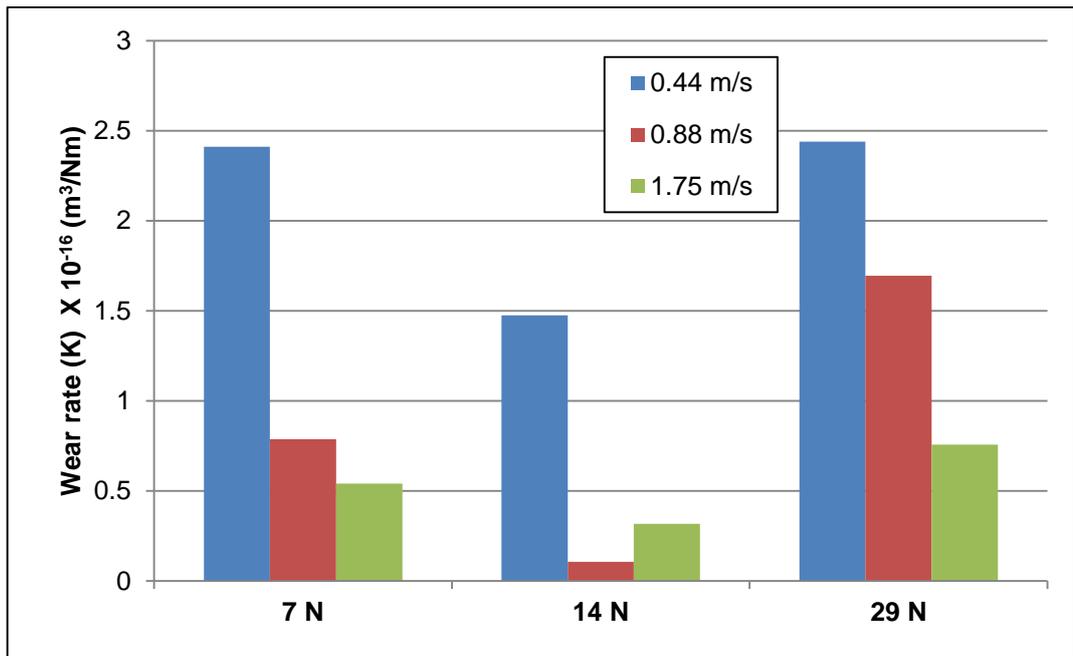
(b)

Figure 6.2 (a) Friction coefficient graph of the average of the last 5 minutes of a 1 hour test for the lubricant additive of MoDTC at temperature of 25⁰C with varying sliding speed (0.44, 0.88 and 1.75 m/s) and load (7 N, 14 N and 29 N). The same lubricant of MoDTC additive was used at the test temperature (25°C). (b) Wear rate values of the ball sample of the HSPOD at the end of 1 hour test for the lubricant additive of MoDTC at temperature of 25⁰C with varying operating speed (0.44, 0.88 and 1.75 m/s) and load (7 N, 14 N and 29 N).
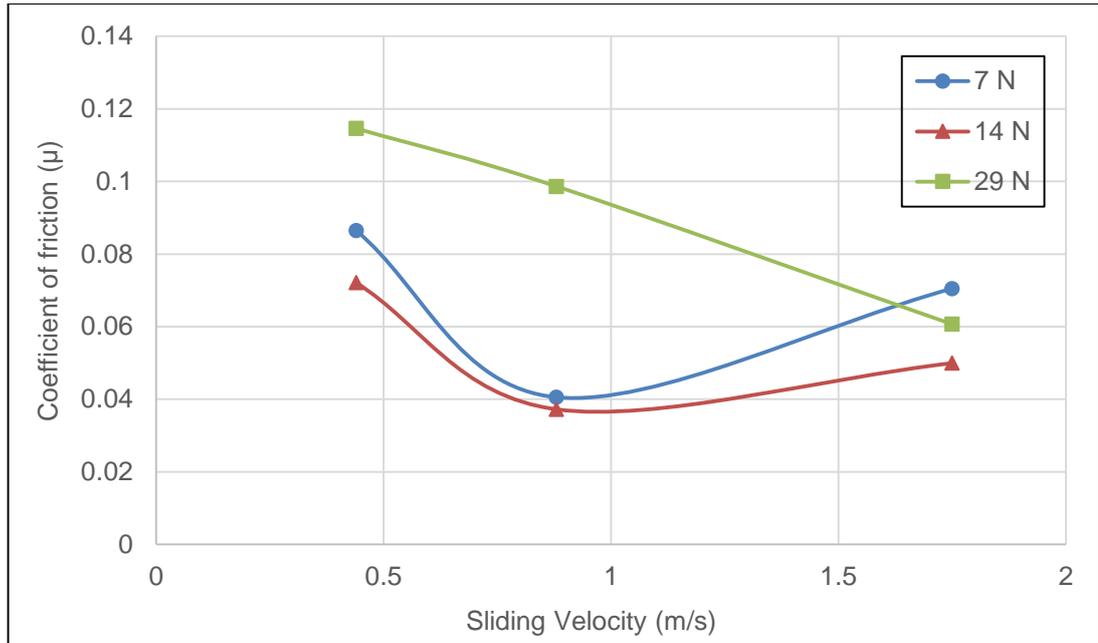
(a)
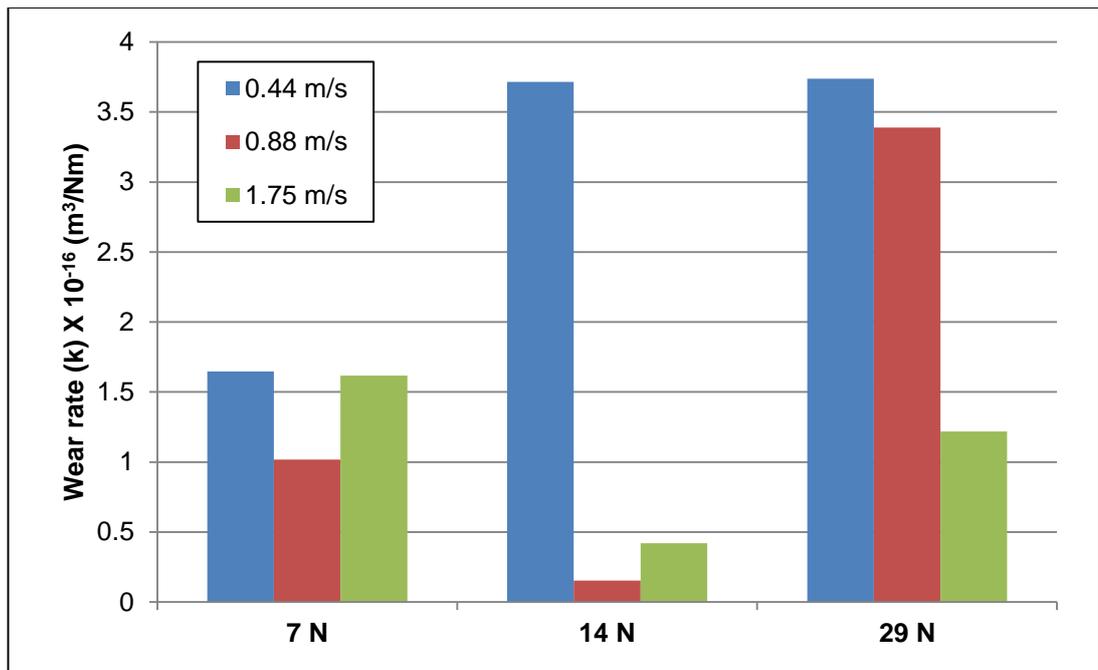
(b)

Figure 6.3 (a) Friction coefficient graph of the average of the last 5 minutes of a 1 hour test for the lubricant additive of MoDTC at temperature of 100ºC with varying sliding velocity (0.44, 0.88 and 1.75 m/s) and load (7 N, 14 N and 29 N). The same lubricant of MoDTC additive was used at the test temperature (100°C). (b) Wear rate values of the ball sample of the HSPOD at the end of 1 hour test for the lubricant additive of MoDTC at temperature of 100ºC with varying sliding speed (0.44, 0.88 and 1.75 m/s) and load (7 N, 14N and 29 N).

Similar characterization test of the MoDTC additive under boundary lubricated conditions at the HSPOD were undertaken with the *in-situ* rig to understand the effect of various tribological parameters on the lubricant additive of MoDTC. Experiments were conducted at room temperature (~25°C) and 100°C for a time period of 1 hour, with varying contact load of 10, 20 and 30 Newton at rotating speeds of 1.02 m/s and 2.04 m/s.

Figure 6.4 provides the friction coefficient for the lubricant additive of MoDTC under boundary lubricated conditions with varying operating parameters. Experiments conducted with load of 30 N shows that with the increase in temperature the average friction coefficient also increases for both rotating speeds (Figure 6.4). The increase in temperature has been described to decrease the viscosity of the lubricant and promote more surface contact. Experiments with loads of 10 N and 20 N, however does not show this effect. The friction coefficient for test conducted with 10N and 20N contact load showed that friction values at 100°C are low compared to the room temperature conditions. Average friction value is however low for all of the tribological conditions with speeds of 2.04 m/s compared to the similar tribological conditions at 1.02 m/s.

Raman analysis was conducted on the wear scar of the samples at the end of the test for all the tribological conditions. Raman analysis showed the presence of E^1_{2g} and A_{1g} peak at 380 and 410 cm^{-1} for MoS_2 tribofilm for test conducted under 100°C temperature with a speed of 2.04 m/s and 20 N contact load. The presence of the MoS_2 peak was also supported with the reduction of friction at the stated tribological conditions (Figure 6.5). Raman spectra of the test conducted with 30 N contact loads were usually supported with an intense peak at 660 cm^{-1}. The Raman response for Fe_3O_4 at 660 cm^{-1} was related with wear due to heavy contact load. Raman analysis at contact load of 10 N showed Raman bands at 220, 288 and 404 cm^{-1}. Similar broad bands was also observed with HSPOD tests conducted at 50°C and 80°C and related to certain form of amorphous chain of Mo – Mo complex. This form of Mo chain was attributed towards the linear drop in friction but the steady state friction is achieved only with the formation of MoS_2 tribofilm.
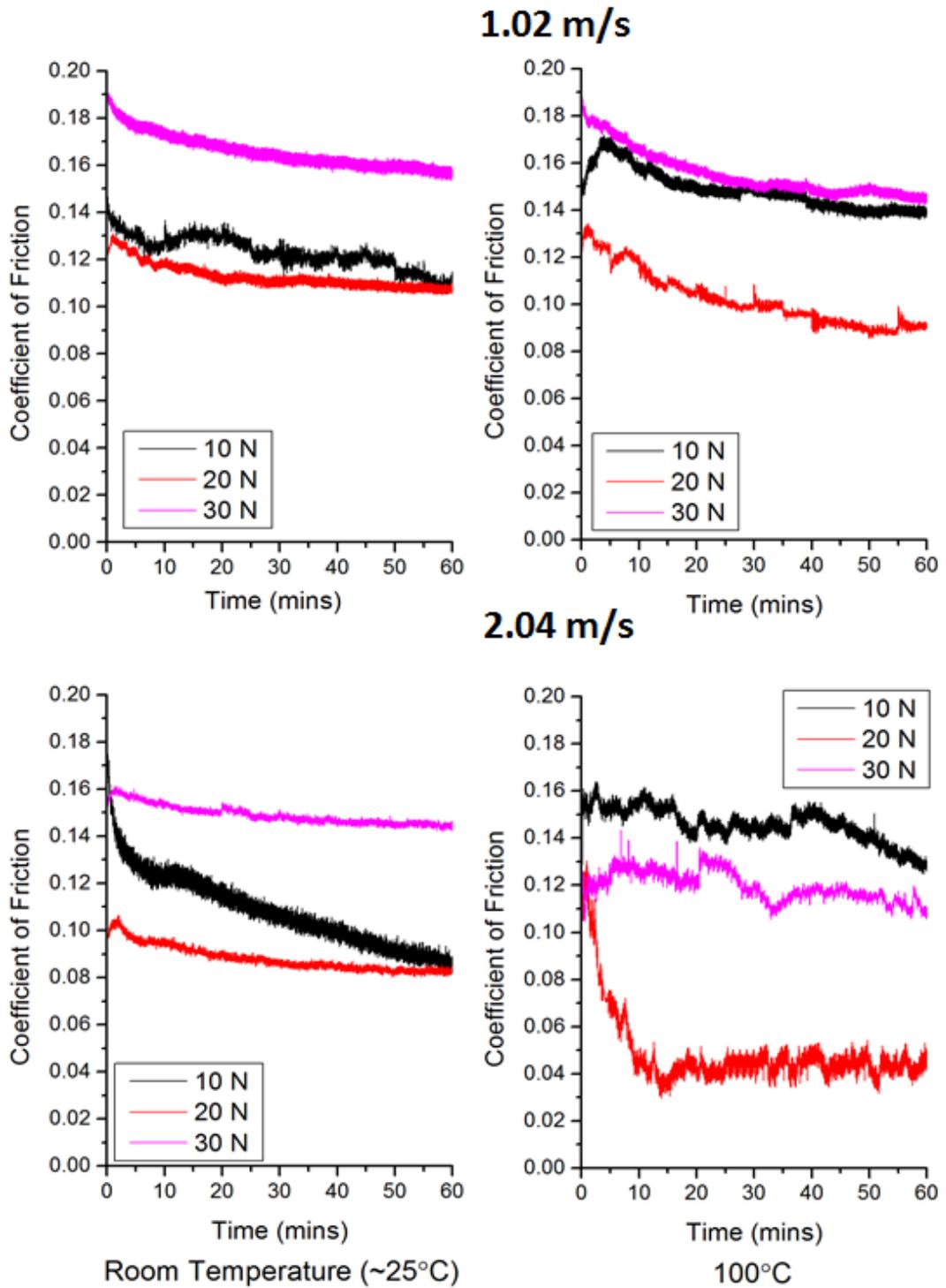
Figure 6.4 Friction coefficient graph conducted in the *in-situ* rig for a time period of 1 hour for the additive of Molybdenum Dialkyldithiocarbamate (MoDTC) at varying operating parameter of temperature (Room temperature and 100 °C), sliding speed (1.02 m/s and 2.04 m/s) and load (10, 20 and 30 N).
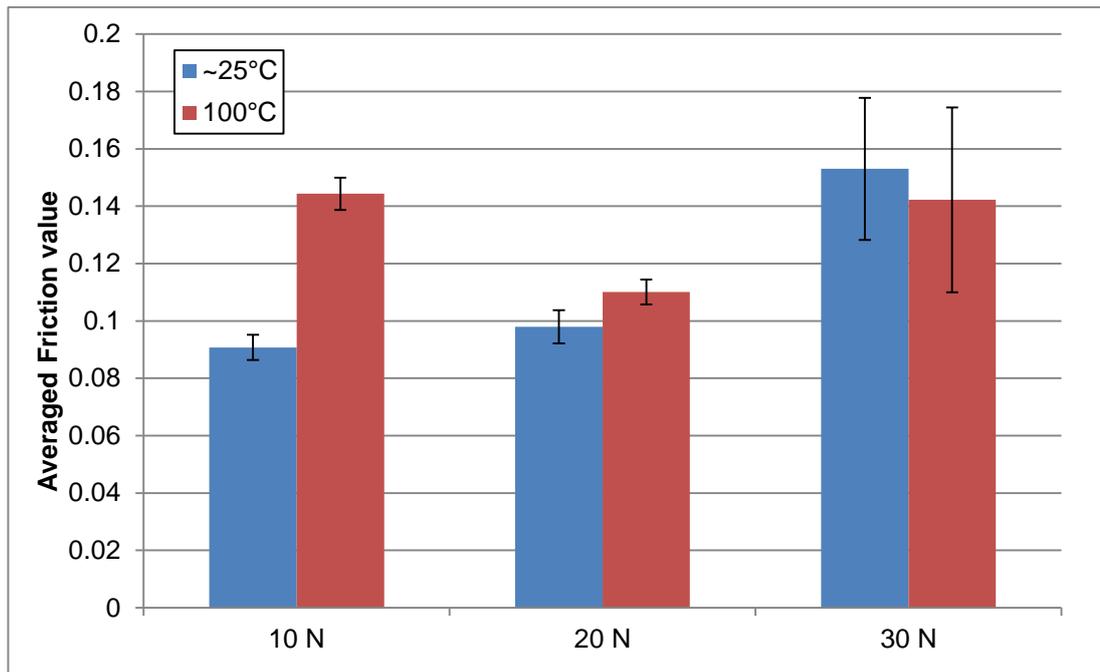
(a)
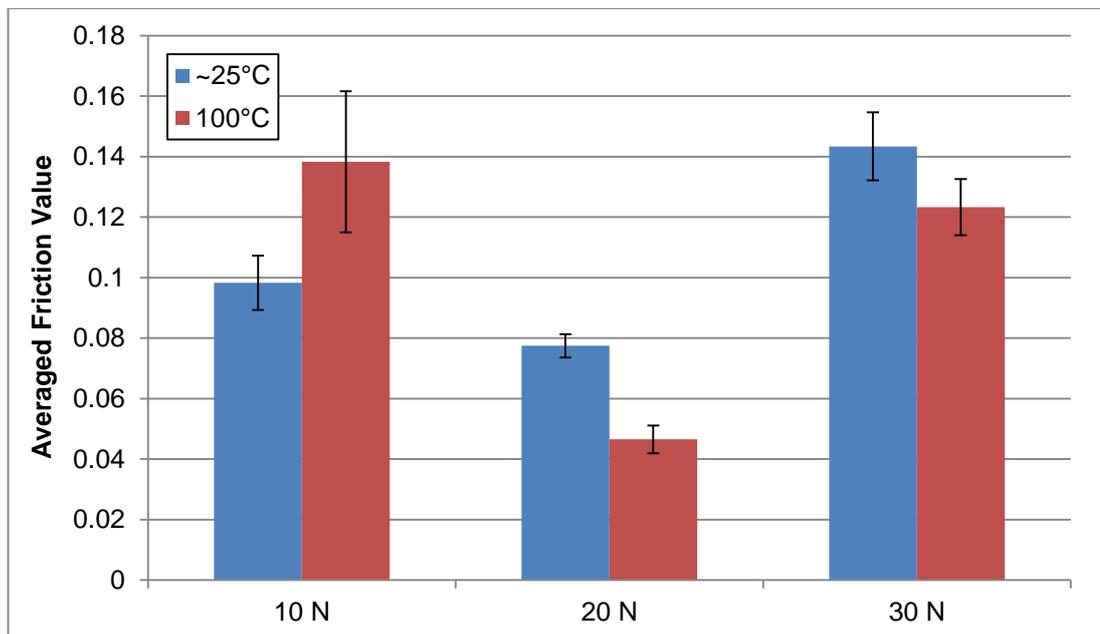
(b)

Figure 6.5 Average of the last 5 minutes friction coefficient graph for the lubricant additive of MoDTC at sliding speed of (a) 1.02 m/s and (b) 2.04 m/s, with temperature of ~25°C and 100°C and loads of 10 N, 20 N and 30 N. Standard deviation of the friction values are shown for repeatability with each condition performed with three tests.

6.1.1 Effect of temperature on the frictional characteristics of MoDTC

In order to understand the effect of the temperature on to the tribofilm formation and its effect on the friction, for the stated tribological condition of 1.5 kg load and 500 rpm sliding speed, experiments are conducted with varying temperatures. At the stated condition, various temperature effect on friction is observed for the MoDTC lubricant.

Figure 6.6 shows the friction coefficient values from test at various temperatures of ~ 25, 50, 80, 100 and 120ºC. Increase in temperature shows a decrease in friction values for the 1 hour time period. At high temperature of 100ºC and 120ºC, a significant drop of friction is observed within the time period of 5 to 10 mins before reaching a steady state.

High temperature conditions of 100ºC promoted the formation of MoS_2 tribofilm onto the surface at the stated tribological conditions. Under higher temperature conditions more solid – solid contact is promoted due to the reduced lubricant viscosity of the oil. Therefore due to more exposed area an initial protective layer could be formed which promotes the formation of MoS_2 onto the surface and has also been reported by various authors [42, 153].
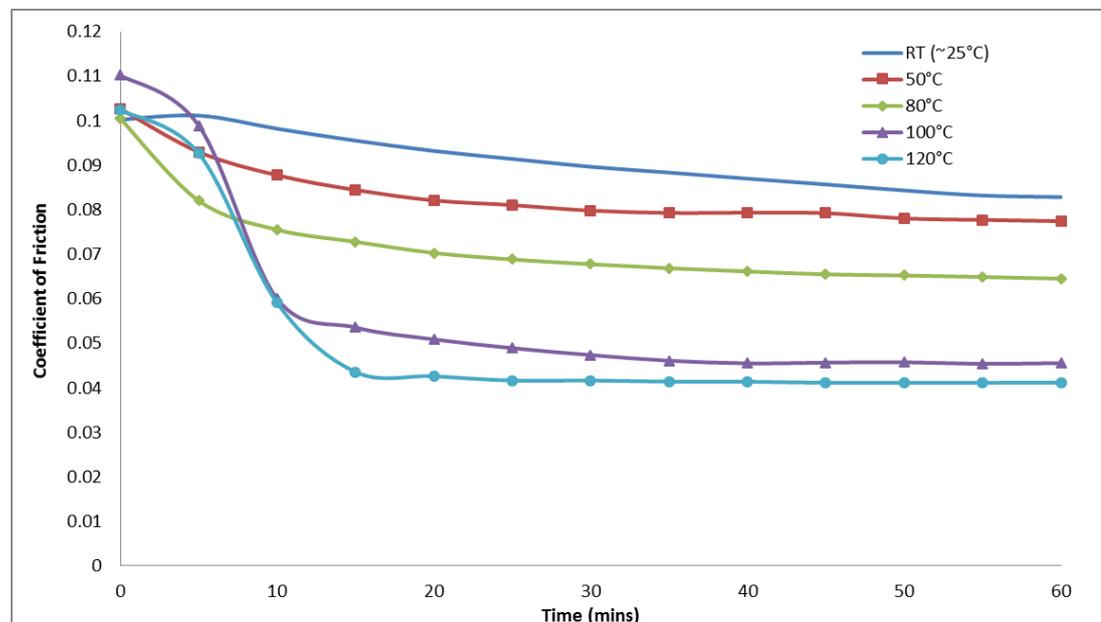
Figure 6.6 Friction coefficient graph for the lubricant additive of MoDTC at the HSPOD tribometer with stated tribological conditions of 1.5 kg and 500 rpm for various temperature of room temperatue (~25ºC), 50ºC, 80ºC, 100ºC and 120ºC.

In lubro Raman analysis were conducted on the contacting samples of the ball and disc wear scar after the test to understand the nature of the tribofilm formed. Raman spectra of the disc and ball samples for test conducted under various temperatures as indicated is presented in Figure 6.7. Under room temperature conditions, (Figure 6.7 (a) and (b)) Raman spectrum of the disc samples observed a peak at 660 cm^{-1} and around 923 cm^{-1} Raman shift.

The broad and intense peak at 660 cm^{-1} has been attributed to the presence of Fe_3O_4 (iron oxide) [150] and occurs due to the wear occurring on the contact because of rubbing.

Raman peak at 923 cm^{-1} has been reported for the Raman mode of $FeMoO_4$ [151] and under room temperature conditions it can be suggested that the formation of MoS_2 tribofilm is not promoted from the additive of MoDTC. The appearance of $FeMoO_4$ could be suggested to suppress the formation of MoS_2 layers which does not contribute towards friction reduction. Analysis on the ball sample shows a similar Raman spectrum for the observed peaks at the disc samples.

Experiments conducted at temperatures of 50°C and 80°C, show the friction decreases compared to the experiment conducted at room temperature. Raman analysis on the disc samples confirms the presence of the peak at 660 cm^{-1} and around 923 cm^{-1} for Fe_3O_4 and $FeMoO_4$ respectively, for both samples.

However, three peaks at 220, 288 and 404 cm^{-1} progressively appear during the analysis of the disc samples. Raman peak at ~220 cm^{-1} has been reported for the Mo-O-Mo deformation mode [154] and peaks around 288 – 280 have been reported for the amorphous MoS_3 molecule [155]. The band at 404 cm^{-1} has been attributed to v(Mo-Mo) and Clark et al [156] stated that this was the highest value for v(Mo-Mo) in any known dimolybdenum compound and is consistent with the uniquely short Mo-Mo bond length in the compound. Raman analysis on the ball samples for both the sample showed similar Raman peak on the spectrum.

Raman peaks corresponding to $FeMoO_4$ are absent on the analysis of the ball samples. The peak corresponding to Fe_3O_4 at 660 cm^{-1} has a broader peak shifting it to around 605 cm^{-1}. Therefore with the increase in temperature, it

can be stated that the molecule of the MoDTC additive breaks down to certain form of amorphous chain of Mo – Mo complex and is attached on both disc and ball wear scars. This form of Mo chain can be attributed towards the linear drop in friction compared to the room temperature friction performance.

At temperatures of 100 and 120°C the decrease in friction is evident with the formation of MoS_2 tribofilm. Raman peaks values at 380 and 410 cm^{-1} for the E^1_{2g} and A_{1g} mode of the MoS_2 tribofilm are present on both the ball and disc samples. Less intense and broad bands at 458 cm^{-1}, 510 cm^{-1} and 553 cm^{-1} are observed on the Raman spectrum of the disc samples. A broad band centred around 454 cm^{-1} was also observed at the Raman spectra for the MoS_2 crystalline powder. This band had been attributed to the 2LA(M) mode for the second order Raman bands of the MoS_2 molecule and a feature present typically because of a resonance effect. Similar peaks at 555 cm^{-1} was also observed with the 785 nm laser wavelength for the MoS_2 crystalline powder and regarded as a combination of various resonance effect and optical mode peaks, giving rise to extensive second order peak.

Frequency band at 510 cm^{-1} was reported by Sourisseau et al. [155] which arises due to the stretching vibrations of $(S_2)^{2-}$ pairs in Lithium supported MoS_3. The stretching vibrations of $(S_2)^{2-}$ pairs for a classic a-MoS_3 has been assigned at a Raman peak value of 522 cm^{-1}. Weak and broad bands at Raman peak values of 660 cm^{-1} for Fe_3O_4 and 925 cm^{-1} for $FeMoO_4$ are also observed onto the disc samples. Raman analysis on the ball samples was usually evident only with the E^1_{2g} and A_{1g} mode of the MoS_2 tribofilm. A detailed discussion of the effect that testing temperature has on tribofilm formation and as a result on friction performance is included in Chapter 8 .
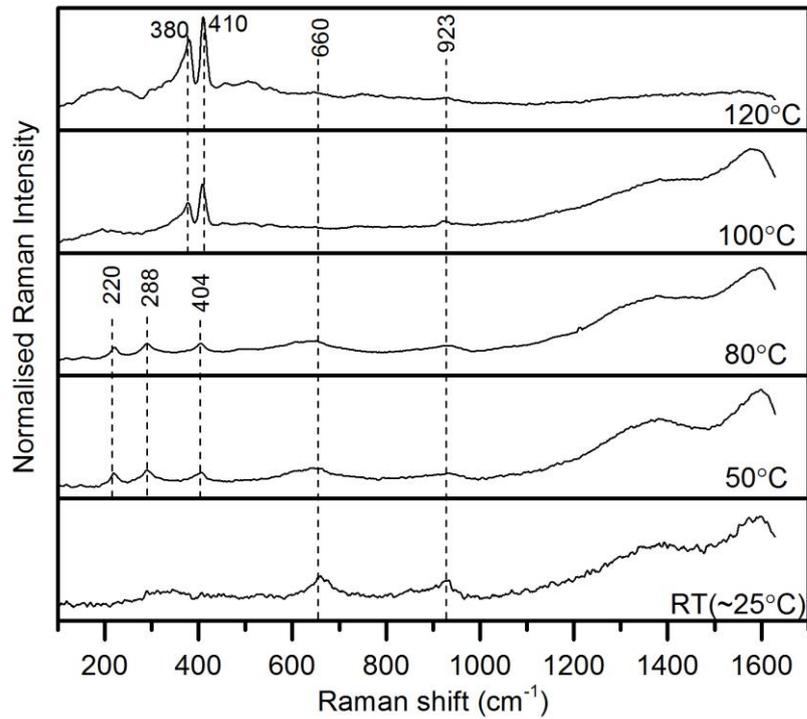
(a)
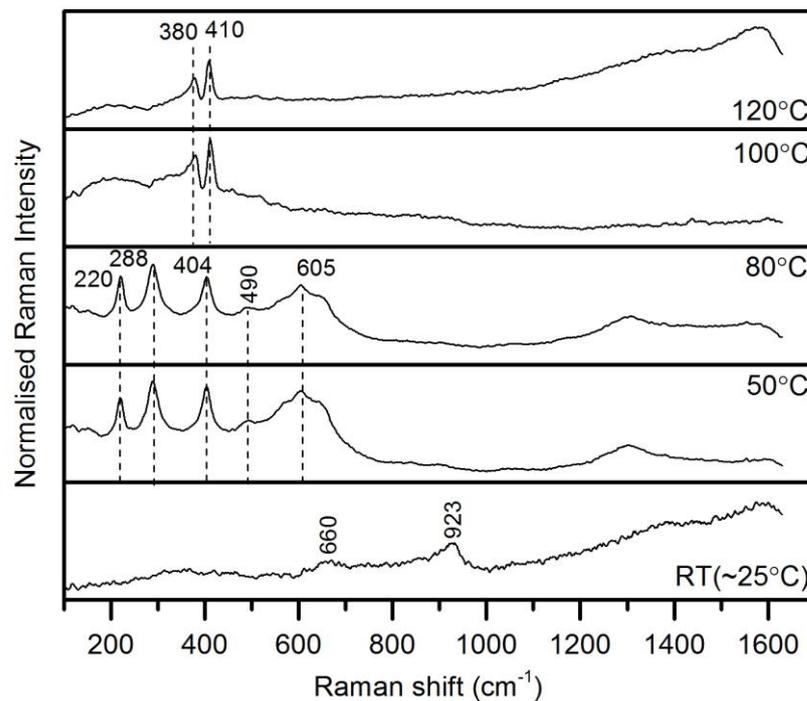
(b)

Figure 6.7 Raman spectra of HSPOD (a) Disc samples and (b) ball samples for the lubricant of MoDTC. Experimental tests are conducted with operating parameters of 1.5 kg load, 500 rpm speed and various temperature of room temperatue (~25ºC), 50ºC, 80ºC, 100ºC and 120ºC. Higher temperature conditions of 100ºC and above is shown to be prominent to activate the additive and lower the friction with the formation of MoS_2 tribofilm.

6.1.2 The effect of lubricant oxidation on the tribological performance of MoDTC

Tribological experiments at high temperature show formation of the friction reducing MoS_2 film from the additive of MoDTC. Under boundary conditions the formation of MoS_2 tribofilm is evident with friction reduction on both contacting samples. However the nature of how the additive of MoDTC reacts with the contacting substrates at high temperature is still not clear. Therefore in order to observe the thermal nature of the lubricant of MoDTC, steel disc samples were immersed in the lubricant of MoDTC and heated at a temperature of 100°C without any contact for a time period of 1 hour. Raman analysis conducted on to the steel surface without any form of solvent cleaning did not show any form of definite peaks except for the broad bands around 1300 cm^{-1} and 1600 cm^{-1} relating to the D and G carbon peaks of the steel substrate. In evidence to the Raman analysis it can be stated under high temperature any sort of thermal absorption of the MoDTC does not occur. Therefore in order to form MoS_2 tribofilm on the surface, sliding and contact conditions are required for the stated boundary conditions.

Furthermore lubricant of MoDTC was heated at a temperature of 100°C for a time period of 1 hour and allowed to cool at a room temperature. The degraded oil was used to conduct tribological experiment under the same conditions as employed before. Experiments at contact load of 1.5 kg and speed of 500 rpm was conducted in room temperature condition for a time period of 1 hour. Figure 6.8 shows the friction coefficient for the lubricant of MoDTC at the stated conditions. In comparison to the friction coefficient of the fresh oil, the degraded oil has an averaged friction lower than that of a fresh oil friction values. Under room temperature conditions, Raman spectrum of the disc samples for fresh oil showed peak values at 660 cm^{-1} and around 923 cm^{-1} and similar peak values at the ball samples (Figure 6.7 (a) and (b)). Raman analysis conducted on the degraded oil test samples observed in Figure 6.9, shows Raman peaks values at 220, 290 and 402 cm^{-1}, along with peaks at 660 cm^{-1} and 923 cm^{-1} for Fe_3O_4 and $FeMoO_4$ for the disc samples. Similar peak values have also been observed for the tribological experiments conducted at 50°C and 80°C temperatures.
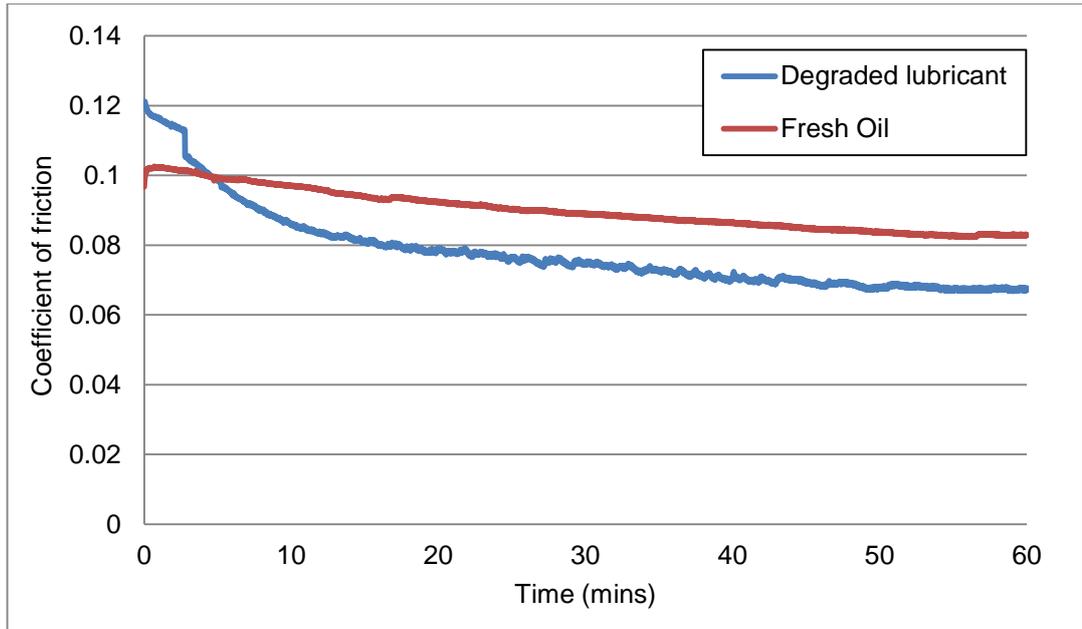
Figure 6.8 Friction coefficient graph of the HSPOD test conducted with the lubricant additive of fresh and degraded MoDTC oil at room temperatue (~25ºC) and experimental conditions of 1.5 kg load and speed of 500 rpm.
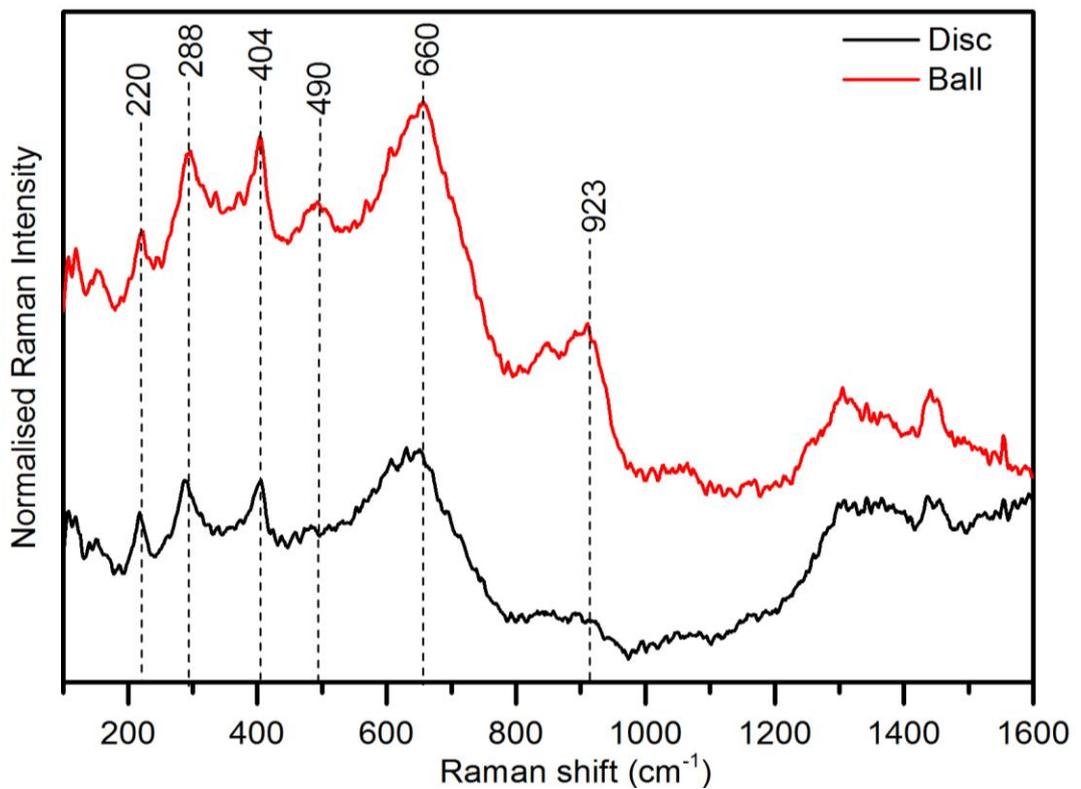
Figure 6.9 Raman spectra of the HSPOD disc and ball samples for test conducted with the degraded lubricant of MoDTC.

6.2 Durability of MoDTC tribofilm

Under contact and sliding conditions, MoDTC lubricant additive is significantly affected with temperature towards the formation of MoS_2 tribofilm. Under room temperature conditions, friction is affected with the formation of $FeMoO_4$ and MoS_2 tribofilm formation is not promoted. Application of high temperature is however noticed towards the tribochemistry understanding of the MoDTC additive. With the increase in temperature an amorphous chain of Mo – Mo complex is observed on the Raman analysis of the samples. High temperatures reduces friction with the formation of MoS_2 tribofilm on both the contacting samples. The friction is reduced as layers of MoS_2 are formed onto the contacting surface until it reaches a steady state condition. Frictional properties of the MoS_2 tribofilm is hence under investigation.

6.2.1 Long duration friction test of MoDTC lubricant additive

Figure 6.10 shows a friction coefficient of the MoDTC lubricant for longer duration friction test of 5 hours at the temperature of 100ºC. Friction value is shown to drop significantly at early time periods as observed with the 1 hour test. However, with the drop in friction, as the friction reaches a steady state condition, the low friction coefficient of the tribological system is maintained towards the end of the test.

Raman analysis on the ball and disc wear track shows the presence of the E^1_{2g} and A_{1g} mode at 380 and 410 cm^{-1} for the MoS_2 tribofilm (Figure 6.11). Hence with the formation of MoS_2 tribofilm onto the wear track, the friction coefficient of the tribological system is maintained even at longer time duration of 5 hours. The formation of MoS_2 tribofilm on the ball and disc wear scar facilitates the easy shearing between the contact and maintains the low friction even at longer duration.
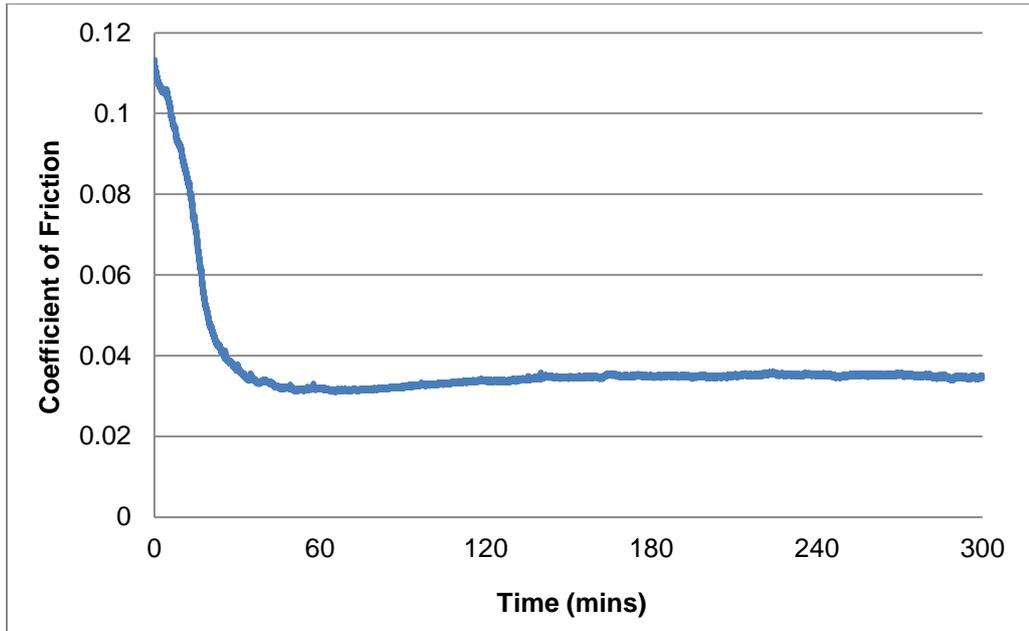
Figure 6.10 Friction coefficient graph for the MoDTC lubricant addtive conducted in the HSPOD at a time period of 5 hour, load of 1.5 kg, 500 rpm and high temperature of 100ºC.
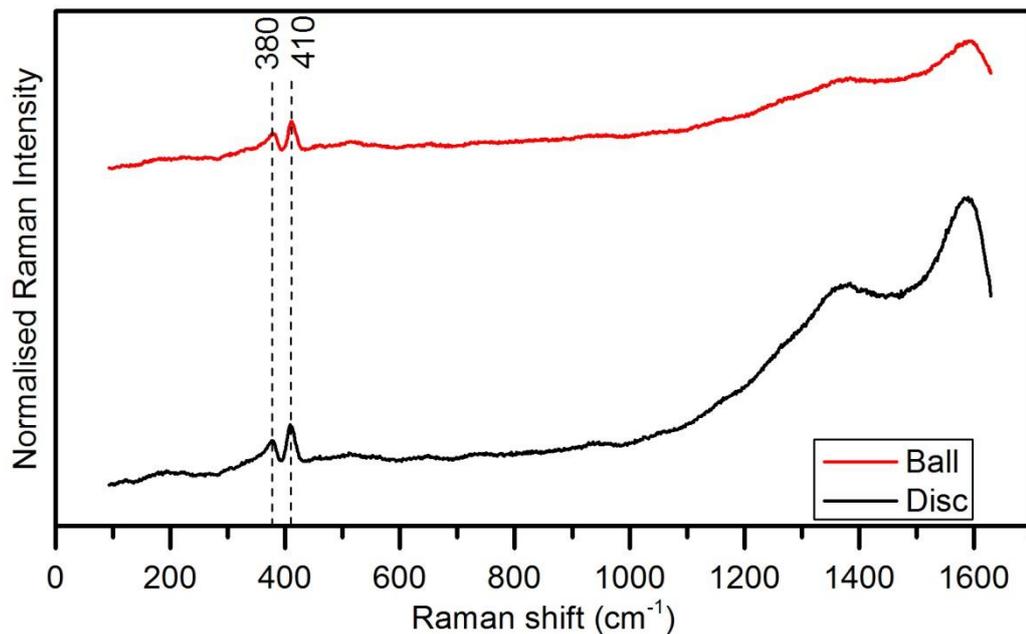
Figure 6.11 Raman spectrum of the HSPOD ball and wear track for a time duration of 5 hour test at 100ºC. The MoS_2 E^1_{2g} and A_{1g} mode at 380 and 410 cm^{-1} is observed on both of the contacting sample.

6.2.2 MoS₂ tribofilm performance under oil scarcity

Low friction is maintained with the formation of MoS₂ tribofilm for the lubricant of MoDTC even in longer duration tests. The formation of this tribofilm on the contacting surface maintains the easy shear and facilitates low friction. Therefore under oil scarcity the following test was conducted to analyse the frictional behaviour of the MoS₂ tribofilm on itself.

Experiments were conducted at 100ºC for a time period of 1 hour to produce the tribofilm of MoS₂ onto the surface. Figure 6.11 shows the low friction of the tribological experiment for the first 1 hour. After a time period of 1 hour, the oil was drained out from the system and dry conditions applied to the system.

As soon as the oil was drained a steady increase in the friction process is observed. The steady increase in friction for the first 5 minutes could be related to the increase in contact pressure as the lubricant is drained from the system. MoS₂ tribofilm formed onto the surface is subjected to higher pressure and reaches a stable friction after which a slow increase in the friction value is observed. Due to the increase in the pressure, layers of MoS₂ tribofilm could be depleted as well and slow rise in friction is observed. The tests was run for another half an hour and Raman analysis were conducted on the ball and disc samples.
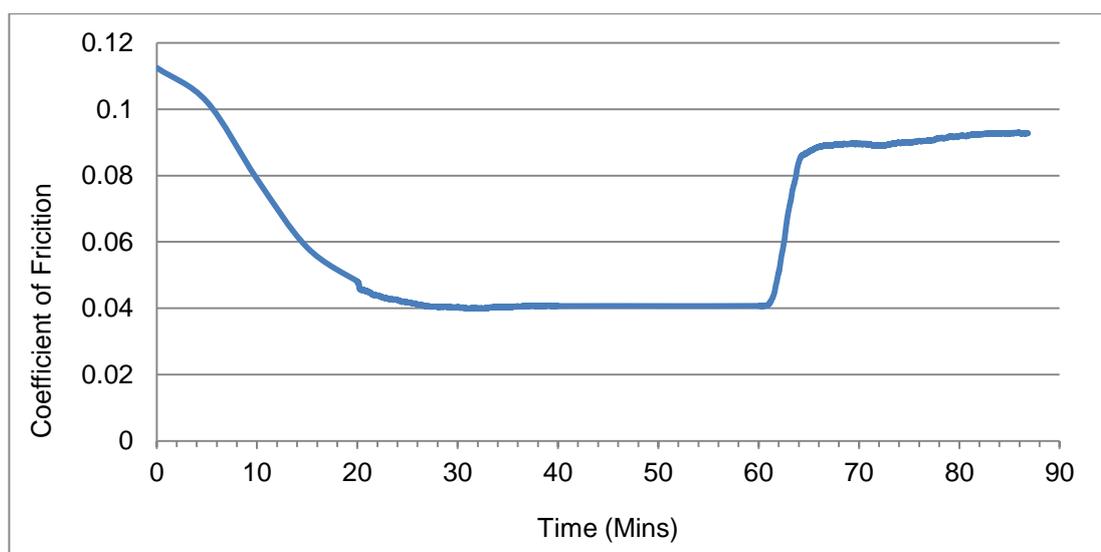
Figure 6.12 Low friction performance of the MoDTC lubricant addtive at HSPOD with the experimental parameters of 1.5 kg load, 500 rpm and high temperature of 100°C for the first hour with the formation of MoS₂ tribofilm and its performance under oil scarcity.

Figure 6.13 shows the Raman spectrum for the disc and ball samples at the end of the test for the MoDTC tribofilm under oil scarcity. Raman analysis of the disc and ball samples showed the presence of the E^1_{2g} and A_{1g} peak of the MoS_2 tribofilm onto the surface. Hence the tribofilm of MoDTC was not completely depleted even under the scarcity of oil.

Close observation on the Raman spectra shows a sharp peak response around 220 cm^{-1} and around 290 cm^{-1}. Similar peak were also observed at test conducted with 50ºC and 80ºC temperature and degraded oil. Peaks at 220 cm^{-1} were reported for Mo-O-Mo deformation mode [154] and peaks around 288 – 280 has been reported for the amorphous MoS_3 molecule. Similarly a broad peak around 501 cm^{-1} also develops on both ball and disc samples. The frequency arising could be due to the stretching vibrations of $(S_2)^{2-}$ pairs due to the development of amorphous MoS_3 from the MoS_2 tribofilm. Therefore under increased pressure the MoS_2 tribofilm is subjected to form an amorphic nature of the film and the presence of the 220 cm^{-1} could indicate that the tribofilm could also be subjected to oxidation with time.
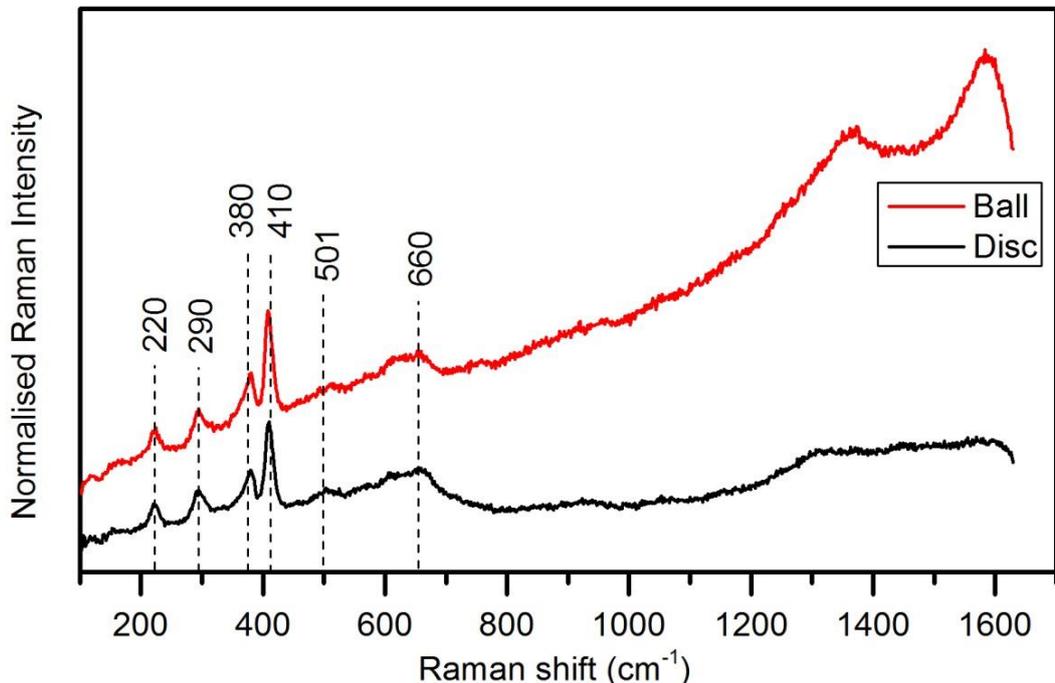
Figure 6.13 Raman spectrum of the HSPOD ball and wear track of the MoDTC lubricant additive samples under oil scarcity. E^1_{2g} and A_{1g} mode of the MoS_2 tribofilm at 380 and 410 cm^{-1} is observed on both of the contacting samples.

6.3 Tribological performance of Molybdenum dialkyldithiocarbamate (MoDTC) interaction with Zinc dialkyldithiophosphate (ZDDP).

Molybdenum dialkyldithiocarbamate reduced friction under boundary conditions with the formation of MoS_2 tribofilm on the contacting surface. The formation of tribofilm was highly dependent upon the tribological parameters and specially depended upon high temperatures. Shift in Raman peak was observed for the E^1_{2g} and A_{1g} peak modes of the MoS_2 tribofilm, with decrease in friction. The shifts were observed with the formation of MoS_2 layer on the contact which decreases friction until a steady state condition was reached. Formation of MoO_3 as reported by various authors [42, 47, 50] was not observed on the tribofilms under any tribological conditions. However Raman peaks corresponding to $FeMoO_4$ was observed on the wear track of the samples. Iron oxide Raman peaks for Fe_3O_4 were also observed on the wear scar of the contacting samples, and occurred due to wear at the rubbing contact. MoS_2 tribofilm maintained low steady friction at longer duration of contact, however under oil scarcity an increase in friction was observed. Raman analysis showed traces of MoS_2 tribofilm along with the characteristic peaks of FeS and Fe_3O_4.

MoDTC was able to reduce friction effectively in the absence of other additives, but the range of tribological condition depended strongly on the temperature. MoDTC has been extensively reported that on its interaction with the additive of ZDDP friction and wear performance of the tribological systems were improved [30, 46, 48, 52-55, 157-161]. ZDDP is a well-known additive and used for its multifunctional properties, namely antiwear and antioxidant actions. ZDDP has been generally agreed to form different chain length of a glassy phosphate film [136, 162, 163] that are responsible for minimizing asperity contact between the contact and reduces wear. Various mechanism for the interaction of the MoDTC with ZDDP has been proposed [53, 54, 164, 165] and further investigation has been conducted on the friction performance of MoDTC with the additive of ZDDP.

6.3.1 MoDTC friction performance with ZDDP at ~25⁰C (room temperature) conditions

Under room temperature conditions, tribological test were carried out for the lubricant additive of MoDTC and ZDDP at boundary conditions for a time period of 1 hour. Tribological experiments were conducted on the HSPOD with the lubricant additive of MoDTC and ZDDP. Experiments are conducted with the same tribological parameters to those conducted with the lubricant additive of MoDTC. A comparative friction graph for the lubricant additive of MoDTC itself at room temperature and its interaction with the lubricant of additive of ZDDP is presented in Figure 6.14. MoDTC was not able to reduce friction at room temperature conditions but lubricant additive combination of MoDTC and ZDDP reduces friction within a time period of 10 minutes. A similar observation was also observed by Muraki et al.[55] and Morina et al. [54] and explained as a synergistic effect on reducing friction obtained from a combination of MoDTC and ZDDP and friction was determined according to which tribofilm dominated the contact area.
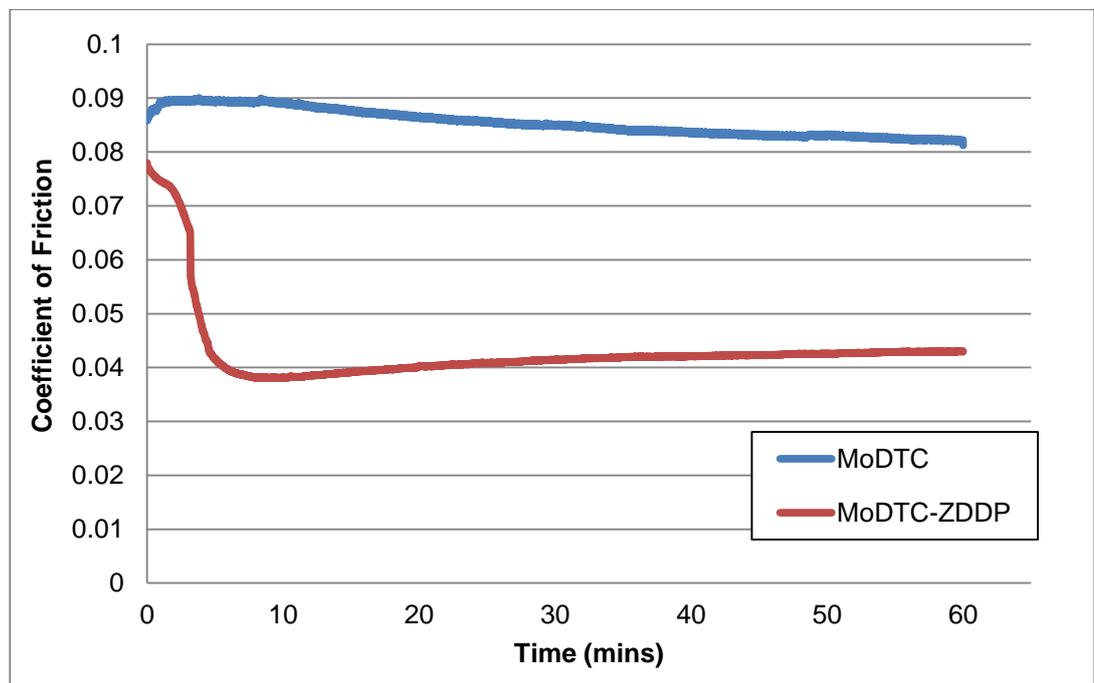
Figure 6.14 A comparative friction graph for the lubricant additive of MoDTC itself and a combination of MoDTC and ZDDP. Experimental test were conducted at the HSPOD for a time period of 1 hour and room temperature conditions, at 1.5 kg load and 500 rpm.

6.3.1.1 Raman analysis on the tribofilm of MoDTC/ZDDP

Raman analysis conducted on the ball and disc wear scar for the lubricant additive of MoDTC and ZDDP showed an intense Raman peak for the E^1_{2g} and A_{1g} vibrating mode of the MoS_2 tribofilm at 383 and 407 cm^{-1} (Figure 6.15). Raman peak values of the MoS_2 tribofilm formed with the lubricant combination of MoDTC and ZDDP at room temperature resembles peak values close to that of the pure MoS_2 sample. Hence, stating the structure of the MoS_2 tribofilm similar to that of the pure MoS_2 sample formed onto the wear scar of the samples. The presence of a mixed MoDTC and ZDDP system has been shown to form decomposition products from both the additives [53,54,165,166] and indicated competitive adsorption onto the surface during the run [55]. ZDDP was credited to improve antiwear properties with the formation of polyphosphate glass and promote the formation of MoS_2 through adsorption and decomposition of MoDTC which results in decrease of the friction. Presence of the Raman peak response of the E^1_{2g} and A_{1g} modes for the MoS_2 tribofilm has been credited to the reduction of friction. As observed for the lubricant additive of MoDTC itself, Raman peaks for $FeMoO_4$ and Fe_3O_4 at 923 and 660 cm^{-1} have not been observed for the lubricant additives of MoDTC and ZDDP at room temperature.
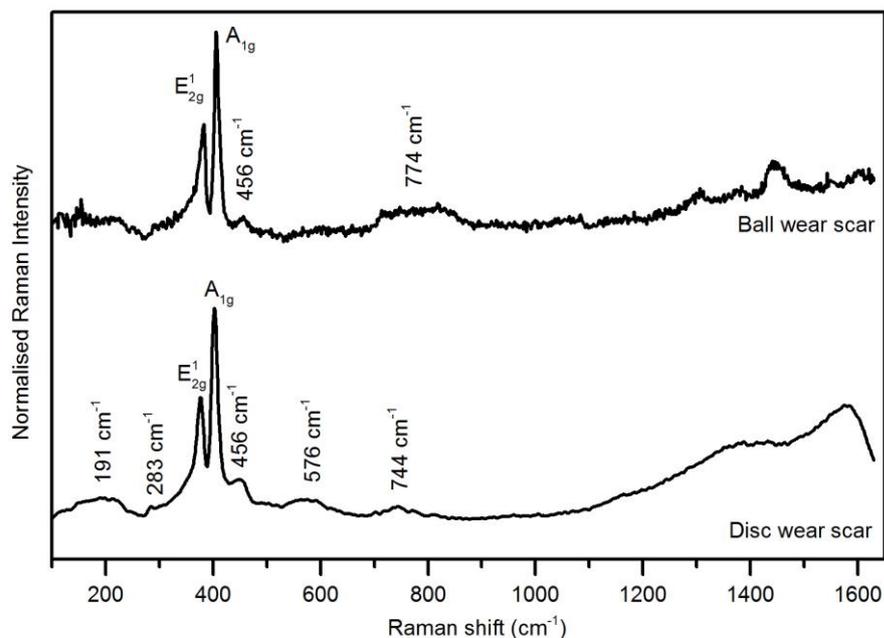
Figure 6.15 Raman spectra (488 nm excitation) of the HSPOD disc and ball samples for test conducted with the lubricant of MoDTC and ZDDP at room temperature conditions.

ZDDP tribofilms have been reported to form even at low temperature under rubbing [108, 162]. Raman spectrum of zinc polyphosphate glass has been reported to exhibit two sets of resonance and assigned in earlier studies of phosphate glasses [167-171]. Symmetric stretching of the bridging P-O bond for the phosphate band has been reported between 600 and 800 cm^{-1} Raman shift. The second band included a series of peaks between 950 and 1400 cm^{-1} relating to various modes of the P-O bonds.

Raman analysis conducted on the wear scar of the disc and ball samples for the lubricant additive of MoDTC and ZDDP does not exhibit any sharp peaks beyond the Raman shift region of 950 cm^{-1}. Disc wear scar samples shows the two broad Raman bands for the D and G Carbon peak arising from the steel substrate of the disc at the Raman region between 1300 – 1600 cm^{-1}. Similarly, the ball samples shows Raman peaks after values of 1200 cm^{-1} which arises from the hydrocarbon bonds exhibited from the base oil. It has been noted that the influence of small amounts of liquid highly influence the collection of Raman data for the polyphosphate bonds [171] and the existence of similar band around the region from the substrate and the oil could also affect the Raman spectra from the polyphosphate bonds.

However, a broad peak has been observed between the Raman peak values of 600 and 800 cm^{-1} on both the disc and ball wear scar. This peak has been associated with the symmetric stretching mode of oxygen atoms bridging two phosphorous atoms (P-O-P) [167] and the Raman band position are shown to increase in peak value with the increase of the zinc content on the glasses [167, 171]. The frequency and intensity of the chain P-O-P symmetric vibration has also been reported to be affected with Raman as the metal cation interaction is weak between the bridging oxygen forming the polyphosphate chain [169]. Therefore with the values of 744 cm^{-1} at the disc samples and 774 cm^{-1} at the ball wear scar, it could be established that the polyphosphate order in the ball sample has a higher order of zinc content on the scar and longer chain of the polyphosphate order. Similar various peaks around 283, and 456 cm^{-1} can also be observed at the Raman spectrum of the wear scar, and related to various order peaks for the MoS_2 tribofilm as observed with the additive of MoDTC itself.

6.3.1.2 TEM analysis of the MoDTC/ZDDP tribofilm under ~25ºC (room temperature) conditions.

TEM analysis conducted onto the MoDTC/ZDDP tribofilm displayed a thickness value ranging between 20 – 40 nm. Thin films are observed to cover the entire surface of the disc wear scar, and as observed in Figure 6.16 (a), a clear glassy structure films are observed in between the tribofilms. This clear glassy film was also observed to fill in the cracks formed on the surface of the steel substrate (Figure 6.16 (b)).

A thicker tribofilm (< 200 nm) are observed where deeper crevices was formed onto the surface of the substrate. These tribofilm as observed in Figure 6.16 (c) has a thicker deposit of tribofilms and tends to level with the thinner films formed on the surface.

Clear glassy structure film dominates the entire structure of the tribofilm, but layers of MoS_2 'eyelash' structure (Figure 6.16 (d)) are observed to dominate the top surface of the tribofilm. Thin layers of MoDTC/ZDDP tribofilm observed at the wear scar area, shows a dominating presence of a clear glassy structure but a few layers of the MoS_2 structure is also present on the top surface of the tribofilm.

Raman analysis conducted on the sample wear scar showed an intense Raman peak for the E^1_{2g} and A_{1g} vibrating mode of the MoS_2 tribofilm at 383 and 407 cm^{-1} (Figure 6.15). Hence the friction reduction in the MoDTC/ZDDP is due to the presence of these MoS_2 layers on the top surface of the tribofilm. The clear glassy structure films has been credited to the formation of phosphate layer near the steel substrate which has been credited towards antiwear properties of the ZDDP film and discussed further in the following section.
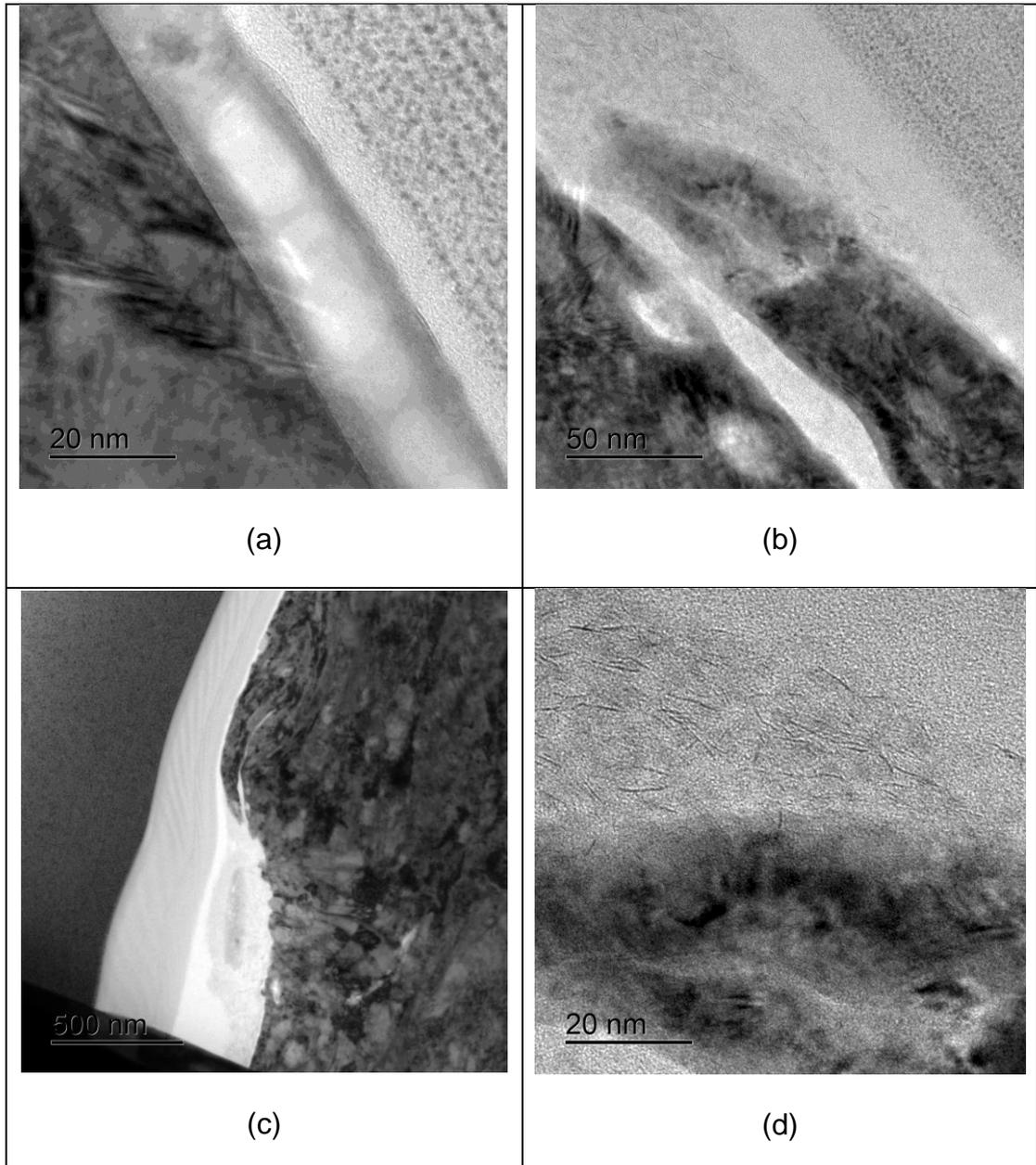
Figure 6.16 TEM images of the MoDTC/ZDDP tribofilm at the HSPOD disc wear scar, for test conducted under room temperature boundary conditions for a time period of 1 hour (a) Clear glassy structure film formed on the tribofilm (b) Clear glass structure formed in between the cracks of the steel substrate (c) Thicker tribofilm formed on the crevices of the steel substrate (d) 'Eyelash' type structure of MoS_2 formed onto the top surface of the tribofilm. (Images according to their relevant scale).

Figure 6.17 (a) provides an indication of the EDX analysis performed on the cross section of the MoDTC/ZDDP tribofilm at a room temperature condition. EDX analysis in conjugation with TEM was performed on the tribofilm to characterize the element on the tribofilm.

EDX1 performed on the steel substrate gave a strong characteristic X-ray (keV) of Fe along with a small amount of Cu, which can be present as an a low alloy element of the substrate. EDX analysis performed on EDX4 showed an intense peak for the element of Platinum which was deposited on the surface to protect the underlying tribofilm. Similar response is also observed for the analysis performed on the point of EDX3. However, analysis performed on the point of EDX2 (Figure 6.17 (b)) shows the presence of Zn, O, P, S and C elements along with the presence of the substrate elements of Fe and Cu.

Raman analysis performed on the tribofilm shows a strong presence of MoS_2 tribofilm onto the wear scar. The EDX analysis shows the presence of S element which corresponds to the MoS_2 structure, however, the (Lα) X-ray mode of Mo and the Kα mode of S overlaps each other in the characteristic X-ray mode [172, 173] and the presence of Mo is subdued.

ZDDP additive are reported to perform with the formation of Zn phosphate tribofilm and a low intense Raman response shows the presence of ZDDP films. The appearance of Zn, P and O elements relates to the presence of phosphate films, and the absence of any metal oxides on the Raman spectrum indicates the O elements responds to the phosphate film on the tribofilm. Hence, indicating the synergistic effect of friction with the formation of Zn phosphate tribofilm on the surface of the steel with the generation of MoS_2.
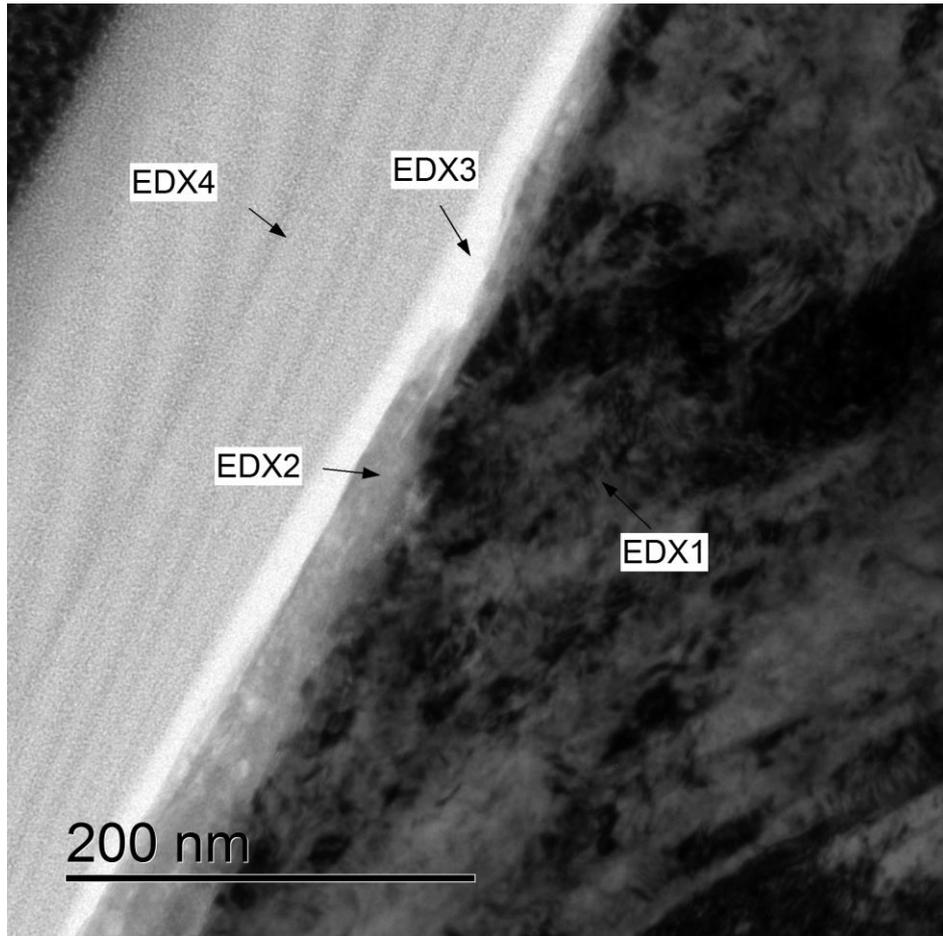
(a)
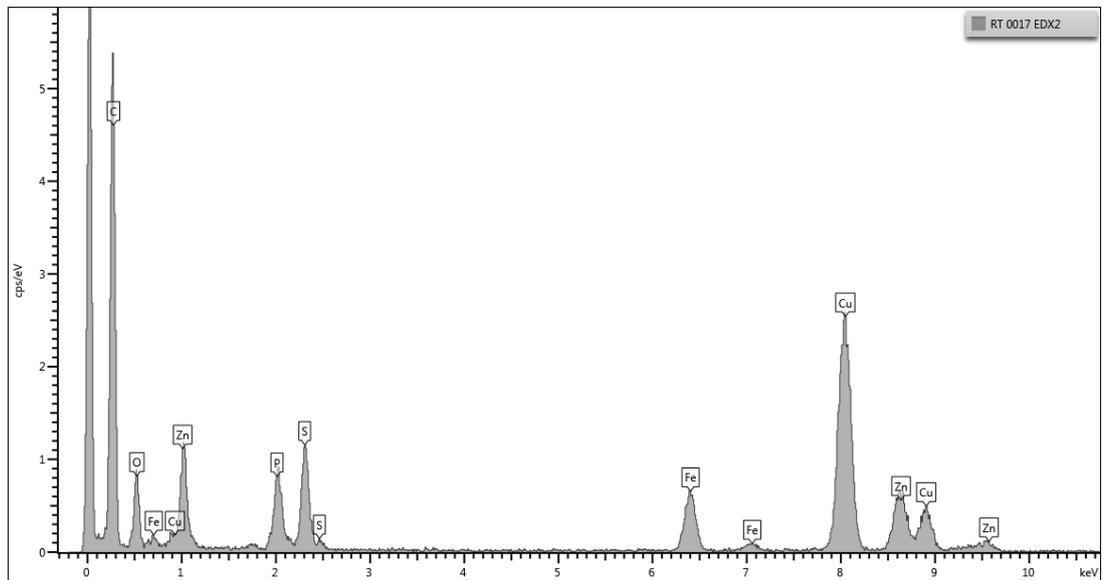
(b)

Figure 6.17 (a) EDX spot analysis performed on the HSPOD MoDTC/ZDDP tribofilm formed under ~ 25°C temperature condition (b) EDX spectrum of the MoDTC/ZDDP tribofilm at the spot area of EDX2.

6.3.1.3 Friction performance of ZDDP under room temperature condition

Figure 6.18 shows the friction coefficient graph for the additive of ZDDP with test performed under room temperature (~25⁰C) at a time period of 1 hour with loads of 1.5 kg and 500 rpm speed. The friction value of the ZDDP additive itself in comparison to the values of MoDTC and its interaction with the ZDDP in Figure 6.11 is much more higher. The high friction maintained with the lubricant of ZDDP could be due to the formation of Zinc polyphosphate films, which is reported to have higher roughness oriented in the direction of sliding [174].

An early drop in the friction is observed which may indicate the formation of an initial, thin reaction film promoting the formation of polyphosphate films. Raman analysis conducted on the wear scar area of the disc and ball did not show response of the polyphosphate bonds. This could be the effect of the oil on the sample surface and also the peaks existing with similar band around the region from the substrate affecting the Raman spectra from the polyphosphate bonds. However in Figure 6.23 section 6.4, the wear value on the ball sample is shown to be rather small compared to the base oil and with the additive of MoDTC. Therefore stating the formation of a thin layer tribofilms which protects the contacting samples.
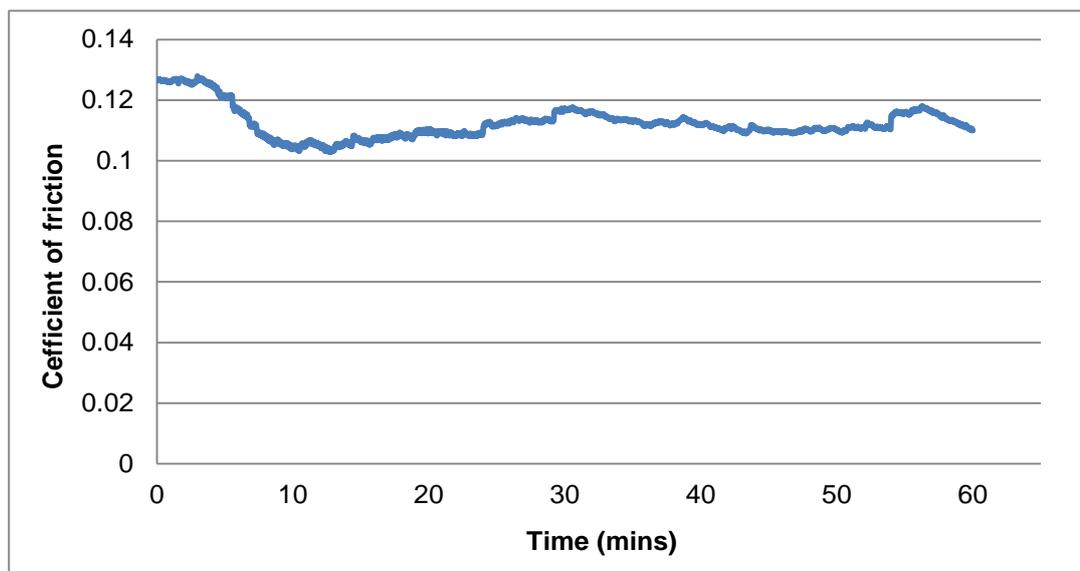
Figure 6.18 Friction coefficient graph for the ZDDP lubricant addtive with test conducted in the HSPOD at a time period of 1 hour, and operating parameters of ~25⁰C, 1.5 kg load and 500 rpm sliding speed.

6.3.2 MoDTC friction performance with ZDDP at 100ºC temperature conditions

Under room temperature (~25ºC) conditions, test carried out with the lubricant additive of MoDTC and ZDDP at boundary conditions showed a decrease in friction, in contrast to the lubricant of MoDTC itself. A comparative friction graph for the lubricant additive of MoDTC itself at 100ºC and its interaction with the lubricant of additive of ZDDP is presented in Figure 6.19. MoDTC reduces friction at higher temperature conditions of 100ºC and is also observed with the lubricant additive combination of MoDTC and ZDDP. The lubricant additive of MoDTC and ZDDP shows a shorter induction period which reduces friction within a time period of 1 or 2 minutes. The lubricant additive of MoDTC takes about 10 minutes to induce a steady state friction value. Lubricant additive of MoDTC and ZDDP, after a drop in friction a slow increase in friction is also observed with a rougher friction steady state around 0.06. Korcek *et al* [52] explained in systems containing ZDDP, extensive oxidation is inhibited by antioxidant reactions of ZDDP, and its ligand exchange products. However, MoDTC is reported to undergo some form of oxidation to reduce friction [42]. Therefore, under higher temperatures extensive oxidation accelerates the consumption of Mo compounds and leads to a premature loss of friction reducing capability.
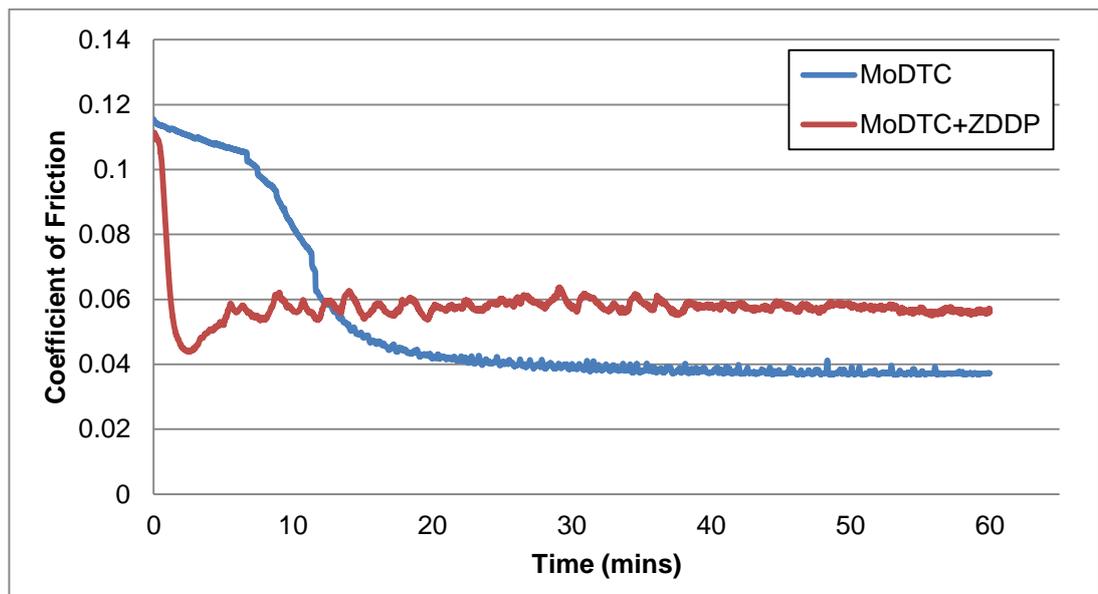
Figure 6.19 A comparative friction graph for the lubricant additive of MoDTC itself and a combination of MoDTC and ZDDP. Test was conducted in the HSPOD for a time period of 1 hour and 100ºC temperature conditions and 1.5 kg load and 500 rpm.

6.3.2.1 Raman analysis on the tribofilm of MoDTC/ZDDP

Raman analysis performed on the ball and disc sample (Figure 6.20) of the lubricant additive of MoDTC/ZDDP at 100ºC showed peak values very similar to that of the room temperature conditions. Raman peaks for $FeMoO_4$ and Fe_3O_4 at 923 and 660 cm^{-1} has not been observed for the lubricant additives of MoDTC and ZDDP at room temperature and also with higher temperature at 100ºC. Raman peaks at 455 and 224 cm^{-1} has been regarded as various order peaks arising from the MoS_2 tribofilm. However low frequency peak values at 585 and 750 cm^{-2} could be arising from bending vibrations of the phosphate tetrahedra [167, 175] and the stretching mode of P-O-P bonds [167-169] respectively. Similarly a sharp response of the E^1_{2g} and A_{1g} peak modes for the MoS_2 tribofilm is observed onto the Raman spectrum of the disc and wear scars. The peak values corresponded to Raman peak values at 381 and 404 cm^{-1} and a Raman shift of 2-3 cm^{-1} is observed in comparison to the room temperature MoDTC/ZDDP Raman values. Effect of layers on the Raman shift of the E^1_{2g} and A_{1g} MoS_2 peak has been reported [176, 177] and hence the loss of friction reducing at high temperatures could be related with the loss of MoS_2 layers on the surface.
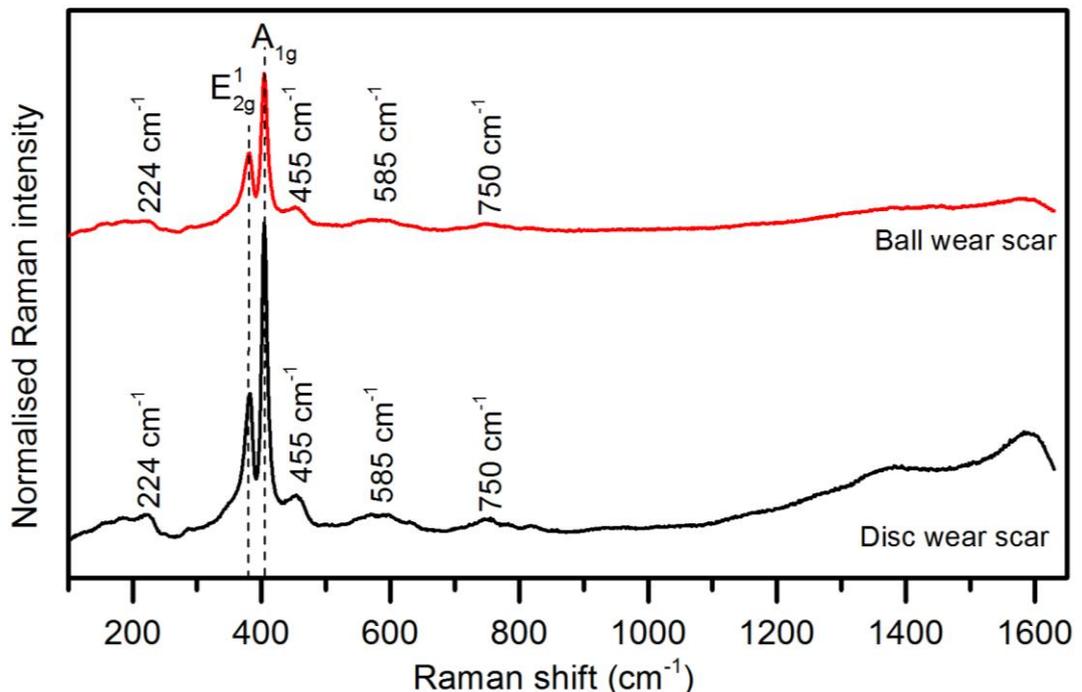
Figure 6.20 Raman spectra (488 nm excitation) of the HSPOD disc and ball samples for test conducted with the lubricant of MoDTC and ZDDP at 100ºC temperature conditions .

6.3.2.2 TEM analysis of the MoDTC/ZDDP tribofilm under 100°C temperature conditions.

TEM images (Figure 6.21) of the 1 hour time period MoDTC/ZDDP tribofilm at 100°C showed similar resemblance to the room temperature samples. The tribofilm showed an overall layer of 40 – 60 nm thickness and as observed with the room temperature tribofilm, thicker deposit of tribofilms were observed at crevices formed onto the surface (Figure 6.21 (a)).

A thicker deposit of tribofilm is observed for the tribofilm of MoDTC/ZDDP at 100°C in comparison to room temperature samples. Clear glassy structure film dominates the entire structure of the tribofilm as observed in Figure 6.21 (c) and (d).

Under room temperature conditions, thicker layers of MoS_2 eyelash structures were observed on the top layer of the tribofilm. TEM images at Figure 6.21 (a) and (b) shows a few layers of MoS_2 on the tribofilm. This few layers of MoS_2 is observed on the top surface of the film and also in between the tribofilm layer.

Raman analysis on the wear scar of the tribofilm showed a shift of the E^1_{2g} and A_{1g} values in comparison to pure Raman values of MoS_2 sample. Shifts in the E^1_{2g} and A_{1g} vibrating mode of the MoS_2 structure has been shown to be highly dependent on the layers of the MoS_2 formed [176, 177] . Hence, as observed with the TEM images, fewer layers of MoS_2 tribofilm formed on to the contacting surface affects the Raman shift values and as observed in Figure 6.18 also affects the friction response of the additive system.

EDX analysis in conjugation with TEM was also performed on the tribofilm to characterize the element of the tribofilm. Figure 6.22 (a) provides an indication of the EDX analysis performed on the cross section of the MoDTC/ZDDP tribofilm at 100°C temperature condition.
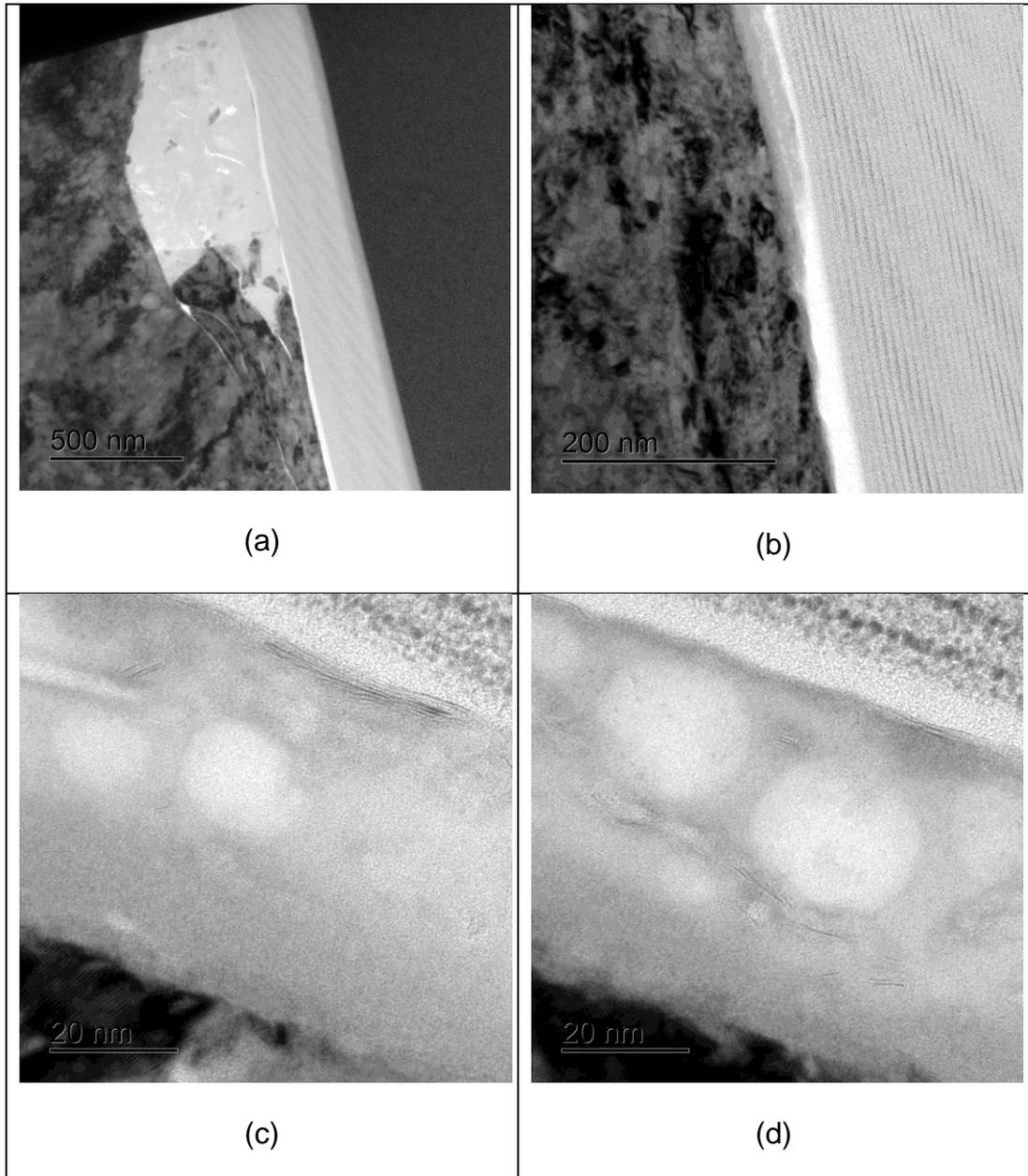
Figure 6.21 TEM images of the MoDTC/ZDDP tribofilm at the HSPOD disc wear scar, for test conducted under 100ºC   temperature boundary conditions for a time period of 1 hour (a) Thicker tribofilm formed on the crevices of the steel substrate (b) Tribofilm thickness ranging between 40 – 60 nm (c) Clear glassy structure film formed on the tribofilm and few layers of MoS_2 on the top surface of the film (d)   'Eyelid' type structure of MoS_2 also observed in between the layers of the tribofilm. (Images according to their relevant scale).

EDX1 showed a characteristic X-ray (keV) of Fe along with a small amount of Cu, which was a typical composition of the steel substrate and also observed with the room temperature condition samples. Similarly EDX3 and EDX4 showed a high response for the Platinum element deposited on the top surface to protect the underlying tribofilm.

EDX analysis performed on the tribofilm layer at the spot of EDX2 is observed at Figure 6.21 (a). EDX spectrum at EDX2 shows a high response for the elements of Iron (Fe) and Copper (Cu) which is present from the steel substrate. Along with the response of Fe and Cu, small traces of the element Chromium (Cr) is also observed on the EDX spectrum. Standard Ball bearing used in the test is an AISI 52100 Chrome Steel and has a high presence of Cr on the sample. Hence, the presence of Cr is justified with the wear of the ball sample and deposited onto the tribofilm layer.

EDX spectrum of EDX2 (Figure 6.22(b)) also shows the presence of Zn, O, P, S and C, similar to the elements observed with the EDX analysis of the room temperature tribofilm. A high carbon element response is observed on the tribofilm which states a rich carbon rich layer is present. Similar to the room temperature tribofilm, the appearance of Zn, P and O elements relates to the presence of phosphate films, and the absence of any metal oxides on the Raman spectrum indicates that the O elements responds to the phosphate film on the tribofilm

 A higher atomic percentage of P and O element in 100ºC sample in comparison to the room temperature sample could indicated the presence of higher Zinc phosphate layer on the sample. TEM images shows that few layers of MoS_2 is formed on the tribofilm, and also confirmed with the response of Raman peaks for MoS_2. However Mo elements are not observed on the EDX spectrum, but S elements are present on the spectrum. Therefore the EDX response of Mo element could have been subdued due to the overlap of energy of S and Mo X-ray mode, or due to the spot analysis resolution not able to cover the entire tribofilm.
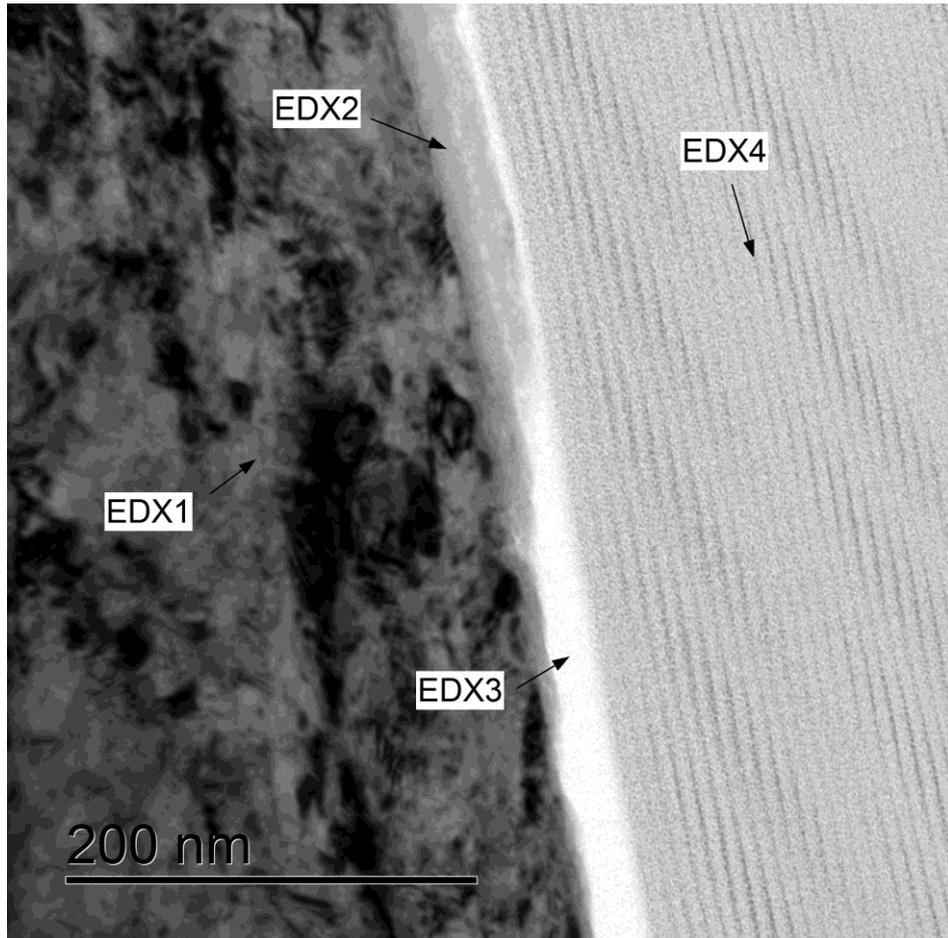
(a)
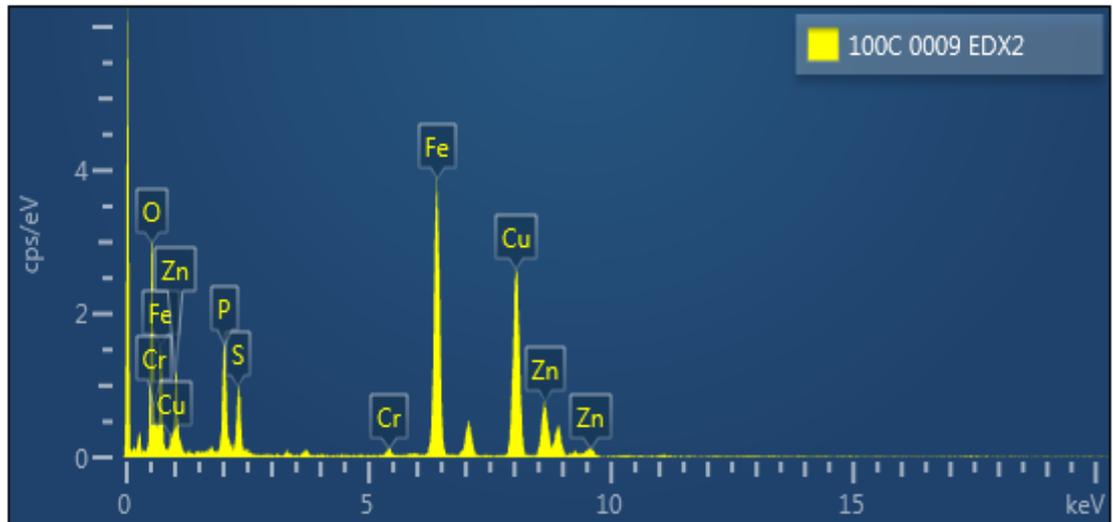
(b)

Figure 6.22 (a) EDX spot analysis performed on the HSPOD MoDTC/ZDDP tribofilm formed at temperature of 100°C condition (b) EDX spectrum of the MoDTC/ZDDP tribofilm at the spot area of EDX2.

6.3.1.3 Friction performance of ZDDP at 100ºC temperature condition

Figure 6.23 shows the friction performance of the lubricant additive ZDDP at a temperature of 100ºC for a 1 hour time period. Fiction value rises for the ZDDP additive at 100ºC to a steady value of around 0.1. Room temperature test shows similar value of friction with time, but a rougher response of friction is observed. Heuberger et al [178] reported at room temperature under tribological stress tribofilm consisted of zinc orthophosphate, which lead to longer chains with increasing temperature. Therefore the thicker the film formed on the contacting surface, the higher the friction coefficient. Hence under rubbing at room temperature, an early drop in the friction is observed which may indicate the formation of an initial, thin reaction film. However at high temperatures the early rise in friction could be related to thicker film of tribofilm forming on the surface. At higher temperature heated ZDDP solution is also reported to form thermal films on the metal surface [162] and which could initiate the formation of the ZDDP tribofilm under tribological contact. Similar to the room temperature (~25°C) samples, Raman analysis conducted on the wear scar area of the disc and ball did not show response of the polyphosphate bonds.
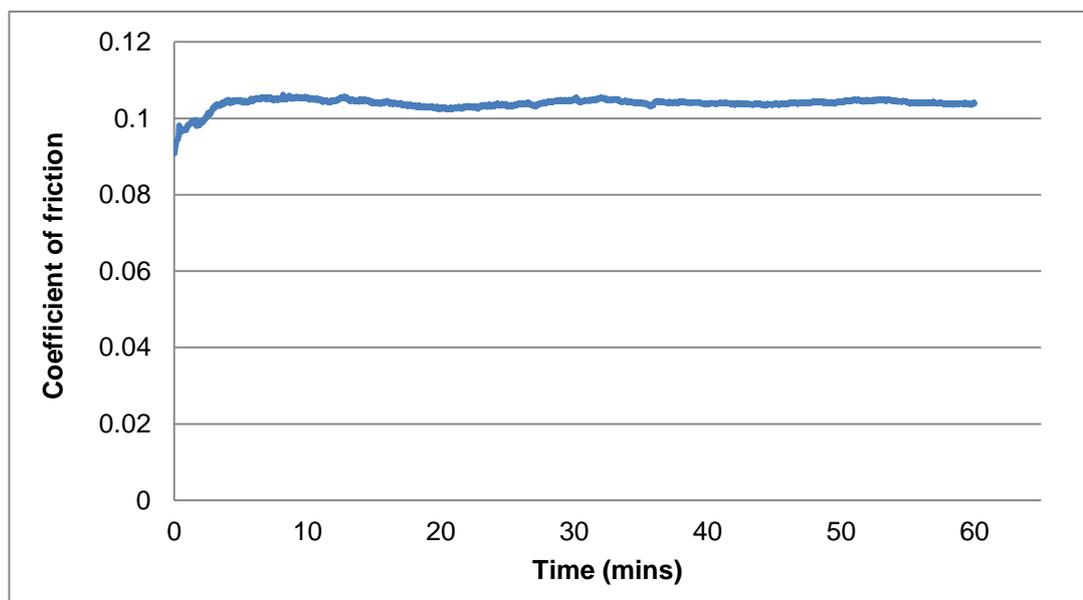
Figure 6.23 Friction coefficient graph for the ZDDP lubricant addtive with test conducted in the HSPOD at a time period of 1 hour, and operating parameters of 100ºC, 1.5 kg load and 500 rpm sliding speed.

6.4 Wear performance

Wear coefficient values for the lubricant additive of MoDTC, MoDTC/ZDDP, ZDDP and base oil PAO4 under room temperature (~25°C) and 100°C at 1.5 kg load and speed of 500 rpm are compared in Figure 6.24. The wear factors are used to indicate the lubricant effectiveness in wear reduction in the overall lubricating system. Surface analyses performed on the disc wear scar showed very small wear values and a compromise was necessary to measure wear accurately.

Wear rate are therefore calculated from the wear scar diameter on the ball and Figure 6.25 shows the wear scar diameter of the different lubricant systems at the end of 1 hour test period. An overall minimum wear is achieve with the lubricant additive of ZDDP, and a decrease in wear rate is observed with the increase in temperature. Similarly, MoDTC in conjugation with ZDDP shows a similar response, but lower friction is also achieved with the lubricant additive system. However, with the lubricant additive of MoDTC on its own and the base oil shows an increase in wear rate with higher temperature. MoDTC at higher temperature is able to reduce friction, however has a higher wear rate value.
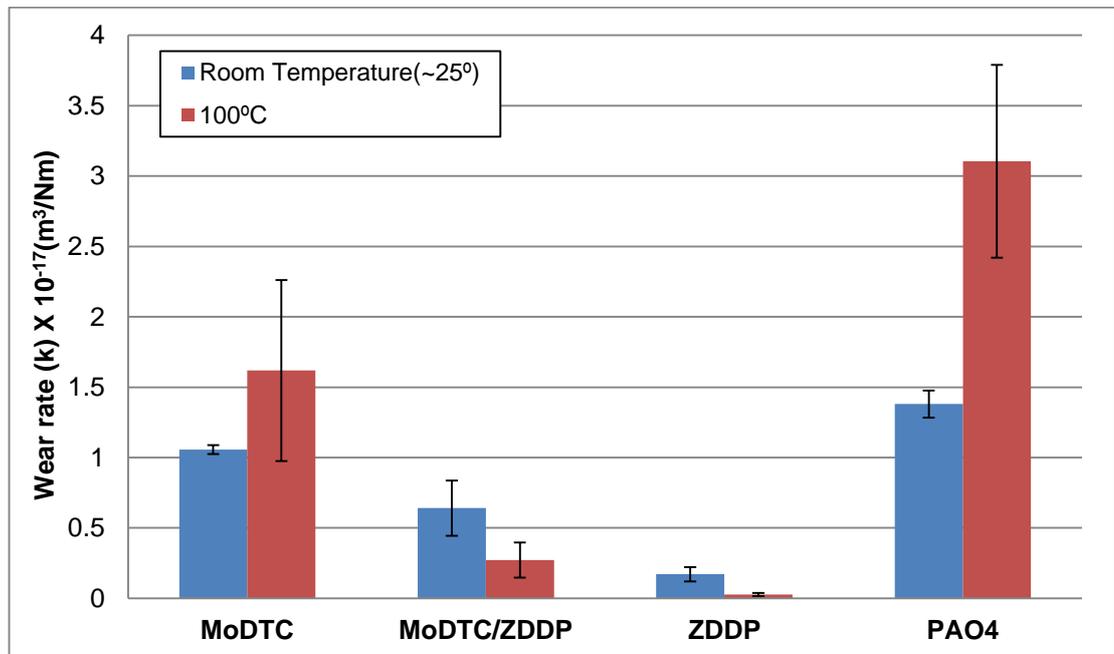
Figure 6.24 Wear rate comparision values at the end of 1 hour HSPOD test for the lubricant additive of MoDTC, MoDTC/ZDDP, ZDDP and base oil PAO4 under room temperature (~25°C) and 100°C at 1.5 kg load and speed of 500 rpm.
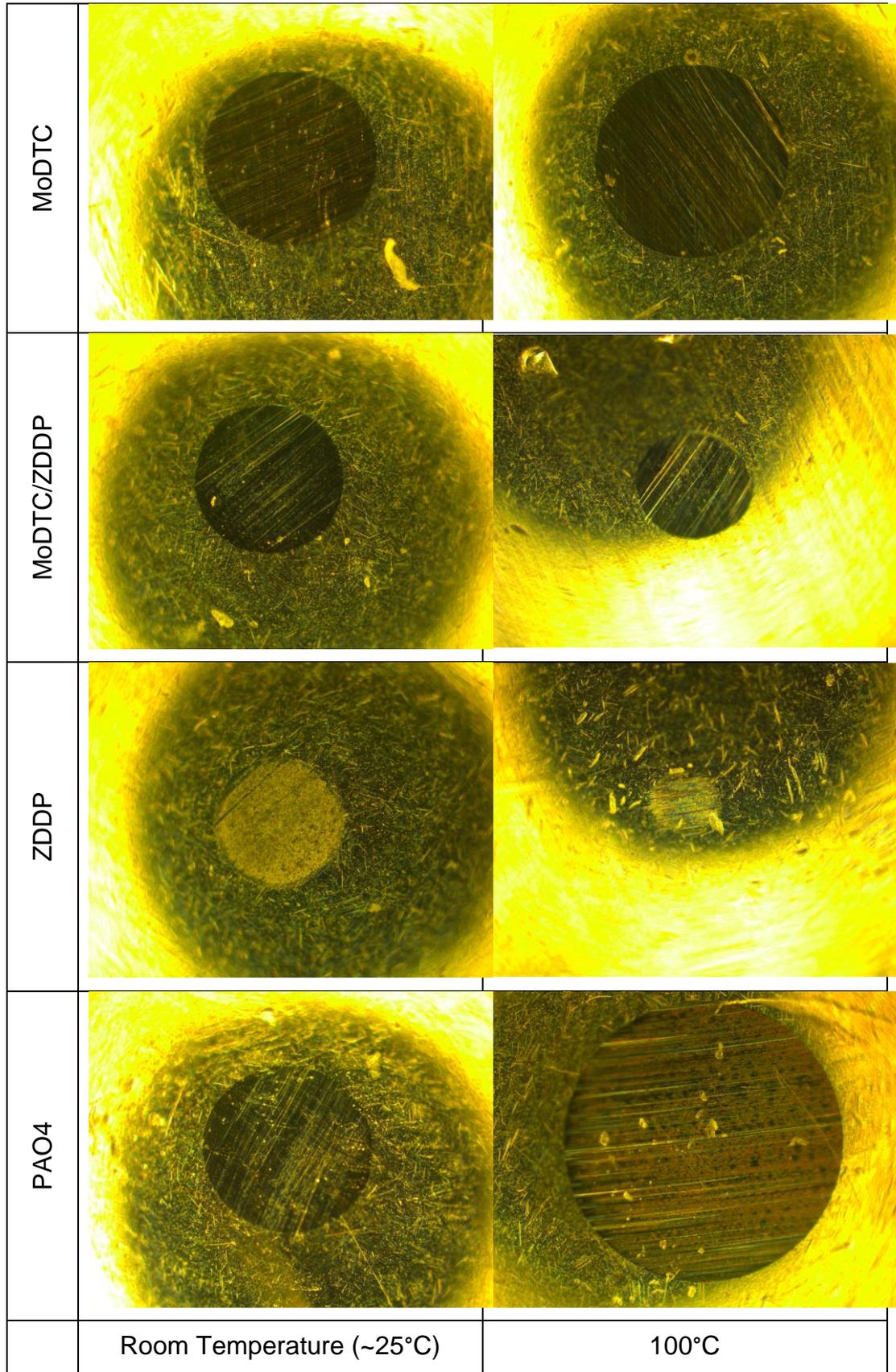
Figure 6.25 Optical images (10 X Objective) of the end of test HSPOD wear scar diameter of the ball sample for the stated lubricant and additive test of 1 hour time period at teperatures of ~25°C and 100°C.

6.5 Summary

In this chapter, tribological performance of the lubricant additive MoDTC under varying parameters and its interaction with the ZDDP additive was presented. The following findings can be summarised in this section.

Tribological performance of the MoDTC lubricant additive was dependent on the varying parameters of load, speed and temperature.

Friction and wear performance of the MoDTC lubricant additive followed similar trend to each other. With the increase in sliding speed, friction and wear usually decreased for a one hour test at the defined load and temperature.

At contact pressure of 1.02 GPa and 500 rpm sliding speed, wear rate was reduced due to the adsorption of MoDTC additive species on the wear scar, which also defined the friction.

The reduction in friction due to the formation of MoS_2 tribofilm was highly dependent on temperature.

With the increase in temperature some form of MoDTC complex is absorbed on the wear scar which defines the friction of the MoDTC system.

At high temperature any sort of thermal absorption of the MoDTC additive does not occur on the sample surface, however some sort of lubricant oxidation reduces the friction at low temperature test conditions.

With the removal of lubricant from the system, MoS_2 tribofilm was not able to maintain low friction on its own. Raman analysis showed the presence of the MoS_2 on both contacting samples, but was subjected to higher stress.

MoDTC additive was able to reduce friction in conjugation with ZDDP additive even under low temperature conditions, with the formation of MoS_2 tribofilm.

The induction period to reduce friction was observed to be shorter with the MoDTC/ZDDP additive at high temperature conditions.

TEM analysis conducted on the MoDTC/ZDDP samples showed the presence of eyelashes type of structure for the MoS_2 film. This structure was present mostly on the top surface of the tribofilm. At higher temperatures fewer layers of these structure was present.

EDX analysis on the tribofilm confirm the presence of phosphate films on the tribofilms and usually present as clear glassy structure on the TEM images.

The additive of ZDDP on its own was not able to reduce friction on its own, and the Raman presence of the zinc phosphate was not observed on the tribofilm.

Comparatively ZDDP additive confirmed overall minimal wear for the analysis conducted on the samples. Similarly, MoDTC/ZDDP samples showed less wear in comparison to using MoDTC lubricant additive on its own.

Chapter 7
Ex-situ and *In-situ* Time Transient Study of Tribofilm Under Boundary Lubricated Conditions

At the defined conditions of tribological test, the effect of temperature is prominent toward the formation of MoS_2 tribofilm for the additive of MoDTC. While there is a good understanding of the end-of-test tribofilm composition, not much is known about the transient processes that lead to the formation of these tribofilms.

The tribofilm formation of MoDTC showed high dependence on the tribological parameter specially with high temperature. The study conducted here utilizes Raman Spectroscopy with *ex-situ* and *in-situ* methods to understand the development of the MoDTC tribofilm as a function of time for conditions of high and low friction systems. A time resolved study has been conducted as a function of rubbing and tribofilm formation to understand the chemical kinetics of the MoDTC lubricant additive.

Chapter 4 provides the description of the small scale, unidirectional tribometer capable of operating in conjunction with a Raman spectroscopy, designed in order to monitor the tribological phenomenon occurring within the boundary lubricated surface. *In-situ* Raman spectroscopy is a technique developed to understand the development of a tribochemical phenomenon occurring on a rubbing surface.

The importance of *in-situ* approaches for tribological interface studies has been highlighted in Chapter 2. Experiments similar to conditions operated with that of the HSPOD tribometer has been conducted on the *in-situ* rig for the lubricant additive of MoDTC. *In-situ* test are conducted as a time transient process with rubbing on the surface for the additive of MoDTC with the analysis of Raman on every time period.

7.1 Time transient study of MoDTC tribofilm development (*ex-situ* analysis)

Tribological experiments were conducted using a High Speed Pin on Disc Tribometer for different time periods of two and a half minutes, five minutes, ten minutes, thirty minutes and one hour. Test were conducted with the boundary conditions stated in earlier test and under temperature of ~25°C (Room temperature) and 100°C. Raman analysis were performed on the disc and ball wear scar after the test where any form of sample cleaning was avoided to analyse the tribofilm. Raman peak values, intensity and Full Width Half Maximum (FWHM) values are related with the analysis performed on the various time period sample.

7.1.1 Effect of rubbing on the tribochemical development of the MoDTC tribofilm at ~25⁰C (room temperature)

Friction results for the lubricant additives of MoDTC are shown in Figure 7.1 for the test conducted at room temperature, respectively at various time periods. Friction for base oil is included too. The MoDTC friction graph at room temperature shows no significant friction reduction, compared to the friction observed at the start of the test. Friction coefficient of the MoDTC lubricant additive stabilizes at a value of 0.08. Shorter time periods demonstrate that the friction coefficient starts at a higher value but along the time period the friction drops gradually and stabilizes at 0.08.

In comparison to the friction coefficient of the base oil, a gradual friction decrease can be observed on Figure 7.1 for the room temperature MoDTC test but not to the level attributed to MoS_2 formation [30, 47, 51]. HSPOD samples after the experiments were analysed with the Raman microscope with a method of In-lubro analysis. Disc and the ball samples were taken off from the test condition, *without rinsing* and sample's wear scar analysed under the Raman microscope. Analysis was carried out on the specimens where an alternative form of sample cleaning was not carried out.
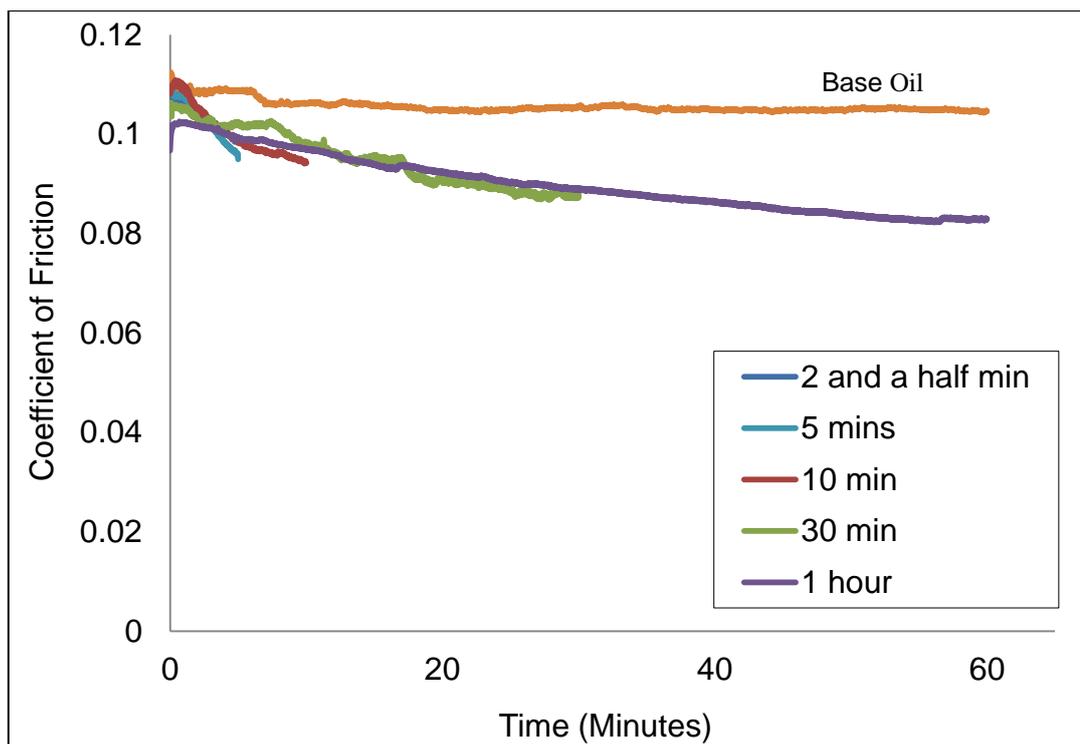
Figure 7.1 Friction coefficient as a function of time for PAO4 (base oil) and the MoDTC lubricant additive, with test conducted in the HSPOD and experimental parameters of 1.5 kg load, sliding speed of 500 rpm and room temperature conditions (~25°C).

Raman response of the wear scar tribofilm of the room temperature MoDTC conditions shows a presence of the Mo-S peaks onto the sample for every time period but not that of the pure MoS_2. Not surprisingly, Raman analysis on the wear scar of the base oil test samples showed an absence of the Raman response as those observed on the room temperature MoDTC test samples.

Samples from different time periods at room temperature showed the two characteristic Raman responses for the particular Mo-S bond as shown in Figure 7.2. These characteristic peaks were observed even at the earliest time period of two and half minutes. The typical Raman spectrum for the wear scar analysed shows a Raman response of the E_{2g} and A_{1g} peak at 375 and 400 cm^{-1}. This response was not observed on every area of the sample's wear scar which indicates the uneven distribution of the tribofilm formation onto the surface. This is confirmed with the Raman mapping results shown later in this section.

Under room temperature conditions for various Raman spectra, an apparent shift of the Raman peak position for various time period samples was not observed. The room temperature tests shows no apparent decrease in friction with time and a pure form of MoS_2 tribofilm is not observed with the Raman spectroscopy onto the sample as well.

The Raman peak position at various time periods has been highlighted at Figure 7.3, performed at different wear scar areas in the sample. For the Room temperature sample the E_{2g} peak value is observed at 375 cm^{-1} for most of the analysed samples. Similarly, the A_{1g} peak assigned to the motion of the S atoms along the z axis of the unit cell is observed at the range of 400 cm^{-1} frequency. Along various wear scar areas analysed, no change in the peak position of the Mo-S frequencies has not been observed.
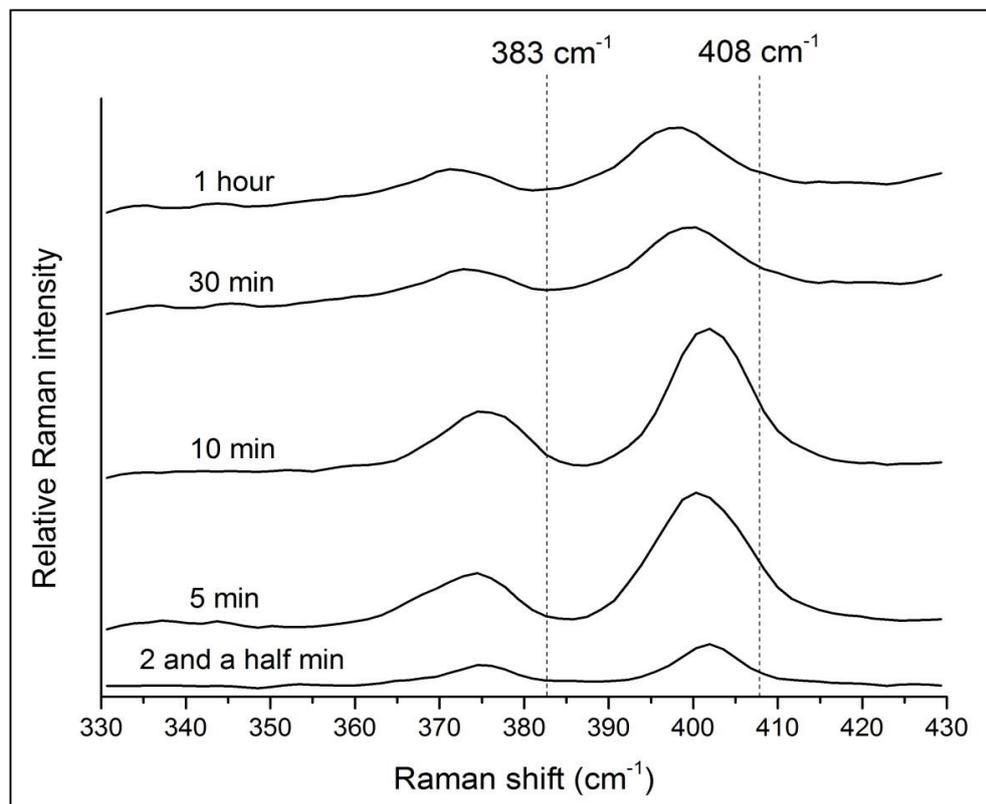
Figure 7.2 Raman response of the E^1_{2g} and A_{1g} vibrating frequency of the Mo-S bonds as a function of rubbing time for room temperature test conditions on the sample disk wear scar. The position of the E^1_{2g} and A_{1g} peak of the pure MoS_2 is highlighted at 383 and 408 cm^{-1}.
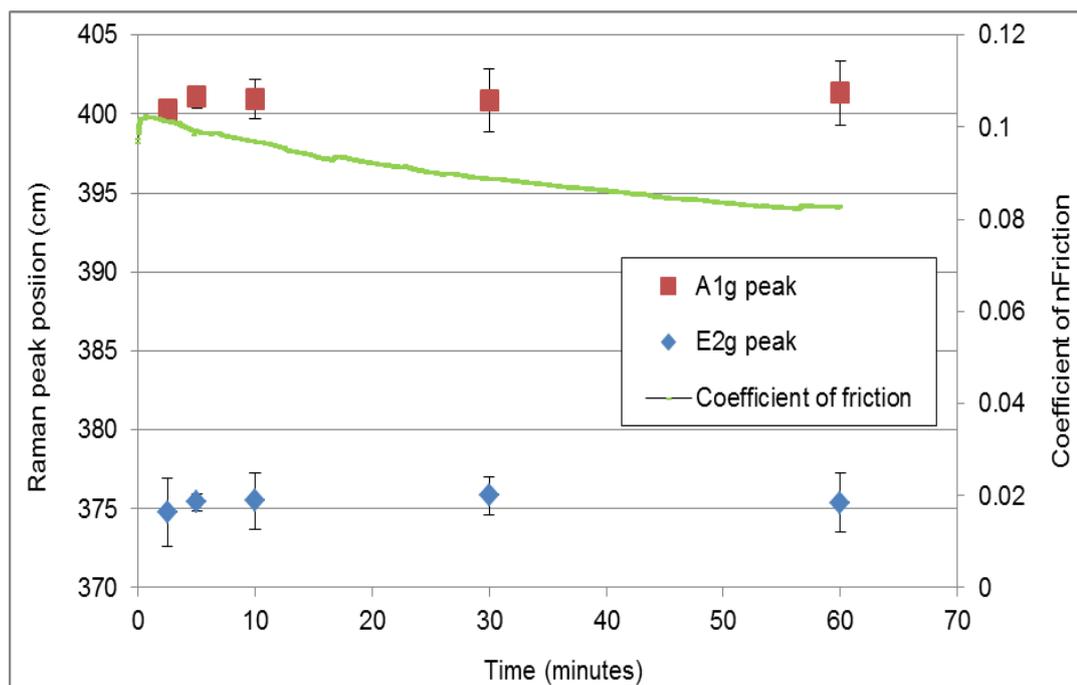
Figure 7.3 Raman peak position of A_{1g} and E^1_{2g} mode for various Room temperature time period disk samples, along with the friction coefficient of the 1 hour room temperature test.

Raman analysis conducted on the wear scar of the ball samples however shows the absence of any Raman response. However, a response at around the Raman shift value of 660 cm^{-1} is observed [Figure 7.4 (a)] on most of the analysed wear scar area for all of the time period samples. These Raman value at 660 cm^{-1} has been accredited to the response of the Fe_3O_4 iron oxide [150], and can be related to the wear of the ball sample occurring with longer duration of time.

A definite peak of MoO_3 at 820 cm^{-1} is not observed on to the Raman spectrum of the room temperature disc sample. However, various peaks in and around 870 and 920 cm^{-1} frequency are observed occasionally on the Raman spectrum of the sample. For tests of less than ten minutes, a Raman peak position 871 cm^{-1} has been observed which gradually becomes less intense with time and disappears with longer duration of test period as shown in Figure 7.4 (b). However, with the disappearance of the 871 cm^{-1} Raman band, a new peak appears around 920 – 930 cm^{-1} Raman shift. This Raman peak is significant for longer duration of test and is observed with every Raman analysis undertaken for the Room temperature test.
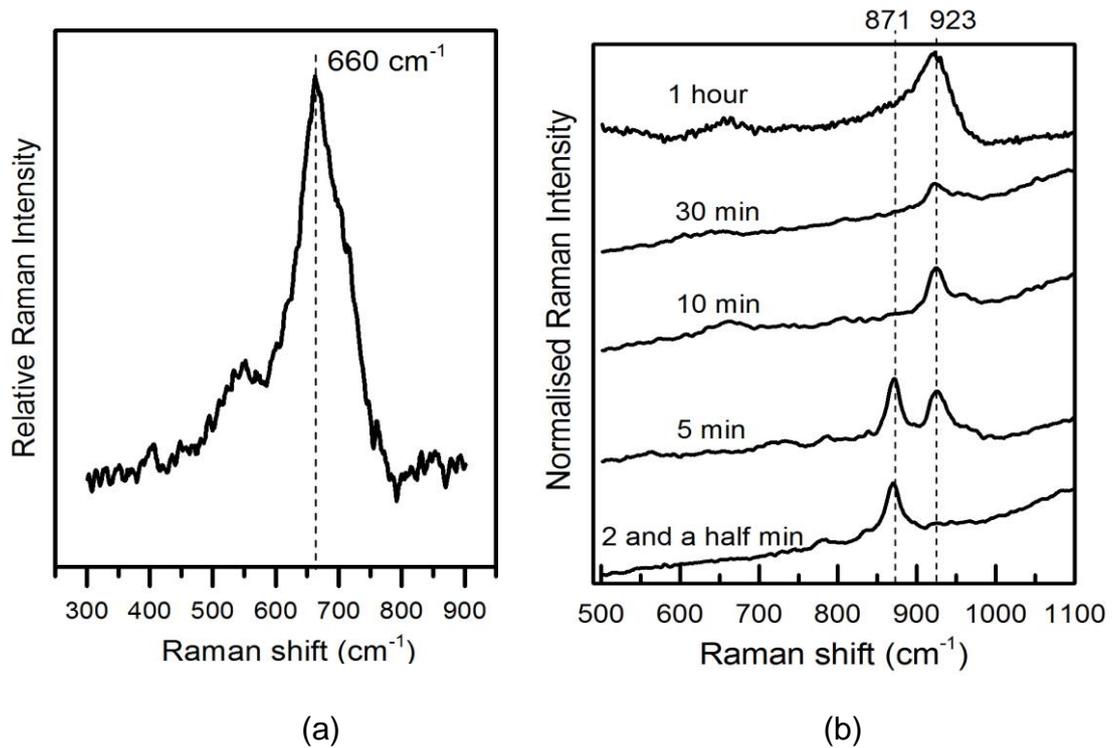
Figure 7.4 (a) Raman response of the room temperature sample ball wear scar for the 1 hour time period. The Raman response of the Fe_3O_4 at 660 cm^{-1} is observed on the various time period ball wear scar. (b) Various Molybdneum oxide bonds observed at different time duration room temperature test disk samples.

Figure 7.5 shows a comparative and averaged Full Width at Half Maximum (FWHM) Raman bands for the Raman response of the two characteristic Mo - S peaks. The Raman peak response at around 375 cm^{-1} assigned to the motion of the Mo - S atoms (E_{2g}) and the assigned motion of the S atoms (A_{1g}) at around 400 to 405 cm^{-1}

Raman frequency, indicates the FWHM value around the range between 10 and 20. The FWHM of the various time duration test show similar values for the two Mo-S peaks at a particular time period.
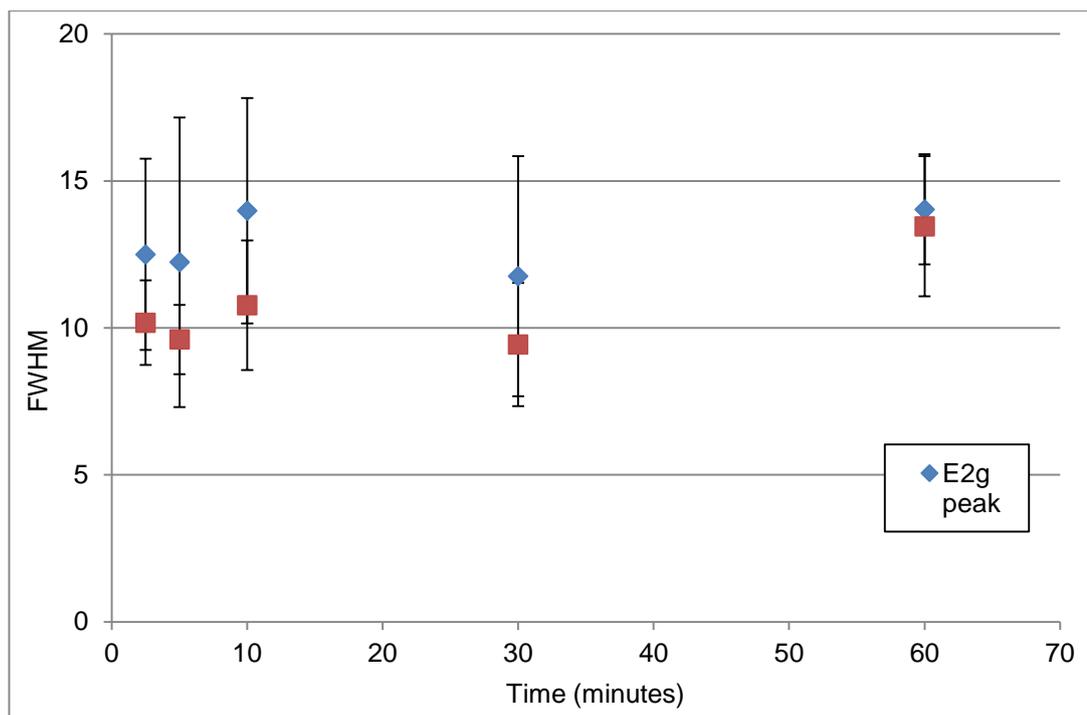
Figure 7.5 Raman response of the E^1_{2g} and A_{1g} vibrating frequency of the Mo-S bonds as a function of rubbing time for room temperature test conditions on the sample disk wear scar. The position of the E^1_{2g} and A_{1g} peak of the pure MoS_2 is highlighted at 383 and 408 cm^{-1}.

To further indicate the formation and distribution of the MoS_2 tribofilm on the sample surface, a Raman map analysis was also carried out onto the surface. The analysis was undertaken with the same parameters to the single point analysis, and a similar mapping analysis was carried out on two to three different areas.

The Raman map was analysed with the distribution of the normalized intensity variations of the 400 cm^{-1} (A_{1g}) Raman response of the tribofilm at room temperature. The response of the Raman peak indicates the distribution of the tribofilm is not uniform on the surface (Figure 7.6). Similarly in relation to the normalized intensity values for the scanned area, the intensity values show similar values for every time period samples.
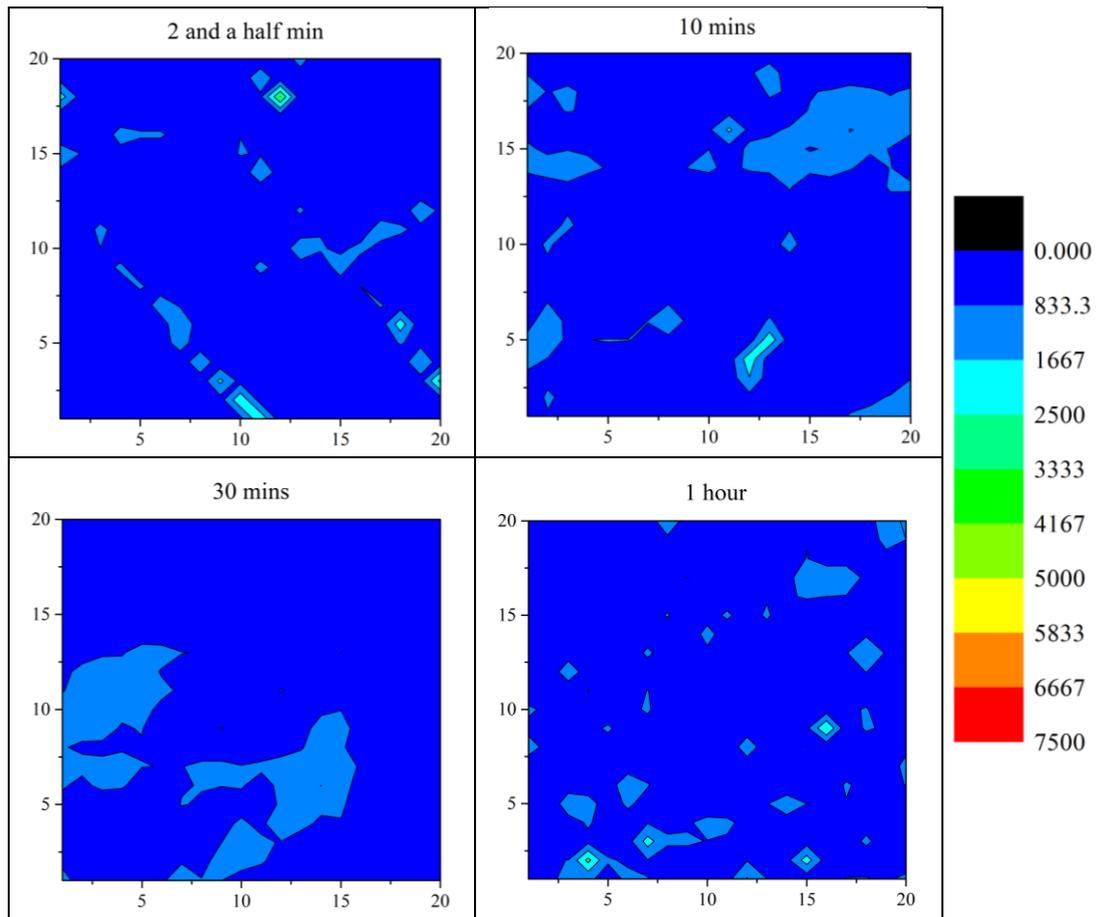
Figure 7.6 Raman map intensities of A_{1g} frequency mode at 400 cm^{-1} at a wear scar area of 20 X 20 µm of the disc samples for the time period of (a) two and a half minutes (b) ten minutes (c) thirty minutes and (d) one hour.

7.1.2 Effect of rubbing on the tribochemical development of the MoDTC tribofilm at 100⁰ C

Friction coefficient graph for the MoDTC additive under a higher lubricant temperature of 100°C shows a gradual drop of the friction (Figure 7.7). The effect of temperature is instantly observed as the friction drops to a value of 0.04 along the time period. Under boundary lubrication, these Molybdenum friction reducing additives have been known to produce very low coefficient of friction values of 0.04 to 0.075 and the effect of temperature has been obvious [43, 44].

The high temperature test with the MoDTC lubricant starts with a higher friction values in comparison to the room temperature conditions. The friction value in high temperature shows a sharp decrease around time limit of five minutes, followed with a steady state friction of 0.04 around the time period of ten minutes. The application of high temperature to the system therefore defines the friction reduction behaviour of the MoDTC lubricant additive. During the time period of five minutes, thermal tribochemical reaction occurs until the period of ten minutes and after which the friction reaches a steady state period.

The tribochemical reaction occurring due to the application of high temperature is an area of interest in order to understand the friction reducing behaviour of these Molybdenum additives. The ability of these additives to reduce friction from values above 0.1 to low friction coefficient of 0.04 within the various time period tests is undertaken in the current study to analyse the development of the MoDTC tribofilm with Raman spectroscopy.
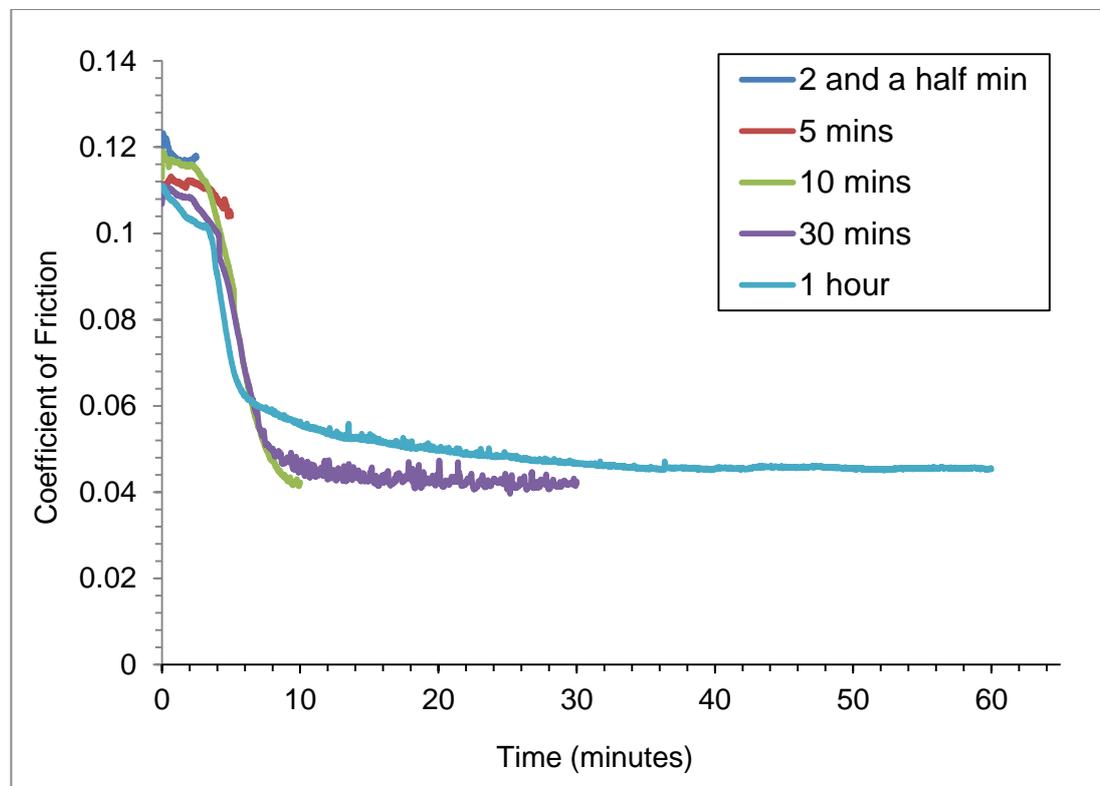
Figure 7.7 Friction coefficient of the MoDTC lubricant additive as a function of time, with test conducted in the the HSPOD and expeimental parameters of 1.5 kg load, sliding speed of 500 rpm and a high temperature of 100°C.

Raman analyses, was performed on the wear scar of the disc and ball samples. The two characteristic peaks peak positions of 379 and 410 cm^{-1} are observed on longer time period when the friction is stable and an apparent shift is observed when the friction starts dropping.

A comparative Raman response of the disc wear scar for various time periods is presented in Figure 7.8 (a). An apparent Raman shift for the A_{1g} frequency mode can be observed, which is not the case with the E^1_{2g} peak. After a time period of two and half minutes, the Raman peak response for the two characteristic peaks has a frequency similar to the ones observed for the Room temperature samples but as stated with the room temperature samples, this peaks were not observed on every area.

The friction coefficient graph also show a high friction value during these time period. Within the time period of five and ten minutes, the friction value starts to drop for the high temperature test. The Raman analysis of the wear scar shows various point analysis at a range of between 400 and 412 cm^{-1} for the A_{1g} frequency mode, and also at a frequency range between 375 and 380 cm^{-1} for the E_{2g} frequency mode.

The low friction of the high temperature test is apparent at time periods of thirty minute where the system starts reaching it steady state friction. The wear scar analyzed showed a sharp Raman response around 410 cm^{-1} and the lower E_{2g} frequency mode between 375 and 380 cm^{-1}, and similar frequency modes were also observed at the wear scar analysis for the one hour time period samples. These frequency modes are the characteristics peak response for the MoS_2 tribofilm.

As the friction drops an evident shift in the A_{1g} is observed which indicates the breakdown of the MoDTC additive towards the formation of a MoS_2 tribofilm. Figure 7.9 shows the distribution of the A_{1g} and E_{2g} Raman peaks for the various time periods along with the friction coefficient of the one hour high temperature test.

Figure 7.8 (b) highlights the Raman response A_{1g} and E_{2g} Raman peaks observed at the wear scar of the ball samples for various time periods. The Raman response of the A_{1g} and E_{2g} Raman peaks of the ball samples shows a similar shift as that observed on the wear scar of the disc samples for different time periods. This Raman shift values are in accordance to the formation of the MoS_2 tribofilms on the ball wear sample and as a result, a friction reduction occurs.

Shorter time period sample, however especially under two and a half minute shows an absence of the A_{1g} and E_{2g} Raman peaks. This response is similar to that of the room temperature ball samples, which showed an absence of the A_{1g} and E_{2g} frequency mode of the Mo-S bonds and the friction is high. Under high temperature, friction tends to drop between time periods of five and ten minutes. The Raman response of the A_{1g} and E_{2g} peaks of a disc sample at ten minute time period shows a value similar to those of the low friction Raman response. However, at a time period of ten minute, the ball sample shows a Raman response of the A_{1g} and E_{2g} Raman value at around 405 and 375 cm^{-1}, which is related to the high friction of the system.
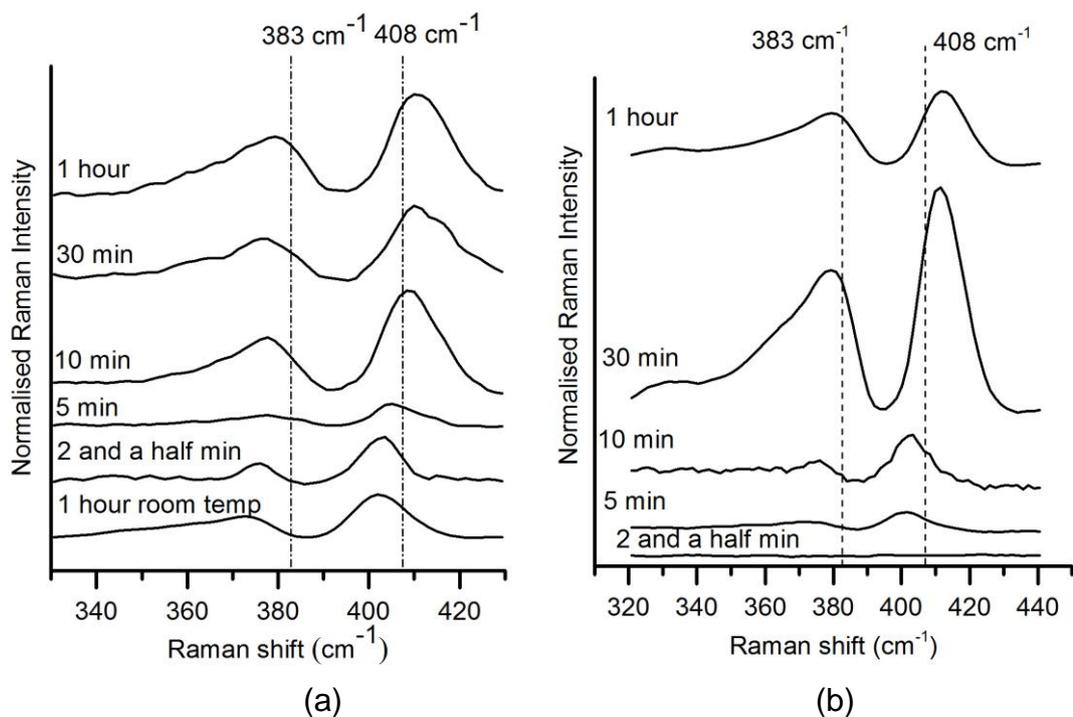
Figure 7.8 Raman response of the E^1_{2g} and A_{1g} vibrating frequency of the Mo-S bonds as a function of rubbing time for high temperature (100° C) test conditions at (a) disc and (b) ball samples. The position of the E^1_{2g} and A_{1g} peak of the pure MoS_2 is highlighted at 383 and 408 cm^{-1}.
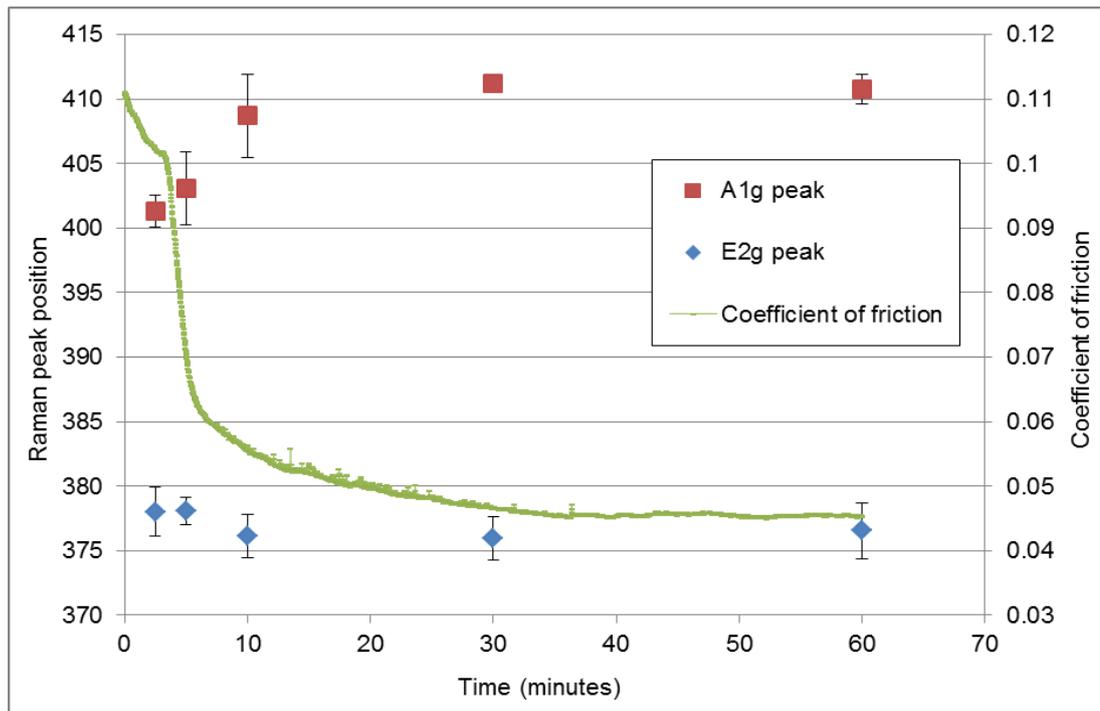
Figure 7.9 Variation of the Raman peak position for different time periods, along with the friction drop at the higher temperature (100°C) test.

Transmission Electron Microscopy (TEM) images shows the presence of an amorphous tribofilm onto the wear scar of the disc sample (Figure 7.10 (a)) for the time period of two and a half minute. An amorphous like structure of tribofilm is formed at time periods of even two and a half min under high temperature onto the sample which has thickness of about 35 nm.

TEM images for the HSPOD 100°C tribofilm for the time period of one hour shows a formation of MoDTC tribofilm with a thickness of about 100nm. Figure 7.10 (b) shows a higher magnification of the tribofilm which, in contrast to the tribofilm formed at room temperature, exhibits a layer like structure arranged on top of one another.

The images confirm the formation of MoS_2 sheets, where this layer-lattice structure of the molybdenum disulphide has facilitated the low friction between the contacts. Similar TEM images were confirmed showing MoS_2 eyelashes at the wear debris showing a lot of highly-dispersed and very flexible bonded MoS_2 single sheets [47].
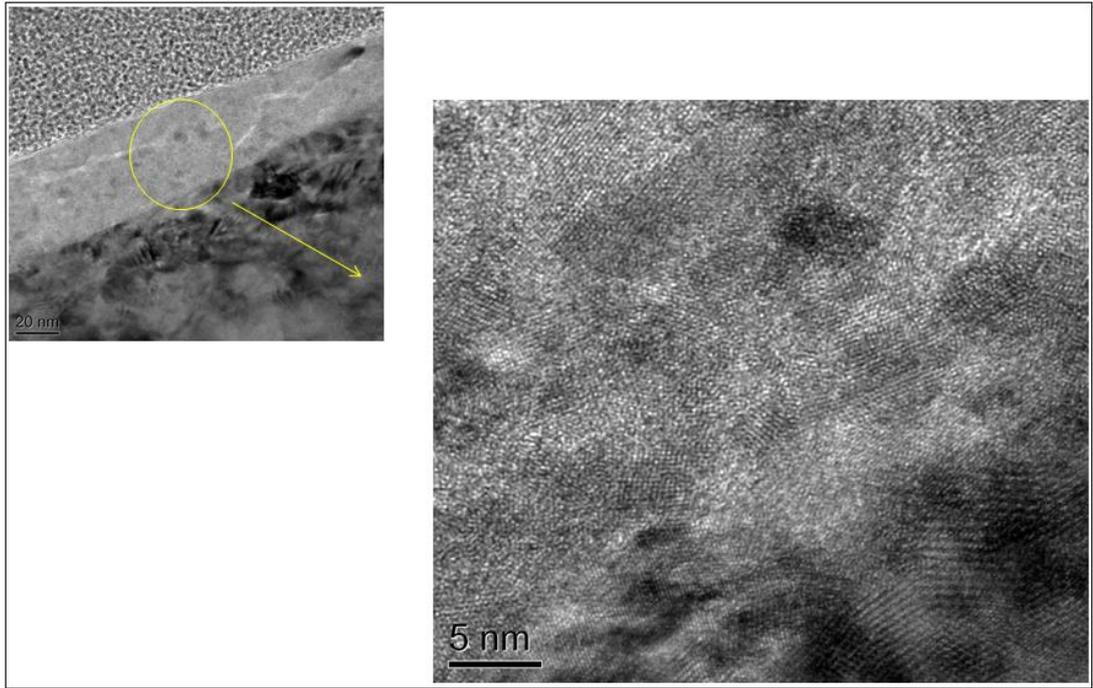
(a)
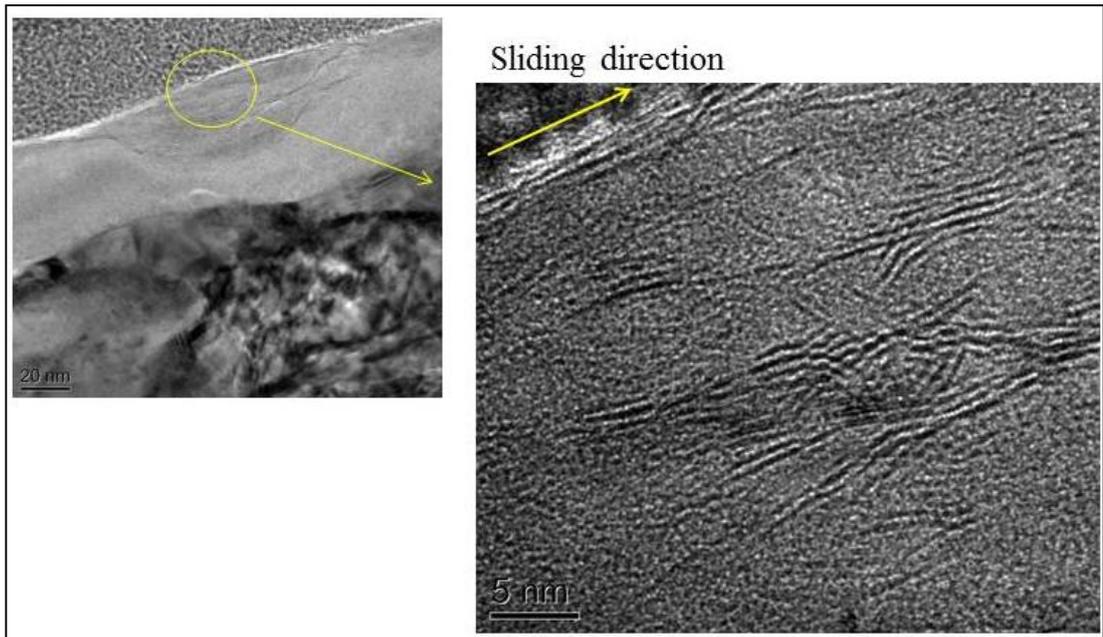
(b)

Figure 7.10 TEM images for the HSPOD 100°C tribofilm for the time period of (a) two and a half minute and (b) one hour.

Similar to the room temperature samples the Raman response of pure MoO_3 at 820 cm^{-1} was not observed at high temperature conditions. The high temperature samples showed a Raman response of the $FeMoO_4$ bonds between the frequency regions of 920 – 930 cm^{-1}. As observed under Room temperature test condition, shorter duration test at high temperature did not show a peak response around 870 cm^{-1} for the Mo-O-Mo entity. Raman response of the $FeMoO_4$ bonds were observed on the sample but it was not very apparent as compared to the room temperature sample. With longer duration of test, a broader peak at the Raman shift between 920 and 930 cm^{-1} can be observed. However along with the $FeMoO_4$ peak, broad Raman peak between 660 and 690 cm^{-1} is more apparent on the high temperature samples. These peaks have been reported for the bonding vibration of the Fe_3O_4 iron oxide peak [150] and have also been observed on previous reports. The Raman response for the iron oxide peak is very apparent at high temperature for longer duration test as observed in Figure 7.11, along with $FeMoO_4$ peak. This iron oxide Raman peak although observed on room temperature samples sometimes, the intensity is less compared to the Moly-oxide bond. However a vice versa affect can be observed with the higher temperature Raman analysed samples and the Moly-oxide bonds becomes less apparent compared to the Fe_3O_4 bonds.
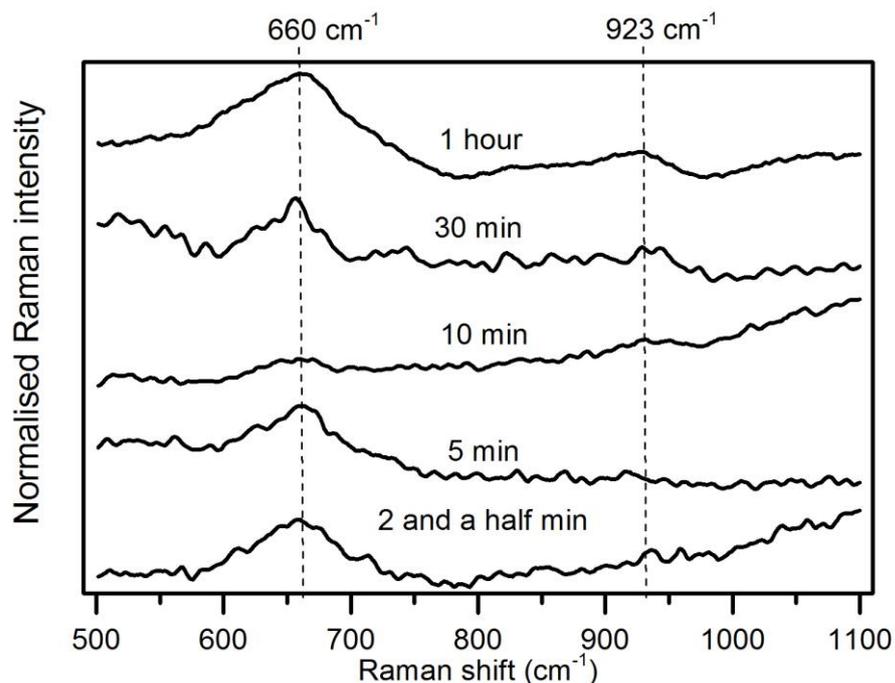
Figure 7.11 Raman intensity variation for Fe_3O_4 and Mo=O peaks of test conducted at 100°C temperature at different time period as stated.

The FWHM of the various time period high temperature (100°C) samples can be observed in Figure 7.12 for the two distinct MoS_2 peak. At a time period of 2 and a half minute, the FWHM values for the two characteristic peak of MoS_2 have a value similar to each other, a feature similar to the room temperature samples.

With longer duration of time the FWHM value for the 408 cm^{-1} (A_{1g}) frequency mode can be observed to be in the range of 10 to 20, similar to the room temperature FWHM values. However, the E_{2g} frequency assigned to the motion of the Mo - S atoms in the x-y layered plane of the unit cell, shows an increase in the FWHM values and lies in the range between 10 and 25.

The increase in the FWHM value for the peak response assigned to the motion of the Mo – S, therefore can be explained in relation to the formation of longer chain of Mo - S and the lattice layer formation. The FWHM value assigned to the motion of the S atoms shows a minimal increase with the effect of high temperature and also with the duration of time. This increase of the FWHM for the S atoms can be regarded due to the effect of temperature.
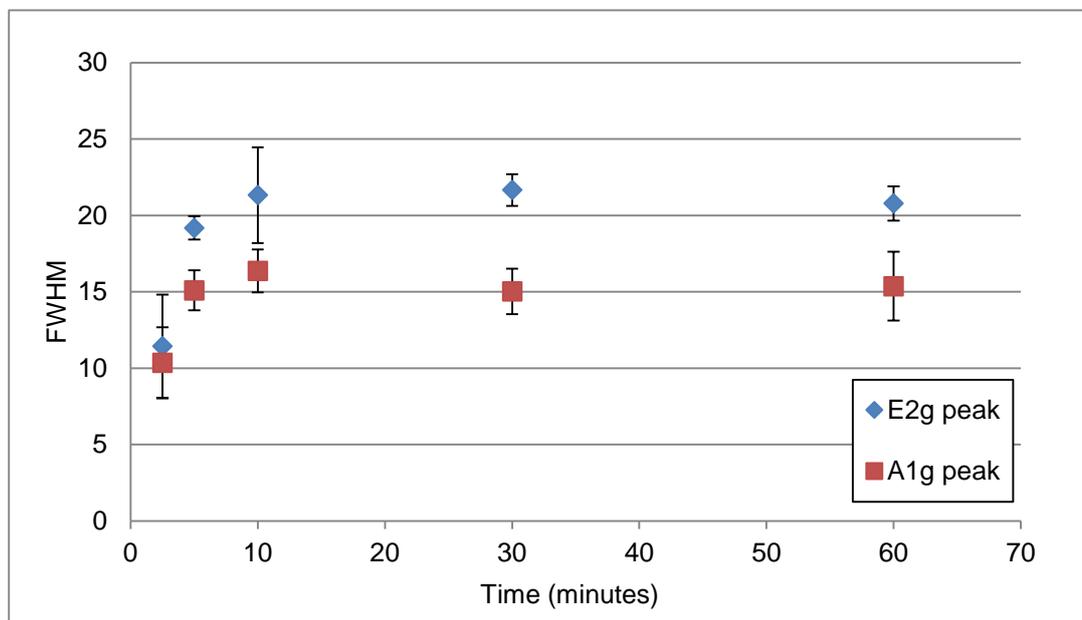
Figure 7.12 FWHM of the various time period high temperature (100°C) HSPOD disc samples.

Raman map analysis of the normalized intensity variations for the MoS_2 (A_{1g}) Raman response of the tribofilm showed an overall increase of the intensity value with time for higher temperature test. Raman analysis were conducted at the wear scar area of 20 X 20 μm of the disk samples. The wider intensity of the MoS_2 tribofilm with time shows a stronger response of the development of the A_{1g} peak onto the sample surface in Figure 7.13.

In comparison to the Raman map analysis of the room temperature samples, the normalized intensity of the high temperature samples are more apparent on to the surface of the tribofilm. The room temperature map area demonstrated an uneven response of the A_{1g} peak on to the surface of the tribofilm and a similar response is also observed on the high temperature scanned area. However, with time duration, high temperature samples shows higher intensity of the A_{1g} peak and the change in the structural transformation is already observed with the Raman shift of this peak.
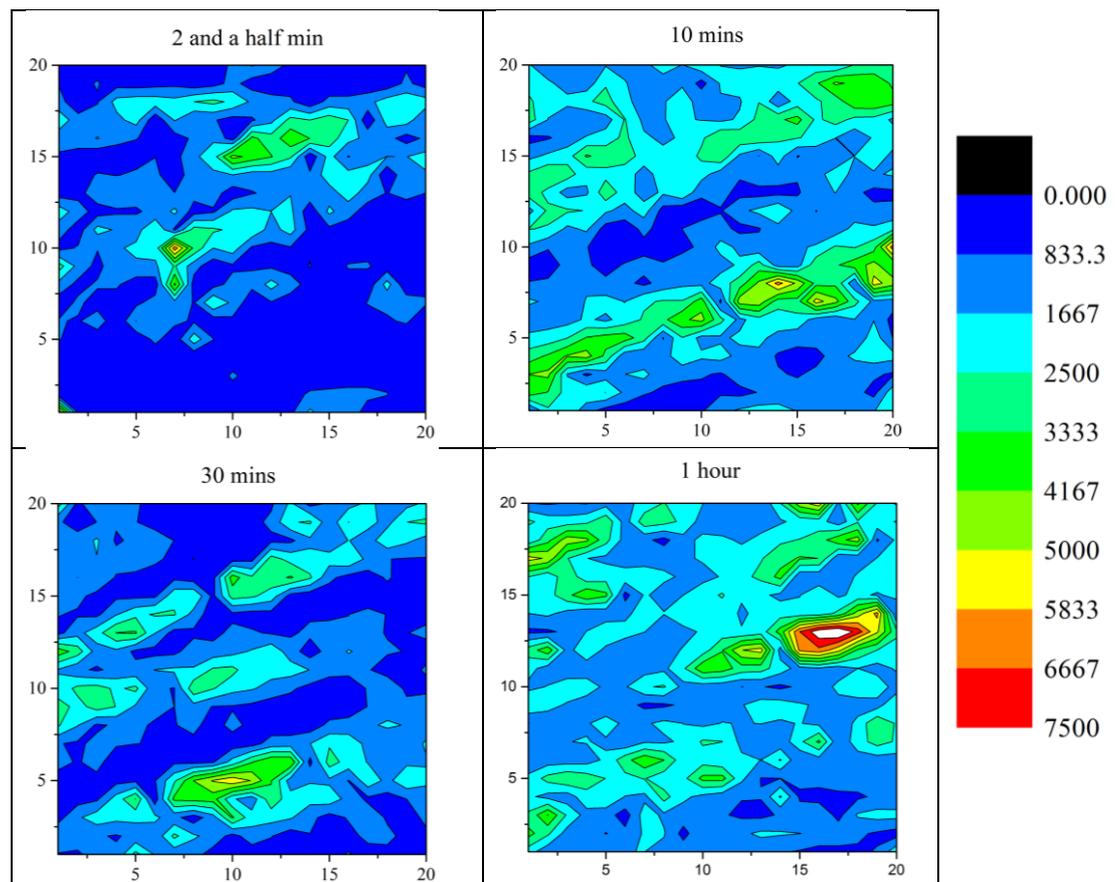
Figure 7.13 Raman map intensities of MoS_2 tribofilm A_{2g} peaks (410 cm^{-1}) at the wear scar area of 20 X 20 μm of the disk samples at high temperature (100°C) for the time period of (a) two and a half minutes (b) ten minutes (c) thirty minutes and (d) one hour.

7.2 Real time *in-situ* analysis of MoDTC additive tribofilm

Time transient test conducted at HSPOD with the lubricant of MoDTC showed that the formation of MoS_2 tribofilm was dependent upon the temperature. Under room temperature conditions, Raman analysis showed a Raman peak for Fe_3O_4 iron oxide and $FeMoO_4$ at most of the wear scar analysed. Raman spectrum for the wear scar analysed also showed a Raman response of the E^1_{2g} and A_{1g} peak at 375 and 400 cm^{-1}. This response was not observed on every area of the sample's wear scar and was related to show the presence of the Mo-S peaks from the additive adsorb onto the wear scar.

At higher temperature of 100ºC, friction value started to drop within a time period of five to ten minutes. The drop in friction was associated with the formation of MoS_2 tribofilm. Shifts in E^1_{2g} and A_{1g} peak of the MoS_2 tribofilm was associated with the formation of MoS_2 layers onto the sample surface, until it reached a value of 380 and 410 cm^{-1} where the friction reaches a steady state. *In-situ* technique benefits the analysis of the tribofilm development under real time conditions, and therefore to understand the tribofilm development in real time conditions *in-situ* analysis of the MoDTC additive was undertaken under similar conditions.

7.2.1 *In-situ* analysis of MoDTC additive under ~25ºC (room temperature) conditions

In-situ tests were conducted under room temperature conditions for the lubricant additive of MoDTC. Experiments were conducted at contact loads of 20 N and speeds of 400 rpm. At time periods of two and a half min, five min, ten min, thirty min and one hour, the test was stopped along with the supply of lubricant and Raman analysis was performed on the wear scar. Before any analysis the contact was removed and rotated for a time period of one minute to remove any excess oil on the sample surface. All of the analysis was performed in dark room conditions to avoid any influence from the ambient light in the room.

Friction coefficient graph for the lubricant of MoDTC under room temperature is shown in Figure 7.14. The friction values correspond to the values with the test performed at the HSPOD under room temperature. After any *in-situ* analysis, the contact between the samples was restored which usually resulted in a high friction at the beginning due to the running in process.

In-situ analysis of the wear scar at different time periods is showcased in Figure 7.15. Under room temperature conditions, peaks around 660 cm^{-1} and 923 cm^{-1} Raman shift were observed on the wear scar of the disc samples. Similar peaks have also been highlighted on the wear scar of the HSPOD room temperature samples. The broad and intense peak at 660 cm^{-1} has been attributed to the presence of Fe_3O_4 (iron oxide) [150] and occurs due to wear occurring on the contact because of rubbing. Raman peak at 923 cm^{-1} has been reported for the Raman mode of $FeMoO_4$ [151] and under room temperature conditions it can be suggested that the formation of $FeMoO_4$ is promoted from the MoDTC additive and the wear of the steel sample, which does not contribute towards friction reduction.
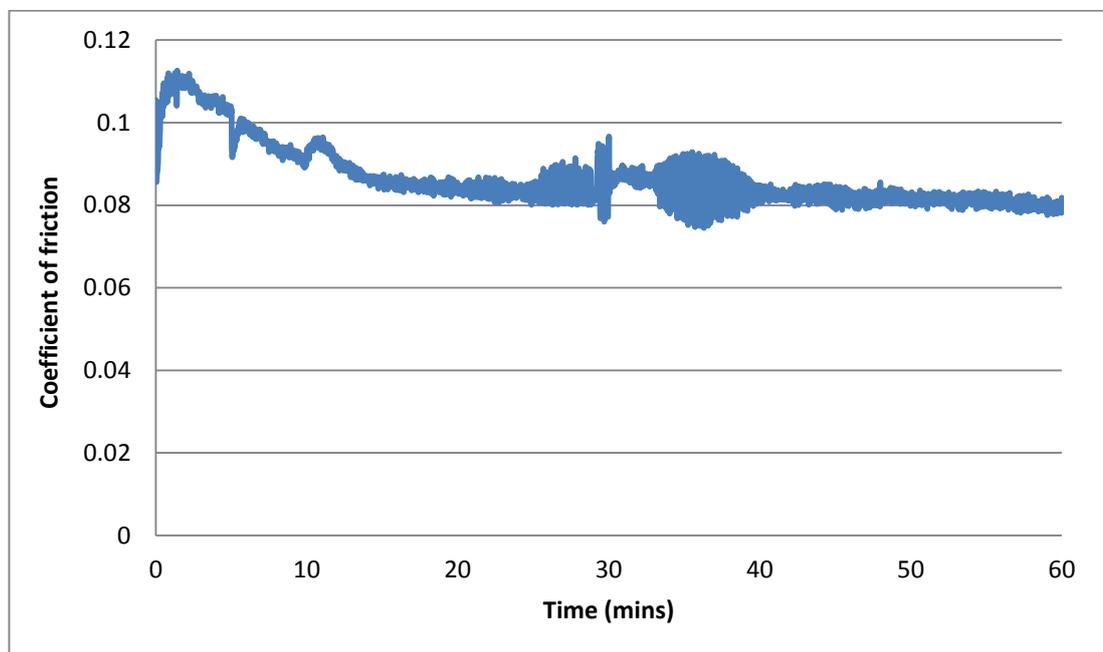
Figure 7.14 Friction coefficient graph of the lubricant additive of MoDTC at loads of 20 N, sliding speed of 400 rpm and 25°C temperature test conducted in the *in-situ* rig.

At shorter time duration, Raman response around 870 cm^{-1} was observed at HSPOD wear scar samples, which gradually decreases with longer duration until the peak of $FeMoO_4$ is observed onto the sample. The Raman peak ~ 870 cm^{-1} has been attributed to the asymmetric stretching mode of the Mo-O-Mo bonds [179, 180] and is absent on the *in-situ* analysis for shorter duration samples wear scar.

Rotational speed (rpm) performed on both of the HSPOD and *in-situ* test are equal but their linear speed are different due to the size of the sample. Larger disc sample of the *in-situ* rig with time covers a longer sliding distance compared to the HSPOD disc samples. Therefore at shorter duration of HSPOD samples, the response of 870 cm^{-1} was observed whereas due to longer sliding distance the Raman response of the 870 cm^{-1} disappeared with the formation of $FeMoO_4$.

Raman response of the E^1_{2g} and A_{1g} peak at 375 and 400 cm^{-1}, as observed with the HSPOD samples were not observed on the *in-situ* rig samples. However, with longer duration of time, broad peaks around 330 and 455 cm^{-1} are observed on the sample of the *in-situ* disc wear track. Similar Raman peak values have been reported for amorphous MoS_2 films grown by pulsed laser deposition [138] and also for amorphous MoS_3 [181, 182].

Bands between 300 – 360 cm^{-1} have been identified with Mo-S stretching mode and the broad profiles of the Raman peak response indicate the amorphous nature of the material. Therefore at room temperature conditions under sliding contact, we expect the MoDTC molecule to adsorb on the contact with the formation of an amorphous structure of MoS_3 and $FeMoO_4$ on the wear scar.

Due to rubbing, presence of Fe_3O_4 (iron oxide) is attributed to the wear of the sample. However presence of E^1_{2g} and A_{1g} peak on the HSPOD samples indicate the start of the amorphous MoS_3 transition towards the tribofilm nature of MoS_2.
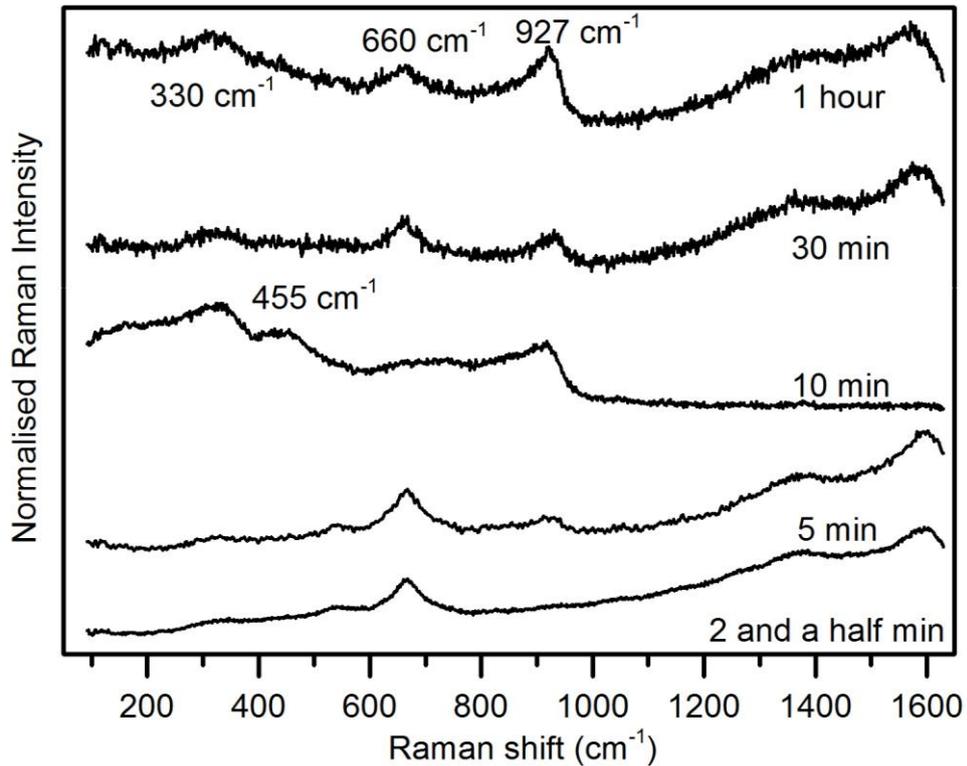
Figure 7.15 Raman spectrum of the MoDTC additive under 25°C temperature at varying time periods.

7.2.2 *In-situ* analysis of MoDTC additive at 100°C temperature

At true boundary conditions, the friction was reduced for the lubricant of MoDTC at high temperatures. Under similar tribological conditions of the *in-situ* room temperature experiment, test at 100°C was conducted with *in-situ* analysis conducted at similar time periods. It can be observed with the friction graph for high temperature experiment at Figure 7.16, the friction starts to drops within a time period of five minutes.

Raman analysis at a time period of two and a half minute shows the response of the E_{2g} and A_{1g} peak at 377 and 406 cm^{-1} (Figure 7.17). Raman analysis on the HSPOD wear scar shows a response around 375 and 400 cm^{-1}, but with no drop in friction. However, at a time period of two and a half min the friction has dropped significantly for the *in-situ* rig. The shift in Raman peak response of the *in-situ* rig samples is due to the effect of layer formation on the wear scar which has been credited towards the drop in friction of the MoDTC lubricated conditions. Due to the longer sliding distance of the *in-situ* rig, the formation of MoS_2 tribofilm has also been accelerated.
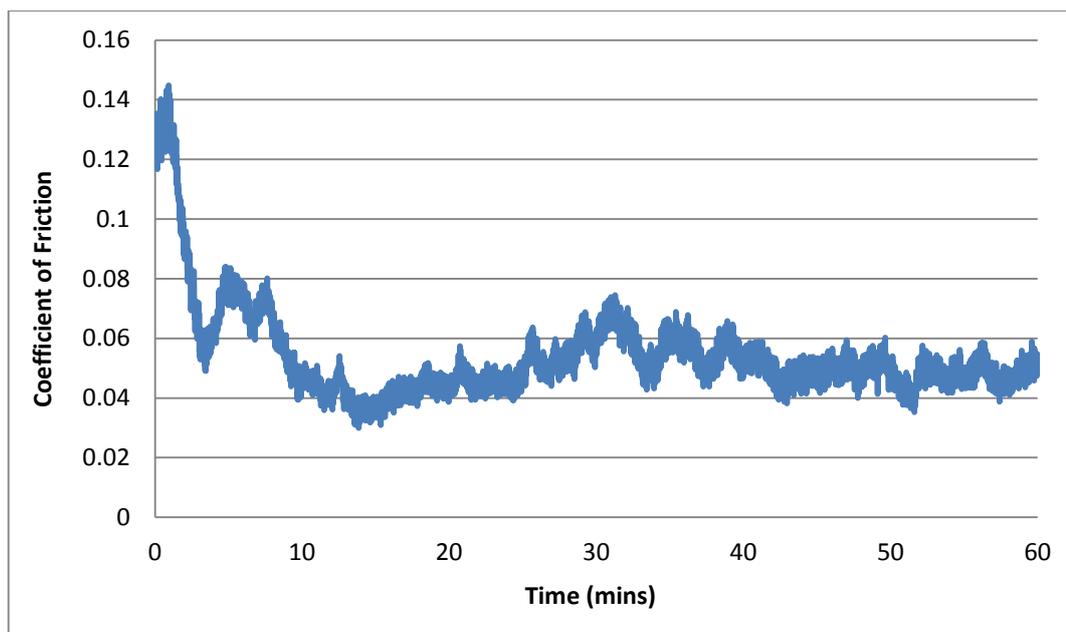
Figure 7.16 Friction coefficient graph of the lubricant additive of MoDTC at loads of 20 N, sliding speed of 400 rpm and 100°C temperature test conducted in the *in-situ* rig.

Raman *in-situ* analysis at the disc wear scar of five min and ten min, the E^1_{2g} and A_{1g} mode of the MoS_2 tribofilm is around 380 and 412 cm^{-1}, which indicates the presence of MoS_2 tribofilm [44] and the low friction present in the system. Similar *in-situ* analysis on the samples of thirty mins and one hour, the E^1_{2g} and A_{1g} mode of the MoS_2 tribofilm has shifted to 377 and 408 cm^{-1}. Friction produced at this time period is still low for the experiment conditions, but the shift could have occurred due to the contact being taking off to rinse the oil from the disc's surface and disturbing the layers of the MoS_2 tribofilm. Raman spectrum also indicated the presence of broad bands around 660 cm^{-1} for iron oxide and 923 cm^{-1} for the presence of $FeMoO_4$ at various time period samples.

In-situ analyses of the MoDTC lubricant at high temperature shows a shift in the E^1_{2g} and A_{1g} mode of the MoS_2 tribofilm when the friction starts to drop (Figure 7.18). This has been accredited to the formation of MoS_2 tribofilm layers and similar shift for pure MoS_2 has also been reported [176, 183]. The friction reaches a steady state condition and no significant change in the Raman spectra for the various time periods samples is observed. Raman response of iron oxide in the sample is observed due to wear and the formation of $FeMoO_4$ occurs which is absorbed onto the contacting surface.
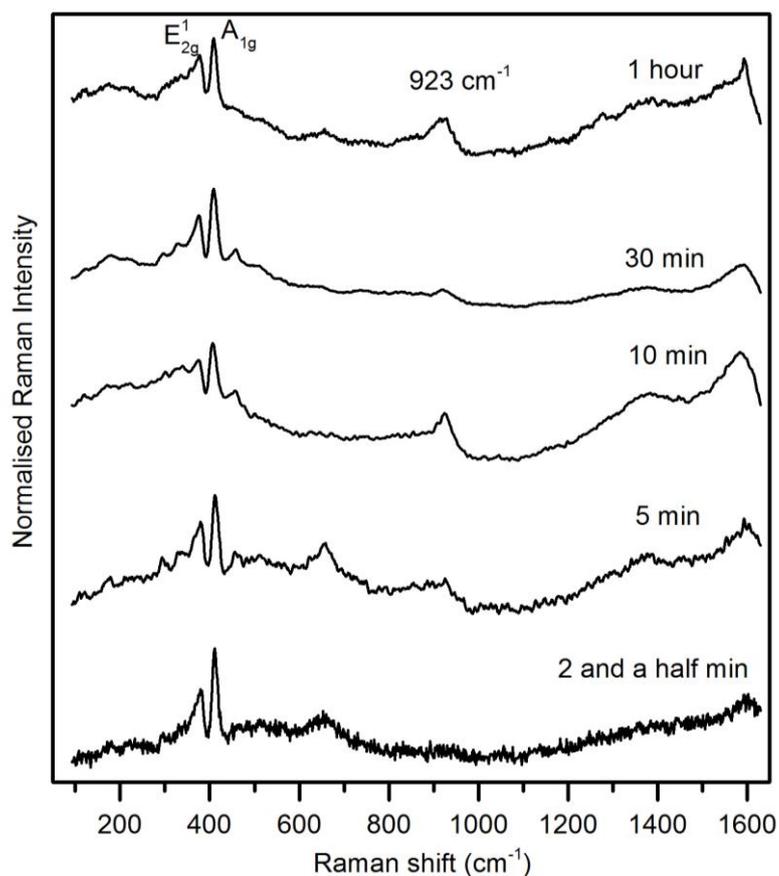
Figure 7.17 Raman spectrum of the MoDTC additive under 100°C temperature at varying time periods.
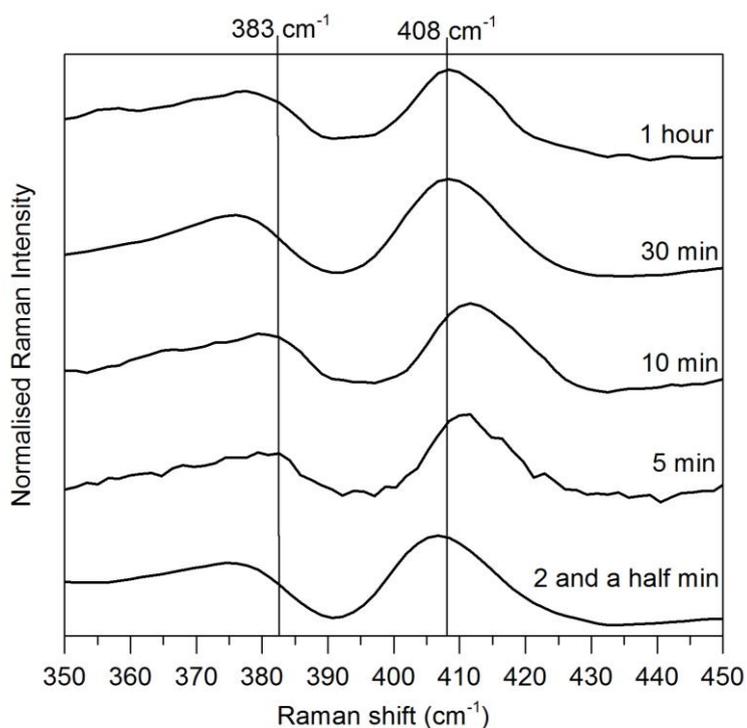
Figure 7.18 Raman response of the E^1_{2g} and A_{1g} vibrating frequency of the MoS_2 bonds as a function of rubbing time at high temperature (100° C) test conditions in the *in-situ* rig.

7.3 Summary

In this chapter *ex-situ* and *in-situ* time resolved study has been conducted as a function of rubbing and tribofilm formation to understand the development of the MoDTC lubricant additive. The findings in this section can be summarized as follows:

- At low temperature conditions *ex-situ* analysis on the tribofilm of MoDTC showed a Raman response of the Mo-S bonds. Raman response of the Mo-S bonds was not evident on every area of the sample.

- Peaks in and around 870 and 920 cm^{-1} Raman shift are observed on the Raman spectrum of the sample at low temperature, which is attributed to various Mo oxides and inhibits the reduction of friction at low temperature.

- *Ex-situ* analysis confirms the reduction in friction at high temperature with the Raman response of MoS_2 characteristic peaks on both contacting samples.

- At shorter time period when the friction is high at high temperature, similar Mo-S bonds were observed on the samples.

- An amorphous like structure of tribofilm is observed with TEM at time periods of even two and a half min under high temperature onto the sample.

- As the friction drops an evident shift in the A_{1g} peak is observed for the MoS_2 tribofilm, which is credited to the formation of MoS_2 layers on the sample which reduces friction. TEM images shows the presence of layer of MoS_2 sheets at the end of 1 hour test.

- Raman spectrum at low and high temperatures shows the response of $FeMoO_4$ and Fe_3O_4 species. At low temperature conditions the intensity of $FeMoO_4$ was stronger compared to Fe_3O_4, and a vice versa effect was observed at high temperature conditions.

- Under low temperature conditions the FWHM of the two characteristic peaks of the Mo-S bonds did not vary, and a broader peak was observed. However, at high temperature conditions an increase in the FWHM value for the peak response was reported.

- Raman map analysed at low temperature conditions showed no increase in intensity for the A_{1g} peak of the Mo-S bond. However, an overall increase in intensity was observed at high temperature conditions with longer duration of time.

- Similar Raman peak values reported for amorphous MoS_2 films grown by pulsed laser deposition and amorphous MoS_3 was observed on the wear track of low temperature *in-situ* test samples. Presence of $FeMoO_4$ and Fe_3O_4 species was also observed on the wear track of the sample.

- Raman analysis on the wear scar of high temperature *in-situ* samples, also observe the shift in Raman peaks for the E^1_{2g} and A_{1g} mode of the MoS_2 tribofilm with the decrease in friction.

- Raman spectrum also indicated the presence of broad bands around 660 cm^{-1} for iron oxide at shorter time periods but a stronger response of $FeMoO_4$ was observed with longer duration of test.

Chapter 8
Discussion

In this chapter, the results presented in Chapters 5, 6 and 7 are discussed. Novel contributions are discussed in relation to current published studies. The discussion is split into two main sections:

- Raman spectroscopy as an *in-situ* tool in tribochemistry; the advantages and disadvantages are discussed and a framework is presented.

- Application of Raman spectroscopy for understanding the MoDTC kinetic tribochemistry processes; how Raman combined with other techniques can advance the understanding of the mechanisms that define formation of low friction films from MoDTC.

The first section discusses the potential of Raman spectroscopy as a surface analytical technique to characterise lubricated samples and the advantages compared to other techniques. Discussion of the *in-situ* tribometer in characterising lubricated surfaces along with its advantages and disadvantages is presented.

The second section contains three parts and covers the tribochemistry of the MoDTC lubricant additive under boundary lubricated conditions. In the first part, the influence of load, speed and temperature parameters is discussed in relation to friction and wear performance on tribochemistry processes. The experimental results showed a key role of temperature on MoDTC low friction performance. A detailed discussion is provided to understand the role of temperature in tribofilm formation.

Secondly, transient processes of MoDTC tribofilm formation as a function of rubbing time and temperature is discussed. With the combination of *in-situ* and *ex-situ* analysis, the tribochemical development of MoDTC tribofilm is presented. The mechanism of MoS_2 formation presented in the literature are critically reviewed and new approaches suggested.

Lastly, durability of the MoDTC tribofilm is also taken into perspective and discussed in this section. The influence of oil oxidation on its frictional performance and oil scarcity is discussed with the observed Raman characteristics on the sample wear scar. In addition, the tribochemical process

of MoDTC and its interaction with the lubricant additive of ZDDP is discussed. Reduction in friction due to the presence of ZDDP additive at varying temperature is discussed with the observed Raman characteristics of the MoDTC/ZDDP tribofilm.

8.1 Raman spectroscopy as a surface analytical technique

With the ease and improvement of instrumentation, Raman spectroscopy as a surface analytical technique has seen its practical application towards various fields of materials, biochemical and medical and other various industrial applications.

8.1.1 Raman spectroscopy in comparison to other surface analytical techniques

Table 8.1 provides comparative overview of the key conditions required for surface analysis using well-known surface techniques utilised in tribological studies. Most of these techniques generally require a condition of sample preparation or cleaning and analysis conducted within UHV environment. Sample preparation or cleaning will inevitably affect the tribochemical nature of the sample being analysed. Being able to analyse tribology samples without any prior sample preparation will lead to new information in tribofilm chemistry.

X-ray methods such as XPS, EDS etc are popular techniques useful for identifying the composition and structure of lubricant tribofilm, however samples must be compatible with high vacuum environment and necessary surface altercation could be imposed when analysing the samples. Tribofilm of MoDTC has always been reported with the formation of MoS_2 and MoO_3 [42, 47, 50] with XPS, however Raman analysis conducted on this thesis shows the presence of MoS_2 layers and $FeMoO_4$ species with an absence of MoO_3. XPS produces a characteristics set of XPS peak for an element at its characteristics binding energy but it can complicate XPS interpretation due to the presence of similar elemental composition. Raman spectroscopy on the other hand provides a detailed molecular composition which acts as a fingerprint for a molecule to be identified.

Table 8.1 Comparison of information obtained from the measurements with respect to the conditions required for the surface analytical techniques utilised in tribological interface studies

	Analysis	**Conditions**
Raman spectroscopy	Chemical/molecular composition, film thickness	Non-contact, No sample preparation
Optical microscope	Surface and cross-section appearances	Chemical information not provided
AFM	Surface topography, friction and elastic properties	Chemical information not provided
TEM	High resolution imaging. Equipped with EDS for elemental analysis	Cross-section area of samples prepared with FIBS, UHV environment
SEM	High resolution imaging. Equipped with EDS for elemental analysis	Analysis in vacuum environment requires dry surfaces
XPS	Elemental and chemical bonding, molecular composition	Sample preparation, UHV environment
SIMS	Elemental, isotopic, or molecular composition	UHV environment
AES	Elemental and molecular composition	Samples must be electrically conductive to be analysed. UHV environment.

Tribofilms formed on the surface could contain various form of molecular structure of a chemical compound, determining the properties of the surface film. Hence, the effect of rinsing, on the characteristics of the tribofilm nature is an important experimental criterion. Solvent washed samples have been reported to remove the outer layers of tribofilms and was not detected with the conventional surface analysis technique [159]. Chapter section 5.2.4 showed Raman spectra of the rinsed and unrinsed samples were similar. Hence, Raman spectroscopy delivers the advantage of sample investigation at ambient conditions, without any form of sample preparation or cleaning.

In this thesis Raman spectroscopy has shown its significance towards analysis of non-rinsed samples, especially with that of MoS_2 tribofilms. Since it is a non-contact technique, it can also be used to analyse sample without destroying it, and analysis conducted within a few seconds with high resolution, hence showing the capability of analysing samples *in-situ* with minimal perturbation. The samples can also be retained after Raman analysis, for additional analysis by other techniques due to its non-destructive nature. In this work, surface analytical techniques of TEM and EDX have been utilised to further analyse the tribological properties of the tribofilm.

General limitations of Raman spectroscopy due to interferences with fluorescence by impurities, sample absorbance of the incident radiation leading to burn or photodecompose etc have limited its application. However in addition to instrumental improvements, methods for processing spectral data with various statistical algorithms have led to high level of data maturity. Sophisticated methods for processing spectra are readily available and accepted. The need for accuracy has also led to a whole new area of chemistry referred to as *chemometrics* [184].

8.1.2 Data processing of Raman spectroscopy in lubricated conditions

Spectral data obtained from the Raman spectrometer is generally dependent of the instrument's operational parameters. In response to understanding the effect of Raman spectrometer parameters, pre-processing techniques in Chapter 5, made data analysis more stable and crucial to obtain accurate

Raman analyses. Care has been taken to record the spectra with exactly the same settings, typically the same acquisition time and accumulations in order to obtain high resolution spectra with a good S/N ratio and repeatability.

One of the most important steps in data-processing is the extraction of peak information. Curve fitting methods are widely used to separate overlapping peaks in the Raman profile [185, 186]. The observed line shape of the vibrating molecule is a function of the transition between the energy levels of the molecules absorbing or scattering. For vibrations, excited state molecules rapidly return to the ground state, where this relaxation is referred to as the lifetime or the amplitude correlation time, τ_a.

Initially, all of the excited molecules are vibrating together (coherently), but motion and slight differences in vibrational frequencies randomizes this over time. As the coherence fades (with coherence lifetime τ_c), the now random components interfere, and effectively cancel one another (called dephasing) [187]. The effective lifetime τ is a combination of these two components, the coherence lifetime τ_c and the amplitude correlation time τ_a, where two interesting limiting cases of $\tau_c \gg \tau_a$ or $\tau_c \ll \tau_a$ exists. The overall line shape originates from the sum of all the individual vibrations, and the exact vibrational frequency of a particular molecule is controlled by its environment [187].

In the first case, where $\tau_c \gg \tau_a$, the excited molecule relaxes before incoherence becomes severe, which occurs mostly in solids, because the environment is not in motion. The various molecules of the solid experience a statistical distribution of environments, and the line shape takes on the bell curve or Gaussian profile. In the second case, where $\tau_c \ll \tau_a$, the incoherence sets in rapidly, so dephasing is the dominant energy loss channel. This occurs in gases where rotation and collisions happen quickly. The resulting line shape is Lorentzian, due to the exponential vibrational population relaxation [187].

Liquids exist in between these limits, where interactions prevent extremely rapid motion, but the molecules are not locked in place. As a result, the two lifetimes can be close, and the line shape has features of both Gaussian and Lorentzian character. The simplest model for this involves the combination

Gaussian-Lorentzian (G-L) profile. A more complex combination of Gaussian and Lorentzian lines is the Voigt profile, where the two characters are convoluted. The functional form for a Voigt profile allows the Gaussian and Lorentzian portions to have different line widths [187]. Raman spectra profile in this research were therefore obtained with the curve fitting form of Voigt function profile, which provided a specific resolution of the Raman spectra under lubricated conditions.

8.1.3 Relevance of Raman spectra profile towards understanding tribofilm nature

Raman spectra profile is characterized by three parameters of location (Raman shift), height (intensity) and line width (FWHM) in the spectra (Figure 8.1). The position of a peak is controlled first by the natural vibrational frequency of the isolated molecule but also depends upon its interactions with the environment. Peak values can red-shift (to lower energy) or blue shift (to higher energy) depending on the characteristics and the environment of the samples [188]. Shift in peak values in the work conducted here shows the dependence of MoS_2 tribofilm layers and more thoroughly discussed in the later section of the chapter.

The intensity of a Raman spectra is governed by a number of factors including incident laser power, the instrument's operating parameters and the sample itself [189]. Similarly, elaboration of the classic eqn in Chapter 3 shows that the intensity of a Raman band due to a molecular vibration depends on the quantity [117]. Quantitative map analysis conducted on the sample in Chapter 7 is measured with the Raman peak position and its intensities relative to the peak position of the sample. Spectral interferences of variable curved background was performed with a baseline subtraction and maps obtained with linear fitting of the sample peak position. Further discussion of the relative sample and the intensity is provided in the later section of the chapters.

Vibrational mode of a molecule gives a peak of finite width and is normally reported as full width at half maximum (FWHM). Three processes of radiation damping, Doppler broadening, and collision broadening, discussed in some detail by Seshadri and Jones [190] are the dominant factors of line widths, of

which the last is the dominating influence in the case of liquid state spectra. All of the molecular dynamics (motion and energy loss) affect the line width, and there are many theories explaining the influence of various environments on line width. Rapid loss of the excitation (short т) results in broad peaks; a long lifetime (long т) leads to narrow peaks. Similarly, collisions between molecules can also enhance energy loss rates, and may broaden peaks [187].
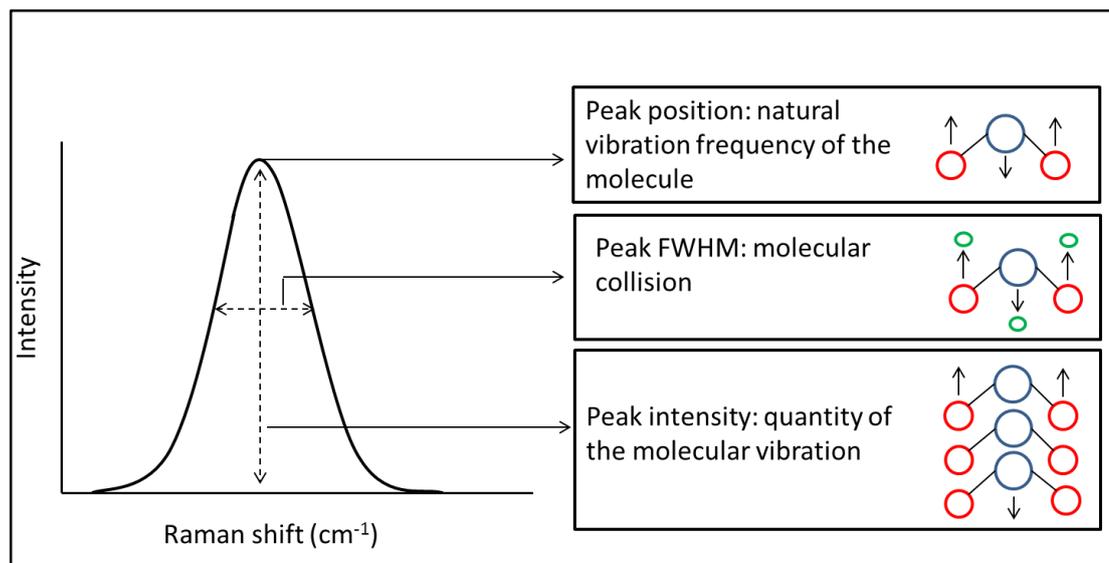
Figure 8.1 Characterisation of the Raman spectra profile and its relevance towards understanding molecular structure.

Under boundary lubrication, the tribological characteristics are determined with the physical and chemical properties of the thin surface films between the contact. As described in this section, properties of the surface film can be obtained with a wealth of information from Raman. Measurement normally requires a short time period compared to other analytical methods, and the signal enhanced through a selection of optimal measuring conditions. However, compared to other techniques Raman measurement of samples omits the requirement of sample cleaning and hence demonstrates *in-situ* and *in-vivo* study capabilities under real time conditions.

8.1.4 *In-situ* Raman tribometer

The *in-situ* tribometer was developed with close attention to parameters replicating a real tribological contact under boundary lubricated conditions. In conjugation with the flexible sampling arm, Raman spectra was obtained with

the *in-situ* tribometer to monitor the lubricant chemistry occurring within the boundary lubricated surface as a function of sliding time and temperature in the tribological experiments.

The two tribometers of high speed pin on disc (HSPOD) and the *in-situ* rig used in this research have a conventional pin on disc set-up and sample materials of the same type (Chapter 4). Hence, promoting similar tribochemical processes occurring within the contact under boundary lubrication conditions. However, sample dimensions vary between the two tribometers, as the *in-situ* rig has a larger disc radius to provide an ease of access towards the wear track. The larger disc radius of the *in-situ* rig however, delivered a longer sliding distance under the same rotational speed as the HSPOD, hence affecting the sliding time of the tribofilm formation. A detailed discussion in relation to the sliding time and distance for the formation of additive tribofilm are discussed in the following chapter sections.

The tribological contact in a HSPOD setup was submerged with the lubricant onto the sample tray and the surface lubricated during experiments with the aid of the copper oil circulator. *In-situ* tribometer contacts was lubricated with the aid of a peristaltic pump and the lubricants poured onto the contact from a lubricant container. Similar experimental set-up was also used by Chandrasekaran and Batchelor [191], which always ensured the flow of oil onto the contact and also allowed the control of the flow.

The *in-situ* rig was developed with the consideration to perform surface analysis on the wear track of the sample disc, outside the contact. This mode avoided any sample cleaning onto the surface and allowed exploration of the adsorbed species and the nature of the lubricant films affecting the tribochemical phenomenon as directly as possible. However, analysis on the wear scar of the ball is restricted due to the setup of the *in-situ* analysis. Muratore et al [33] employed a similar set-up to examine solid coatings of MoS_2 and VN-Ag and successfully correlate the changes occurring on coating surfaces to simultaneous measurements of friction coefficient.

Raman promotes the analysis of the surface to be undertaken at ambient conditions, where no form of sample preparation is required and negates the

influence of solvent, rinsing etc. as used in vacuum based surface analytical methods. However, as observed in Chapter 5, presence of oil on the surface could produce a high background on the Raman spectrum and the response of weak Raman scatterer could be attenuated. Hence, before any *in-situ* analysis, oil drained from the surface by rotating the sample disc without any contact minimised the effect of background on the analysed Raman spectra.

In-situ analysis performed on the wear scar in the research experiments were conducted with the set-up of a *post mortem* analysis. Raman analysis were performed after the friction test for a certain time criterion. This mode allowed a higher flexibility of the Raman analysis performed on to the surface and the choice of appropriate area on the sample. *In-situ* post mortem analysis also provided suitable measurement of time scale, along with the analysis of the wear scar to establish a time transient understanding of the tribofilm development. *Pre mortem in-situ* analysis promotes the analysis to be carried out during the rotation of the disc interface. However the analysed area continuously changes due to the rotational motion of the contact. Sample focusing was difficult to achieve and the acquisition time was not quick enough to obtain a spectra from a specific sample area during rotation, and usually resulting in distorted Raman signal.

The *in-situ* rig therefore successfully correlates the tribological phenomenon in an optimal boundary conditions with the optimal *post mortem in-situ* mode to obtain the best Raman response for *in-situ* purposes. The disadvantage lies in the restricted set-up condition which does not allow the analysis of the ball wear scar during *in-situ* analysis. Raman spectroscopy enhances the understanding of the development processes of these tribofilms formed onto the surface. In addition the time scale criterion successfully related with the tribochemical reactions processes, providing valuable information in the transient processes that lead to tribofilm formation.

8.2 Tribological performance of Molybdenum dialkyldithiocarbamate (MoDTC) lubricant additive under boundary lubricated conditions

Most of the experiments in this research have been conducted in the presence of MoDTC lubricant additive. Similarly, with the large amount of tribochemistry studies conducted for the lubricant additive MoDTC, most of the understanding is based on the end-of-test tribofilm composition (Refer to sub-chapter 2.3.1.1 and 3.3). The transient processes that lead to the formation of these tribofilms are still unclear and hence *in-situ* Raman tribometry highlights a greater benefit of understanding the kinetics of formation of tribofilms and the relative roles of tribochemical processes. MoS_2 tribofilm of MoDTC is reported to have a significant Raman response [43, 44] (Refer to sub-chapter 5.1) which allows us to determine the usefulness of *in-situ* Raman tribometry.

8.2.1 Tribological performance of MoDTC additive with varying boundary lubricated conditions

Under boundary conditions, MoS_2 tribofilms of MoDTC are reported to form on the rubbing surface in the presence of air and oxygen and able to reduce friction [42, 43, 146, 192, 193]. This level of friction reduction depends on the MoDTC type and concentration, operational temperature and the type of the tribological system such as geometry of the contact, contact pressure, surface roughness, type of base oil, sliding mode (reciprocating, continuous), lubrication mode etc [43]. The results presented in sub-chapter 6.1 examine the friction behaviour of MoDTC in the absence of other additives and running parameters.

8.2.1.1 Influence of sliding speed and contact pressure

At low speed of 0.44 m/s in HSPOD and 1.02 m/s in the *in-situ* rig, the friction values are maximum compared to increasing sliding speed. Arai and Yamamoto [194] reported that in a reciprocating sliding test of steel on aluminium, the MoDTC friction response dependent upon the sliding speed, with the additive becoming more effective at high sliding speed. With high sliding speed of 1.75 m/s in HSPOD, the friction response is minimal but no response of MoDTC tribofilm is observed onto the surface. Under high sliding

speed of 1.75 m/s, the running conditions leads to a thicker entrained oil film hence promoting conformal lubricated contact at the surface and thus less solid-solid contact and a decrease in friction. Graham et al [192], also reported that the friction reduction was more dependent on the stroke length of the reciprocating sliding then the mean sliding speed. In the current study, linear speed of 0.877 m/s in the HSPOD at high temperature shows a drop in friction. A drop in friction is not observed under sliding speed of 1.02 m/s in the *in-situ* rig (Figure 6.4 and 6.5 (a)). Sliding speed of 2.04 m/s in the *in-situ* rig shows the drop of friction due to formation of MoS_2 tribofilm under high temperature conditions. As observed in Figure 8.2, the reduction in friction is related to the formation of MoS_2 tribofilm in the HSPOD and *in-situ* rig at 0.88 m/s and 2.04 m/s sliding speed relatively. At sliding speed of 1.02 m/s in the *in-situ* rig, formation of this tribofilm is not observed in the Raman spectrum but a formation of Fe_3O_4 due to wear is present. Hence suggesting the formation of MoDTC tribofilm is dependent on the exposure time of contacting surfaces and also the load on a pin on disc setup.
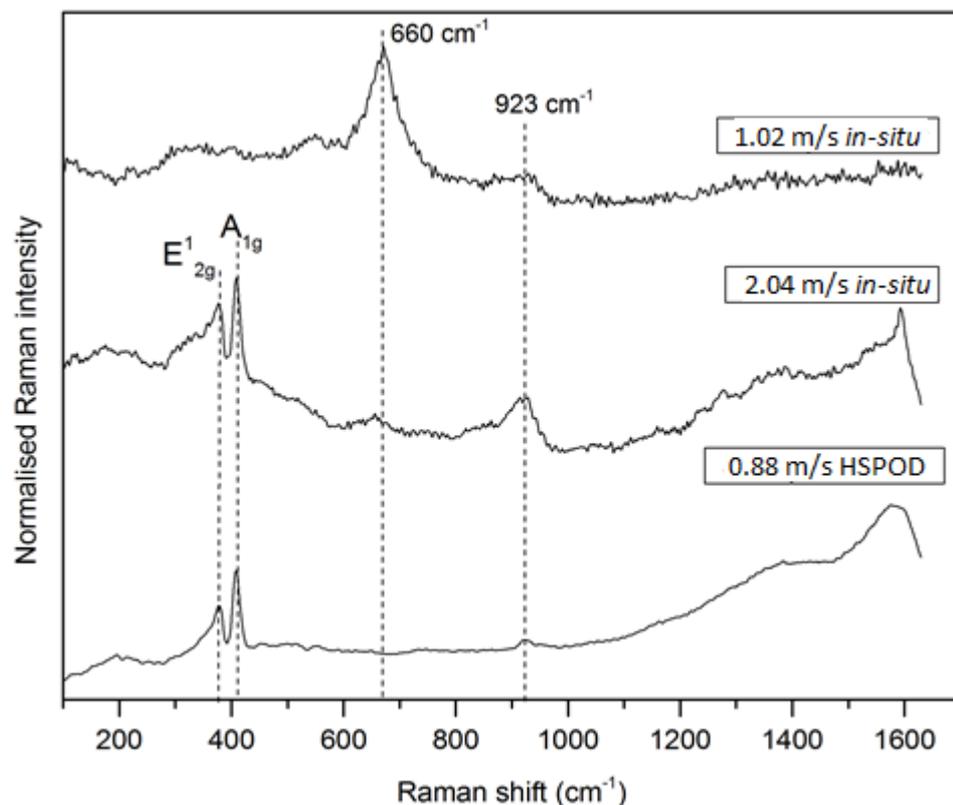
Figure 8.2 Raman spectrum at the end of 1 hour test with the MoDTC lubricant additive at high temperatures, and sliding speed of 0.88 m/s in the HSPOD and 1.02 m/s and 2.04 m/s in the *in-situ* rig.

Eqn 1-4 shows that the dimensional wear factor is indirectly proportional to the sliding distance. Therefore for a certain time criterion lower speed accounts to shorter sliding distance, and with increasing speed, longer sliding distance is achieved. With lower sliding speed therefore higher wear rate is generated, which decreases with an increase in speed. In relation to 0.44 m/s, the sliding distance for a one hour test only covers about one-fourth of the sliding distance for the speed of 1.75 m/s. Hence, in relation to sliding distance it can be stated that wear factor is generated at a higher rate when the contact is initially produced. However, with longer sliding distance wear induces conformal lubricated contact at the surface promoting mixed or elastohydrodynamic lubrication within the contact. Under this lubrication regime, a thicker entrained oil film is produced which leads to less solid contact and the wear rate is decreased along with the friction.

At slow speed of 0.44 m/s, Figure 6.2 (b) and 6.3 (b) shows a high wear rate and in high speeds of 1.75 m/s, a lower wear rate is observed usually. Wear rate for speed of 0.88 m/s usually lies in between the two low and high speed, however at contact load of 14 N, minimum wear is observed on the HSPOD pin. Avoidance of the excessive wear could be through a formation of a protective film under boundary lubricated contacts, hence providing a nominal conditions for the formation of MoDTC tribofilm.

An apparent increase in friction value with the increase in load, is associated with the increase in contact pressure which lead to more surface contact onto the surface (Figure 6.2 (a) and 6.3 (a)). Relative loads of 29 N in an HSPOD and the *in-situ* rig shows a higher friction value compared with the low loads of 7 N and 10 N in both HSPOD and *in-situ* rig. Similarly, wear rate values for the HSPOD pin, under higher load is greater compared to the low load at similar conditions of temperature and speed. Raman analysis conducted on the samples were also usually supported with the presence of Fe_3O_4 spectra, which occurred as a result of wear on the surface.

However, friction reduction is observed to be minimum with the load of 14 N in HSPOD and 20 N in the *in-situ* rig under most of the conditions, except for room temperature conditions and sliding speed of 0.88 m/s in the HSPOD (Refer to Figure 6.1). Wear rate value is also minimum under this load at 0.88

m/s in the HSPOD for both temperatures. Hence indicating, under these conditions of boundary lubrication, lubricant additive is physically adsorbed onto the contacting surface, and the properties of the additive film formed on the surface define the wear and friction properties of the tribological system.

8.2.1.2 Influence of temperature

With the increase in temperature, the friction values were usually observed to increase in comparison to low temperature conditions for most of the parameters. A similar observation is accompanied in the wear rate values. Increase in temperature results in the reduction of fluid viscosity, therefore promoting more solid – solid contact and hence increasing friction and wear. Except for conditions of 500 rpm sliding speed and loads of 7.36 N and 14.72 N, which promotes the formation of MoS_2 tribofilm. Influence of temperature on MoS_2 tribofilm formation is discussed further in the following section.

A significant drop in friction, due to the formation of MoS_2 tribofilm is evident with the conditions of 500 rpm sliding speed and loads of 7.36 N and 14.72 N (Refer to Figure 6.2 (a) and 6.3 (a)). Raman spectroscopy confirmed the presence of MoS_2 tribofilm and its formation is shown to be highly dependent on high temperature conditions. Under similar conditions, the *in-situ* rig also showed the dependency of high temperature conditions to form MoS_2 tribofilm.

At condition of 14.72 N and 500 rpm, high temperature conditions shows the drop in friction for MoDTC additive but is absence in low temperature conditions. Wear data presented however suggested the wear rate of the ball sample of the HSPOD is minimal for this conditions compared to other parameters. Therefore suggesting under this conditions some form of molecules are adsorbed onto the contacting samples and also provides the decrease in wear rate values.

8.2.2 Effect of temperature on the MoDTC tribofilm composition and its frictional characteristics

Raman analysis conducted on the steel disc samples immersed in the lubricant of MoDTC and heated at a temperature of 100ºC for a time period of 1 hour did not show any presence of MoS_2. Similarly, Kasrai *et al* [46] showed that MoS_2 was not deposited under high thermal conditions and thermally generated films of MoDTC were shown that a major part of sulphur in the films experienced oxidation to form sulphate. Therefore stating that MoDTC does not thermally decompose to form MoS_2 and the phenomenon of contact rubbing is necessary to from MoS_2 on the surface.

Yamamoto and Gondo [50] showed that with the oil containing MoDTC, the coefficient of friction decreased with an increase in the oil temperature, giving friction value of below 0.05. Increase in temperature also showed a decrease in friction values for the time period of 1 hour tests (Figure 8.3 (b)). At temperatures above 100ºC a significant drop of friction is observed which reaches a steady state friction value of around 0.04.

With the increase in oil temperature, oxidized products are generated but they did not seem to exert a harmful influence on the friction and wear characteristics (Figure 6.7). Yamamoto and Gondo [50] stated this was probably due to forming a surface film effective in enhancing the wear and friction properties at the low temperature stage and the action of MoDTC as an antioxidant.

| | (a) | | (b) |
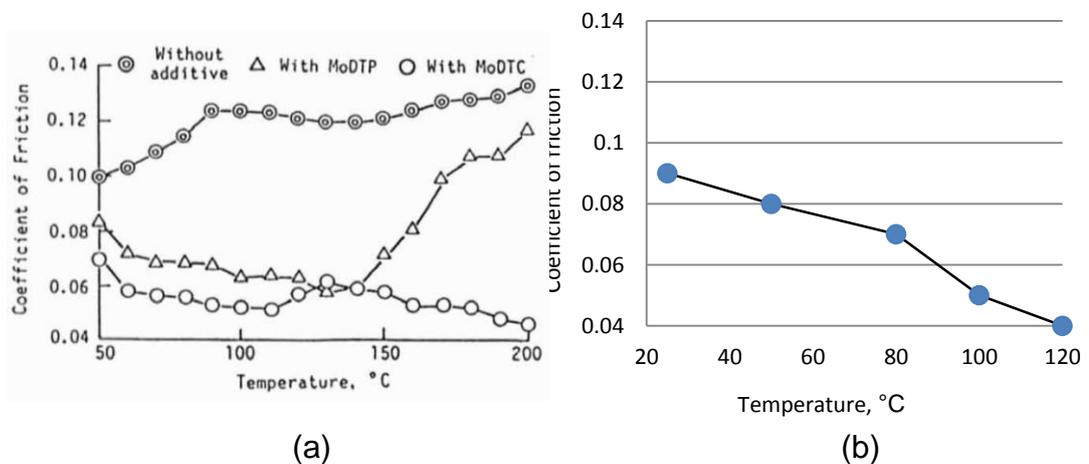
Figure 8.3 (a) Change in the coefficient of friction with temperature for MoDTP and MoDTC as shown by Yamamoto and Gondo [50] (b) Change in coefficient of friction with temperature for MoDTC.

At temperatures above 100ºC, the contacting samples consist mostly of MoS_2 film which lower the friction in the tribological system. Morina *et al* [54] reported that even at low temperature (30ºC) MoDTC film formation was observed and the amounts of MoDTC constituents Mo and S increases with the increase in temperature. Higher amount of Mo oxides was formed in the 30ºC tribofilm and they suggested with the high presence of oxides in the tribofilm, the effectiveness of Mo sulphides in reducing friction is reduced. Raman spectra of disc and ball samples in Figure 6.7 show a higher intensity response for $FeMoO_4$ and Fe_3O_4 at low temperatures of 25ºC, where the friction is high and the presence of MoS_2 is not observed.

Raman analysis conducted on the disc and ball wear scar of the HSPOD samples (Figure 6.7) show that at temperatures above 100ºC, MoS_2 tribofilm is formed which initiates friction reduction at low values. Oxidation products of $FeMoO_4$ and Fe_3O_4 are evident on all of the temperature conditions. However, with an increase in temperature a more complex form of MoDTC tribofilm is formed onto the surface of the wear scar. This complex form of tribofilm is related with the reduction in friction observed with temperature conditions of 50 and 80ºC, but a lower friction is not observed as the formation of MoS_2 is not initiated.

Peaks observed at 220, 288 and 404 cm^{-1} for the complex molybdenum tribofilm have also been reported with similar Raman values for a corroded steel. Raman spectra around 217, 285 and 400 cm^{-1} were reported for poorly crystallized iron sulphide due to ageing of steel [195, 196]. Similarly, Isoyama and Sakurai [45] reported that diethyldithiocarbamate dimolybdenum decomposed to MoS_2 on frictional surfaces, of which the particles adhered to the porous iron sulphide film produced by the reaction of the decomposed sulphur compounds and iron surfaces, and that these components made an extreme pressure or antiwear film.

However, under the conditions of FeS formation as an extreme pressure film, MoS_2 film was required to form initially under boundary lubricated conditions [45]. MoS_2 reacted chemically with the metal surface at high friction temperature which then leads to the formation of FeS films. Therefore negating the fact that FeS is formed on the surface with the increase in

temperature, as the criteria of MoS_2 film formation which is related to low friction needs to be formed initially.

Hence, with the increase in temperature a complex film of MoDTC derived film is adsorbed onto the surface containing Mo–S–0 complexes with reported Raman frequency of Mo-O-Mo deformation mode, amorphous MoS_3 molecule and v(Mo-Mo) for the dimolybdenum compound (Refer to Chapter sub-section 6.1.1).

Experiments conducted with the MoDTC degradation time period of 1 hour under 25ºC temperature shows a lower friction compared to the fresh oil (Refer to Figure 6.7). Raman analysis shows the presence of similar oxidation products of Fe_3O_4 and $FeMoO_4$ at 660 cm^{-1} and 923 cm^{-1} on both of the samples. The degraded lubricant samples also shows Raman peaks which are similar and observed for the fresh oil tribological experiment conducted at 50ºC and 80ºC temperatures (Refer to Figure 6.7 and 6.9). Friction was observed to reduce for this temperatures of 50ºC and 80ºC compared to the low temperature conditions and a similar friction trend observed for the degraded lubricant. It is stated with the increase in temperature a complex film of MoDTC additive is adsorbed onto the surface containing Mo–S–O complexes.

De Feo *et al* [197] showed that with degradation time the frictional behaviour of MoDTC containing oil, showed an increasing induction period for friction reduction. The fresh MoDTC tribofilm chemical composition was suggested with the formation of Molybdenum disulphide, where low friction was observed. At various degradation time period, friction reduction with induction time was related with the formation of molybdenum oxi-sulphide species (with high and low oxygen content). A significant friction reduction is observed, with enough quantity of low oxygen content oxisulphide and vice versa affect with longer time period degraded oil.

Hence, it can be stated with the increase in temperature, a slow decomposition of additive occurs which initiates the formation of molybdenum oxi-sulphide species on the contacting surface. Frictional characteristics of the MoDTC is directly influenced with the high and low oxygen content on the

species. Under low temperature conditions, high presence of oxides in the tribofilm inhibits friction reduction. The reduction in friction is generated with the formation of MoS_2 tribofilms but the friction characteristics is highly influenced with the oxygen content within the Mo-S species in the tribofilm.

Hence under nominal conditions of load and speed, and a constant MoDTC concentration of 100 ppm, friction performance of the MoDTC additive is dependent of the adsorbed films formed on the contacting surfaces. With the increase in temperature, the friction performance could be related to the removal of oxide film due to increasing contact pressure, promoting the formation of Mo-S containing tribofilm. Increase in temperature also leads to reduction in lubricant viscosity promoting more solid-solid interaction, where asperity contacts may produce very high, local flash temperature and initiates the adsorption of MoDTC moieties onto the surface. Further discussion of MoDTC rubbing process and its time transient tribofilm development is discussed in the following section.

8.3 Time transient development of the MoDTC tribofilm

Ex-situ and *in-situ* surface analysis of samples produced from both room temperature and high temperature lubricated tests show formation of a relatively thin tribofilm from the lubricant additive of MoDTC. The characteristic Raman peaks observed at the room temperature sample showed that a pure MoS_2 tribofilm was not formed on the sample, explaining the lack of friction reduction.

In contrast the analysis of the tribofilm formed on high temperature test samples confirms the formation of MoS_2 tribofilm on both of the contacting surfaces. In these tests, it took around 5-10 minutes of rubbing for the friction to reduce to the low friction value typical for the MoS_2 tribofilm. It is obvious that an appropriate combination of rubbing and lubricant temperature is necessary for formation of the MoS_2 tribofilm on the interface.

8.3.1 Effect of rubbing on the tribochemical development of the MoDTC tribofilm

Under room temperature conditions (~25°C), the gradual friction drop of the friction in comparison to the base oil test indicates the presence of the additive itself initiates the slow friction drop when the tribological components are in contact (Refer to Figure 7.1). The tribological contact therefore initiates the adsorption of the MoDTC additive within the contact, but at this temperature formation of the MoS_2 layers is not promoted.

Formation of the Mo-S tribofilm from MoDTC could be explained with the Grossiord chemical model on MoDTC decomposition [47]. According to this model, the MoDTC molecule decomposes first to a core Mo-S-O molecule and two N-containing chain ends. The following step of the chemical model is the decomposition of Mo-S-O molecule to form MoS_2. In the current study the formation of pure MoS_2 tribofilms has not been observed in low temperature of 25°C test samples.

Raman response of the 25°C temperature *ex-situ* test samples shows a Mo-S spectrum with the two characteristic peaks along with the Mo-O bonds on the sample's wear scar surface. However, characteristics peaks of the Mo-S spectrum is not observed with *in-situ* analysis, but a broader peak relating to the amorphous MoS_2 films and amorphous MoS_3 has been reported. Therefore under a tribological contact, the MoDTC additive decomposes to form free radicals of Mo-S-O which adsorb onto the wear scar, experimentally supporting the theoretical model proposed in [47].

Under *ex-situ* analysis, Raman response for the characteristic peaks of the Mo-S species has also been reported not to be observed on every area of the sample's wear scar. The low shift of the A_{1g} Raman peak for MoS_2 has been reported for few-layered MoS_2 [177, 183, 198], hence stating that reduction in friction by MoS_2 depends on the layer of MoS_2 formed onto the surface. The rate of MoS_2 formation is therefore critical of the chemical activation kinetics which the increase with temperature.

High temperature condition reduces the lubricant viscosity of the oil and results in more solid – solid contact [19]. The rubbing phenomenon is therefore

subjected to affect the nascent Fe surface and the Raman response of Fe_3O_4 at around 660 – 690 cm^{-1} is more observable under high temperature (Figure 7.11). At low temperature conditions the intensity of the Mo oxides peak are stronger with the presence of the Fe_3O_4 Raman shift, but a vice versa affect is observe under high temperature samples. Raman response of Fe_3O_4 on the rubbing samples is a product of wear process occurring on the contact, however the response of Mo oxides can be related with the frictional characteristics of the MoDTC.

At high temperature conditions, therefore rubbing result in a higher wear rate compared with low temperature conditions (Refer to sub-chapter 6.4) which could provide the adsorption of Mo-S-O radical on to the wear scar to decompose further to form the MoS_2. Recently, it was also shown that MoDTC decomposed to form MoS_2 in the presence of Fe_3O_4 iron oxide at high temperatures [199]. Therefore under higher temperature the MoDTC is exposed to rapid formation of the MoS_2 tribofilm due to rubbing and the formation of iron oxides on the contacting surface.

An amorphous tribofilm structure is observed at time period of 2 and a half minute, where the friction is high. TEM images for 1 hour time period show a formation of 'eyelashes' like structure which has been attributed to the formation of MoS_2 sheets [47] which enable low friction. These highly dispersed layers of MoS_2 are detected on most part of the 100°C tribofilm, but close to the substrate an amorphous like structure similar to the ones observed at high friction is observed. A prerequisite to form an initial layer before these layers of MoS_2 has been reported by various authors [42, 153]. Similar with the Raman response of Mo-S and Mo-O bonds at high friction, a layer is deposited close to the steel surface, which then further promotes the formation of MoS_2 layer under high temperature.

The role of the Mo oxide on the mechanism of MoDTC tribofilm, if any, is not clear. Gondo and Yamamoto [146] indicated that a prerequisite to form MoS_2 on the rubbing surfaces was that MoO_3 be formed in advance. In the current study, the Raman response of the pure MoO_3 tribofilm at 820 cm^{-1} is not observed on any of the wear scars. This is in contrast to previous work conducted in vacuum with XPS on tribofilms [165] and dry sliding MoS_2

coating Raman studies [33].

A various broader Raman peak is however observed onto the Raman spectrum of the tribofilm at a frequency range of 850 – 1000 cm^{-1} Raman shift (Refer to Figure 7.4 (b)). This Raman shift corresponds to the long chain of Mo-O bonds [142], which is formed due to the further decomposition of the MoDTC molecule under tribology contact. Under room temperature the Mo-O-Mo entity Raman response at 871 cm^{-1} (Figure 7.4 (b)) can be observed for shorter duration of test which further disintegrates to form Mo=O bonds which is apparent with longer duration test [141, 200, 201]. Raman peak observed around 920 – 930 cm^{-1} Raman shift has been reported for $FeMoO_4$ [151]. Iron and molybdenum both show a strong affinity towards oxygen, but iron oxides are formed as a result of wear occurring on the sample contact. Higher response of $FeMoO_4$ under low temperature conditions therefore affects the friction of the tribological system, which also further inhibits the formation of MoS_2 to reduce friction under low temperature conditions.

8.3.2 Effect of temperature on the tribochemical development of the MoDTC tribofilm

Previous work has demonstrated the effectiveness of temperature for the formation of the MoS_2 tribofilm from the MoDTC additive [43, 193]. The characteristic Raman active modes for the MoS_2 tribofilm approximately at 379 and 410 cm^{-1} are observed at samples where the friction drops to a value of 0.04. The MoS_2 tribofilm formed under high temperature however shows a shift of 2-3 cm^{-1} compared to that of the pristine MoS_2 spectrum (Figure 8.4). The shift in the tribofilm could be as a result of the induced pressure which probes vibrational changes in the multilayered MoS_2 [147]. It was also noted that the intensity of the MoS_2 powder was much more higher compared to the MoDTC tribofilm, which can be attributed to the crystalline nature of the MoS_2 powder. Similarly, E^1_{2g} and A_{1g} peak of the MoDTC tribofilm are much more broader than those of the powder sample. Broadening of the Raman peak has been highly attributed to the disorder in the molecular arrangement. (Refer to Chapter sub-section 3.2.2), and the broadening of the tribofilm peaks could be related to the disorder of the Mo and S atoms in the x–y plane as a result of induced pressure.

At the high temperature test during the high friction induction period, the Raman response of the samples corresponds with that of the low temperature test samples. The synergy of temperature and rubbing on obtaining the low friction could be achieved only after a certain induction time. This was achieved at a shorter time for the *in-situ* test, due to the effect of rotational speed and the longer sliding distance occurring in the rig. However, this indicates that the higher lubricant temperature does not result in a different MoDTC additive bulk decomposition mechanism and temperature input is mainly related to the change of contact conditions due to the lower viscosity at higher temperature.
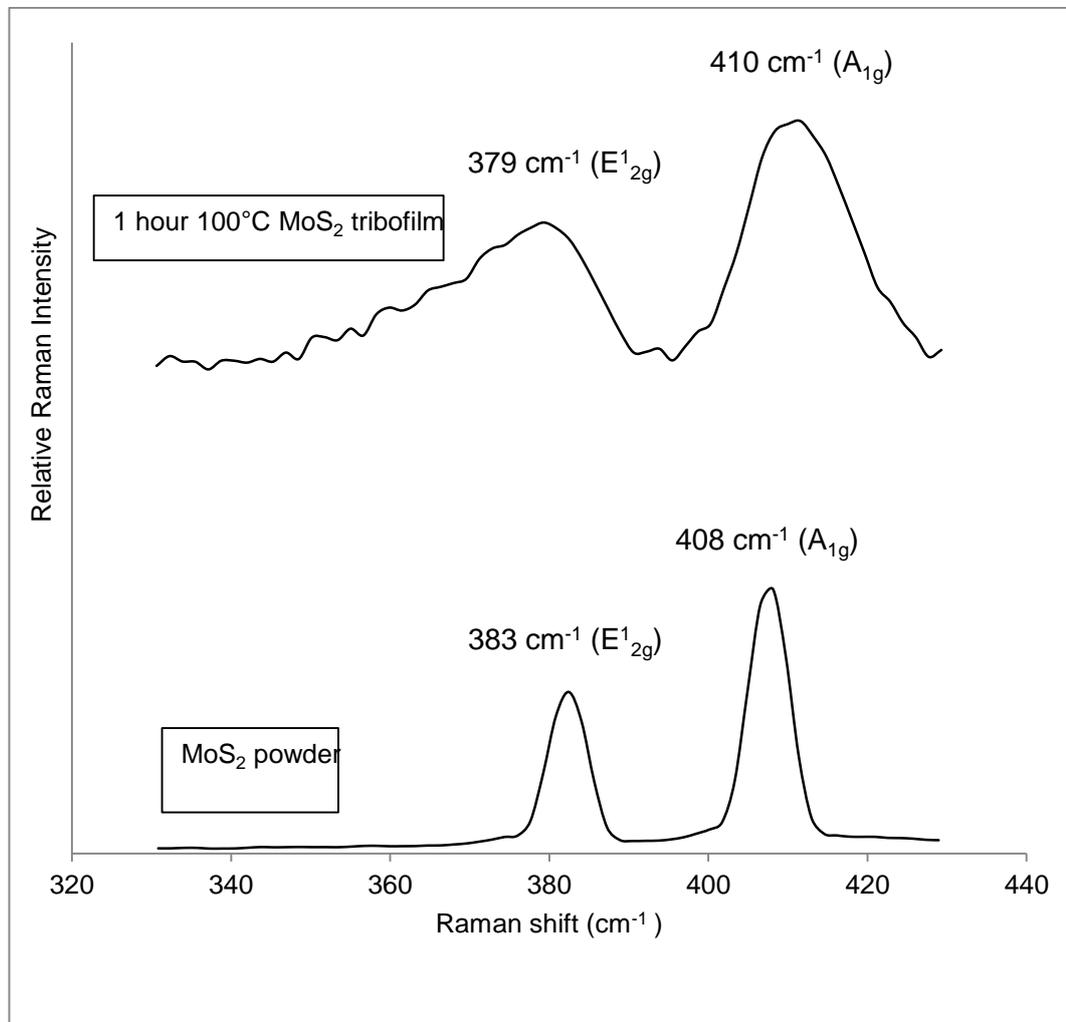
Figure 8.4 Raman spectra of the E^1_{2g} and A_{1g} peak for the 1 hour high temperature MoS_2 tribofilm, in comparison to the E^1_{2g} and A_{1g} peak of a pure MoS_2 powder.

With the increase in temperature it was shown that friction coefficient decreases for the MoDTC lubricant additive. At higher temperatures, oxidation processes can be accelerated and due to reduction in lubricant viscosity the wear phenomenon is observed with higher intensity of Fe_3O_4 in Raman. The influence of iron wear particles from the contacting substrate on the formation of the MoS_2 tribofilm is not very clear. However, under rubbing process the formation of $FeMoO_4$ could be influenced with the amount of iron oxide formed on the surface. Raman spectrum shows higher intensity of Fe_3O_4 at high temperatures, which could support the hypothesis that the formation of $FeMoO_4$ is controlled with high temperature and wear process. Low temperature conditions therefore does not initiate the formation of MoS_2 tribofilms, due to high level presence of $FeMoO_4$ on the surface. At higher temperatures, the presence of $FeMoO_4$ is controlled with the wear particles of Fe_3O_4, and the formation of MoS_2 films is initiated.

Following on this hypothesis adjustments on the chemical process on the formation of MoS_2 from MoDTC as proposed by Grossiord et al [47] is made in Figure 8.5. Grossiord et al considers the chemical breakdown process of MoDTC without the influence of substrate on the formation of the tribofilms. The revised version of the chemical process of the formation of MoS_2 from MoDTC considers the phenomenon of rubbing and temperature as observed from the research conducted here.
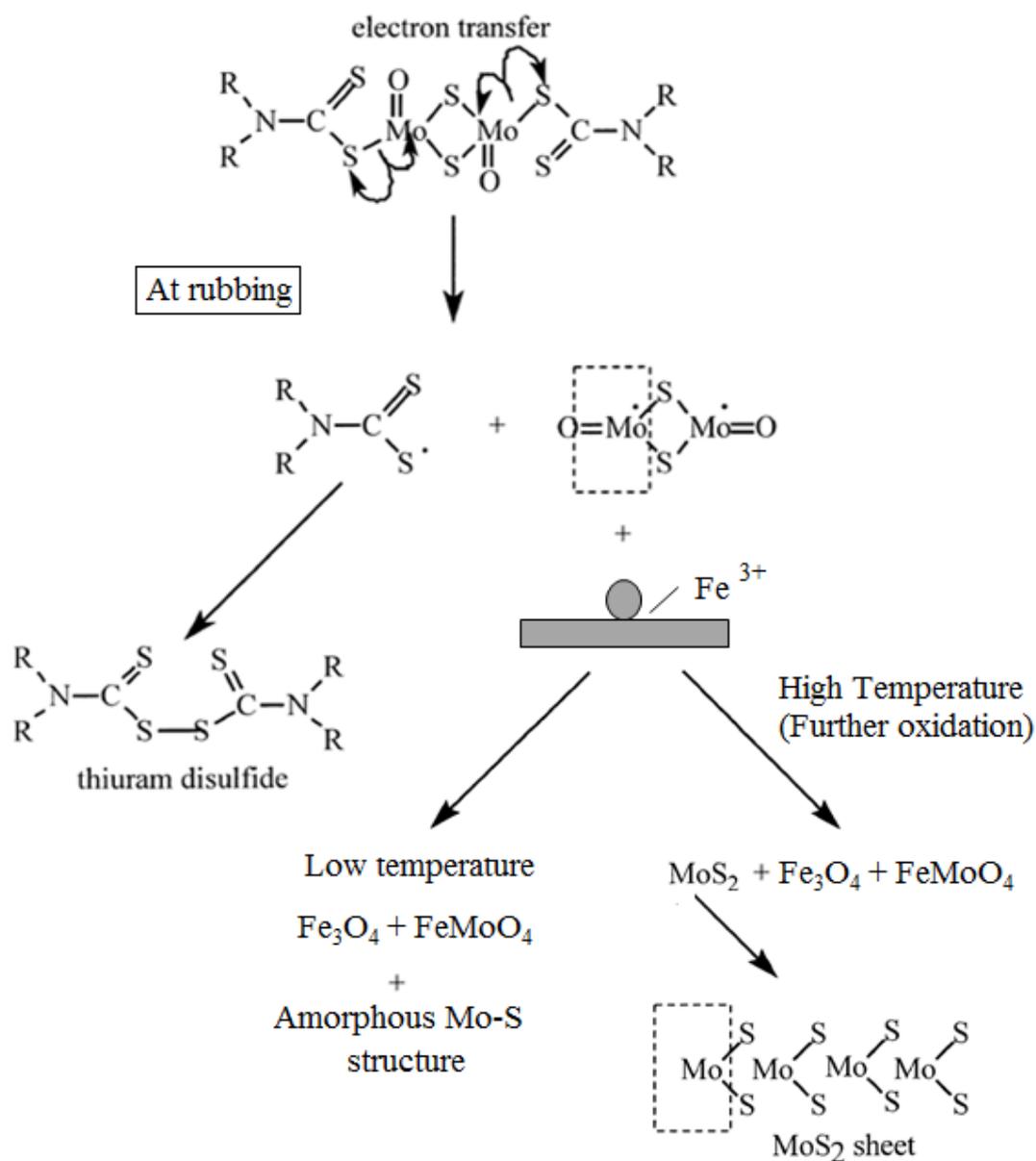
Figure 8.5 Revised version of the chemical process of the formation of MoS₂ from MoDTC as proposed by Grossiord et al [47]. The phenomenon of rubbing and temperature has been included in the process of MoS₂ tribofilm. The first phase corresponds to electron transfer on Mo-S bonding due to rubbing and wear on the contacting surface, and leading towards the formation of free radicals. The second phase represents the influence of temperature on the formation of MoDTC tribofilm. Formation of thiuram disulphide as described by Grossiord et al was not observed for the work conducted here. Similarly, formation of MoO₃ species was not observed in this work.

One key observation from Raman results is that under high temperature conditions, a shift in the A_{1g} Raman peak position with longer duration of rubbing could be observed (Figure 7.8 and 7.17). This shift also aligned well with the increase in FWHM of both A_{1g} and E_{2g} Raman peaks (Figure 7.12). A recent published study on model MoS_2 film suggests that position of A_{1g} Raman peak in relation to E_{2g} could be used as a convenient diagnostic of the layer thickness of the MoS_2 samples [177]. Lee et al [177] characterized single and few layers of MoS_2 films by Raman spectroscopy and concluded that the frequency of the E_{2g} mode decreases and that of A_{1g} mode increases with increasing the number of MoS_2 monolayers.

In the current study, it appears that the shift of the A_{1g} Raman peak observed from tribofilm analyses signifies the formation of the MoS_2 layers onto the wear scar which then lead to low friction (Figure 8.6). This is also supported by the TEM images at low friction samples in Figure 7.10 which show the lattice layer structure of the tribofilm formed at the sliding interface. The shift of the E_{2g} and A_{1g} modes of the MoDTC tribofilm formed at high temperature therefore confirms the increase of the MoS_2 number of layers with time resulting in low friction of the system.
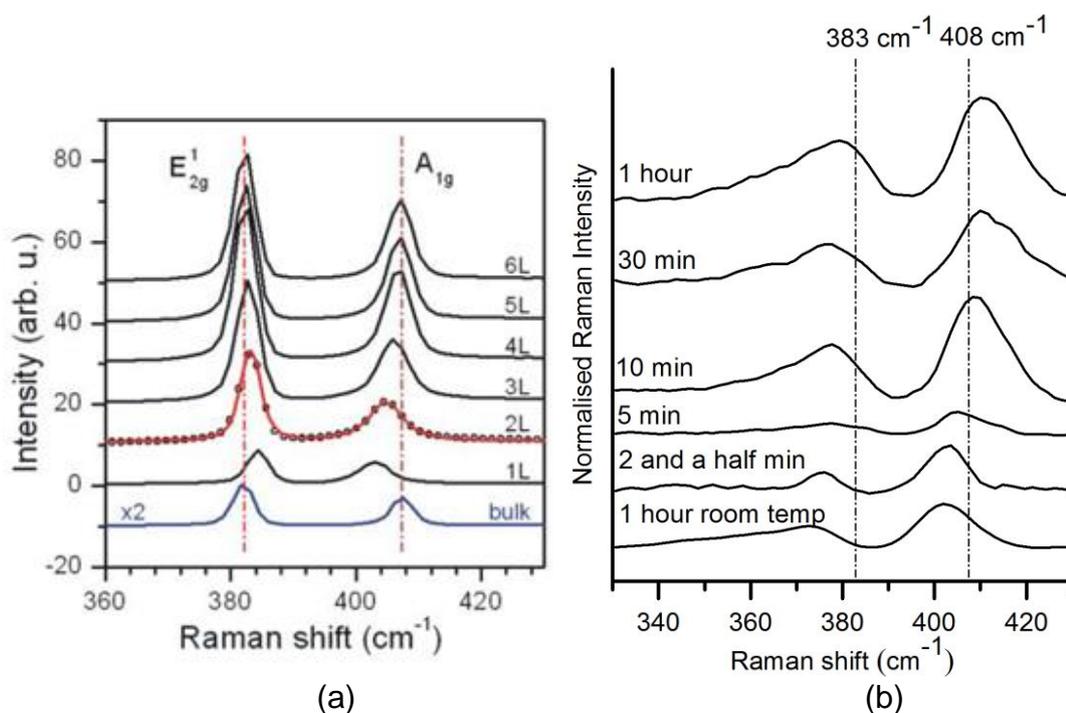
Figure 8.6 (a) Raman spectra of E^1_{2g} and A_{1g} Raman modes of thin (nL) and bulk MoS_2 films [177] and (b) A_{1g} and E^1_{2g} Raman peaks of time derived MoS_2 tribofilm.

Hence, reduction of friction in the tribological system of MoDTC is activated with the formation of MoS_2 layers on both rubbing samples. The rate of MoS_2 formation is inhibited with the formation of $FeMoO_4$ species in the tribofilm and higher lubricant temperature is mainly related to the change of contact conditions due to the lower viscosity of the oil achieved. However, higher temperature oxidation and wear processes accelerates the formation of Fe_3O_4 wear particles which controls the presence of $FeMoO_4$ on to the surface and initiates formation of MoS_2 films.

8.4 Durability of MoDTC friction reducing capability

The lubricating ability of MoDTC additive has been reported to be greatly degraded under severe conditions of very high temperature, shear stress and chemical attack by fuel combustion products in an engine [39, 202, 203]. The formation of MoS_2 tribofilm which reduces friction in an oil containing MoDTC is subjected to high lubricant temperature changing the tribological contact conditions, which initiates the formation of MoS_2 layers. During engine operations, additives were reported to be consumed during oil use and the friction reducing benefits were lost.

At high temperature oxidizing conditions, MoDTC additives decay linearly through oxidation, where the friction reducing capability was found to initially improve, before being abruptly lost when the MoDTC concentration was reduced below a certain concentration [204]. Under short oil degradation time, MoDTC oil performance was shown to lower the friction compared to fresh oil (Refer to chapter sub-section 6.1.2) at low temperature conditions. This frictional performance was observed to be similar to the fresh oil test conducted at elevated temperatures of $50^{\circ}C$ and $80^{\circ}C$. The tribofilm properties on the wear scar were observed with similar characteristics. Hence certain level of oxidation supports the breakdown of MoDTC additive on the contacting sample.

Friction reducing ability of the MoDTC oil was reported to be lost with longer duration of oil degradation, as the MoDTC concentration was depleted [192, 204]. De Feo *et al* [197], reported for the Mo(IV) in XPS, a progressive chemical shift of the Mo3d photopeak to higher values was observed as the

degradation time increase. They considered that the peak may arise from molybdenum oxisulphide species ($MoS_{2-x}O_x$) and that there is a chemical shift in its position to higher binding energy, which became greater and greater as the oxygen replaces sulphur in the Mo-oxisulphide structure. Raman analysis conducted on the degraded test tribofilms has been reported with a complex Mo–S–O species, which can be related to the Mo oxisulphide species present in the tribofilm. The friction characteristics of the oil is therefore related with the oxygen content on these molybdenum oxisulphides compounds.

Graham et al [192] indicated a substantially reduced friction after up to three hours oxidation for the MoDTC additive but after four and five hours oxidation they lost this ability as Mo concentration in the form of MoDTC fell below 180 ppm. Similarly, De Feo *et al* [197] reported an induction period was necessary to obtain the reduction in friction coefficient and the delay to reach the low steady-state value increased as the ageing time increases.

However, longer duration tribological test conducted with fresh MoDTC additive showed that the friction reduction ability was not affected (Refer to chapter sub-section 6.2.1). Raman analysis confirmed the formation of MoS_2 tribofilm on the contacting samples, with similar characteristics as that observed with a 1 hour time period samples. Hence, once the MoS_2 is formed on the contacting samples, the low friction characteristic is maintained even with longer time duration, and the effect of oxidation is negated.

Morina et al [205] assessed the low-friction tribofilm formation from MoDTC containing lubricants and its removal by applying "changing lubricants" procedure. The low friction achieved with the MoDTC lubricant was maintained when the lubricant was changed to a fresh MoDTC lubricant as the process does not disrupt the tribofilm. However, change of friction was instantaneous with the change in other additive lubricants. They suggested instantaneous change of low-friction obtained from MoDTC once the additive is removed from the lubricant suggests that replenishment of the low-friction film is essential in maintaining the low-friction.

Under oil scarcity, the frictional response of the MoDTC lubricant increases as the lubricant is drained from the system (Refer to Chapter sub section 6.2.2).

The MoS$_2$ tribofilm formed on the contacting surface is therefore exposed to higher pressure as the load carrying capacity of the lubricant is negated. Similarly, replenishment of the MoDTC film in maintaining the low-friction is stopped and the pure tribofilm exposed to dry sliding contacts.

Grossiord et al [47] confirms that even one MoS$_2$ sheet is sufficient to lubricate the contact. However, after the removal of the oil and 30 minutes of sliding exposure, Raman analysis conducted on the wear scar of the contacting surface shows the presence of E$^1_{2g}$ and A$_{1g}$ mode of the MoS$_2$ film. Therefore, the steady increase of friction could be related to the removal of the MoS$_2$ sheets formed on the contacting surface, as the removal of lubricant does not allow the replenishment of the MoDTC film. However, certain thickness of MoS$_2$ layer is required to maintain the low friction properties.

Equally, similar Raman peaks observed at test conducted with 50ºC and 80ºC temperature and degraded oil response was observed around 220 cm^{-1} and 290 cm^{-1}. This peak has been reported for Mo-O-Mo deformation mode at 220 cm^{-1} [154] and peaks around 288 – 280 have been reported for the amorphous MoS$_3$ molecule. Hence with the removal of oil, the MoS$_2$ film is subjected to increased contact stress but the MoS$_2$ film is not completely depleted from the contact even after half an hour of dry sliding. However due to increased contact pressure, reduction in friction is not maintained with the removal of lubricant and the replenishment of MoDTC film is disturbed. The contact pressure induces a disorder in the arrangement of the MoS$_2$ species on the surface, which shows characteristics of moly oxisulphide species along with MoS$_2$ tribofilms based on Raman results.

Low friction properties of the MoDTC additive are therefore maintained with the formation of the MoS$_2$ on the contacting surface. The friction is maintained with the availability of lubricant in the tribological system. Longer oxidation period is reported to lose the ability of low friction for the MoDTC additive, as the Mo concentration was reported to fell [42, 192]. However, as the MoDTC film is formed on the surface, these film maintain the low friction properties even at longer time period of high temperature and sliding exposure (Chapter section 6.2.1). However as the lubricant is removed within the system, friction reduces dramatically and the MoS$_2$ film on its own does not support the

increased contact pressure to maintain the low friction (Chapter section 6.2.2) . Hence, replenishment of these MoDTC film in maintaining low-friction on the contact is necessary.

8.4.1 Tribological performance of Molybdenum dialkyldithiocarbamate (MoDTC) and its interaction with Zinc dialkyldithiophosphate (ZDDP)

MoDTC lubricant additive is shown to reduce friction with the absence of other additives in the base oil (Figure 5.8) [41, 43, 44, 50]. The reduction in friction is contributed with the formation of MoS_2 tribofilm layers on both the contacting surface, and its formation is critically dependent on high temperature, where a certain level of oxidation is necessary. However, in the presence of an additive containing sulphur and phosphorous, molybdenum complexes are reported to reduce friction and wear significantly [41]. MoDTC in conjugation with ZDDP has been reported to reduce friction and wear, which is attributed to the formation of MoS_2 and polyphosphates films [46, 53, 54, 160, 206].

Tests performed under ZDDP/MoDTC lubricant tribological conditions as with MoDTC only, show that friction reduction occurs on both low and high temperature conditions (Refer to Chapter section 6.3) (Figure 6.14 and 6.19). Raman analysis conducted onto the contacting samples shows the presence of MoS_2 films, which is credited for low friction on both low and temperature conditions for the additives of MoDTC and ZDDP [54]. EDX analysis performed on the sample analysis shows the presence of Zn, O and P elements, which relates to the presence of phosphate films. The absence of any metal oxides response in the Raman also indicated the O elements relates to the phosphate film on the tribofilm.

Hence, the reduction in friction for the lubricant additive of MoDTC and ZDDP is credited to the presence of zinc phosphate layer which provides suitable conditions for the formation of MoS_2 tribofilm on the contacting surface. The tribochemical reactions between the additive of MoDTC and ZDDP have been explained on the basis of the hard and soft acid and base (HSAB) principle [30, 160]. A two-step reaction was proposed where firstly, a reaction between phosphate and iron oxide occurred, and second, a reaction between the

nascent iron surface and a sulphide species. These reactions occur through material transfer between the two counterfaces [30].

Under low temperature conditions of 25ºC, the friction reduction for the additive of MoDTC/ZDDP occurred with an initial induction period, which was similar to the friction response of MoDTC additive at high temperature conditions. At high temperature conditions, MoDTC additive achieved low friction after a certain induction time due to the synergy of temperature and rubbing which is mainly related to the change of contact conditions due to the lower viscosity at higher temperature. Low friction was however, not observed with the additive of MoDTC at low temperature conditions. Therefore at low temperature conditions, rubbing initiates the formation of zinc phosphate glass from ZDDP initially in the additive mixture of MoDTC/ZDDP. This polyphosphate tribofilm then promotes the formation of MoS_2 through adsorption and decomposition of MoDTC which results in the decrease of the friction.

The induction period of MoDTC/ZDDP lubricant additive at high temperature was much more earlier in comparison to the low temperature conditions (Refer to Figure 6.19). At high temperatures, ZDDP has also been reported to form transparent, solid, reaction films on the metal surface [207, 208]. These thermal films have been reported to have a similar composition to ZDDP tribofilms, which consists mainly of a thin, outer layer of polyphosphate grading to pyro- or orthophosphate in the bulk, where the rate of thermal film formation increases with temperature [207]. Similarly, the thermal films phosphate form is also affected by the presence of MoDTC where generally, short chain polyphosphates were found for the thermal films [46]. Hence at high temperature condition, the accelerated process of ZDDP thermal film formation enhances the formation of MoS_2 tribofilm on the surface and supported with an earlier low friction induction period.

After a certain time period, however an increase in friction for the MoDTC/ZDDP additive is observed at higher temperature conditions. The friction-reducing capabilities of the MoDTC and ZDDP additive systems are very much affected by oxidative conversion occurring during inhibited oxidation [52]. Korcek et al [52] describes initially the rate of ZDDP tribofilm

with increasing oxidation time affects the friction response and with its decrease rate of formation, the oxidation properties of the tribofilm formed affects the friction response due to the formation of MoS_2.

An intense Raman peak for the E^1_{2g} and A_{1g} vibrating mode of the MoS_2 tribofilm along with the 'Eyelid' type structure of MoS_2 layers formed onto the top surface of the tribofilm explains the low friction observed in low temperature test conditions for MoDTC/ZDDP lubricant. However, a shift in the E^1_{2g} and A_{1g} vibrating mode of the MoS_2 tribofilm is observed with the high temperature conditions. TEM images also indicate that thicker layers of MoS_2 tribofilm is absent on the tribofilm (Figure 6.21). Friction response is therefore related with the layers of MoS_2 formed onto the surface.

At earlier time periods when the friction is low for MoDTC/ZDDP additive at high temperature conditions, Raman peak of the E^1_{2g} and A_{1g} vibrating mode of the MoS_2 tribofilm formed showed similar response to that of the low temperature conditions. However, with longer time duration a shift occurs to lower value, which is responsive of the few layers of MoS_2 on the contacting surface (Figure 8.7). Under high temperature conditions, hence the rate of MoS_2 formation is accelerated with the formation of ZDDP tribofilms onto the surface Morina et al [54] also reported the increase in friction due to the increase in Zn phosphate and Mo phosphate formation at this temperature.. With longer time duration the formation of MoS_2 is deteriorated with longer oxidation time and the friction response is directly related with the layers of MoS_2 formed onto the surface.

The E^1_{2g} and A_{1g} Raman modes of the MoS_2 tribofilm therefore indicate that the MoS_2 film is dependent of the layer formed onto the surface. Figure 8.8 shows a comparative E^1_{2g} and A_{1g} Raman peak at the end of the test MoS_2 tribofilm formed from MoDTC and MoDTC/ZDDP at different temperature. The higher shift (blue shift) of the A_{1g} peak in the MoS_2 tribofilm formed with the additive of MoDTC itself, is a result of the induced pressure which probes vibrational changes in the multilayered MoS_2 [147].
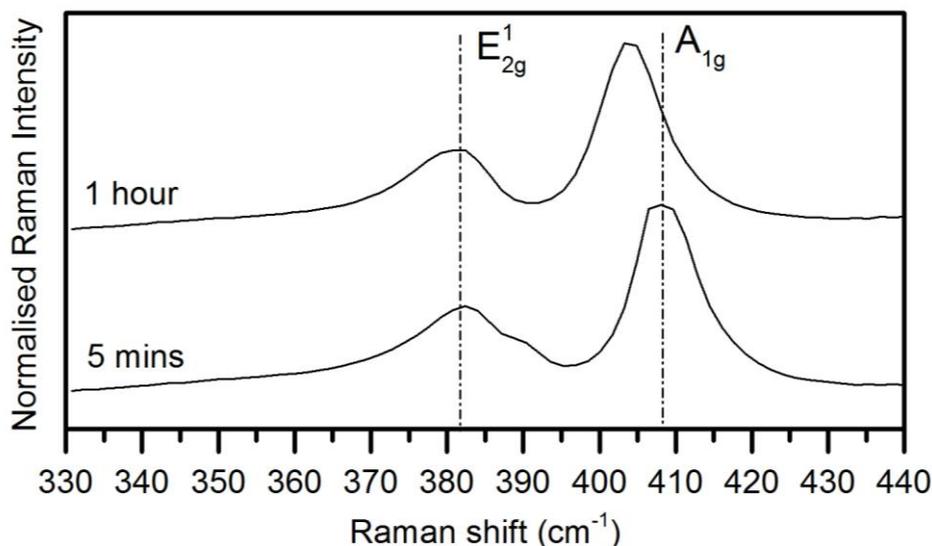
Figure 8.7 Raman peak comparison of the E^1_{2g} and A_{1g} mode of the MoS$_2$ tribofilm formed at time periods of 5 mins and 1 hour for the MoDTC/ZDDP additive under high temperature conditions of 100ºC.

With the additive of MoDTC/ZDDP under low temperature conditions, the MoS$_2$ Raman peak resembles that of a pure MoS$_2$ powder. Bec *et al* [159] reported that the contact pressure was found to be a critical parameter for the orientation of MoS$_2$ sheets present in the outer layer of the tribofilms formed from MoDTC containing lubricants. Higher contact pressures were attained when ZDDP was used together with MoDTC as one of the main characteristics of ZDDP additives is to form protective anti-wear tribofilms under boundary lubrication. Hence the induced pressure is distributed with the formation of ZDDP tribofilms and the influence of blue shifts in the MoS$_2$ tribofilm due to induced pressure is not observed. The red shift of the E^1_{2g} and A_{1g} mode observed for the MoS$_2$ tribofilm of MoDTC and ZDDP at high temperatures is due to the layer effect.

Typically Raman response of zinc phosphate glasses has been reported in earlier studies [167-171, 175]. Raman analysis conducted on the additive of ZDDP and MoDTC/ZDDP however, did not show a definite peak of the ZDDP tribofilms on the sample. Uy *et al* [150] observed less intense phosphate peak around 1009 cm^{-1} in the samples of the ball-on-flat experiment, but this response was much more stronger on the cylinder-on-flat experiments. Similarly, Berkani *et al* [209] reported a P–O band located at 968 cm^{-1} for a ZDDP tribofilm and attributed it to the anti-symmetric stretching modes. They

indicate that the phosphate tetrahedra are strongly distorted, possibly because of the presence of a mixed Fe/Zn phosphate compound in the tribofilm. Raman analysis conducted on the ZDDP tribofilm did not show any response even with the lubricant additive of ZDDP on its own. Weak Raman response was however observed in between 500 and 800 cm^{-1} for the additive of MoDTC/ZDDP which has been related to the stretching mode of P-O-P bonds.

Hence, the characterization of the ZDDP tribofilm was not feasible with the Raman spectroscopy in this work. The formation of highly amorphous nature of the ZDDP tribofilm could subdue the response of the sample, and the spectra of films formed, due to the presence of oil could mask the Raman peaks of the ZDDP film.
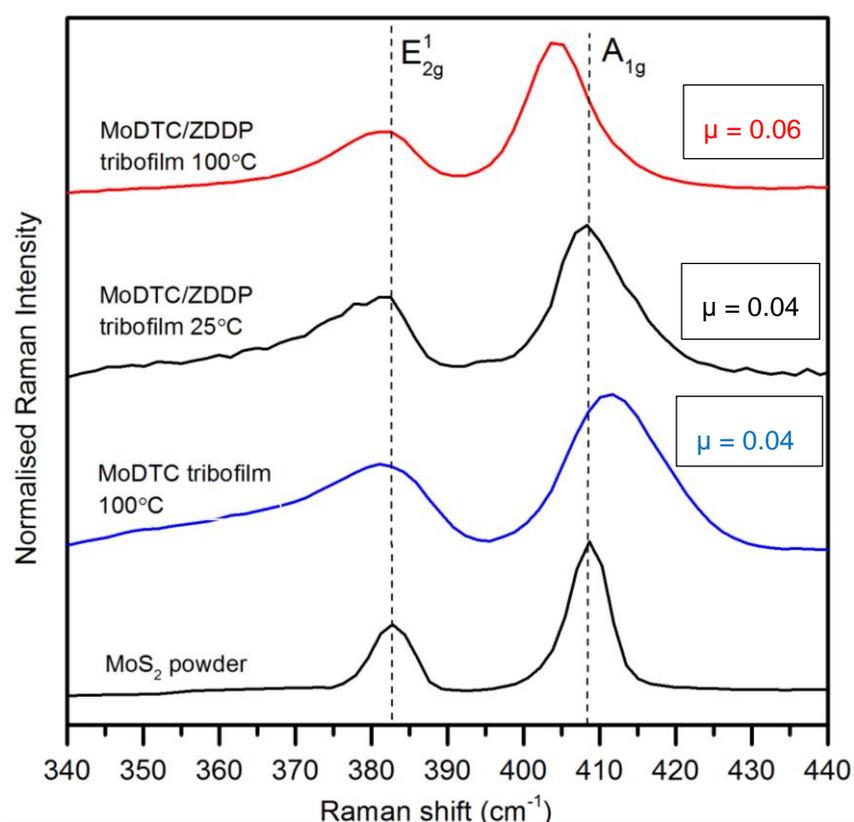
Figure 8.8 Comparison of the E^1_{2g} and A_{1g} Raman mode of the MoS_2 powder and the MoS_2 tribofilm formed at time periods of 1 hour for the MoDTC and MoDTC/ZDDP additive under same tribological conditions and stated temperature. Coefficient value of friction (μ) at the end of 1 hour test for the lubricant additive tribological conditions is given.

Chapter 9
Conclusion and Future Work

With this thesis, an *in-situ* Raman tribometer has been used to show its usefulness for chemically characterising the tribochemical film formation under boundary lubricated conditions. End of test surface analysis are usually applied for a broader understanding of the tribochemical nature of the tribofilm. *In-situ* Raman studies has allowed a time development understanding and chemical characterisation of the tribofilm formed on the surface contact as a function of sliding time and temperature.

Application of Raman spectroscopy for determining the physical and chemical properties of the tribofilms formed on the surface is demonstrated with a wealth of information obtained from the analysis. Based on the research of this project, the following conclusion has been established with the *ex-situ* and *in-situ* analysis of Raman conducted here in this research.

9.1 Influence of varying parameters on the tribological performance of MoDTC

- Reduction in friction for the lubricant additive of molybdenum dialkyldithiocarbamate (MoDTC) is initiated with the formation of MoS_2 tribofilm on the contacting surface.

- The formation of MoS_2 tribofilm is dependent on the contact pressure, sliding speed and temperature which defines true boundary lubrication conditions.

- Low sliding speed conditions initiates high friction and wear rate, as the condition for the adsorption of MoDTC additive on the surface is not promoted. Higher sliding speed initiates lower friction values and low wear rate, as conformal lubricated contact at the surface is promoted. The surfaces in contact are transformed that leads to entrain thicker oil film and conditions of elastohydrodynamic and mixed lubrication is achieved.

- Under true boundary conditions reduction in friction was achieved with the formation of MoS_2 tribofilm, and occurred with a contact pressure of 1 GPa, sliding speed of 0.88 m/s and temperature of 100°C in this study.

- The formation of MoDTC tribofilm on the HSPOD and *in-situ* rig could be suggested with the exposure time of the lubricant additive within the contact and the load, as the formation of the tribofilm varies in terms of sliding speed in the different rigs.

- At higher temperatures, MoDTC tribofilm does not thermally decompose to form MoS_2 and the phenomenon of contact rubbing is necessary to form MoS_2 on the surface.

- With the increase in temperature, the frictional characteristic of the MoDTC lubricant was influenced with the adsorbed species on the contacting surface. A complex form of MoDTC additive containing Mo-O-S species was observed to adsorb on the contacting surface. The frictional characteristics of the MoDTC is directly influenced with the oxygen content on the Mo-O-S species and could be related with the removal of oxide film due to increasing contact pressure, promoting the formation of Mo-S containing film.

9.2 Time transient processes of the lubricant additive of MoDTC

- Time transient study of the MoDTC tribofilm, showed under low temperature conditions, the reduction in friction is inhibited with the formation of $FeMoO_4$ species on the tribofilm.

- Raman analysis shows the presence of the two characteristics peaks for the Mo-S spectrum, but not observed on every area of the sample's wear scar. The low shift of the A_{1g} Raman peak has been reported for a few layered MoS_2, hence stating that under rubbing few MoS_2 layer could be formed but not enough to support the contact pressure induced. *In-situ* analysis shows the formation of amorphous MoS_2 films and MoS_3 which is adsorbed onto the wear scar.

- High temperature conditions promotes the formation of MoS_2 on the contacting sample. Earlier induction period with higher friction shows similar tribofilm characteristics as that observed with low temperature conditions. TEM images shows that at even at earlier time period a form of tribofilm is adsorbed on the contacting samples.

- The initiation of low friction in the MoDTC additive is evident with the shift in the A_{1g} peak for the MoS_2 tribofilm. This shift is related with the formation of MoS_2 layers on the sample, which decreases friction with the increase in layers.

- The reduction in friction is observed with the formation of MoS_2 layers on the contacting samples, and a steady state low friction is achieved with a certain thickness of MoS_2 layers. TEM images shows the formation of eyelashes type of structure of the MoS_2 sheets. At high temperature, hence change of contact conditions due to lower viscosity of oil, induces arrangement of the adsorbed MoDTC species to form MoS_2 layers.

9.3 Durability performance of MoDTC and its interaction with ZDDP

- Durability test performed on the additive of MoDTC shows that some form of oxidation is necessary to lower the friction of the tribological systems.

- As the MoS_2 tribofilm is formed on the contacting surface, the low friction is maintained, but the removal of lubricant shows that the tribofilm does not support low friction on its own. The induced pressure exerts the removal of MoS_2 layers as the load carrying capacity of the lubricant is absent. Hence stating the replenishment of the low-friction film is essential in maintaining low friction. The tribofilm is however not fully removed and shows the presence of MoS_2 along with the molybdenum oxide species.

- MoDTC along with the additive of ZDDP shows a reduction of friction and wear. The reduction in friction is related with the formation of MoS_2 tribofilm and the reduction of wear with the formation of Zinc phosphate films.

- Friction reduction was generated even at low temperatures, which is in contrast with the additive of MoDTC used on its own. Contact pressure which is a critical parameter for the orientation of MoS_2 sheets, were obtained with ZDDP films which distributes the induced pressure. This is also exhibited with the Raman response of the MoS_2 tribofilm, as blue shift of the A_{1g} peak occurs with higher pressure induced in the MoS_2 tribofilm formed with the additive of MoDTC itself.

- Higher temperature conditions show an earlier induction period for the friction reduction with the additive of MoDTC/ZDDP lubricant. The earlier reduction in friction is related to the formation of ZDDP thermal films, which accelerates the rate of MoS_2 formation on the surface. Under this conditions Raman response shows the formation of similar MoS_2 structure as that of the low temperature conditions. The friction reducing capabilities of the MoDTC and ZDDP are reported to be affected with the oxidative conversion and the formation of MoS_2 inhibited. Raman and TEM analysis shows the presence of fewer layers of MoS_2.

- Characterization of ZDDP tribofilm was not very constant with the Raman spectroscopy. The formation of glassy like structure and its amorphous form could affect the response of the tribofilm in Raman. Similarly the presence of oil could mask the Raman speaks of the ZDDP film.

9.4 Recommendation for future work

The research at hand shows the formation of MoDTC tribofilms is dependent upon true boundary conditions for a concentration of 100 ppm of Mo. At the defined contact pressure and sliding speeds of true boundary conditions, MoDTC additives are adsorbed onto the contacting surface and the frictional performance related with the type of films formed on the contacting surface.

The formation of MoS_2 tribofilm which is related to low friction is critically dependent on high temperatures and some form of oxidation is required. At higher concentration it has been reported the rate of MoS_2 film formation is accelerated and an earlier induction period is observed. To further understand the kinetics of the MoDTC tribofilm formation, test with higher concentration

could be undertaken to understand its influence on the formation of MoS_2 layers and its relevance to low friction characteristics.

MoS_2 film formation has also been linked with the roughness of the substrate, where a certain roughness is required to adsorb the MoDTC additive to form MoS_2 films. Graham et al [192] showed that with smoother surface under the same tribological parameters, the formation of MoS_2 tribofilm was inhibited. Hence, this provides a platform to understand the asperity contacts of the substrate, for a logical definition of the MoDTC molecular adsorption on the contacting surface. Although physical adsorption of the additives are observed with this research, the molecular arrangement of how this adsorbed species forms MoS_2 eyelid type structure is still vague.

The influence of lubricant viscosity on the formation of MoS_2 tribofilm is also as important parameter. The study conducted here is obtained with a base oil of PAO4 where its viscosity characteristics remains the same. However considering other base oil and its influence on the MoDTC characteristics should also be considered.

In-situ analysis of the tribofilm formed presented a time developed tribochemical characteristics and performance for the lubricant additive. As mentioned replenishment of the films formed on the wear scar is an important phenomenon in maintaining the tribological properties of the tribofilm. Further test to understand and develop the durability of the lubricant additives could be performed with the *in-situ* rig to understand the performance of these additives under boundary lubrication.

With the recent development of surface treatments, surface coatings such as diamond like carbon (DLC) are extensively applied to machine component surfaces operating in lubricated systems. Conventional lubricants formulated for a steel/steel surface are still used for DLC coated surfaces. However, the surface properties of these coatings are quite different from those of steel. Hence, the interaction of additive molecules with the coatings should be considered with the use of Raman spectroscopy. Raman spectroscopy has been utilized to characterize the structural form of carbon in DLC, which shows a definite Raman feature of the D and G peak for the sp^3 and sp^2 bonds

content in DLC films. Hence with the utilisation of *in-situ* analysis, progressive development and tribochemical interactions could be analysed as a function of sliding time and its friction and wear properties.

List of References

1. Dick, K. and F.B. Thomas, *Organic Friction Modifiers*, in *Lubricant Additives*. 2009, CRC Press. p. 195-210.

2. Wieting, T.J. and J.L. Verble, *Infrared and Raman Studies of Long-Wavelength Optical Phonons in Hexagonal MoS$_2$*. Physical Review B, 1971. **3**(12): p. 4286-4292.

3. Dowson, D., *History of tribology*. 2nd ed. 1998, London: Professional Engineering Pub. xxiv, 768 p.

4. Stachowiak, G.W. and A.W. Batchelor, *Engineering tribology*. 3rd ed. 2005, Amsterdam ; Boston: Elsevier Butterworth-Heinemann. xxiv, 801 p.

5. Heinicke, G. and H.-P. Hennig, *Tribochemistry*. 1984, München: C. Hanser. 495 p.

6. Pawlak, Z., *Tribochemistry of lubricating oils*. Tribology and interface engineering series. 2003, Amsterdam ; Boston: Elsevier. xiv, 368 p.

7. Torbacke, M., s.K. Rudolphi, and E. Kassfeldt, *Lubricants Introduction to Properties and Performance*. 2014, Wiley: Hoboken. p. 1 online resource (219 p.).

8. Popov, V.L., *Contact Mechanics and Friction - Physical Principles and Applications*. 2010, Springer: Heidelberg ; New York.

9. Archard, J.F., *Contact and Rubbing of Flat Surfaces.* Journal of Applied Physics, 1953. **24**(8): p. 981-988.

10. Archard, J.F. and W. Hirst, *The Wear of Metals under Unlubricated Conditions*. Vol. 236. 1956. 397-410.

11. Hutchings, I.M., *Tribology : friction and wear of engineering materials*. 1992, London: Edward Arnold. viii, 273 p.

12. Taylor, C.M., *Lubrication Regimes and the Internal Combustion Engine*, in *Tribology Series*, C.M. Taylor, Editor. 1993, Elsevier. p. 75-87.

13. Mortier, R.M., et al., *Chemistry and technology of lubricants*. 2010, Springer: Dordrecht ; London. p. xiv, 560 p.

14. Hamrock, B.J. and D. Dowson, *Isothermal Elastohydrodynamic Lubrication of Point Contacts .3. Fully Flooded Results.* Journal of Lubrication Technology-Transactions of the Asme, 1977. **99**(2): p. 264-276.

15. Hamrock, B.J., S.R. Schmid, and B.O. Jacobson, *Fundamentals of fluid film lubrication*, in *Mechanical engineering 169*. 2004, Marcel Dekker: New York. p. xiv, 699 p.

16. Czichos, H. and K.H. Habig, *Lubricated wear of metals*. Mixed Lubrication and Lubricated Wear, Proc. 11th Leeds-Lyon Symp. on Tribology, Leeds, September 4–7, 1984, ed. D. Dowson and C.M. Taylor. 1985, London: Butterworths.

17. Rudnick, L.R., *Lubricant additives chemistry and applications*, in *Chemical industries 124*. 2009, CRC Press: Boca Raton. p. xvi, 777 p.

18. Korcek, S., et al., *Automotive lubricants for the next millennium.* Industrial Lubrication and Tribology, 2000. **52**(5): p. 209-220.

19. Holmberg, K., P. Andersson, and A. Erdemir, *Global energy consumption due to friction in passenger cars.* Tribology International, 2012. **47**: p. 221-234.

20. Hamrock, B.J. and D. Dowson, *Isothermal Elastohydrodynamic Lubrication of Point Contacts .1. Theoretical Formulation.* Journal of Lubrication Technology-Transactions of the Asme, 1976. **98**(2): p. 223-229.

21. Hamrock, B.J. and D. Dowson, *Isothermal Elastohydrodynamic Lubrication of Point Contacts .2. Ellipticity Parameter Results.* Journal of Lubrication Technology-Transactions of the Asme, 1976. **98**(3): p. 375-383.

22. Ai, X.L. and H.S. Cheng, *The effects of surface texture on EHL point contacts.* Journal of Tribology-Transactions of the Asme, 1996. **118**(1): p. 59-66.

23. Patir, N. and H.S. Cheng, *An Average Flow Model for Determining Effects of Three-Dimensional Roughness on Partial Hydrodynamic Lubrication.* Journal of Lubrication Technology, 1978. **100**(1): p. 12-17.

24. Dowson, D., C.M. Taylor, and G. Zhu, *A transient elastohydrodynamic lubrication analysis of a cam and follower.* Journal of Physics D: Applied Physics, 1992. **25**(1A): p. A313.

25. Williams, J.A., *Engineering tribology*. 1994, Oxford ; New York: Oxford University Press. xix, 488 p.

26. Bovington, C.H., *Friction, Wear and the Role of Additives in Controlling Them*, in *Chemistry and Technology of Lubricants*, R.M. Mortier, M.F. Fox, and S.T. Orszulik, Editors. 2010, Springer Netherlands. p. 77-105.

27. Matveevskii, R.M., *Problems of Boundary Lubrication.* Tribology International, 1995. **28**(1): p. 51-54.

28. Gunsel, S., H.A. Spikes, and M. Aderin, *Insitu Measurement of Zddp Films in Concentrated Contacts.* Tribology Transactions, 1993. **36**(2): p. 276-282.

29. Cann, P.M. and H.A. Spikes, *In-contact IR spectroscopy of hydrocarbon lubricants.* Tribology Letters, 2005. **19**(4): p. 289-297.

30. Martin, J.M., et al., *Transfer films and friction under boundary lubrication.* Wear, 2000. **245**(1-2): p. 107-115.

31. Piras, F.M., A. Rossi, and N.D. Spencer, *In situ Attenuated Total Reflection (ATR) spectroscopic analysis of tribological phenomena.* Boundary and Mixed Lubrication: Science and Applications, 2002. **40**: p. 199-206.

32. Himmel, D., et al., *In Situ Raman Microspectrometry of Lubricated Tribologic Contacts. Part Two: Simultaneous Measurements of Pressure, Lubricant Film Thickness and Temperature Distributions in a Running EHD Contact.* Tribology Letters, 2011. **41**(1): p. 131-144.

33. Muratore, C., et al., *In situ Raman spectroscopy for examination of high temperature tribological processes.* Wear, 2011. **270**(3-4): p. 140-145.

34. Totten, G.E., S.R. Westbrook, and R.J. Shah, *9. Additives and Additive Chemistry*, in *Fuels and Lubricants Handbook - Technology, Properties, Performance, and Testing: (MNL 37WCD)*. ASTM International.

35. Mang, T. and W. Dresel, *Lubricants and lubrication.* 2001, Weinheim ; New York: Wiley-VCH. xxxix, 759 p.

36. Canter, N., *Fuel economy The role of friction modifiers and VI improvers.* Tribology & Lubrication Technology, 2013. **69**(9): p. 14-27.

37. Kano, M., et al., *Ultralow friction of DLC in presence of glycerol mono-oleate (GMO).* Tribology Letters, 2005. **18**(2): p. 245-251.

38. Minami, I., et al., *Investigation of tribo-chemistry by means of stable isotopic tracers, part 2: Lubrication mechanism of friction modifiers on diamond-like carbon.* Tribology Transactions, 2007. **50**(4): p. 477-487.

39. Braithwaite, E.R. and A.B. Greene, *Critical Analysis of Performance of Molybdenum Compounds in Motor Vehicles.* Wear, 1978. **46**(2): p. 405-432.

40. Mitchell, P.C.H., *Oil-Soluble Mo-S Compounds as Lubricant Additives.* Wear, 1984. **100**(1-3): p. 281-300.

41. Yamamoto, Y., et al., *Organoamine and Organophoshpate Molybdenum Complexes as Lubricant Additives.* Wear, 1987. **120**(1): p. 51-60.

42. Yamamoto, Y. and S. Gondo, *Environmental-Effects on the Composition of Surface-Films Produced by an Organomolybdenum Compound.* Tribology Transactions, 1994. **37**(1): p. 182-188.

43. Graham, J., H. Spikes, and S. Korcek, *The friction reducing properties of molybdenum dialkyldithiocarbamate additives: Part I - Factors influencing friction reduction.* Tribology Transactions, 2001. **44**(4): p. 626-636.

44. Miklozic, K.T., J. Graham, and H. Spikes, *Chemical and physical analysis of reaction films formed by molybdenum dialkyl-dithiocarbamate friction modifier additive using Raman and atomic force microscopy.* Tribology Letters, 2001. **11**(2): p. 71-81.

45. Isoyama, H. and T. Sakurai, *The lubricating mechanism of di-u-thio-dithio-bis (diethyldithiocarbamate) dimolybdenum during extreme pressure lubrication.* Tribology, 1974. **7**(4): p. 151-160.

46. Kasrai, M., et al., *The chemistry of antiwear films generated by the combination of ZDDP and MoDTC examined by X-ray absorption spectroscopy.* Tribology Transactions, 1998. **41**(1): p. 69-77.

47. Grossiord, C., et al., *MoS$_2$, single sheet lubrication by molybdenum dithiocarbamate.* Tribology International, 1998. **31**(12): p. 737-743.

48. Korcek, S., et al., *Fuel efficient engine oils, additive interactions, boundary friction, and wear.* Lubrication at the Frontier, 1999. **36**: p. 13-24.

49. Lansdown, A.R., *Molybdenum disulphide lubrication.* 1st ed. Tribology series. 1999, Amsterdam ; New York: Elsevier. xxvi, 380 p.

50. Yamamoto, Y. and S. Gondo, *Friction and Wear Characteristics of Molybdenum Dithiocarbamate and Molybdenum Dithiophosphate.* Tribology Transactions, 1989. **32**(2): p. 251-257.

51. Graham, J. and H. Spikes, *The behaviour of molybdenum dialkyldithiocarbamate friction modifier additives.* Lubrication at the Frontier, 1999. **36**: p. 759-766.

52. Korcek, S., R.K. Jensen, and M.D. Johnson, *Interactions leading to formation of low friction films in systems containingmolybdenum dialkyldithiocarbamate and zinc dialkyldithiophosphate additives*, in *Tribology Series*, M.P. D. Dowson, C. M. Taylor, P. Ehret, T. H. C. Childs, G. Dalmaz, A. A. Lubrecht, Y. Berthier, L. Flamand, J. M. Georges, Editor. 2000, Elsevier. p. 399-407.

53. Morina, A., et al., *ZDDP and MoDTC interactions and their effect on tribological performance - tribofilm characteristics and its evolution.* Tribology Letters, 2006. **24**(3): p. 243-256.

54. Morina, A., et al., *ZDDP and MoDTC interactions in boundary lubrication - The effect of temperature and ZDDP/MoDTC ratio.* Tribology International, 2006. **39**(12): p. 1545-1557.

55. Muraki, M., Y. Yanagi, and K. Sakaguchi, *Synergistic effect on frictional characteristics under rolling-sliding conditions due to a combination of molybdenum dialkyldithiocarbamate and zinc dialkyldithiophosphate.* Tribology International, 1997. **30**(1): p. 69-75.

56. Korcek, S., *Engine oil fuel efficiency - Practical issues.* Tribology for Energy Conservation, 1998. **34**: p. 25-33.

57. Martin, J.M., et al., *Effect of oxidative degradation on mechanisms of friction reduction by MoDTC.* Boundary and Mixed Lubrication: Science and Applications, 2002. **40**: p. 207-213.

58. Stachowiak, G.W., A.W. Batchelor, and G.B. Stachowiak, *Experimental methods in tribology.* 1st ed. Tribology series. 2004, Amsterdam, The Netherlands ; San Diego, CA: Elsevier. xviii, 354 p.

59. Bhushan, B., *Modern tribology handbook.* Mechanics and materials science series. 2001, Boca Raton, FL: CRC Press.

60. Totten, G.E. and H. Liang, *Mechanical tribology materials, characterization, and applications.* 2004, Marcel Dekker: New York. p. ix, 496 p.

61. Gellman, A.J. and N.D. Spencer, *Surface chemistry in tribology.* Proceedings of the Institution of Mechanical Engineers Part J-Journal of Engineering Tribology, 2002. **216**(J6): p. 443-461.

62. Christophe, D. and M. Jean-Michel, *Problem-Solving Methods in Tribology with Surface-Specific Techniques*, in *Handbook of Surface and Interface Analysis*. 2009, CRC Press. p. 351-388.

63. Bharat, B., *Surface Roughness Analysis and Measurement Techniques*, in *Modern Tribology Handbook, Two Volume Set*. 2000, CRC Press.

64. Schuh, C.A., *Nanoindentation studies of materials.* Materials Today, 2006. **9**(5): p. 32-40.

65. Davidson, M.W. and M. Abramowitz, *Optical microscopy.* Encyclopedia of Imaging Science and Technology, ed. J. Hornak. Vol. 2. 2002: Wiley.

66. *Low-Coherence Interference Microscopy*, in *Optical Imaging and Microscopy*. 2007, Springer Berlin Heidelberg. p. 329-345.

67. Petzing, J., Coupland, J*, Leach, R K, *The measurement of rough surface topography using coherence scanning interferometry.*, ed. D. Measurement Good Practice Guide No. 116. December 2010.

68. Perry, S.S., *Scanning Probe Microscopy Measurements of Friction.* Mrs Bulletin, 2004. **29**(07): p. 478-483.

69. Carpick, R.W. and M. Salmeron, *Scratching the surface: fundamental investigations of tribology with atomic force microscopy.* Chemical Reviews, 1997. **97**(4): p. 1163-1194.

70. Klein, T., E. Buhr, and C. Georg Frase, *Chapter 6 - TSEM: A Review of Scanning Electron Microscopy in Transmission Mode and Its Applications*, in *Advances in Imaging and Electron Physics*, W.H. Peter, Editor. 2012, Elsevier. p. 297-356.

71. Torbacke, M., Å.K. Rudolphi, and E. Kassfeldt, *Surface Characterization*, in *Lubricants: Introduction to Properties and Performance, First Edition*. 2014, John Wiley & Sons, Ltd.

72. Mayer, J., et al., *TEM sample preparation and FIB-induced damage.* Mrs Bulletin, 2007. **32**(5): p. 400-407.

73. Egerton, R., *Analytical Electron Microscopy*, in *Physical Principles of Electron Microscopy*. 2005, Springer US. p. 155-175.

74. Watts, J.F. and J. Wolstenholme, *Electron Spectroscopy: Some Basic Concepts*, in *An Introduction to Surface Analysis by XPS and AES*. 2005, John Wiley & Sons, Ltd. p. 1-15.

75. Williams, P., *Secondary ion mass spectrometry.* Annual Review of Materials Science, 1985. **15**(1): p. 517-548.

76. Sathyanarayana, D.N., *Vibrational spectroscopy: theory and applications*. 2007: New Age International.

77. Sawyer, W.G. and K.J. Wahl, *Accessing Inaccessible Interfaces: In Situ Approaches to Materials Tribology.* Mrs Bulletin, 2008. **33**(12): p. 1145-1148.

78. Spikes, H., *In Situ Methods for Tribology Research.* Tribology Letters, 2003. **14**(1): p. 1-1.

79. Albahrani, S., et al., *A review of in situ methodologies for studying elastohydrodynamic lubrication.* Proceedings of the Institution of Mechanical Engineers, Part J: Journal of Engineering Tribology, 2015.

80. Wahl, K.J. and W.G. Sawyer, *Observing Interfacial Sliding Processes in Solid-Solid Contacts.* Mrs Bulletin, 2008. **33**(12): p. 1159-1167.

81. Krick, B.A., et al., *Optical In Situ Micro Tribometer for Analysis of Real Contact Area for Contact Mechanics, Adhesion, and Sliding Experiments.* Tribology Letters, 2012. **45**(1): p. 185-194.

82. Keith, J.H., *Design of a Pin-on-disk Tribometer with in Situ Optical Profilometry*. 2010, University of Florida.

83. Bongaerts, J.H.H., et al., *In situ confocal Raman spectroscopy of lubricants in a soft elastohydrodynamic tribological contact.* Journal of Applied Physics, 2008. **104**(1).

84. Scharf, T.W. and I.L. Singer, *Monitoring transfer films and friction instabilities with in situ Raman tribometry.* Tribology Letters, 2003. **14**(1): p. 3-8.

85. Singer, I.L., et al., *Third body processes and friction of solid lubricants studied by in situ optical and Raman tribometry.* Boundary and Mixed Lubrication: Science and Applications, 2002. **40**: p. 327-336.

86. Piras, F.M., A. Rossi, and N.D. Spencer, *Growth of tribological films: in situ characterization based on attenuated total reflection infrared spectroscopy.* Langmuir, 2002. **18**(17): p. 6606-6613.

87. Wang, J.J., et al., *The formation of carbon nanostructures by in situ TEM mechanical nanoscale fatigue and fracture of carbon thin films.* Nanotechnology, 2009. **20**(30).

88. Lim, S.C. and J.H. Brunton, *A Dynamic Wear Rig for the Scanning Electron-Microscope.* Wear, 1985. **101**(1): p. 81-91.

89. Rabe, R., et al., *Observation of fracture and plastic deformation during indentation and scratching inside the scanning electron microscope.* Thin Solid Films, 2004. **469–470**: p. 206-213.

90. Eswara-Moorthy, S.K., et al., *An In Situ SEM-FIB-Based Method for Contrast Enhancement and Tomographic Reconstruction for Structural Quantification of Porous Carbon Electrodes.* Microscopy and Microanalysis, 2014. **20**(05): p. 1576-1580.

91. Idziak, S.H.J., et al., *Structure under confinement in a smectic-A and lyotropic surfactant hexagonal phase.* Physica B: Condensed Matter, 1996. **221**(1–4): p. 289-295.

92. Idziak, S.H.J., et al., *The x-ray surface forces apparatus: Structure of a thin smectic liquid crystal film under confinement.* Science, 1994. **264**(5167): p. 1915-1918.

93. Golan, Y., et al., *The x-ray surface forces apparatus for simultaneous x-ray diffraction and direct normal and lateral force measurements.* Review of Scientific Instruments, 2002. **73**(6): p. 2486-2488.

94. Sch, J., T. Schneider, and E. Santner, *Development of a combined AFM-tribometer test rig.* Tribotest, 1998. **4**(4): p. 345-353.

95. Grierson, D.S., E.E. Flater, and R.W. Carpick, *Accounting for the JKR–DMT transition in adhesion and friction measurements with atomic force microscopy.* Journal of Adhesion Science and Technology, 2005. **19**(3-5): p. 291-311.

96. Le Mogne, T., J.M. Martin, and C. Grossiord, *Imaging the chemistry of transfer films in the AES/XPS analytical UHV tribotester.* Lubrication at the Frontier, 1999. **36**: p. 413-421.

97. Pepper, S.V., *Auger analysis of films formed on metals in sliding contact with halogenated polymers.* Journal of Applied Physics, 1974. **45**(7): p. 2947-2956.

98. Oyarce, A., et al., *In-situ Measurements of Contact Resistance and In-situ Durability studies of Steels and Coatings to be used as Bipolar Plates in PEMFCs.* Proton Exchange Membrane Fuel Cells 9, 2009. **25**(1): p. 1791-1801.

99. Laedre, S., et al., *In Situ and Ex Situ Contact Resistance Measurements of Stainless Steel Bipolar Plates for PEM Fuel Cells.* Proton Exchange Membrane Fuel Cells 9, 2013. **50**(2): p. 829-839.

100. Cann, P.M. and H.A. Spikes, *In Lubro Studies of Lubricants in Ehd Contacts Using Ftir Absorption-Spectroscopy.* Tribology Transactions, 1991. **34**(2): p. 248-256.

101. Rossi, A., et al., *Surface analytical studies of surface-additive interactions, by means of in situ and combinatorial approaches.* Wear, 2004. **256**(6): p. 578-584.

102. Piras, F.M., A. Rossi, and N.D. Spencer, *Combined in situ (ATR FT-IR) and ex situ (XPS) study of the ZnDTP-iron surface interaction.* Tribology Letters, 2003. **15**(3): p. 181-191.

103. Mangolini, F., A. Rossi, and N.D. Spencer, *In Situ Attenuated Total Reflection (ATR/FT-IR) Tribometry: A Powerful Tool for Investigating Tribochemistry at the Lubricant-Substrate Interface.* Tribology Letters, 2012. **45**(1): p. 207-218.

104. Ratoi, M., *In situ study of metal oleate friction modifier additives (vol 14, pg 33, 2003).* Tribology Letters, 2003. **15**(1): p. 73-73.

105. Glovnea, R.P., et al., *Measurement of sub-nanometer lubricant films using ultra-thin film interferometry.* Tribology Letters, 2003. **15**(3): p. 217-230.

106. Fujita, H. and H.A. Spikes, *Study of zinc dialkyldithiophosphate antiwear film formation and removal processes, part II: Kinetic model.* Tribology Transactions, 2005. **48**(4): p. 567-575.

107. Spikes, H.A., *Thin films in elastohydrodynamic lubrication: the contribution of experiment.* Proceedings of the Institution of Mechanical Engineers Part J-Journal of Engineering Tribology, 1999. **213**(J5): p. 335-352.

108. Fujita, H. and H.A. Spikes, *The formation of zinc dithiophosphate antiwear films.* Proceedings of the Institution of Mechanical Engineers Part J-Journal of Engineering Tribology, 2004. **218**(J4): p. 265-277.

109. Martin, J.M., et al., *Low-temperature friction in the XPS analytical ultrahigh vacuum tribotester.* Tribology Letters, 2003. **14**(1): p. 25-31.

110. Grossiord, C., et al., *UHV friction of tribofilms derived from metal dithiophosphates.* Tribology Letters, 1999. **6**(3-4): p. 171-179.

111. Lauer, J.L. and M.E. Peterkin, *Analysis of Infrared-Spectra of Fluid Films in Simulated Ehd Contacts.* Journal of Lubrication Technology-Transactions of the Asme, 1975. **97**(2): p. 145-150.

112. Lauer, J.L. and M.E. Peterkin, *Infrared-Emission Spectra of Liquids in a Diamond Anvil Cell by Interferometry.* Applied Spectroscopy, 1975. **29**(1): p. 78-79.

113. Cann, P.M., *In-Contact Molecular Spectroscopy of Liquid Lubricant Films.* Mrs Bulletin, 2008. **33**(12): p. 1151-1158.

114. Smith, E. and G. Dent, *Introduction, Basic Theory and Principles*, in *Modern Raman Spectroscopy – A Practical Approach.* 2005, John Wiley & Sons, Ltd. p. 1-21.

115. Larkin, P., *Chapter 2 - Basic Principles*, in *Infrared and Raman Spectroscopy*, P. Larkin, Editor. 2011, Elsevier: Oxford. p. 7-25.

116. Ferraro, J.R., K. Nakamoto, and C.W. Brown, *Chapter 1 - Basic Theory*, in *Introductory Raman Spectroscopy (Second Edition)*, J.R.F.N.W. Brown, Editor. 2003, Academic Press: San Diego. p. 1-94.

117. Vandenabeele, P., *Theoretical Aspects*, in *Practical Raman Spectroscopy – An Introduction.* 2013, John Wiley & Sons, Ltd. p. 1-38.

118. McCreery, R.L., *Introduction and Scope*, in *Raman Spectroscopy for Chemical Analysis.* 2005, John Wiley & Sons, Inc. p. 1-14.

119. Bernath, P.F., *Spectra of atoms and molecules.* 2nd ed. 2005, New York ; Oxford: Oxford University Press. xiv, 439 p.

120. Turrell, G. and J. Corset, *Raman microscopy : developments and applications.* 1996, London ; San Diego: Harcourt Brace. xxviii, 463 p.

121. Kazemi-Zanjani, N., et al., *Tip-Enhanced Raman Imaging and Nano Spectroscopy of Etched Silicon Nanowires.* Sensors, 2013. **13**(10): p. 12744.

122. Vandenabeele, P., *Raman Instrumentation*, in *Practical Raman Spectroscopy – An Introduction.* 2013, John Wiley & Sons, Ltd. p. 61-100.

123. Mathieu, J.P., Société française de physique., and Société de chimie physique., *Proceedings of the third International Conference on Raman Spectroscopy : University of Reims, France, September, 1972.* Advances in Raman spectroscopy. 1973, London ; New York: Heyden. 1 , xiii, 639 p.

124. Dvorak, S.D., K.J. Wahl, and I.L. Singer, *In situ analysis of third body contributions to sliding friction of a Pb-Mo-S coating in dry and humid air.* Tribology Letters, 2007. **28**(3): p. 263-274.

125. Singer, I.L., S.D. Dvorak, and K.J. Wahl, *Investigation of third body processes by in vivo Raman tribometry.* 9th Nordic Symposium on Tribology Nordtrib 2000, Vol 1, 2000. **200**: p. 31-41.

126. Singer, I.L., et al., *Role of third bodies in friction and wear of protective coatings.* Journal of Vacuum Science & Technology A, 2003. **21**(5): p. S232-S240.

127. Scharf, T.W. and I.L. Singer, *Role of third bodies in friction behavior of diamond-like nanocomposite coatings studied by in situ tribometry.* Tribology Transactions, 2002. **45**(3): p. 363-371.

128. Chromik, R.R., H.W. Strauss, and T.W. Scharf, *Materials Phenomena Revealed by In Situ Tribometry.* Jom, 2012. **64**(1): p. 35-43.

129. Mcdevitt, N.T., M.S. Donley, and J.S. Zabinski, *Utilization of Raman-Spectroscopy in Tribochemistry Studies.* Wear, 1993. **166**(1): p. 65-72.

130. Temple, P.A. and C.E. Hathaway, *Multiphonon Raman-Spectrum of Silicon.* Physical Review B, 1973. **7**(8): p. 3685-3697.

131. Li, J., *Advanced Techniques in TEM Specimen Preparation*. The Transmission Electron Microscope, ed. K. Maaz. 2012, Rijeka: InTech.

132. Porto, S.P.S. and R.S. Krishnan, *Raman Effect of Corundum.* Journal of Chemical Physics, 1967. **47**(3): p. 1009-&.

133. Kadleikova, M., J. Breza, and M. Vesely, *Raman spectra of synthetic sapphire.* Microelectronics Journal, 2001. **32**(12): p. 955-958.

134. Palanza, V., et al., *Micro-Raman spectroscopy applied to the study of inclusions within sapphire.* Journal of Raman Spectroscopy, 2008. **39**(8): p. 1007-1011.

135. Totten, G.E., S.R. Westbrook, and R.J. Shah, *10. Synthetic Lubricants - Non Aqueous*, in *Fuels and Lubricants Handbook - Technology, Properties, Performance, and Testing: (MNL 37WCD)*. ASTM International.

136. Barnes, A.M., K.D. Bartle, and V.R.A. Thibon, *A review of zinc dialkyldithiophosphates (ZDDPS): characterisation and role in the lubricating oil.* Tribology International, 2001. **34**(6): p. 389-395.

137. Windom, B.C., W.G. Sawyer, and D.W. Hahn, *A Raman Spectroscopic Study of MoS$_2$ and MoO$_3$: Applications to Tribological Systems.* Tribology Letters, 2011. **42**(3): p. 301-310.

138. Mcdevitt, N.T., J.S. Zabinski, and M.S. Donley, *The Use of Raman-Scattering to Study Disorder in Pulsed-Laser Deposited MoS$_2$ Films.* Thin Solid Films, 1994. **240**(1-2): p. 76-81.

139. Chen, J.M. and C.S. Wang, *Second-Order Raman-Spectrum of MoS$_2$.* Solid State Communications, 1974. **14**(9): p. 857-860.

140. Stacy, A.M. and D.T. Hodul, *Raman spectra of IVB and VIB transition-metal disulfides using laser energies near the absorption edges.* Journal of Physics and Chemistry of Solids, 1985. **46**(4): p. 405-409.

141. Py, M.A. and K. Maschke, *Intralayer and Interlayer Contributions to the Lattice-Vibrations in MoO₃.* Physica B & C, 1981. **105**(1-3): p. 370-374.

142. Hardcastle, F.D. and I.E. Wachs, *Determination of Molybdenum Oxygen Bond Distances and Bond Orders by Raman-Spectroscopy.* Journal of Raman Spectroscopy, 1990. **21**(10): p. 683-691.

143. Zolper, T., et al., *Lubrication Properties of Polyalphaolefin and Polysiloxane Lubricants: Molecular Structure-Tribology Relationships.* Tribology Letters, 2012. **48**(3): p. 355-365.

144. Praveena, M., et al., *Total internal reflection Raman spectroscopy of poly(alpha-olefin) oils in a lubricated contact.* Rsc Advances, 2014. **4**(42): p. 22205-22213.

145. McCreery, R.L., *Raman spectroscopy for chemical analysis.* 2000, New York Chichester: John Wiley & Sons. xxiv, 420 p.

146. Gondo, S. and Y. Yamamoto, *Mechanism of Surface-Film Formation of Modtc and Effect of Rubbing Materials.* Journal of Japanese Society of Tribologists, 1991. **36**(3): p. 242-248.

147. Nayak, A.P., et al., *Pressure-induced semiconducting to metallic transition in multilayered molybdenum disulphide.* Nature Communications, 2014. **5**.

148. Liu, K.K., et al., *Growth of Large-Area and Highly Crystalline MoS₂ Thin Layers on Insulating Substrates.* Nano Letters, 2012. **12**(3): p. 1538-1544.

149. Lanzillo, N.A., et al., *Temperature-dependent phonon shifts in monolayer MoS₂.* Applied Physics Letters, 2013. **103**(9).

150. Uy, D., et al., *Characterization of anti-wear films formed from fresh and aged engine oils.* Wear, 2007. **263**: p. 1165-1174.

151. Wang, Y.H., et al., *Novel FeMoO₄/graphene composites based electrode materials for supercapacitors.* Composites Science and Technology, 2014. **103**: p. 16-21.

152. Morina, A., et al., *Role of friction modifiers on the tribological performance of hypereutectic Al-Si alloy lubricated in boundary conditions.* Proceedings of the Institution of Mechanical Engineers Part J-Journal of Engineering Tribology, 2011. **225**(J6): p. 369-378.

153. Grossiord, C., et al., *In situ MoS₂ formation and selective transfer from MoDPT films.* Surface & Coatings Technology, 1998. **108**(1-3): p. 352-359.

154. Hu, H.C., I.E. Wachs, and S.R. Bare, *Surface-Structures of Supported Molybdenum Oxide Catalysts - Characterization by Raman and Mo L(3)-Edge Xanes.* Journal of Physical Chemistry, 1995. **99**(27): p. 10897-10910.

155. Sourisseau, C., O. Gorochov, and D.M. Schleich, *Comparative IR and Raman studies of various amorphous MoS$_3$ and Li$_x$MoS$_3$ phases.* Materials Science and Engineering B-Solid State Materials for Advanced Technology, 1989. **3**(1-2): p. 113-117.

156. Clark, R.J.H., A.J. Hempleman, and M. Kurmoo, *Infrared, Raman, and Resonance-Raman Spectra of [Mo$_2$(O$_2$CCH$_3$)$_4$] and [Mo$_2$(O$_2$CCD$_3$)$_4$].* Journal of the Chemical Society-Dalton Transactions, 1988(4): p. 973-981.

157. Bouchet, M.I.D., et al., *Mechanisms of MoS$_2$ formation by MoDTC in presence of ZnDTP: effect of oxidative degradation.* Wear, 2005. **258**(11-12): p. 1643-1650.

158. Shea, T.M. and A.J. Stipanovic, *Solution phase reactions of organomolybdenum friction modifier additives for energy conserving engine oils.* Tribology Letters, 2002. **12**(1): p. 13-22.

159. Bec, S., et al., *Synergistic effects of MoDTC and ZDTP on frictional behaviour of tribofilms at the nanometer scale.* Tribology Letters, 2004. **17**(4): p. 797-809.

160. Grossiord, C., et al., *Friction-reducing mechanisms of molybdenum dithiocarbamate zinc dithiophosphate combination: New insights in MoS$_2$ genesis.* Journal of Vacuum Science & Technology a-Vacuum Surfaces and Films, 1999. **17**(3): p. 884-890.

161. Unnikrishnan, R., et al., *Additive-additive interaction: an XPS study of the effect of ZDDP on the AW/EP characteristics of molybdenum based additives.* Wear, 2002. **252**(3-4): p. 240-249.

162. Spikes, H., *The history and mechanisms of ZDDP.* Tribology Letters, 2004. **17**(3): p. 469-489.

163. Nicholls, M.A., et al., *Review of the lubrication of metallic surfaces by zinc dialkyl-dithlophosphates.* Tribology International, 2005. **38**(1): p. 15-39.

164. Martin, J.M., et al., *Tribochemistry in the analytical UHV tribometer.* Tribology International, 1999. **32**(11): p. 617-626.

165. Martin, J.M., et al., *Synergistic effects in binary systems of lubricant additives: a chemical hardness approach.* Tribology Letters, 2000. **8**(4): p. 193-201.

166. De Barros, M.I., et al., *Friction reduction by metal sulfides in boundary lubrication studied by XPS and XANES analyses.* Wear, 2003. **254**(9): p. 863-870.

167. Brow, R.K., et al., *The Short-Range Structure of Zinc Polyphosphate Glass.* Journal of Non-Crystalline Solids, 1995. **191**(1-2): p. 45-55.

168. Meyer, K., *Characterization of the structure of binary zinc ultraphosphate glasses by infrared and Raman spectroscopy.* Journal of Non-Crystalline Solids, 1997. **209**(3): p. 227-239.

169. Nelson, B.N. and G.J. Exarhos, *Vibrational Spectroscopy of Cation-Site Interactions in Phosphate-Glasses.* Journal of Chemical Physics, 1979. **71**(7): p. 2739-2747.

170. Tallant, D.R., C. Nelson, and J.A. Wilder, *Effects on Glass Structure of Bao Substitution in Alkali Meta-Phosphate Glasses.* Physics and Chemistry of Glasses, 1986. **27**(2): p. 71-74.

171. Tischendorf, B., et al., *A study of short and intermediate range order in zinc phosphate glasses.* Journal of Non-Crystalline Solids, 2001. **282**(2-3): p. 147-158.

172. Arslan, E., F. Bülbül, and I. Efeoglu, *The Structural and Tribological Properties of MoS$_2$-Ti Composite Solid Lubricants.* Tribology Transactions, 2004. **47**(2): p. 218-226.

173. *X-ray Data Booklet*, ed. A.C. Thompson and D. Vaughan. 2009: Lawrence Berkeley National Laboratory, University of California.

174. Taylor, L., A. Dratva, and H.A. Spikes, *Friction and wear behavior of zinc dialkyldithiophosphate additive.* Tribology Transactions, 2000. **43**(3): p. 469-479.

175. Berkani, S., et al., *Structural Changes in Tribo-Stressed Zinc Polyphosphates.* Tribology Letters, 2013. **51**(3): p. 489-498.

176. Li, H., et al., *From Bulk to Monolayer MoS$_2$: Evolution of Raman Scattering.* Advanced Functional Materials, 2012. **22**(7): p. 1385-1390.

177. Lee, C., et al., *Anomalous Lattice Vibrations of Single- and Few-Layer MoS$_2$.* Acs Nano, 2010. **4**(5): p. 2695-2700.

178. Heuberger, R., A. Rossi, and N.D. Spencer, *XPS study of the influence of temperature on ZnDTP tribofilm composition.* Tribology Letters, 2007. **25**(3): p. 185-196.

179. Vuurman, M.A. and I.E. Wachs, *Insitu Raman-Spectroscopy of Alumina-Supported Metal-Oxide Catalysts.* Journal of Physical Chemistry, 1992. **96**(12): p. 5008-5016.

180. Tytko, K.-H., et al., *Mo Molybdenum hydrous molybdates of groups VA to VIB metals (system nos. 18 to 52)*, in *Gmelin handbook of inorganic chemistry 4.* 1985, Springer: Berlin.

181. Chang, C.H. and S.S. Chan, *Infrared and Raman studies of amorphous MoS3 and poorly crystalline MoS$_2$.* Journal of Catalysis, 1981. **72**(1): p. 139-148.

182. Bhattacharya, R.N., et al., *Optical study of amorphous MoS3: Determination of the fundamental energy gap.* Journal of Non-Crystalline Solids, 1987. **91**(2): p. 235-242.

183. Chakraborty, B., et al., *Layer-dependent resonant Raman scattering of a few layer MoS₂.* Journal of Raman Spectroscopy, 2013. **44**(1): p. 92-96.

184. Shaver, J.M., *Chemometrics for Raman Spectroscopy*, in *Handbook of Raman Spectroscopy*, I.R. Lewis and H.G.M. Edwards, Editors. 2001, Marcel Dekker, Inc.: New York , Basel.

185. Ferraro, J.R., K. Nakamoto, and C.W. Brown, *Chapter 5 - Analytical Chemistry*, in *Introductory Raman Spectroscopy (Second Edition)*, J.R.F.N.W. Brown, Editor. 2003, Academic Press: San Diego. p. 267-293.

186. Maddams, W.F., *The Scope and Limitations of Curve Fitting.* Applied Spectroscopy, 1980. **34**(3): p. 245-267.

187. Bradley, M., *Curve Fitting in Raman and IR Spectroscopy: Basic Theory of Line Shapes and Applications.* USA: Thermo Fisher Scientific.

188. Strube, G., *Raman Scattering.* Optical Measurements:Techniques and Applications, ed. F. Mayinger. 1994, Berlin: Springer. 215-241.

189. McCreery, R.L., *Magnitude of Raman Scattering*, in *Raman Spectroscopy for Chemical Analysis.* 2005, John Wiley & Sons, Inc. p. 15-33.

190. Seshadri, K.S. and R.N. Jones, *The Shapes and Intensities of Infrared Absorption Bands - a Review.* Spectrochimica Acta, 1963. **19**(6): p. 1013-1085.

191. Chandrasekaran, M. and A.W. Batchelor, *In situ observation of sliding wear tests of butyl rubber in the presence of lubricants in an X-ray microfocus instrument.* Wear, 1997. **211**(1): p. 35-43.

192. Graham, J., H. Spikes, and R. Jensen, *The friction reducing properties of molybdenum dialkyldithiocarbamate additives: Part II - Durability of friction reducing capability.* Tribology Transactions, 2001. **44**(4): p. 637-647.

193. Yamamoto, Y. and S. Gondo, *On Properties of Surface-Films Formed with Modtc under Different Conditions.* Journal of Japanese Society of Tribologists, 1991. **36**(3): p. 235-241.

194. Arai, K. and Y. Yamamoto, *Effect of molybdenum dithiocarbamate on friction and wear properties between aluminum alloy and steel.* Tribology Transactions, 2000. **43**(1): p. 45-50.

195. El Mendili, Y., A. Abdelouas, and J.F. Bardeau, *Insight into the mechanism of carbon steel corrosion under aerobic and anaerobic conditions.* Physical Chemistry Chemical Physics, 2013. **15**(23): p. 9197-9204.

196. El Mendili, Y., et al., *Phase transitions of iron sulphides formed by steel microbial corrosion.* Rsc Advances, 2013. **3**(48): p. 26343-26351.

197. De Feo, M., et al., *Ageing impact on tribological properties of MoDTC-containing base oil.* Tribology International, 2015. **92**: p. 126-135.

198. Golasa, K., et al., *Resonant Raman scattering in MoS$_2$-From bulk to monolayer.* Solid State Communications, 2014. **197**: p. 53-56.

199. Khaemba, D., A. Neville, and A. Morina, *A methodology for Raman characterisation of MoDTC tribofilms and its application in investigating the influence of surface chemistry on friction performance of MoDTC lubricants.* Tribology Letters, 2015. **59**(3): p. 1-17.

200. Seguin, L., et al., *Infrared and Raman-Spectra of MoO$_3$ Molybdenum Trioxides and MoO$_3$-xH$_2$O Molybdenum Trioxide Hydrates.* Spectrochimica Acta Part a-Molecular and Biomolecular Spectroscopy, 1995. **51**(8): p. 1323-1344.

201. Desikan, A.N., L. Huang, and S.T. Oyama, *Oxygen-Chemisorption and Laser Raman-Spectroscopy of Unsupported and Silica-Supported Molybdenum Oxide.* Journal of Physical Chemistry, 1991. **95**(24): p. 10050-10056.

202. Sorab, J., Korcek, S., and Bovington, C, *Friction Reduction in Lubricated Components Through Engine Oil Formulation.* SAE Technical Paper 982640. 1998.

203. Arabyan, S.G., et al., *An investigation of the effectiveness of antifriction additives in motor oils by laboratory methods and engine tests.* Lubrication Science, 1993. **5**(3): p. 241-256.

204. Korcek, S., Jensen, R., Johnson, M. and Clausing, E, *Antioxidant Reactions of Engine Oil Additive Systems Containing Friction Modifiers.* International Tribology Conference, Yokohama 1995, ed. N.J. Gakkai. 1996, Tokyo: JST. 733 - 737.

205. Morina, A. and A. Neville, *Understanding the composition and low friction tribofilm formation/removal in boundary lubrication.* Tribology International, 2007. **40**(10-12): p. 1696-1704.

206. Martin, J.M., et al., *Tribochemistry of ZDDP and MoDDP chemisorbed films.* Tribology Letters, 1996. **2**(3): p. 313-326.

207. Fuller, M.L.S., et al., *Solution decomposition of zinc dialkyl dithiophosphate and its effect on antiwear and thermal film formation studied by X-ray absorption spectroscopy.* Tribology International, 1998. **31**(10): p. 627-644.

208. Fuller, M., et al., *Chemical characterization of tribochemical and thermal films generated from neutral and basic ZDDPs using X-ray absorption spectroscopy.* Tribology International, 1997. **30**(4): p. 305-315.

209. Berkani, S., et al., *Model formation of ZDDP tribofilm from a mixture of zinc metaphosphate and goethite.* Tribology International, 2014. **79**: p. 197-203.

Appendix A
# Contact geometry

A.1 Hertzian Contact pressure

Figure A.1 shows a contact area between the pin and disc tribometer configuration. The contact area between the surface is regarded as a contact between a sphere and a plane surface.
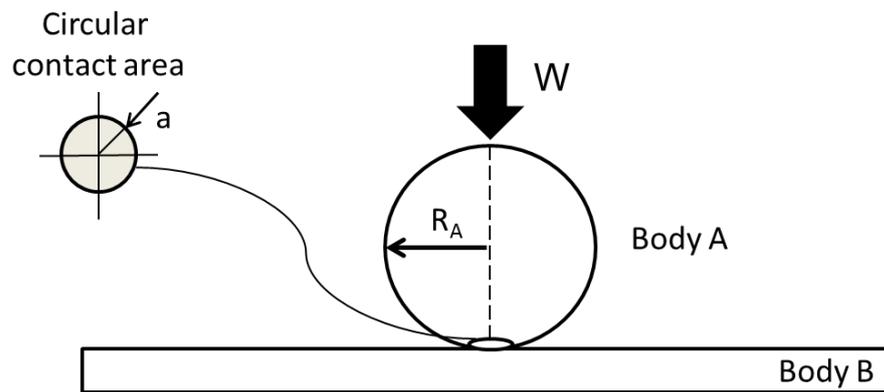
Figure A.1 Contact geometry between a sphere and a flat surface.

The contact parameters for this configuration are calculated according to the formula extracted from the Hertz contact theory. Table A.1 lists the formulae for the contact parameters between the sphere and a plane surface.

Table A.1 Formulae for contact parameters between a sphere and a flat surface

Contact area dimensions	Maximum contact pressure	Average contact pressure
$a = \left(\dfrac{3WR'}{E'}\right)^{1/3}$	$P_{max} = \dfrac{3W}{2\pi a^2}$	$P_{average} = \dfrac{W}{\pi a^2}$
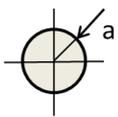
[Stachowiak, G.W. and A.W. Batchelor, 7 - Elastohydrodynamic Lubrication, in Engineering Tribology (Third Edition), G.W.S.W. Batchelor, Editor. 2006, Butterworth-Heinemann: Burlington. p. 287-362.]

where:

- a = semi-major axes of the contact ellipse [m];

- W = normal load [N];

- R' = reduced radius of curvature between the sphere and the flat surface in contact [m], which is given by:

$$\frac{1}{R'} = \frac{1}{R_x} + \frac{1}{R_y} = \frac{1}{R_{ax}} + \frac{1}{R_{bx}} + \frac{1}{R_{ay}} + \frac{1}{R_{by}}$$

Since one of the contacting surfaces is a plane then it has infinite radii of curvature, therefore

$$R_{bx} = R_{by} = \infty$$

And the reduced radius of curvature becomes

$$\frac{1}{R'} = \frac{1}{R_x} + \frac{1}{R_y} = \frac{1}{R_{ax}} + \frac{1}{R_{ay}}$$

where:

R_x and R_y is the radius of the sphere in the 'x' and 'y' coordinate

Radius of HSPOD sphere ($R_x = R_y$) – 0.003175 m

Radius of *in-situ* rig sphere ($R_x = R_y$) – 0.00275 m

- *E* = reduced Young's modulus [Pa], defined as:

$$\frac{1}{E'} = \frac{1}{2}\left[\frac{1 - \vartheta_A^{\,2}}{E_A} + \frac{1 - \vartheta_B^{\,2}}{E_B}\right]$$

where:

ϑ_A and ϑ_B are the Poisson's ratios of the contacting bodies '**A**' and '**B**' respectively,

E_A and E_B are the Young's moduli of the contacting bodies '**A**' and '**B**' respectively,

Table A.2 Mechanical properties of the steel and ball sample

Material	Young's modulus (E)	Poisson's ratio (ϑ)
Spring steel AISI 1050 disc	210 GPa	0.3
AISI 52100 Chrome Steel Ball Bearings	210 GPa	0.3

Calculations of Hertzian contact pressure with the stated formulae and properties have been conducted prior to performing any experiments. Contact pressure formula are dependent of the contact area dimensions and the change in the diameter of the ball sample of the HSPOD and the *in-situ* rig affects the contact pressure of the tribological system.